University of Cyprus

DEPARTMENT OF CHEMISTRY

INVESTIGATION OF THE ENHANCEMENT OF THE MECHANICAL PROPERTIES OF POLYMER NETWORK HYDROGELS VIA NETWORK MULTIPLICITY, AMPHIPHILICITY, AND REVERSIBILITY

DOCTOR OF PHILOSOPHY DISSERTATION

PANAYIOTA PANTELI

2019

University of Cyprus

DEPARTMENT OF CHEMISTRY

INVESTIGATION OF THE ENHANCEMENT OF THE MECHANICAL PROPERTIES OF POLYMER NETWORK HYDROGELS VIA NETWORK MULTIPLICITY, AMPHIPHILICITY, AND REVERSIBILITY

PANAYIOTA PANTELI

A Dissertation Submitted to the University of Cyprus in Partial Fulfillment of the Requirements for the Degree of Doctor of Philosophy

May 2019

VALIDATION PAGE

Doctoral Candidate: Panayiota Panteli

Doctoral Dissertation Title: Investigation of the Enhancement of the Mechanical Properties of Polymer Network Hydrogels via Network Multiplicity, Amphiphilicity, and Reversibility.

The present Doctoral Dissertation was submitted in partial fulfillment of the requirements for the Degree of Doctor of Philosophy at the ***Department of Chemistry*** *and was approved on the 6th of May 2019 by the members of the* ***Examination Committee****.*

Examination Committee:

Research Supervisor: Costas S. Patrickios, Professor, University of Cyprus

Costas S. Patrick .....

Committee Member: Epameinondas Leontidis, Professor, University of Cyprus

.....

Committee Member: Anastasios Keramidas, Professor, University of Cyprus

.....

Committee Member: Pavletta Shestakova, Professor, Bulgarian Academy of Sciences

.....

Committee Member: Vasileios Koutsos, Professor, University of Edinburgh

.....

DECLARATION OF DOCTORAL CANDIDATE

The present doctoral dissertation was submitted in partial fulfillment of the requirements for the degree of Doctor of Philosophy of the University of Cyprus. It is a product of original work of my own, unless otherwise mentioned through references, notes, or any other statements.

SANS measurements were performed at the Helmholtz-Zentrum in Berlin (HZB), Germany.

Nano-indentation experiments were performed at the Cyprus University of Technology in Limassol by Assistant Professor Georgios Constantinides and Dr. Marios Constantinou.

20/05/2019

Panayiota Panteli

ΠΕΡΙΛΗΨΗ

Η παρούσα Διδακτορική Διατριβή πραγματεύεται τη διερεύνηση τριών στρατηγικών για την ενίσχυση των μηχανικών ιδιοτήτων πολυμερικών υδροπλεγμάτων. Αυτές οι στρατηγικές ήταν η πολλαπλότητα, η αμφιφιλικότητα, και η αντιστρεπτότητα των δικτύων. Οι πρώτες δύο στρατηγικές αποδείχθηκαν επιτυχείς, με το πλέγμα με τη μεγαλύτερη πολλαπλότητα, ίση με 5, και τη μεγαλύτερη συγκέντρωση μονομερούς, ίση με 5 M, να παρουσιάζει την πολύ υψηλή τάση θραύσης συμπίεσης των 51 MPa, και το καλύτερο αμφιφιλικό πολυμερικό δίκτυο, με ενδιάμεση περιεκτικότητα σε υδρόφοβο μονομερές, να παρουσιάζει επίσης την υψηλή τάση θραύσης συμπίεσης των 11 MPa. Στην περίπτωση των πολλαπλών υδροπλεγμάτων, η τάση θραύσης αυξήθηκε με αύξηση και της πολλαπλότητας του δικτύου και της συγκέντρωσης του μονομερούς, ως συνέπεια της προστασίας των προηγούμενων δικτύων από τα επόμενα δίκτυα ως προς τη δημιουργία και διάδοση ρωγμών. Στην περίπτωση των αμφιφιλικών πολυμερικών δικτύων, η τάση θραύσης τους αυξήθηκε με το ποσοστό του υδρόφοβου μονομερούς ως αποτέλεσμα της μειωμένης πρόσληψης νερού, αλλά, κυρίως, λόγω των ελκτικών αλληλεπιδράσεων μεταξύ των επαναλαμβανόμενων μονάδων του υδρόφοβου μονομερούς. Τα πιο αραιά διασταυρωμένα αμφιφιλικά πολυμερικά δίκτυα παρουσίασαν την ιδιότητα «μνήμης σχήματος» (“shape memory”), μία πολύ σημαντική ιδιότητα που μπορεί να αξιοποιηθεί σε πολλές εφαρμογές στην τεχνολογία και στην ιατρική. Σχετικά με την αντιστρεπτότητα του δικτύου, ο συγκεκριμένος δυναμικός ομοιοπολικός δεσμός που χρησιμοποιήθηκε για τις αντιστρεπτές διασταυρώσεις ήταν πολύ σταθερός και δύσκολο να επιτευχθεί η ανταλλαγή του.

Η προαναφερθείσα στρατηγική για τα πολλαπλά πλέγματα είναι αρκετά καινοτόμα, καθώς αποτελεί την επέκταση της κλασικής προσέγγισης των διπλών πλεγμάτων σε πενταπλά πλέγματα. Το μονομερές που χρησιμοποιήθηκε για τα πολλαπλά πλέγματα ήταν το ουδέτερο υδρόφιλο μονομερές *N*,*N*-διμεθυλακρυλαμίδιο (DMAAm). Το ίδιο μονομερές χρησιμοποιήθηκε επίσης στην παρασκευή των αμφιφιλικών πολυμερικών δικτύων, σε συνδυασμό με το σπανίως χρησιμοποιούμενο υδρόφοβο και κρυσταλλικό μονομερές *N*-δωδεκυλακρυλαμίδιο (DDAAm). Μέχρι πολύ πρόσφατα, το τελευταίο μονομερές δεν ήταν εμπορικά διαθέσιμο και έπρεπε να συντεθεί στο εργαστήριο. Παρόλο που κάποιες από τις συνθέσεις των πολυμερών περιλάμβαναν πολυμερισμό ελευθέρων ριζών, αρκετές από τις συνθέσεις πραγματοποιήθηκαν με χρήση μίας ελεγχόμενης μεθόδου πολυμερισμού ριζών, και, συγκεκριμένα, τον πολυμερισμό μεταφοράς αλυσίδας μέσω αντιστρεπτής προσθήκης και απόσπασης.

ABSTRACT

This PhD Thesis involves the exploration of three strategies for the improvement of the mechanical properties of polymer network hydrogels. These strategies were network multiplicity, network amphiphilicity, and network reversibility. The first two strategies were proven successful, with the multiple network possessing the highest multiplicity, equal to 5, and prepared at the highest monomer concentration, 5 M, presenting a very high compressive fracture stress of 51 MPa, and the strongest amphiphilic polymer conetwork, bearing an intermediate content of the hydrophobic monomer, also exhibiting a high compressive fracture stress of 11 MPa. In the case of the multiple network hydrogels, fracture stress increased both with network multiplicity and monomer concentration, a result of the protection of the earlier networks from the later networks with regard to crack formation and crack propagation. In the case of the amphiphilic polymer networks, their strength increased with the content in the hydrophobic monomer, a consequence of the reduced water uptake, but, more importantly, the associations among the hydrophobic monomer repeating units. Interestingly, the more loosely cross-linked amphiphilic polymer networks displayed shape memory, a very useful property which can be exploited in many applications in technology and medicine. Regarding network reversibility, the particular dynamic covalent bond employed for the reversible cross-links in this investigation was too stable and, consequently, difficult to exchange.

Our above-mentioned multiple network strategy was highly innovative, in that it greatly extended the classical approach of double network hydrogels to quintuple (5-fold) network hydrogels. The monomer employed for these multiple networks was the nonionic hydrophilic *N*,*N*-dimethylacrylamide (DMAAm). The same monomer was also employed for the preparation of the amphiphilic polymer networks, in combination with the rarely used hydrophobic and crystalline *N*-dodecylacrylamide (DDAAm) monomer. Until very recently, this latter monomer was not commercially available and had to be prepared in the laboratory. Although several of our polymer syntheses employed free radical photopolymerization, many of the synthesis used a controlled radical polymerization method, and, in particular, reversible addition-fragmentation chain transfer (RAFT) polymerization.

ACKNOWLEDGMENTS

First of all, I would like to thank my supervisor, Professor Costas S. Patrickios, for the valuable help, guidance and excellent cooperation during the course of my Doctoral studies at the University of Cyprus.

Moreover, I would like to thank Professor Michael Gradzielski and Ms. Miriam Simon of the Technical University of Berlin (TUB), and Dr. Daniel Clemens of the Helmholtz-Zentrum in Berlin (HZB), for their help with our SANS measurements, and HZB for the neutron beam time.

I would also like to thank Assistant Professor Georgios Constantinides and Dr. Marios Constantinou of the Cyprus University of Technology in Limassol for performing for us the nano-indentation experiments.

Furthermore, I would like to thank Professor Epameinondas Leontidis for providing to us access to his rheometer for our rheology measurements, and Associate Professor Triantafyllos Stylianopoulos and Dr. Chrysovalantis Voutouri at the Department of Mechanical and Manufacturing Engineering of the University of Cyprus for performing for us preliminary compression and tensile measurements.

In addition, I would like to thank Professor Epameinondas Leontidis and Professor Anastasios Keramidas of our Department of Chemistry at the University of Cyprus, Professor Vasileios Koutsos of the Institute for Materials at the University of Edinburgh and Professor Pavletta Shestakova of the Bulgarian Academy of Sciences in Sofia for their participation in my Doctoral Examination Committee.

I would like to thank the members of the Polymer Science Research Group for our excellent cooperation.

Finally, I would like to thank my family and my friends for their valuable support over all these years!

PUBLICATIONS

- Panayiota A. Panteli and Costas S. Patrickios, Complex Hydrogels Based on Multiply-interpenetrated Polymer Networks: Enhancement of Mechanical Properties via Network Multiplicity and Monomer Concentration. *Macromolecules* **2018**, *51*, 7533-7545.
- Panayiota A. Panteli, Costas S. Patrickios, Marios Constantinou, and Georgios Constantinides, Multiple Network Hydrogels: A Study of Their Nanoindentation Hardness. *Macromolecular Symposia* **2019**, In press.
- Panayiota A. Panteli and Costas S. Patrickios, Multiply Interpenetrating Polymer Networks: Preparation, Mechanical Properties, and Applications. *Gels* **2019**, In press.
- Panayiota A. Panteli and Costas S. Patrickios, Determination of the Degree of Interconnection within Nonionic Double Network Hydrogels with the Use of a Degradable Cross-linker. In preparation.
- Panayiota A. Panteli, Miriam Simon, Michael Gradzielski, Daniel Clemens, and Costas S. Patrickios, Synthesis and Characterization of Linear Amphiphilic Diblock Copolymers of *N*,*N*-Dimethylacrylamide (DMAAm) and *N*-Dodecylacrylamide (DDAAm) Prepared Using RAFT Polymerization. In preparation.
- Panayiota A. Panteli and Costas S. Patrickios, Randomly Cross-linked Amphiphilic Polymer Conetworks with Shape Memory: Random Combination of *N*-Dodecylacrylamide (DDAAm) and *N*,*N*-Dimethylacrylamide (DMAAm). In preparation.
- Panayiota A. Panteli and Costas S. Patrickios, Amphiphilic Polymer Conetworks Based on End-Linked Pentablock Terpolymers of *N*-Dodecylacrylamide (DDAAm) and *N*,*N*-Dimethylacrylamide (DMAAm) Prepared using RAFT Polymerization. In preparation.
- Panayiota A. Panteli and Costas S. Patrickios, Amphiphilic Polymer Conetworks Based on End-Linked Pentablock Terpolymers Prepared via RAFT Polymerization and Cross-linked via Oxime Bonds. In preparation.
- Florian Jung, Panayiota A. Panteli, Costas S. Patrickios, Christine M. Papadakis, Structural Properties of a Telechelic Pentablock Terpolymer with pH-responsive Mid-blocks and Temperature-responsive Random Copolymer End-blocks in Aqueous Solution. In preparation, April 2019.

ABBREVIATIONS

AAc	Acrylic acid
AAm	Acrylamide
AFM	Atomic force microscopy
AIBN	2,2´-Azobis(isobutyronitrile)
AMPS	2-Acrylamido-2-methyl-1-propanesulfonic acid
APCN	Amphiphilic polymer conetwork
APS	Ammonium persulfate
ATRP	Atom transfer radical polymerization
BDA	Butanediol diacrylate
BFAECs	Bovine fetal aorta endothelial cells
BMPA	2-Bromo-2-methylpropionic acid
BzHA	*O*-Benzylhydroxylamine hydrochloride
CEC	*N*-Carboxyethyl chitosan
CTA	Chain transfer agent
Đ	Molecular weight dispersity
DAAm	Diacetone acrylamide
DCC	*N,N′*-Dicyclohexylcarbodiimide
DCM	Dichloromethane
DDAAm	*N*-Dodecylacrylamide
DHEBA	*N*,*N´*-(1,2-Dihydroxy-ethylene)bisacrylamide
DLS	Dynamic light scattering
DMAAm	*N*,*N*-Dimethylacrylamide
DMAEA-Q	2-(Trimethylamino)ethyl acrylate, chloride quaternary salt
DMAP	4-Dimethylaminopyridine
DMAPAA-Q	3-(Acrylamidopropyl)trimethylammonium chloride
DMF	*N*,*N*-Dimethylformamide
DMPA	2-(Dodecylthiocarbonothioylthio)-2-methylpropionic acid
DMPAP	2,2-Dimethoxy-2-phenylacetophenone
DMSO	Dimethylsulfoxide
***d*$_6$-DMSO**	Deuterated dimethylsulfoxide
DN	Double-network
DP	Degree of polymerization
DPPH	2,2-Diphenyl-1-picrylhydrazyl hydrate
DS	Degree of swelling
E	Young's/Elastic modulus
EA	Ethyl acrylate
EDOT	3,4-Ethylenedioxythiophene

EtOAc	Ethyl acetate
EtOH	Ethanol
FAAm	*N*-Formylacrylamide
FTIR	Fourier-transform infrared
G	Fracture energy
G′	Storage/elastic modulus
G″	Loss/viscous modulus
GPC	Gel permeation chromatography
GTP	Group transfer polymerization
H	Hardness
HDDA	1,6-Hexanediol diacrylate
HEA	2-Hydroxyethyl acrylate
HRMAS	High-resolution magic angle spinning
HUVECs	Human umbilical vein endothelial cells
INC	Internetwork cross-linking
KPS	Potassium perfulfate
MA	Methyl acrylate
MBAAm	*N*,*N′*-Methylenebisacrylamide
MeOH	Methanol
MHA	Methacrylated hyaluronan
M_n	Number-average molecular weight
MSCs	Mouse mesenchymal stem cells
M_w	Weight-average molecular weight
MW	Molecular weight
$M_{w,micelle}$	Molecular weight of micelle
N_{agg}	Aggregation number
NaSS	Sodium 4-styrenesulfonate
NC	Nanocomposite
NIPAAm	*N*-Isopropylacrylamide
NMR	Nuclear magnetic resonance
ODEX	Partially oxidized dextran
OXG	2-Oxoglutaric acid
PAAc	Poly(acrylic acid)
PAAm	Polyacrylamide
PAMPS	Poly(2-acrylamido-2-methyl-1-propanesulfonic acid)
PBS	Phosphate-buffered saline
PC	Physically cross-linked
PDH	*O*,*O′*-1,3-Propanediylbishydroxylamine dihydrochloride
PDMAAm	Poly(*N*,*N*-dimethylacrylamide)

PEDOT	Poly(3,4-ethylenedioxythiophene)
PEG	Poly(ethylene glycol)
PEG DMPA	Poly(ethylene glycol) bis[2-(dodecylthiocarbonothioylthio)-2-methylpropionate]
PEGDA	Poly(ethylene glycol) diacrylate
PEGDMA	Poly(ethylene glycol) dimethacrylate
PEGMA	Poly(ethylene glycol) methyl ether methacrylate
PHEA	Poly(2-hydroxyethyl acrylate)
PMA	Poly(methyl acrylate)
PMHA	Poly(methacrylated hyaluronan)
PMMA	Poly(methyl methacrylate)
PNaSS	Poly(sodium 4-styrenesulfonate)
PPEGMA	Poly[poly(ethylene glycol) methyl ether methacrylate]
PSAMPS	Poly(2-acrylamido-2-methyl-1-propanesulfonic acid sodium salt)
PSAPS	Poly(sodium 3-sulfopropyl acrylate)
PSS	Poly(styrene sulphonic acid)
PSty	Polystyrene
PVA	Poly(vinyl alcohol)
QN	Quadruple network
RAFT	Reversible addition-fragmentation chain transfer
R_g	Radius of gyration
RGD	Arginine-glycine-aspartic acid
R_h	Hydrodynamic radius
$R_{max}^{micelle}$	Maximum radius for micelles
R_{min}^{unimer}	Minimum radius for unimers
RSTFCs	Rabbit synovial tissue-derived fibroblast cells
S	Shear modulus
SAMPS	2-Acrylamido-2-methyl-1-propanesulfonic acid sodium salt
SANS	Small-angle neutron scattering
SDS	Sodium dodecyl sulfate
SLD	Scattering length density
SN	Single network
SR	Slide ring
TAPEG	Tetra-amine-terminated four-arm poly(ethylene glycol)
TEA	Triethylamine
TEMED	*N*,*N*,*N*′,*N*′-tetramethylethylenediamine
TFA	Trifluoroacetic acid
T_g	Glass transition temperature
THF	Tetrahydrofuran

T_m	Melting temperature
TN	Triple network
TNPEG	Tetra-ester-terminated four-arm poly(ethylene glycol)
TPEG	Four-arm poly(ethylene glycol)
UV/Vis	Ultraviolet/visible
VA-044	2,2′-Azobis[2-(2-imidazolin-2-yl)propane] dihydrochloride
ε_{max}	Fracture strain
σ_{max}	Fracture stress
5×N	Quintuple network

LIST OF TABLES

LIST OF FIGURES

pH 4.5, and (b) $DMAAm_{100}$-*co*-$DAAm_{10}$ cross-linked using PDH and prepared at the stoichiometric ratio at total solids concentrations of (b) 10.0, (c) 12.5, and (d) 15.0% w/v in aqueous buffer solutions of pH 4.5.

Figure 3.7.8. Evolution of *G′* and *G″* during the formation of the oxime cross-linked APCNs based on $DAAm_6$-*b*-$DMAAm_{50}$-*b*-EG_{46}-*b*-$DMAAm_{50}$-*b*-$DAAm_6$ cross-linked using PDH prepared at total solids concentrations of (a) 10.0, (b) 12.5, and (c) 15.0% w/v at the stoichiometric ratio in aqueous buffer solutions of pH 4.5.

Figure 3.7.9. Evolution of *G′* and *G″* during the formation of the oxime cross-linked APCNs based on (a) the $DAAm_3$-*b*-$DMAAm_{50}$-*b*-EG_{46}-*b*-$DMAAm_{50}$-*b*-$DAAm_3$ and (b) the $DAAm_{12}$-*b*-$DMAAm_{50}$-*b*-EG_{46}-*b*-$DMAAm_{50}$-*b*-$DAAm_{12}$ pentablock terpolymers cross-linked using PDH and prepared in aqueous buffer solutions of pH 4.5 at the stoichiometric ratio at a total solids concentration of 15.0% w/v.

Figure 3.7.10. Dependence of *G′* and *G″* on the angular frequency of the randomly cross-linked copolymer networks cross-linked via oxime bonds formed using PDH and (a) $DMAAm_{100}$-*co*-$DAAm_5$, and (b) $DMAAm_{100}$-*co*-$DAAm_{10}$ prepared at the stoichiometric ratio at a total solids concentration of 15.0% in aqueous buffer solutions of pH 4.5. The experiments were performed at a 10% strain.

Figure 3.7.11. Dependence of *G′* and *G″* on the angular frequency of the oxime cross-linked APCNs based on (a) the $DAAm_6$-*b*-$DMAAm_{50}$-*b*-EG_{46}-*b*-$DMAAm_{50}$-*b*-$DAAm_6$ and (b) the $DAAm_{25}$-*b*-$DMAAm_{50}$-*b*-EG_{46}-*b*-$DMAAm_{50}$-*b*-$DAAm_{25}$ pentablock terpolymers. The gels were prepared at the stoichiometric ratio at a total solids concentration of 15.0% in an aqueous buffer solution of pH 4.5 and in an EtOH : buffer solution of pH 4.5 at a volume ratio of 1:2, respectively. Both experiments were performed at a 10% strain.

Figure 3.7.12. Dependence of *G′* and *G″* on the angular frequency of the oxime cross-linked APCN prepared from the reaction of the $DAAm_{25}$-*b*-$DMAAm_{50}$-*b*-EG_{46}-*b*-$DMAAm_{50}$-*b*-$DAAm_{25}$ pentablock terpolymer and PDH. The gel was prepared at a total solids concentration of 15.0% at the stoichiometric ratio in an EtOH : buffer solution of pH 4.5 at a volume ratio of 1:2, and it was then equilibrated in an aqueous buffer solution of pH 7.4. The experiment was performed at a 10%

strain.

Figure 3.7.13. Effect of the DAAm content in the linear polymer precursors on the equilibrium aqueous degrees of swelling (aqueous buffer solution of pH 7.4) of the oxime cross-linked polymer networks. The gels were initially formed at the stoichiometric ratio at a total solids concentration of 15.0% w/v in an aqueous buffer solution of pH 4.5 or in an EtOH : buffer solution of pH 4.5 mixture at a 1:2 volume ratio.

Figure 3.7.14. Compressive stress-strain curves for the oxime cross-linked polymer networks formed from PDH and (a) the $DMAAm_{100}$-*co*-$DAAm_{10}$ random copolymer, (b) the $DAAm_{6}$-*b*-$DMAAm_{50}$-*b*-EG_{46}-*b*-$DMAAm_{50}$-*b*-$DAAm_{6}$ pentablock terpolymer (total solids concentration = 15% w/v, aqueous buffer solution of pH 4.5), and (c) the $DAAm_{25}$-*b*-$DMAAm_{50}$-*b*-EG_{46}-*b*-$DMAAm_{50}$-*b*-$DAAm_{25}$ pentablock terpolymer (total solids concentration = 15% w/v, EtOH : buffer solution of pH 4.5 mixture of a 1:2 volume ratio and equilibrium swollen in a buffer solution of pH 7.4).

Figure 3.8.1. Procedure followed for the synthesis of the linear amphiphilic ABCBA pentablock terpolymers and the final ABCDCBA heptablock quaterpolymers, which were subsequently used for the preparation of the oxime cross-linked APCNs.

Figure 3.8.2. GPC traces of (a) the $DMAAm_{50}$-*b*-EG_{46}-*b*-$DMAAm_{50}$ triblock copolymer precursor and the $DDAAm_{x}$-*b*-$DMAAm_{50}$-*b*-EG_{46}-*b*-$DMAAm_{50}$-*b*-$DDAAm_{x}$ pentablock terpolymers and (b) the final $DAAm_{y}$-*b*-$DDAAm_{x}$-*b*-$DMAAm_{50}$-*b*-EG_{46}-*b*-$DMAAm_{50}$-*b*-$DDAAm_{x}$-*b*-$DAAm_{y}$ heptablock quaterpolymers.

Figure 3.8.3. ^{1}H NMR spectra in $CDCl_3$ of (a) the $DMAAm_{50}$-*b*-EG_{46}-*b*-$DMAAm_{50}$ triblock copolymer precursor, (b) the $DDAAm_{12}$-*b*-$DMAAm_{50}$-*b*-EG_{46}-*b*-$DMAAm_{50}$-*b*-$DDAAm_{12}$ pentablock terpolymer and (c) the $DAAm_{14}$-*b*-$DDAAm_{12}$-*b*-$DMAAm_{50}$-*b*-EG_{46}-*b*-$DMAAm_{50}$-*b*-$DDAAm_{12}$-*b*-$DAAm_{14}$ heptablock quaterpolymer.

Figure 3.8.4. Effect of the volume ratio of ethanol : aqueous buffer solution mixture on the gel formation time of the oxime cross-linked APCNs based on PDH and the (a) $DAAm_{10}$-*b*-$DDAAm_{9}$-*b*-$DMAAm_{50}$-*b*-EG_{46}-*b*-$DMAAm_{50}$-*b*-$DDAAm_{9}$-*b*-$DAAm_{10}$ and (b) $DAAm_{12}$-*b*-$DDAAm_{17}$-*b*-$DMAAm_{50}$-*b*-EG_{46}-*b*-$DMAAm_{50}$-*b*-$DDAAm_{17}$-*b*-$DAAm_{12}$ heptablock quaterpolymers. The reactions were performed at the stoichiometric

ratio at a total solids concentration of 15% w/v in a mixture of EtOH and an aqueous buffer solution of pH 4.5 at a final buffer concentration of 200 mM.

Figure 3.8.5. Dependence of the minimum volume ratio of ethanol to the aqueous buffer solution in their mixture on the DDAAm content in the linear amphiphilic heptablock quaterpolymers required for complete polymer solubility. The reactions were performed at the stoichiometric ratio at a total solids concentration of 15% w/v in an EtOH : aqueous buffer solution of pH 4.5 at a final buffer concentration of 200 mM.

Figure 3.8.6. Effect of (a) DDAAm content and (b) DAAm content in the heptablock quaterpolymers on the gel formation time of the oxime cross-linked APCNs. The reactions were performed at the stoichiometric ratio in a solvent mixture containing the minimum volume fraction of ethanol (to ascertain polymer solubility; different for each polymer) and an aqueous buffer solution of pH 4.5 at a final buffer concentration in the mixture of 200 mM.

Figure 3.8.7. Effect of total solids concentration on the gel formation time of the oxime cross-linked APCNs. The reactions were performed at the stoichiometric ratio in mixtures of EtOH and aqueous buffer solution of pH 4.5 at a final buffer concentration in the mixtures of 200 mM.

Figure 3.8.8. Dependence of G' and G'' on the angular frequency of the oxime cross-linked APCNs based on PDH and (a) the $DAAm_{14}$-*b*-$DDAAm_{12}$-*b*-$DMAAm_{50}$-*b*-EG_{46}-*b*-$DMAAm_{50}$-*b*-$DDAAm_{12}$-*b*-$DAAm_{14}$, (b) the $DAAm_{12}$-*b*-$DDAAm_{17}$-*b*-$DMAAm_{50}$-*b*-EG_{46}-*b*-$DMAAm_{50}$-*b*-$DDAAm_{17}$-*b*-$DAAm_{12}$, and (c) the $DAAm_{14}$-*b*-$DDAAm_{22}$-*b*-$DMAAm_{50}$-*b*-EG_{46}-*b*-$DMAAm_{50}$-*b*-$DDAAm_{22}$-*b*-$DAAm_{14}$ heptablock quaterpolymers, prepared at the stoichiometric ratio at a total solids concentration of 15% in EtOH : aqueous buffer solution of pH 4.5 mixtures of different volume ratios. The measurements were performed at a 10% strain.

Figure 3.8.9. Effect of the DDAAm content on the equilibrium degrees of swelling of the prepared oxime cross-linked APCNs. The polymer networks were formed in mixtures of EtOH and aqueous buffer solution of pH 4.5 of different volume ratios.

Figure 3.8.10. Compressive stress-strain curves for the oxime cross-linked APCNs formed using PDH and (a) the $DAAm_{16}$-*b*-$DMAAm_{50}$-*b*-EG_{46}-*b*-

$DMAAm_{50}$-*b*-$DAAm_{16}$ pentablock terpolymer, (b) the $DAAm_{14}$-*b*-$DDAAm_{12}$-*b*-$DMAAm_{50}$-*b*-EG_{46}-*b*-$DMAAm_{50}$-*b*-$DDAAm_{12}$-*b*-$DAAm_{14}$, (c) the $DAAm_{12}$-*b*-$DDAAm_{17}$-*b*-$DMAAm_{50}$-*b*-EG_{46}-*b*-$DMAAm_{50}$-*b*-$DDAAm_{17}$-*b*-$DAAm_{12}$, and (d) the $DAAm_{14}$-*b*-$DDAAm_{22}$-*b*-$DMAAm_{50}$-*b*-EG_{46}-*b*-$DMAAm_{50}$-*b*-$DDAAm_{22}$-*b*-$DAAm_{14}$ heptablock quaterpolymers. The APCNs were prepared at the stoichiometric ratio at a total solids concentration of 20.0% w/v in DMF in the presence of 10.0% v/v aniline, and then swollen in water.

Figure 3.8.11. Dependence of (a) the fracture stress and (b) the fracture strain on the DDAAm content in the oxime cross-linked APCNs.

TABLE OF CONTENTS

CHAPTER 1: THEORETICAL SECTION

1.1 Introduction, Goal and Innovation

The aim of this PhD Thesis is the contribution towards the improvement of the mechanical properties of polymeric hydrogels which are infamously fragile. This was done through the design, preparation and characterization of polymer networks possessing enhanced mechanical properties. In particular, three types of polymer networks were prepared. The first type consisted either of multiply interpenetrated hydrophilic polymer network hydrogels up to 5-fold, or of degradable hydrophilic double-network hydrogels. The second type was based on the introduction of a hydrophobic monomer to hydrophilic polymer network hydrogels for the preparation of amphiphilic polymer networks, which were either randomly cross-linked, or well-defined, prepared through the end-linking of linear amphiphilic multiblock copolymers. Finally, the third type of polymer networks were well-defined amphiphilic polymer conetworks also prepared through the end-linking of linear amphiphilic multiblock copolymers, but, using dynamic covalent bonds as cross-links.

Polymer network hydrogels are soft and wet materials capable of absorbing large quantities of water. The high water content in the hydrogels endows them with poor mechanical performance, thereby, limiting their applications. In the last two decades, numerous studies on the mechanical reinforcement of conventional chemically cross-linked polymer network hydrogels have been reported. Amongst the suggested structures, double-network (DN) hydrogels, consisting of two interpenetrated polymer networks with opposite physical properties (a highly cross-linked ionic first polymer network and a loosely cross-linked nonionic second polymer network), exhibited extraordinary mechanical strength and toughness in compression and tensile experiments. However, the applications of the DN hydrogels are relatively limited due the presence of ionic charges in the first network, which are sometimes undesired for particular applications. Recently, triple network (TN) hydrogels based on solely nonionic components were reported, which also exhibited enhanced mechanical properties in compression experiments. More recently, the preparation of quadruple network (QN) hydrogels was reported, which also consisted only

of nonionic components, and these hydrogels exhibited high fracture stretch ratios and high fracture stress values in tensile experiments.

The first specific goal in this Thesis is to extend the concept of double and triple networks by preparing multiple network hydrogels of up to five polymer networks based also on nonionic components (*N*,*N*-dimethylacrylamide (DMAAm) monomer and *N*,*N*′-methylenebisacrylamide (MBAAm) cross-linker). In addition to the variation of network multiplicity, monomer concentration in the polymer networks was also systematically varied. The dependence of the degrees of swelling and mechanical properties on network multiplicity and monomer concentration in the multiple network hydrogels was investigated. Some particular multiple network hydrogels, the ones with the lowest monomer concentration, were also characterized in terms of their hardness using nanoindentation, which allowed for the determination of hardness, elastic modulus, and percentage of recoverable energy.

In addition to the preparation of multiple network hydrogels with enhanced mechanical performance, a second specific goal in this study is to investigate the structure of the DN hydrogels in terms of the degree of interconnection between the first and the second polymer networks. Previous studies have shown that the superior mechanical properties of the DN hydrogels are partially attributed to the presence of covalent junctions between the two interpenetrating polymer networks, and particularly in the case of DN hydrogels containing a second, linear, non cross-linked polymeric component rather than a second cross-linked polymer network. These junctions are created from the grafting of linear polymer chains of the second polymer component onto the unreacted double bonds of the cross-linker in the first network, as a certain percentage of double bonds remain active after the synthesis of the first network. To achieve our goal and determine the degree of interconnection between the two polymer networks, partially degradable DN hydrogels were prepared using combinations of degradable and non-degradable cross-linkers. The resulting DN hydrogels were subjected to degradation, and the masses of the remaining gel fraction and soluble fraction were used to determine the degree of interconnection. To our knowledge, the quantitative determination of the grafting percentage in DN hydrogels was yet to be reported.

The second general aim of this study is to introduce a hydrophobic monomer, and, in particular, *N*-dodecylacrylamide (DDAAm), in the hydrophilic polymer network hydrogels for the preparation of amphiphilic polymer networks, and their characterization in terms of their degrees of swelling and mechanical properties. The DDAAm monomer was chosen as the hydrophobic comonomer, as it contains a dodecyl group in the pendant, thereby being capable of establishing hydrophobic associations among the side groups that can contribute to the improvement of the mechanical performance of the produced polymer networks. In addition, owing to its relatively large length, the dodecyl side group exhibits a melting point at the moderate temperature of 55-57 ^{o}C, conferring upon the materials containing it thermoreversible transition behavior, and, possibly, shape-memory.

To this end, randomly cross-linked copolymer networks of various compositions consisting of the hydrophilic DMAAm and the hydrophobic DDAAm monomers were prepared using conventional free radical photopolymerization. To our knowledge, this is the first example of the preparation of randomly cross-linked copolymer networks using this particular combination of monomers. In addition to the variation of the composition of the randomly cross-linked copolymer networks, the cross-linking density was also varied. All the obtained gels were characterized in terms of their degrees of swelling in various solvents and mechanical properties in water, in order to elucidate the dependence of these properties on their composition and cross-linking density. Finally, the water-swollen randomly cross-linked copolymer networks were evaluated in terms of their shape-memory behavior.

The second specific goal of the preparation of amphiphilic polymer networks is the preparation of well-defined amphiphilic polymer conetworks (APCNs) consisting of the hydrophilic DMAAm and the hydrophobic DDAAm monomers using the controlled polymerization method reversible addition-fragmentation chain transfer (RAFT) polymerization. To our knowledge, this is also the first example of the preparation of APCNs based on these particular monomers. The APCNs comprise covalently interconnected hydrophilic and hydrophobic segments, and, upon their swelling in water, hydrophobic associations are established among the hydrophobic segments leading to microphase separation, in addition to low values of degrees of swelling and high polymer volume fractions, resulting in increased mechanical performance. Furthermore, due to the presence of hydrophobic associations, crystalline domains are formed which act as

physical/reversible cross-links, and, consequently, provide an additional energy dissipation mechanism, rendering the gels mechanically stronger.

However, prior to the preparation of the APCNs, the corresponding linear amphiphilic diblock copolymer counterparts were synthesized and characterized. To our knowledge, this is the second example in the literature concerning the preparation of diblock copolymers based on the hydrophobic DDAAm monomer using a controlled polymerization method. Two series of amphiphilic diblock copolymers were prepared, $DMAAm_x$-*b*-$DDAAm_y$ and $DDAAm_x$-*b*-$DMAAm_y$, in which the degree of polymerization of the first block was kept constant, while the degree of polymerization of the second block was systematically varied. Then, the amphiphilic diblock copolymers were characterized in terms of their self-assembly in water using dynamic light scattering (DLS) and small-angle neutron scattering (SANS), while atomic force microscopy (AFM) was employed for the investigation of their morphology. From these measurements, the dependence of the hydrodynamic radius (R_h) and radius of gyration (R_g) on molecular weight, composition, and block sequence in the diblock copolymers was elucidated.

Subsequently, the preparation of the well-defined APCNs was performed. Initially, linear amphiphilic pentablock terpolymers with a range of compositions consisting of DMAAm and DDAAm monomers were synthesized, using RAFT polymerization. These linear precursors, similarly to the amphiphilic diblock copolymers, were also characterized using DLS and SANS to investigate their self-assembly in water. Then, the well-defined APCNs were prepared through the end-linking of the linear precursors. The thus-prepared APCNs were characterized in terms of their degrees of swelling in various solvents and mechanical properties in water, in order to investigate the effect of composition on these parameters.

The final general goal of the amphiphilic polymer networks is the preparation of well-defined APCNs by the end-linking of amphiphilic pentablock terpolymers and amphiphilic heptablock quaterpolymers using reversible covalent oxime bonds. In order to achieve the end-linking of the linear precursors through oxime bonds, the hydrophobic diacetone acrylamide (DAAm) monomer, bearing a ketone group in the pendant, was incorporated in the end-blocks of the linear precursors, while the cross-linking was accomplished through the reaction of the linear precursors with a difunctional *O*-alkoxyamine. To our knowledge,

this is the first example concerning the preparation of well-defined APCNs cross-linked via oxime bonds. The dependence of the degrees of swelling in various solvents and mechanical properties in water on the composition of the oxime cross-linked APCNs was investigated. Finally, the self-healing ability and the gel-to-sol transition of the oxime cross-linked APCNs were evaluated.

1.2 Literature Review

1.2.1 Polymers and Polymer Networks

1.2.1.1 Amphiphilic Block Copolymers

Amphiphilic block copolymers represent an important class of polymers possessing unique characteristics. They comprise segments of hydrophilic and hydrophobic monomer repeating units conferring upon them self-organization in selective solvents with the formation of a variety of morphologies including spherical and cylindrical micelles, vesicles, rods and lamellae.[1-8] When the selective solvent is water, only the hydrophilic segments are solvated, while the hydrophobic segments avoid contact with water. Hence, the inner part of these morphologies comprises hydrophobic repeating units, while the outer part consists of hydrophilic repeating units, as shown in Figure 1.2.1. To date, amphiphilic block copolymers are used as materials for a large spectrum of applications, including drug delivery, environmental remediation, food processing, coatings, detergents, and personal care products.[1,2,6]

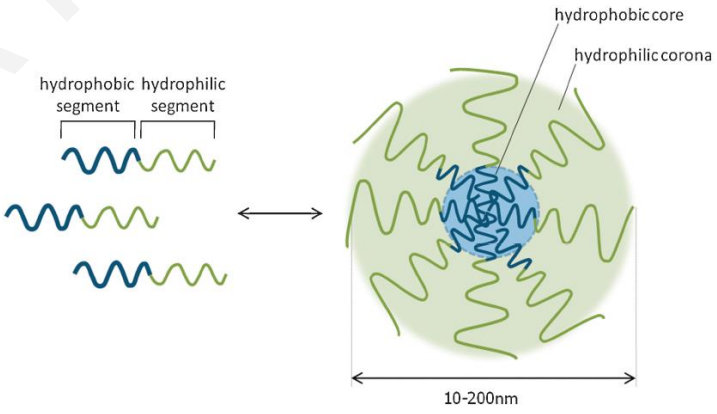

Figure 1.2.1. Schematic representation of the micelle structure, consisting of a hydrophobic core and a hydrophilic corona, formed upon the self-assembly of a diblock copolymer in water, a selective solvent for the hydrophilic segment.[4]

Amphiphilic block copolymers are usually prepared using controlled/living polymerization methods, such as RAFT polymerization, atom transfer radical polymerization (ATRP) and group transfer polymerization (GTP). In all these procedures, the block copolymers are obtained in several steps depending on the number of the constituent blocks, while a great variety of monomers have been used. Such monomers include acrylates and methacrylates monomers, whereas acrylamides and methacrylamides have been employed much less.

1.2.1.2 Hydrogels and Amphiphilic Polymer Conetworks

Polymer network hydrogels consist of cross-linked hydrophilic polymers capable of absorbing large quantities of water (up to 99%), without dissolving, thereby possessing a hybrid nature with both solid-like and liquid-like characteristics.[9] The high-water content endows hydrogels with biocompatibility, which, together with their solid-like nature, renders polymeric hydrogels the appropriate materials for use in biomedicine and technology. Applications in the biomedical field include drug delivery, tissue engineering, and soft contact lenses, whereas technological applications concern water retention in agriculture, urine and blood retention in baby and hygienic diapers, actuation, and sensing.[10-13] However, these applications are often limited by the poor mechanical properties of hydrogels, arising from their high-water content. Conventional chemically cross-linked hydrogels usually exhibit low modulus and fragile/brittle behavior owing to the easy crack formation and rapid crack propagation that takes place from low strain. In contrast, due to the absence of solvent, bulk elastomers possess an increased resistance to crack formation and propagation through viscoelastic and crystallization/melting energy dissipation mechanisms.

Another type of polymer networks with unique features are APCNs,[14-16] comprising covalently interconnected hydrophilic and hydrophobic segments, in contrast to the conventional polymer network hydrogels which comprise solely hydrophilic components. This constitution confers upon APCNs the ability to absorb both organic solvents and water, with the amount of water absorbed being lower than that absorbed by simple hydrogels, due to the presence of the hydrophobic segments in APCNs.

APCNs in water exhibit superior mechanical properties compared to conventional hydrogels which are infamously fragile. This is due to the lower water content in APCNs (resulting in higher concentration of elastic chains), and also to the formation of hydrophobic associations among the hydrophobic segments leading to the formation of hydrophobic cores. These hydrophobic associations reversibly deform or even dissociate upon the application of strain, thereby offering an important mechanism for the dissipation of mechanical energy.

1.2.2 Network Structures with Improved Mechanical Properties

The conventional chemically cross-linked hydrogels possess poor mechanical properties arising from their high-water content, limiting the application potential of these hydrogels. The toughening of polymeric hydrogels has always been a challenge for the scientific community. This challenge has been addressed relatively recently with the development of a great variety of new hydrogel structures with enhanced mechanical strength, including the topological/slide ring (SR) gels,[17] nanocomposite (NC) gels,[18] DN hydrogels,[19-21] TN hydrogels,[22-36] and QN hydrogels.[37-38] From these hydrogel structures, the hydrogels consisting of two or more polymer networks stand out for their ease of preparation and excellent mechanical properties, which can be tuned by the number of networks, monomer type, concentration of monomer, cross-linking density in the first network, and cross-linking density in the higher networks.

1.2.2.1 Double-Network (DN) Hydrogels

The preparation of DN hydrogels was reported in 2003 by Gong, Osada and co-workers.[19] DN hydrogels are based on two interpenetrating polymeric hydrogels with large differences in their mechanical properties, cross-linking density, and electric charge. In particular, the first network is brittle, consisting of a relatively highly cross-linked polyelectrolyte network of poly(2-acrylamido-2-methyl-1-propanesulfonic acid) (PAMPS), containing 4 mol%, relative to the 2-acrylamido-2-methyl-1-propanesulfonic acid (AMPS) monomer of MBAAm cross-linker, while the second network is ductile, based on a relatively loosely cross-linked polyacrylamide (PAAm) nonionic network, containing 0.1 mol% MBAAm cross-linker relative to the monomer. These DN hydrogels are prepared in two steps. In the first step, the PAMPS single network (SN) is prepared. In the second step,

this SN hydrogel is allowed to reach swelling equilibrium in an aqueous solution of 2 M acrylamide (AAm) monomer, containing MBAAm cross-linker and 2-oxoglutaric acid (OXG) photoinitiator, followed by the subsequent photopolymerization of the AAm-MBAAm solution absorbed within the PAMPS first network, resulting in the formation of the second network and the final DN composite network. After their preparation, the mechanical properties of the SN and the DN hydrogels are evaluated using compression experiments. The PAMPS/PAAm DN hydrogels exhibit extraordinary mechanical performance in comparison with the PAAm and PAMPS SN hydrogels, and, in particular, values of compressive fracture stress, σ_{max}, of 17.2 MPa, compressive fracture strain, ε_{max}, of 92%, and compressive fracture energy of up to ~300 J m^{-2}, despite their high water content (~90% w/w).[19] Furthermore, decreasing the MBAAm cross-linker concentration in the second PAAm network leads to further enhancement of the mechanical properties of the DN hydrogels. The greater enhancement is observed when the second network consists of linear, uncross-linked PAAm chains, with the obtained DN hydrogels exhibiting values of fracture energy, G, of up to 1000 J m^{-2}.[20] Figure 1.2.2 illustrates the structure of the two different polymer networks in the DN hydrogel (part (a)), and a photograph of a tough DN hydrogel containing 90% w/w water (part (b)).

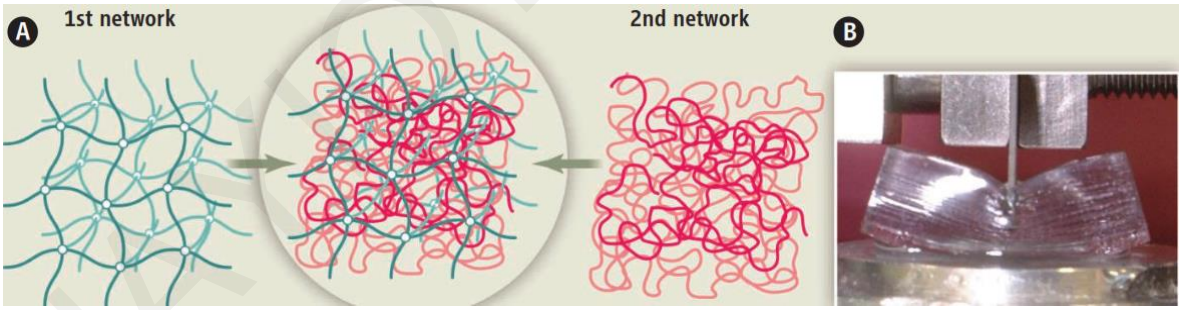

Figure 1.2.2. (A) Schematic presentation of a DN hydrogel prepared from the combination of two different polymer networks. (B) Photograph of a tough DN hydrogel containing 90% w/w water.[21]

1.2.2.2 Triple Network (TN) Hydrogels

Table 1.1 summarizes the composition and mechanical properties of the TN hydrogels reported in the literature. Many of these TN hydrogels comprise DN hydrogels plus a third polymer network. In several cases, the afore-mentioned DN hydrogel is the classical PAMPS/PAAm DN hydrogel developed by Gong, Osada and co-workers.[19-21] In some cases, the third component is not a polymer network, but rather a linear (not cross-linked)

polymer, or some other polymer architecture, such as a polymeric microgel. This non-cross-linked polymer entity may be the first, the second, or the third component of the TN hydrogels. Thus, the presented TN hydrogels may not necessarily comprise three polymer networks, but just two, with the third component being physically entrapped within the overall network structure.

The three first columns in the table contain the polymer components of the TN hydrogels, and, in particular, the names of the monomers or polymers used and their concentration, as well as the name and the concentration of the cross-linker. The chemical structures and names of the monomers employed in the preparation of the TN hydrogels are presented in Table 1.2. In some cases, the TN hydrogels were cross-linked through physical interactions, hence these examples will be referred to as "physically cross-linked" (PC). The following columns contain the type of mechanical testing, whether compressive or tensile, and the mechanical properties of the SN, DN and TN hydrogels, and, in particular, the fracture stress (σ_{max}, in MPa), fracture strain (ε_{max}, in %), and Young's modulus (E, also in MPa).

Table 1.1. Summary of all prepared triple network (TN) hydrogels and their mechanical properties, fracture stress (σ_{max}), fracture strain (ε_{max}), and Young's modulus (E), in comparison with the mechanical properties of their SN and DN precursors.

Gel Components			**Method**	**Mechanical Properties of SN**			**Mechanical Properties of DN**			**Mechanical Properties of TN**			**Ref**
1st Network	**2nd Network**	**3rd Network**		σ_{max} **(MPa)**	ε_{max} **(%)**	E **(MPa)**	σ_{max} **(MPa)**	ε_{max} **(%)**	E **(MPa)**	σ_{max} **(MPa)**	ε_{max} **(%)**	E **(MPa)**	
(a) Simple Triple Networks													
PAMPS-1 MBAAm-8	PAAm-2-MBAAm-0.1	PAMPS-1 MBAAm-0.1	Compression	-	-	-	4.60	65	0.84	4.80	57	2.00	**22**
		PAMPS-1 MBAAm-0								9.20	70	2.10	
PSAMPS-1 MBAAm-4	PDMAAm-3 MBAAm-0.1	PSAMPS-*co*-PDMAAm (F=0.5)-1-MBAAm-0	Compression	0.26	57	0.19	-	-	-	3.00	71	0.32	**23**
		PSAMPS-*co*-PDMAAm (F=0.5)-1-MBAAm-2					-	-	-	2.31	65	0.65	
		PSAMPS-*co*-PDMAAm (F=0.5)-1 MBAAm-4					-	-	-	1.36	47	0.88	
Odex	Teleostean	CEC	-	-	-	-	-	-	-	-	-	-	**24, 25**
PAAm-1.40 PEGDMA-4	PAAm-0.7-7.0 MBAAm-0	PAAm-0.7-7.0 MBAAm 0	Compression	0.15	70	-	9.20	95	-	25.00	99	0.10	**26**
PDMAAm-1 PEGDMA-4-10	PDMAAm-0.5-5.0 MBAAm-0	PDMAAm-0.5-5.0 MBAAm-0	Compression	0.17	47	-	-	-	-	26.10	95	2.00	

EA-5 BDA-1.45	EA-9.4 BDA-0.01	EA-9.4 BDA-0.01	Tension	1.20	-	0.60	10.00	260	0.80	16.00	220	1.50	**27**
EA-5 BDA-1.45	MA-11 BDA-0.01	MA-11 BDA-0.01		0.50	-	0.80	8.00	240	1.30	22.00	260	2.20	
EA-5 BDA-2.81				0.50	-	1.50	6.50	190	2.00	29.00	190	4.20	
EA-5 BDA-5.81				0.50	-	2.30	3.00	160	2.30	-	-	-	
MHA (20 g L^{-1})	DMAAm-3 MBAAm-0.05	DMAAm-3 MBAAm-0.05	Compression	0.05	40	0.017	12.00	93	0.37	22.00	96	0.40	**28**
M_i-x_i, C_i -y_i: M_i, x_i, C_i, and y_i state the abbreviation of the polymer's name, the molar concentration of monomer, the abbreviation of the cross-linker's name, and the cross-linker loading feed in mol% with respect to the monomer, respectively. **P.C.:** physically cross-linked.													
(b) Triple Networks with a 1st Polymer Network Based on Microgels													
PSAMPS-1 MBAAm-4	PAAm-2 MBAAm-0.01	PAAm-4 MBAAm-0.01	Tension	-	-	-	0.15	130	0.05	2.46	1270	0.22	**29, 30**
PAAm-1- MBAAm-4				-	-	-	0.41	1010	0.03	1.37	910	0.05	**30**
PDMAPAA-Q-1 MBAAm-4				-	-	-	-	-	-	0.94	970	0.15	
PNaSS-*co*-PDMAEA-Q (F=0.5)-1- MBAAm-4				-	-	-	-	-	-	0.75	530	0.07	
PSAMPS+ PDMAPAA-Q (F=0.5)-1 MBAAm-4				-	-	-	-	-	-	0.51	410	0.07	

(c) Triple Networks with a Linear Polyelectrolyte Stent as the 2nd Polymeric Component													
PAAm-1.2 MBAAm-4	PAMPS-1 MBAAm-0	PAAm-2 MBAAm-0.02	Tension	-	-	-	-	-	-	0.83	1000	-	
PDMAAm-0.7 MBAAm-3				-	-	-	-	-	-	1.95	-	-	
PDMAAm-1 MBAAm-2				-	-	-	-	-	-	1.57	-	-	
PNIPAAm-0.7 MBAAm-2				-	-	-	-	-	-	1.02	-	-	
PAAc-1 MBAAm-4	PAMPS-0.7 MBAAm-0	PAAm-2 MBAAm-0.02	Tension	-	-	-	-	-	0.067	0.70	-	-	**31**
PAAm-1 MBAAm-4				0.031	-	-	-	-	0.15	0.69	-	-	
PHEA-1 MBAAm-4				0.037	-	0.054	-	-	-	0.82	-	-	
	PNaSS-1 MBAAm-0						-	-	-	0.34	-	-	
	PDMAPAA-Q-1 MBAAm-0						-	-	-	0.47	-	-	
	PDMAEA-1 MBAAm-0						-	-	-	0.47	-	-	
PTPEG-2×10^{-5}	PAMPS-0.6 MBAAm-0		Tension	-	-	-	0.20	600	-	2	2200	-	**32**
	PAMPS-1.0 MBAAm-0									-	-	-	

(d) Triple Networks with a Mold Used in the 1st Polymeric Component													
PVA-P.C.	PAMPS-1 MBAAm-4	PAAm-2-MBAAm-0	Tension	-	-	-	0.30	300	-	0.80	900	-	**33**
(e) Triple Networks Containing an Electrically Conducting Polymer in the 3rd Component													
PAAc-1.5 MBAAm-6	PAAc-6 MBAAm-0.1	PEDOT (0.48 M)-PNaSS (0.10 M) P.C.	Tension	0.10	37	-	0.60	61	-	1.00	68	-	**34**
		PEDOT-PNaSS (No. 2) - P.C.								1.10	70	-	
		PEDOT-PNaSS (No. 3) - P.C.								1.30	72	-	
		PEDOT-PNaSS (No. 4) - P.C.					0.60	61	-	1.60	73	-	
		PEDOT-NaSS (No. 5) - P.C.								1.80	78	-	
PAMPS-1 MBAAm-4	PAAm-2 MBAAm-0.1	PEDOT (No. 1)	Tension	-	-	-	1.19	134	0.37	1.38	154	0.33	**35**
		PEDOT (No. 2)								2.07	235	0.56	
PNaSS-1 MBAAm-10	PDMAAm-1.5 MBAAm-0	PEDOT	Compression	-	-	-	0.39	45	0.71	1.27	45	3.48	**36**
	PDMAAm-2.0 MBAAm-0						1.08	81	0.95	1.98	76	2.97	
PPEGMA-0.18 MBAAm-4	PAAc-2.78 MBAAm-0.1	PEDOT (0.46 M) + NaPSS (0.48 M) P.C.	Tension	-	-	-	0.48	340	0.40	0.60	240	0.11	**37**
			Compression				8.50	81	-	11.60	78	-	

Table 1.2. Chemical structures and names of monomers and polymers employed in the preparation of the TN hydrogels.

Chemical Structure	Name
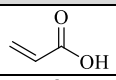	**AAc**, Acrylic acid
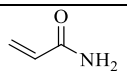	**AAm**, Acrylamide
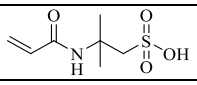	**AMPS**, 2-Acrylamido-2-methyl-1-propanesulfonic acid
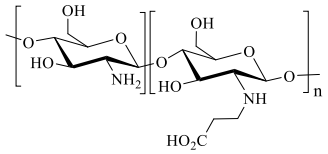	**CEC**, *N*-Carboxyethyl chitosan
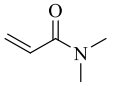	**DMAAm**, *N*,*N*-Dimethylacrylamide
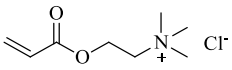	**DMAEA-Q**, 2-(Trimethylamino)ethyl acrylate, chloride quaternary salt
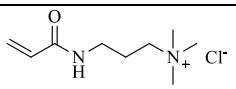	**DMAPAA-Q**, 3-(Acrylamidopropyl)trimethylammonium chloride
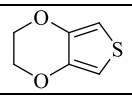	**EDOT**, 3,4-Ethylenedioxythiophene
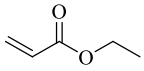	**EA**, Ethyl acrylate
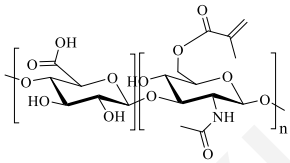	**MHA**, Methacrylated hyaluronan
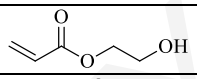	**HEA**, 2-Hydroxyethyl acrylate
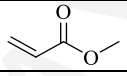	**MA**, Methyl acrylate
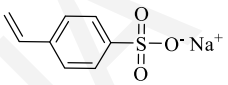	**NaSS**, Sodium 4-styrenesulfonate
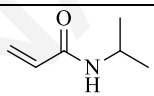	**NIPAAm**, *N*-Isopropylacrylamide
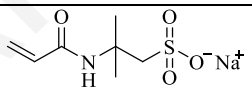	**SAMPS**, 2-Acrylamido-2-methyl-1-propanesulfonic acid sodium salt
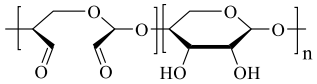	**ODEX**, Partially oxidized dextran
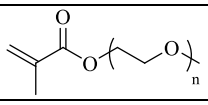	**PEGMA**, Poly(ethylene glycol) methyl ether methacrylate
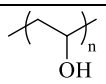	**PVA**, Poly(vinyl alcohol)

1.2.2.2.1 Simple Triple Networks

In 2005, the research group of Gong and Osada[22] reported the synthesis of two new materials with enhanced mechanical properties and low frictional coefficients, prepared by introducing a third component in the already developed PAMPS/PAAm DN hydrogels,[19] either a loosely cross-linked PAMPS network to prepare a triple network (TN) hydrogel, or a linear PAMPS chain to prepare a TN hydrogel, denoted as DN-L. Thus, the TN hydrogels consisted of a highly cross-linked PAMPS network as the first network, a loosely cross-linked PAAm network as the second network, and a loosely cross-linked PAMPS polymer network or non cross-linked PAMPS linear polymer chains as the third component. The thus-prepared DN, TN and DN-L hydrogels were characterized in terms of their mechanical properties using compression experiments which indicated a substantial increase in the Young's modulus values of the TN and DN-L (~2 MPa), a slight increase in the fracture stress value of the TN (4.8 MPa), and a two-fold increase in the fracture stress of the DN-L hydrogel (9.2 MPa) in comparison with the DN hydrogel (σ_{max} = 4.60 MPa, E=0.84 MPa), despite their identical water content. These increases in the Young's moduli were attributed to the presence of the third polymer network, PAMPS, and not in the presence or absence of the MBAAm cross-linker. The enhancement of the fracture stress value of the DN-L hydrogel was attributed to the absence of the MBAAm cross-linker in the third network, leading to a linear PAMPS chain that can dissipate fracture energy most efficiently than the loosely cross-linked network counterpart. Finally, the DN-L hydrogel exhibited an ultra-low frictional coefficient (~10^{-5}) against a glass substrate, which, together with its high mechanical toughness, renders this hydrogel an important candidate as material for artificial articular cartilage.

Three years later, the same research group[23] prepared TN hydrogels with increased mechanical toughness that were also investigated in terms of their ability to promote cell spreading and proliferation using three kinds of cells, bovine fetal aorta endothelial cells (BFAECs), human umbilical vein endothelial cells (HUVECs), and rabbit synovial tissue-derived fibroblast cells (RSTFCs). The first network consisted of a densely cross-linked 2-poly(2-acrylamido-2-methyl-1-propanesulfonic acid sodium salt) (PSAMPS) network, the second network consisted of a loosely cross-linked poly(*N*,*N*-dimethylacrylamide) (PDMAAm) network, and the third network consisted of an equimolar random copolymer

of DMAAm and 2-acrylamido-2-methyl-1-propanesulfonic acid sodium salt (SAMPS), randomly cross-linked with 0, 2, and 4 mol% MBAAm cross-linker. The resulting SN, DN, and TN hydrogels were then characterized in terms of their mechanical performance using compression experiments. The TN hydrogels exhibited improved mechanical properties in comparison with their SN counterparts, and, in particular, fracture stress values of 1-3 MPa, fracture strain values of 47-71%, and Young's modulus values of 0.32-0.88 MPa. Increasing the MBAAm cross-linker loading in the third polymer network resulted in increased Young's modulus values and decreased values of fracture stress and fracture strain. Finally, the TN hydrogels were evaluated in terms of their ability to serve as a matrix for cell spreading and proliferation, as the presence of the ionic component SAMPS on the surface of the gel is known to promote cell adhesion and proliferation. It was found that cell proliferation was only observed in the cases of the TN hydrogels containing MBAAm cross-linker in the third polymer network, as the TN hydrogel consisting of linear polymer chains as the third polymeric component did not exhibit cell proliferation, because the linear polymer chains do not facilitate cell spreading due to their increased mobility.

In 2011, Zhang et al.[24,25] reported the preparation of injectable triply interpenetrating network hydrogels[24] and monodispersed spherical microgels with a triply interpenetrating structure,[25] both containing three different natural components: partially oxidized dextran (Odex) prepared by oxidation of dextran using sodium periodate ($NaIO_4$), *N*-carboxyethyl chitosan (CEC) synthesized from the reaction of chitosan and acrylic acid (AAc), and Teleostean. The aqueous solutions of the three natural components at varying polymer concentrations were mixed together in an aqueous buffer solution of pH 7.4 in the order: first Odex, then Teleostean, and finally CEC at a constant Odex : Teleostean : CEC volume ratio of 2:1:1 in order to form the triply interpenetrating hydrogels. Figure 1.2.3 illustrates the chemical structures of the three components employed in the preparation of these hydrogels. CEC is an amphoteric natural polymer as it contains both $–NH_2$ and $–CO_2H$ groups, Teleostean contains $–NH_2$ groups, and Odex contains –CHO groups. Thus, Odex acts as a macromolecular cross-linker both for CEC and Teleostean through imine (Schiff base) bond formation. Hence, the triply interpenetrating hydrogels are cross-linked through both covalent Schiff base bonds and ionic interactions between the amine and the carboxylic acid groups. After their preparation, these hydrogels were evaluated in terms of

their mechanical properties using burst strength testings. The triple hydrogels exhibited higher mechanical performance than their doubly interpenetrating hydrogel counterparts. Furthermore, increasing the polymer concentration, and, consequently, the number of cross-linking $–NH_2$, $–CO_2H$, and –CHO groups, resulted in increased mechanical performance of the final hydrogels.

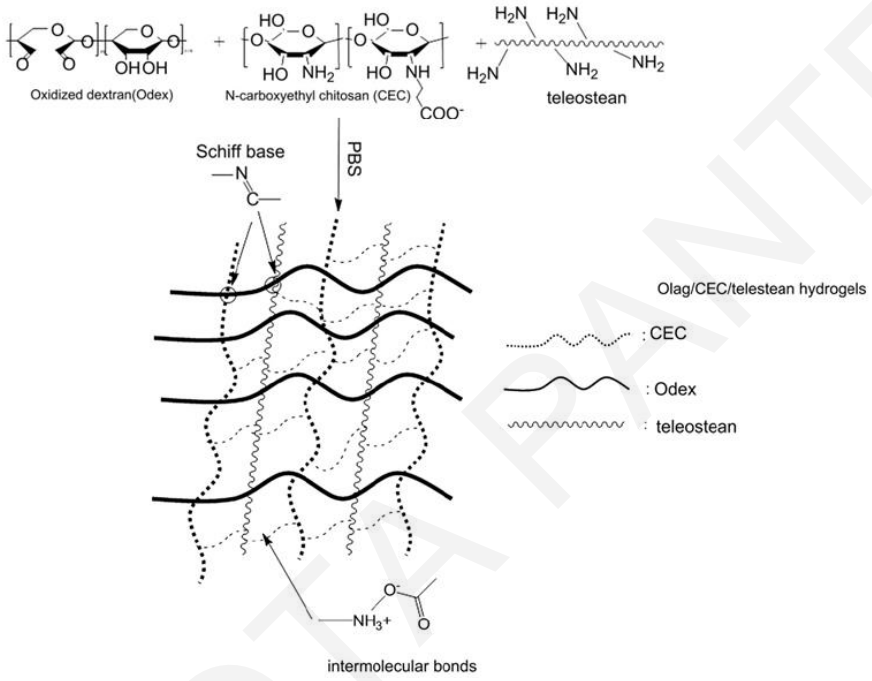

Figure 1.2.3. Structure of the three polymeric components used to prepare the TN hydrogels.[24]

In 2014, Okay and co-workers[26] developed nonionic TN hydrogels based on the hydrophilic AAm or DMAAm monomers and the poly(ethylene glycol) dimethacrylate (PEGDMA) cross-linker, prepared using redox polymerization, with ammonium persulfate (APS) serving as the initiator and *N*,*N*,*N*′,*N*′-tetramethylethylenediamine (TEMED) as the polymerization accelerator. The PAAm/PAAm/PAAm TN hydrogels consisted of an inhomogeneous highly cross-linked first polymer network of AAm, with a PEGDMA cross-linker loading up to 4 mol% with respect to monomer, and linear, uncross-linked PAAm chains as the second and third TN components. Similarly to the PAAm-based TN hydrogels, the PDMAAm/PDMAAm/PDMAAm TN hydrogels also consisted of an inhomogeneous highly cross-linked first polymer network of DMAAm, but with a PEGDMA cross-linker loading ranging between 4 and 10 mol% with respect to monomer, and linear PDMAAm chains as the second and third TN components. In contrast to the AAm or DMAAm concentration in the first network which was constant, the AAm or

DMAAm concentration in the second and third polymer networks acquired values between 0.7 and 7 M or 0.5 and 5 M, respectively, so as to obtain DN and TN hydrogels with varying molar ratios of the second to the first network units, n_{21}, and second and third to the first network units, $n_{32/1}$, respectively, thereby leading to the preparation of a large number of DN and TN hydrogels. All the hydrogels were evaluated in terms of their mechanical behavior using compression experiments. Figure 1.2.4 presents the typical stress-strain curves for particular DN and TN hydrogels as the dependence of the nominal fracture stress (σ_{nom}, solid curves) and true fracture stress (σ_{true}, dashed curves, $\sigma_{true} = \lambda \times \sigma_{nom}$) on the deformation ratio, λ. Both the PAAm-based and PDMAAm-based TN hydrogels exhibited excellent mechanical properties, with nominal fracture stress values of 25 and 26 MPa, respectively, fracture strain values of 99 and 95%, respectively, and Young's modulus values of up to 2 MPa. Increasing the molar ratio of the repeating units in the higher networks to the repeating units in the first network, n_{21} and $n_{32/1}$, resulted in a greater enhancement of the mechanical properties of the DN and TN hydrogels, respectively. Finally, cyclic compressive tests on a particular TN hydrogel revealed the presence of hysteresis in the first cycle due to permanent internal fracture taking place in the first network, and a nearly elastic behavior in the subsequent cycles due to the presence of the ductile PAAm or PDMAAm components that prevented the sample from failure.

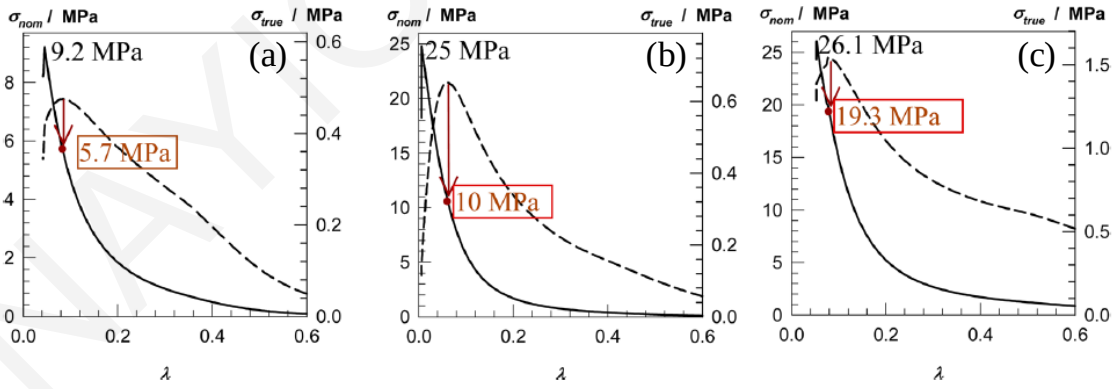

Figure 1.2.4. Stress-strain curves for the hydrogels as the effect of the deformation ratio, λ, on the nominal fracture stress (solid curves) and true fracture stress (dashed lines). Red circles are taken as the points of failure in the gel samples. (a) PAAm/PAAm DN hydrogel formed at 4 mol% PEG DMA. n_{21}=3.6. (b) PAAm/PAAm/PAAm TN hydrogel formed at 4 mol% PEG DMA. n_{21}=2.6, $n_{32/1}$= 17. (c) PDMAAm/PDMAAm/PDMAAm TN hydrogel prepared using 10 mol% PEG-DMA. n_{21}=4.0, $n_{32/1}$= 33.[26]

At about the same time as Okay et al.,[26] Creton et al.[27] prepared TN elastomers rather than TN hydrogels, consisting only of the hydrophobic components ethyl acrylate (EA,

always in the first network, and in some cases in the second and third networks as well) or methyl acrylate (MA, the component of the second and third networks in most cases) as monomers, and butanediol diacrylate (BDA) as cross-linker. The concentration of EA monomer in the first network was always constant and equal to 5 M, while the concentration of BDA cross-linker in the first network acquired values of 1.45 (denoted with 0.5), 2.81 (denoted with 1), and 5.81 mol% (denoted with 2) with respect to monomer. In the higher networks, the concentration of EA and MA was 9.4 and 11 M, respectively, while the concentration of the BDA cross-linker was very low, and, in particular, 0.01 mol% relative to monomer. The prepared TN elastomers were subsequently evaluated in terms of their mechanical performance using tensile measurements, and these measurements indicated extraordinary mechanical properties with fracture stress and Young's modulus values up to 29 MPa and 4.2 MPa, respectively, surpassing those of the corresponding DN elastomers by 4 and 3 times, respectively. Figure 1.2.5 presents the true stress-stretch curves for the EA_1 SN, EA_1MA DN, EA_1MAMA TN, and the poly(methyl acrylate) (PMA) second network alone, MA_{2N}, at 60 ^oC (45 ^oC above the glass transition temperature, T_g, of PMA), while part (b) of the figure presents the effect of cross-linker concentration in the EA first network on the EA_xMA DN elastomers. Increasing the network multiplicity resulted in increased values of fracture stress, while decreasing the BDA cross-linker loading in the first network led to increased values of both fracture stress and fracture strain of the DN elastomers. Similar to the DN hydrogels, the origin of the toughening mechanism in the TN elastomers was also attributed to the prevention of large crack formation by the higher (second and third) networks, and stress level (and hence stiffness) control by the fracture of the covalent bonds in the first network. The latter was nicely proven experimentally via the use of a chemiluminescent cross-linker incorporated in the first network, which, upon fracturing, emitted light whose total intensity was proportional to the cumulative mechanical hysteresis for a given value of the stretch ratio, as shown in Figure 1.2.6.

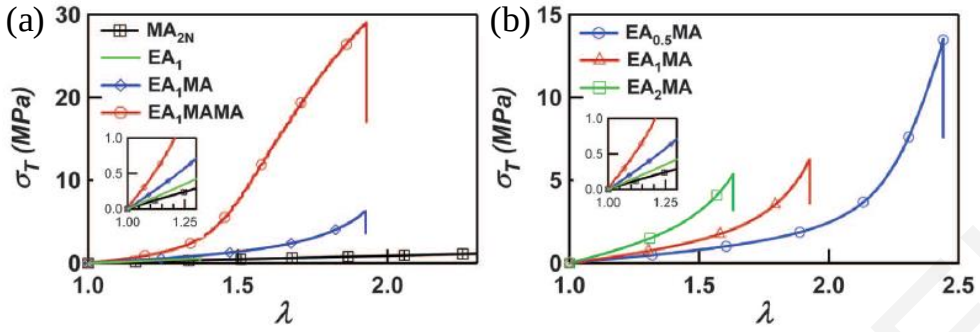

Figure 1.2.5. Mechanical behavior of the SN, DN and TN elastomers. (a) True stress-stretch curves for the EA_1, EA_1MA, EA_1MAMA and PMA second network alone (MA_{2N}) at 60 °C. (b) Effect of the cross-linker loading in the EA first network on the EA_xMA DN elastomers.[27]

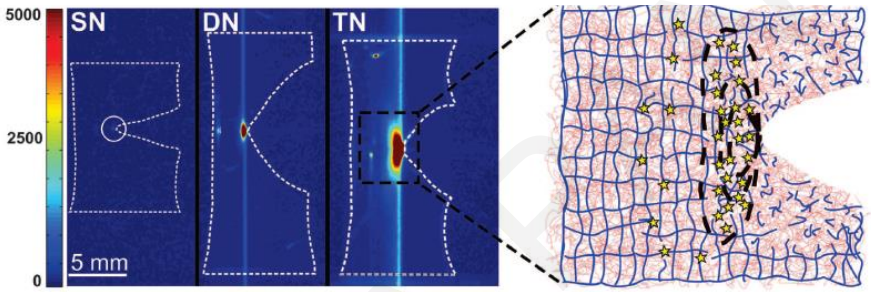

Figure 1.2.6. Mapping of where bonds break during crack propagation. (Left) Intensity-colored images of propagating cracks on notched samples containing dioxetane cross-linker in the first network, showing light emission due to breaking of bonds in SN, DN, and TN samples. (Right) Schematic of the sacrificial bond-breaking mechanism in front of the crack tip for the DN and TN; the first network is represented in blue, and the second and third networks are in red.[27]

In 2015, the research group of Okay[28] prepared DN and TN hydrogels based on methacrylated hyaluronan (MHA) macromonomer, DMAAm monomer, and MBAAm cross-linker, using sequential free radical photopolymerizations. In particular, these TN hydrogels consisted of poly(methacrylated hyaluronan) (PMHA) as the first network, and two loosely cross-linked polymer networks of PDMAAm as the second and third networks. A great variety of SN, DN, and TN hydrogels were prepared, afforded by the variation of the methacrylation degree in hyaluronan from 4 to 25%, the concentration of DMAAm monomer in the second network from 1 to 5 M and in the third network from 1 to 3 M, and the ratio of MBAAm cross-linker to the DMAAm monomer in the second and third networks from 0.0 to 0.5 mol%. After their preparation and equilibrium swelling in water, all the prepared hydrogels were characterized in terms of their mechanical properties using compression experiments. The optimum methacrylation degree in MHA and the optimum ratio of MBAAm cross-linker to DMAAm monomer were found to be equal to 4% and

0.05 mol%, respectively. Similar to the previous work from Okay and co-workers,[26] the key factor for obtaining tough hydrogels was the molar ratio of the repeating units in the higher networks to the repeating units in the first network. Thus, increasing this ratio led to a greater enhancement of the mechanical properties. The toughest DN hydrogel presented a fracture stress value of 12 MPa, a fracture strain of 93%, and a Young's modulus of 0.37 MPa. In the case of the TN hydrogels, the best-performing hydrogel exhibited a fracture stress of 22 MPa, a fracture strain of 95%, and a Young's modulus of 0.4 MPa. Finally, the cyclic compressive test on a particular TN hydrogel indicated the same behavior as the behavior of a particular PAAm/PAAm/PAAm TN hydrogel, that exhibited hysteresis in the first cycle and an elastic behavior in the subsequent cycles.

1.2.2.2.2 Triple Networks with a 1st Polymer Network Based on Microgels

In 2011, the research group of Gong[29,30] reported the preparation of TN hydrogels consisting of microgels as the first component, and loosely cross-linked PAAm networks as the second and third components. Five different monomers were employed in the preparation of the microgels. These were AAm, SAMPS, sodium 4-styrenesulfonate (NaSS), 2-(trimethylamino)ethyl acrylate, chloride quaternary salt (DMAEA-Q), and 3-(acrylamidopropyl)-trimethylammonium chloride (DMAPAA-Q). For each monomer, a different microgel was prepared, and, from that, the corresponding DN and TN hydrogels were formed. The preparation of the five different TN hydrogels was accomplished through three steps. Figure 1.2.7 illustrates the synthetic route for the preparation of the PSAMPS/PAAm/PAAm TN hydrogels. After their preparation, the microgel precursors were allowed to reach swelling equilibrium in an aqueous solution of AAm, containing MBAAm and OXG photoinitiator, and after their photopolymerization, they were again allowed to reach swelling equilibrium in an aqueous solution of AAm, MBAAm, and OXG, and photopolymerized in order to obtain the final TN hydrogels. The evaluation of the TN hydrogels in terms of their mechanical properties using tensile measurements indicated values of fracture stress, fracture strain, and Young's modulus for the PSAMPS/PAAm/PAAm TN hydrogels similar to that of the conventional PAMPS/PAAm DN hydrogels.[19] In the next report,[30] these authors investigated the dependence of the mechanical properties of the PSAMPS/PAAm/PAAm TN hydrogels on several parameters, such as the concentration of microgel, the concentration of sodium chloride in the second

network, the concentration of AAm in the second and third network, and the concentration of MBAAm in the second network. Increasing the concentration of microgel or the concentration of AAm in the second and third network and, therefore, the molar ratio of PAAm to PSAMPS, resulted in great improvement of the mechanical properties of the final TN hydrogels.

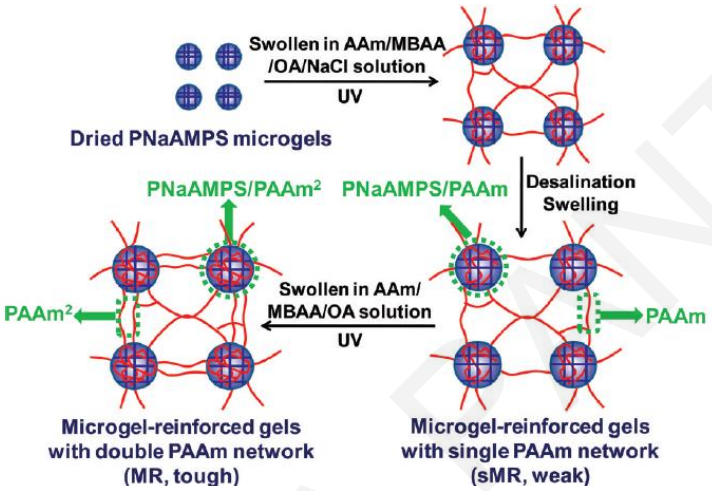

Figure 1.2.7. Preparation route followed for the synthesis of the PAMPS/PAAm/PAAm TN hydrogels.[30]

1.2.2.2.3 Triple Networks with a Linear Polyelectrolyte Stent as the 2nd Polymeric Component

In 2012, the same research group[31] proposed a new method for the toughening of nonionic DN hydrogels by introducing the molecular stent approach. This approach was based on the introduction of a linear polyelectrolyte, PAMPS, between the first and the second polymer networks consisting of nonionic components, in order to induce a higher osmotic pressure, and, consequently, a higher degree of swelling in the first network, which would ultimately lead to enhanced mechanical properties. To this end, after its preparation, the nonionic SN hydrogel was immersed in the ionic AMPS monomer solution, and after its equilibrium swelling, was photopolymerized in order to obtain the DN hydrogel. Then, the DN hydrogel was immersed in an aqueous solution of AAm monomer, and photopolymerized, resulting in the preparation of the TN hydrogel. Figure 1.2.8 presents the synthetic route followed for the preparation of the TN hydrogels based on the molecular stent approach. In order to investigate the universality of this method, several monomers were used in the preparation of the first network, including AAc, AAm,

DMAAm, *N*-isopropylacrylamide (NIPAAm), and 2-hydroxyethyl acrylate (HEA), whereas the third network was common for all hydrogels and consisted of loosely cross-linked PAAm polymer chains. The corresponding DN hydrogels without the presence of a PAMPS chain as the second component/stent were also prepared, in order to compare the mechanical properties of the two series of hydrogels. Characterization of all the prepared hydrogels revealed a significant improvement of the tensile mechanical properties of the stent-based TN hydrogels in comparison with the corresponding DN hydrogels lacking the linear PAMPS stent. Furthermore, the tensile mechanical properties of the prepared stent-based TN hydrogels were very similar, and in some cases better, than those of the conventional PAMPS/PAAm DN hydrogels.[19]

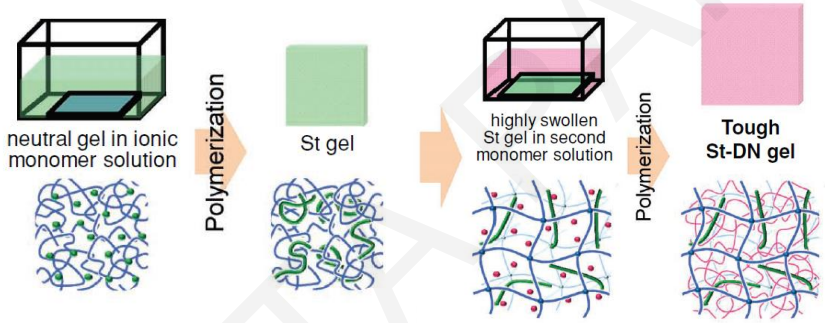

Figure 1.2.8. Schematic representation of the preparation of the TN hydrogels containing a polyelectrolyte molecular stent as the second network.[31]

One year later, the same research group[32] developed TN hydrogels consisting of a well-defined four-arm poly(ethylene glycol) (TPEG) gel as the first polymer network, a linear PAMPS molecular stent chain as the second component, and a loosely cross-linked nonionic PAAm network as the third network, as shown in Figure 1.2.9. The TPEG gel was obtained from the reaction of a tetra-amine-terminated four-arm poly(ethylene glycol) (TAPEG) star polymer with an activated tetra-ester-terminated four-arm poly(ethylene glycol) (TNPEG) star polymer. In order to induce a higher osmotic pressure, and, consequently, a higher degree of swelling in the first network which was well-defined, the first network was immersed in an AMPS monomer solution and was UV-irradiated to obtain a DN hydrogel. This DN hydrogel was subsequently immersed in an AAm monomer/MBAAm cross-linker solution, and was also UV-irradiated to prepare the final TN hydrogel. Furthermore, the corresponding PAMPS/PAAm and TPEG/PAAm DN hydrogels were also prepared, in order to perform the comparison between the three types

of hydrogels. Characterization of the obtained hydrogels in terms of their mechanical behavior using tensile experiments indicated the superior mechanical properties of the TN hydrogels in comparison with the TPEG/PAAm DN hydrogels without the stent, and the conventional PAMPS/PAAm DN hydrogels.

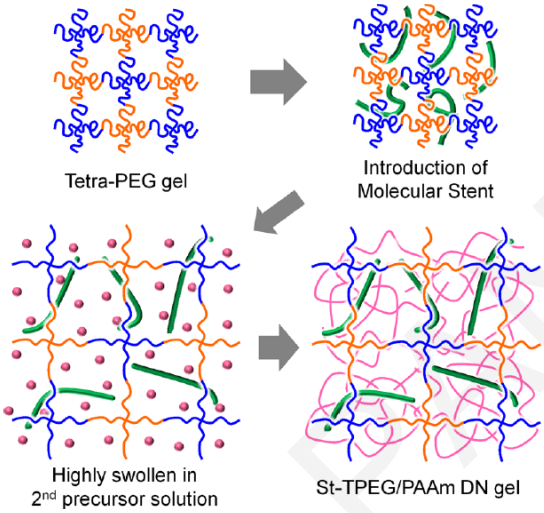

Figure 1.2.9. Schematic representation of the TN hydrogels based on a well-defined TPEG gel first polymer network.[32]

1.2.2.2.4 Triple Networks with a Mold Used in the 1st Polymeric Component

In 2010, the same research group[33] reported the fabrication of TN hydrogels consisting of poly(vinyl alcohol) (PVA) as the first component, a highly cross-linked PAMPS second component, and a loosely cross-linked PAAm third network. For comparison, PVA/PAMPS DN and PVA/PAAm DN hydrogels were also prepared. The PVA/PAMPS/PAAm TN hydrogels possessed increased flexibility owing to the highly flexible PVA which acted as an internal mold, and toughness due to the presence of the PAMPS/PAAm DN structure. Figure 1.2.10 presents photographs for the PVA/PAMPS/PAAm TN hydrogels which could possess various shapes. Subsequently, the mechanical properties of the prepared PVA/PAMPS DN and PVA/PAAm DN and TN hydrogels were evaluated using tensile measurements. The TN hydrogels exhibited improved mechanical properties in comparison with their DN counterparts, and this was attributed to the presence of the PAMPS/PAAm DN structure.

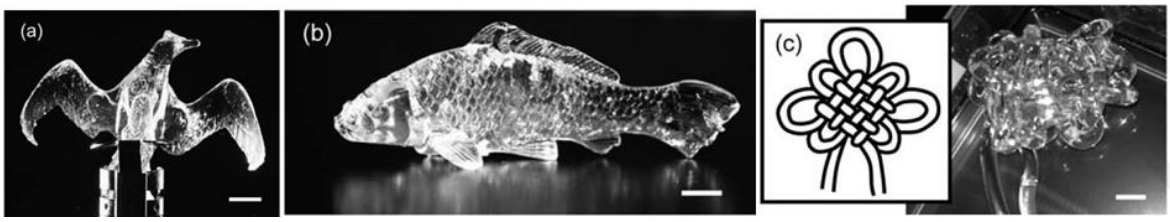

Figure 1.2.10. Pictures for the PVA/PAMPS/PAAm TN hydrogels with the shape of (a) bird, (b) fish, and (c) Chinese knot. Scale bars: 1 cm.[33]

1.2.2.2.5 Triple Networks Containing an Electrically Conducting Polymer in the 3rd Component

In 2009, the research group of Lu[34] were the first to report the preparation of electrically conducting TN hydrogels with good mechanical performance, prepared using the conducting poly(3,4-ethylenedioxythiophene) (PEDOT) as the third component, together with poly(sodium 4-styrenesulfonate) (PNaSS, molecular weight = 70 kg mol^{-1}). In particular, these TN hydrogels consisted of a highly cross-linked PAAc as the first network, a loosely cross-linked PAAc as the second network, and a PEDOT-PNaSS homopolymer mixture as the third component. The polymerization of the 3,4-ethylenedioxythiophene (EDOT) monomer was accomplished through chemical oxidation and was initiated using iron (III) nitrate nonahydrate [$Fe(NO_3)_3 \cdot 9H_2O$], while the iron (III) cation (Fe^{3+}) also acted as a physical cross-linker for the NaSS monomer repeating units through ionic interactions, leading to the formation of a physically cross-linked polymer network. In total, five different TN hydrogels were prepared, differing in their PEDOT content with respect to their dry mass, ranging between 8.0 and 18.4% w/w, while PAAc SN and PAAc/PAAc DN hydrogels were also prepared. The characterization of the conducting TN and their PAAc SN and PAAc/PAAc DN hydrogels precursors in terms of their mechanical performance using both compression and tensile experiments indicated higher values of fracture stress and fracture strain for the TN hydrogels in comparison with their SN and DN hydrogel precursors. In addition, the mechanical properties of these TN hydrogels were found to increase upon increasing the PEDOT content, with the TN hydrogel with the highest PEDOT content, 18.4% w/w, exhibiting a compressive fracture stress of 1.8 MPa and a compressive fracture strain of 78%. Finally, the TN hydrogels exhibited high values of electrical conductivity, up to 10^{-3} *S* cm^{-1}, and this value was found to increase when increasing the PEDOT content.

In a later report, the research group of Kishi[35] prepared electrically conducting TN hydrogels with satisfactory mechanical properties by introducing a third polymer consisting of PEDOT to the conventional PAMPS/PAAm DN hydrogels. The DN hydrogels were prepared according to Gong's procedure,[19] while the TN hydrogels were prepared in the same manner as previously[34] but using iron (III) *p*-toluenesulfonate hexahydrate [Fe(III) *p*-TS·$6H_2O$] as the initiator for the polymerization of the EDOT monomer. Two TN hydrogels with different PEDOT amounts were obtained, and this amount was dependent on the duration of the polymerization of the EDOT monomer. The mechanical properties of the prepared DN and TN hydrogels were evaluated using tensile measurements. The values of fracture stress, fracture strain, and Young's modulus of the TN hydrogels were higher than the corresponding values of the DN hydrogels. Furthermore, these values were found to improve when the PEDOT amount in the TN hydrogels increased. This increase was attributed to the hydrophobic nature of the EDOT monomer repeating units and the rigid main chain of PEDOT. These TN hydrogels also exhibited electrical conductivity with similar values as in the previous report, in the order of 10^{-3} *S* cm^{-1}, which increased with increasing the PEDOT content.

Two years later, the same research group[36] prepared electrically conducting and mechanically robust TN hydrogels based on poly(styrene sulphonic acid) (PSS), PDMAAm, and PEDOT. In particular, the first network consisted of a highly cross-linked PSS network, the second network contained a loosely cross-linked PDMAAm network, and the third network comprised a PEDOT chain. The TN hydrogels were prepared according to the above-mentioned procedure, using Fe(III) *p*-TS·$6H_2O$ as the initiator for the polymerization of the EDOT monomer, while the corresponding PSS/DMAAm DN hydrogels were also prepared. Two different DN hydrogels, and, consequently, two different TN hydrogels were obtained, by varying the DMAAm monomer concentration in the second network from 1.5 to 2.0 M, resulting in PEDOT content values in the TN hydrogels equal to 19.4 and 20.3% w/w, respectively. The characterization of the DN and TN hydrogels in terms of their mechanical properties using compression measurements showed a significant enhancement in fracture stress and Young's modulus of the TN hydrogels in comparison with their DN hydrogel counterparts, whereas the fracture strain was slightly reduced or remained constant. Furthermore, the values of fracture stress and

Young's modulus of the TN hydrogels were found to increase upon increasing the PEDOT content. Finally, these TN hydrogels exhibited very high values of electrical conductivity, ~1 *S* cm^{-1}, much higher than those in the previous reports, indicating their great potential for application as actuators and sensors.

1.2.2.3 Quadruple Network (QN) Hydrogels

In 2012, Naficy and co-workers[37] developed electrically conductive, mechanically robust, and pH sensitive TN and QN hydrogels consisting of poly[poly(ethylene glycol) methyl ether methacrylate] (PPEGMA), PAAc, and PEDOT-PNaSS (PNaSS : molecular weight = 70 kg mol^{-1}). The first network consisted of a highly cross-linked PPEGMA network, the second network consisted of a loosely cross-linked PAAc network, and the third network consisted of PEDOT-PNaSS physically cross-linked with Fe^{3+}. The preparation of the DN and TN hydrogels was accomplished in two or three steps, respectively, while, after the preparation of the TN hydrogel, this was again immersed in the aqueous dispersion containing EDOT monomer and PNaSS and polymerized after reaching swelling equilibrium, which resulted in the formation of the QN hydrogel. All the prepared hydrogels were characterized in terms of their mechanical performance using compression and tensile measurements. Increasing the amount of the incorporated PEDOT led to a significant increase in the values of both the compressive and tensile fracture stress, whereas the values of compressive fracture strain remained almost constant or were slightly decreased. However, increasing this amount resulted in a significant decrease in the values of the tensile fracture strain. Furthermore, these mechanical properties were found to exhibit a great dependence on pH. Increasing the pH from 3 to 5 led to a great reduction in the values of fracture stress and fracture strain, due to the deprotonation of the carboxylic acid in the AAc monomer repeating units, leading to electrostatic repulsion between them which resulted in higher values of degrees of swelling, and, consequently, in poorer mechanical properties. Finally, this QN hydrogel exhibited increased electrical conductivity, and, in particular, 4.3 *S* cm^{-1}, which is a value higher than the values reported for the TN hydrogels in the previous section, making these materials potential candidates as soft strain sensors.

In 2016, Shams Es-haghi and Weiss[38] reported the preparation and characterization of

nonionic QN hydrogels. These hydrogels were based on AAm monomer and MBAAm cross-linker, while all four PAAm networks were prepared using a relatively high monomer concentration, 4 M, and a very low MBAAm cross-linker concentration (0.01 mol% relative to the monomer), in order to achieve high extensibility and allow for tensile measurements. The thus-prepared SN, DN, TN, and QN hydrogels were characterized in terms of their mechanical properties using both compression and tensile measurements. It was found from the tensile measurements that the SN and DN hydrogels exhibited high stretch ratios at break, 1020 and 820%, respectively, while the stretch ratios at break of the TN and QN hydrogels were found to be slightly lower, around 780%. In contrast, the tensile fracture stress increased with network multiplicity, from 0.2 MPa for the SN to at least 1.8 MPa for the QN, which did not break but slipped out of the clamp fixture. A similar trend was observed in the case of the compression experiments. Increasing the network multiplicity led to increased fracture stress values, from ~0.5 MPa for the SN to ~7 MPa for the QN hydrogel, and decreased fracture strain values, from 88% for the SN to 78% for the QN hydrogel. Figure 1.2.11 displays the tensile stress-strain curves (part (a)) and the compressive stress-strain curves for the SN, DN, TN, and QN hydrogels (part (b)). The TN and QN hydrogels were found to exhibit strain localization during tensile deformation. Unloading before strain localization did not lead to network damage. However, unloading after strain localization resulted in a large hysteresis due to energy dissipation arising either from the damage of microgel-like cross-linked clusters created from the high network multiplicity or from translation of the cross-link junctions in the loosely cross-linked networks during deformation.

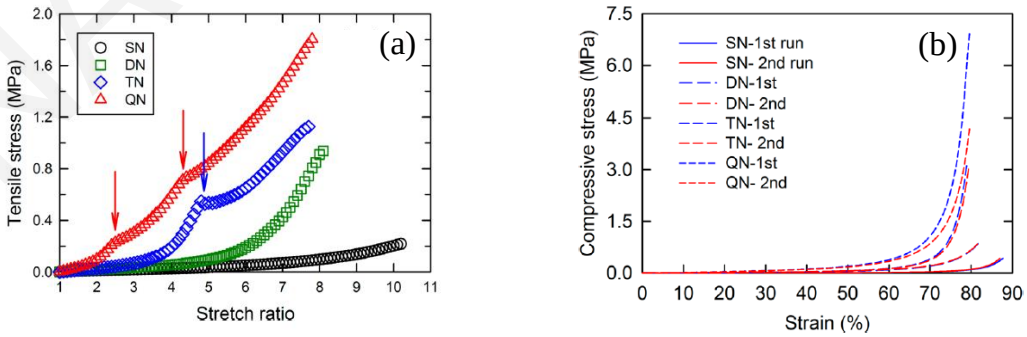

Figure 1.2.11. (a) Tensile stress-strain curves for the SN, DN, TN, and QN hydrogels. Arrows show the strain localization in the TN and QN hydrogels. (b) Compressive stress-strain curves for the SN, DN, TN, and QN hydrogels. Blue lines show the first compression run on the sample, and the red lines show the second compression after the first run on the same sample.[38]

1.2.3 Applications of the Multiple Network Hydrogels

The multiple network hydrogels, e.g., the DN, TN, and QN hydrogels, are excellent candidates in applications that require mechanical strength and toughness. For example, the conventional PAMPS/PAAm DN hydrogels meet these criteria as they possess enhanced mechanical performance, and hence they are potential candidates in applications that require both soft and wet materials, such as soft robotics, including artificial articular cartilages and artificial tendons.[19] In addition, in order for the hydrogels to be able to serve in these applications that include motion, the hydrogels must also exhibit low frictional coefficients, as in the case of the PAMPS/PAAm/PAMPS TN hydrogels.[22]

Furthermore, the DN, TN, and QN hydrogels with increased mechanical properties can serve as scaffolds in tissue engineering, due to their biocompatibility and non-cytotoxicity. For example, TN hydrogels based on DMAAm and SAMPS[23] with satisfactory mechanical performance, exhibited the ability to induce cell spreading and proliferation for particular types of cells. However, the hydrogels must also be biodegradable in order to enable their clearance from the body.

Injectable TN microgels composed of Odex, Teleostean, and CEC[24] may be applied in biomedical applications such as drug delivery, because these materials have the appropriate size to serve as injectable materials, and, at the same time, they can be degraded once they are administered in the body owing to their biodegradable constituents. Finally, the TN hydrogels containing an electron conducting component, e.g., PEDOT, in their structure and exhibit satisfactorily enhanced mechanical properties may be employed in the technology field, in applications such as sensing and actuating.[34-38]

1.2.4 Structure of the DN Hydrogels

The PAMPS/PAAm DN hydrogels[19] possess extraordinary mechanical toughness arising from the combination of the two distinct polymer networks with opposite physical properties. In addition, these mechanical properties are further enhanced when the second polymer network in the DN hydrogels consists of linear, non cross-linked PAAm chains. However, this high mechanical toughness of the particular DN hydrogels cannot be simply

explained by taking into account the unique structure of their constituents. Until now, several groups have attempted to reveal the true structure of the DN hydrogels and correlate it to their mechanical performance. The research group of Gong[39] have tried to shed more light to the structure of DN hydrogels. They assumed that a percentage of double bonds belonging to MBAAm cross-linker remained active after the preparation of the first PAMPS network. This allowed for the grafting of the linear PAAm chains in the second component onto the active double bonds in the PAMPS network. To test this assumption, they synthesized two PAMPS networks with different structures. First, they prepared the PAMPS hydrogel according to the previous procedure,[19] which was called *active*-PAMPS (*α*-PAMPS) hydrogel. After its polymerization, this hydrogel was immersed in an aqueous solution of 0.1 M OXG photoinitiator and, after reaching swelling equilibrium, it was UV-irradiated, resulting in the preparation of the *inert*-PAMPS (*i*-PAMPS) hydrogel, due to the expected deactivation of the remaining double bonds. Subsequently, samples of both the *α*-PAMPS and the *i*-PAMPS hydrogels were immersed in the aqueous solution of AAm (2 M) with or without MBAAm cross-linker (0-0.3 mol%). The photopolymerization of the *α*-PAMPS and *i*-PAMPS hydrogels led to the preparation of the *connected*-DN (*c*-DN) hydrogels and the *truly independent*-DN (*t*-DN) hydrogels, respectively. Figure 1.2.12 presents the structures of both the *c*-DN and *t*-DN hydrogels. The characterization of all the prepared DN hydrogels in terms of their mechanical behavior using compression experiments revealed initially the superior mechanical properties of the *c*-DN hydrogels in comparison with the *t*-DN hydrogels. In particular, the *c*-DN hydrogels exhibited higher values of fracture stress and fracture strain than the corresponding values of the *t*-DN hydrogels. This was attributed to the formation of internetwork cross-linking (INC) points in the *c*-DN hydrogels between the active double bonds of MBAAm in the first PAMPS network and the non cross-linked linear PAAm chains in the second component. During the compression test, these INC points act as bridges between the two networks, leading to a more extensive energy dissipation mechanism which results in enhanced mechanical properties for the *c*-DN hydrogels. Furthermore, it was found that the fracture energy values for both the *c*-DN and *t*-DN hydrogels could be tuned by the cross-linking density in the second PAAm network. In particular, the *c*-DN hydrogels consisting of a second non cross-linked PAAm chain exhibited the highest value of fracture energy, ~1200 J m^{-2}, whereas in the case of the *t*-

DN hydrogels, the highest value of fracture energy, ~2200 J m^{-2}, was obtained when the cross-linking density in the second PAAm network was 0.01 mol%. Finally, it was found that the percentage of the INC points in the *c*-DN hydrogels could be tuned by the OXG photoinitiator concentration used for the preparation of the PAMPS network. Increasing the OXG concentration resulted in a decreased amount of INC points in the *c*-DN hydrogels, while an optimum OXG concentration of 0.6 mol% was found to result in a reduced amount of INC points, and at the same time, in enhanced values of fracture stress, Young's modulus, and fracture energy.

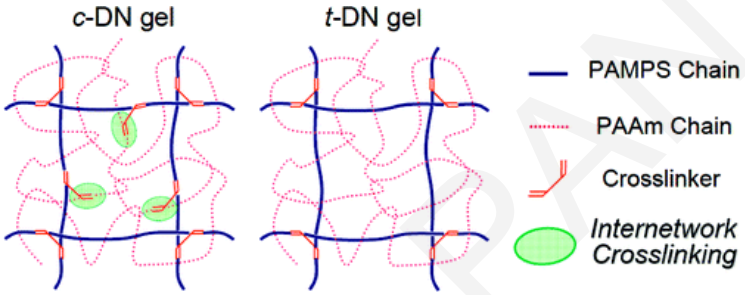

Figure 1.2.12. Structures of the *connected*-DN (*c*-DN) hydrogels and *truly independent*-DN (*t*-DN) hydrogels.[39]

In 2014, the research group of Leonov and Weiss[40] provided some evidence for the presence of grafted chains between the two networks in the DN hydrogels, where, in this case, the hydrogels consisted of poly(sodium 3-sulfopropyl acrylate) (PSAPS) as the first network, and poly(2-hydroxyethyl acrylate) (PHEA) or PAAm as the second network. Similar to the procedure reported in the previous study[39] for the deactivation of the remaining active double bonds of MBAAm cross-linker, a PSAPS hydrogel was immersed in an aqueous solution of 0.1 M OXG photoinitiator, and, after its swelling equilibrium, this hydrogel was UV-irradiated in order to prepare the inert PSAPS hydrogel. A sample of the same PSAPS hydrogel was also immersed in an aqueous solution of 0.1 M 2,2′-azobis[2-(2-imidazolin-2-yl)propane] dihydrochloride (VA-044) thermal initiator, and, after reaching swelling equilibrium, the hydrogel was subjected to a thermally induced deactivation for the preparation of the inert PSAPS hydrogel. After the preparation of the corresponding PSAPS/PHEA DN and the deactivated PSAPS – OXG/PHEA and PSAPS – VA-044/PHEA DN hydrogels, all the SN and DN hydrogels were characterized using Fourier-transform infrared (FTIR) spectroscopy. This characterization revealed the presence of the C=C absorption band at ~1650 cm^{-1} in the case of the PSAPS SN hydrogel

which corresponded to the remaining double bonds of MBAAm cross-linker in the first network, whereas the particular absorption band was absent in the FTIR spectrum of the PSAPS/PHEA DN hydrogel, indicating the grafting of the PHEA chains onto the double bonds of MBAAm cross-linker in the PSAPS network. Furthermore, it was found from the FTIR spectroscopy that the deactivation of the remaining double bonds of the MBAAm cross-linker was more efficient when the VA-044 thermal initiator was used instead of the OXG photoinitiator. In order to compare the mechanical properties of the particular DN hydrogels with the conventional PAMPS/PAAm DN hydrogels,[19] the corresponding DN and deactivated DN hydrogels were prepared using AAm as the second monomer instead of HEA, and their characterization was performed using tensile measurements. It was found that the completely deactivated PSAPS – VA-044 SN hydrogel exhibited a brittle behavior in comparison with the partially deactivated PSAPS – OXG SN and the PSAPS SN hydrogel, and it was so brittle that it could not be characterized using tensile testing. Finally, it was observed that the PSAPS/PAAm DN hydrogel exhibited higher values of tensile fracture stress and stretch ratio at fracture than the PSAPS – OXG/PAAm, as a consequence of the grafted polymer chains of the second network onto the double bonds of the MBAAm cross-linker in the PSAPS network in the case of the PSAPS/PAAm DN hydrogel.

Last but not least, Shestakova and co-workers[41] used high-resolution magic angle spinning nuclear magnetic resonance (HRMAS NMR) spectroscopy to characterize the conventional PAMPS/PAAm DN hydrogels and proved the existence of grafted chains of the PAAm network onto the double bonds of the MBAAm cross-linker in the PAMPS network. The SN and DN hydrogels were prepared following the procedure reported by Gong's group,[19] but, with the difference that, in this case, the polymerizations were performed using potassium persulfate (KPS) as initiator. In addition, the AAm monomer concentration in the second network was varied, and, in particular, it acquired values of 1, 2, and 3 M. After the preparation of the SN and DN hydrogels, their structure was investigated using HRMAS ^{1}H and ^{13}C NMR spectroscopy. It was found that a set of peaks corresponding to the vinyl protons or vinyl carbons were present in the ^{1}H and ^{13}C NMR spectra, respectively, for both the PAMPS and PAAm SN hydrogels. The same set of peaks was also present in some ^{1}H NMR spectra of the PAMPS/PAAm DN hydrogels. In

particular, increasing the AAm monomer concentration from 1 to 3 M in the second network resulted in a lower intensity of these particular peaks, indicating a higher percentage of intercross-linking/grafting, leading to a lower amount of the remaining active double bonds after the preparation of the DN hydrogels. Thus, when the AAm monomer concentration was equal to 3 M, the particular peaks were not observed in the ^{1}H NMR spectrum of the particular PAMPS/PAAm DN hydrogel, which indicated that all the double bonds of the MBAAm cross-linker were reacted with AAm upon the formation of the DN hydrogel. Furthermore, they also proved the formation of hydrogen bonds in the DN hydrogels between the –NH groups of the PAMPS network which act as hydrogen donors and the –C=O groups in the PAAm network which act as hydrogen acceptors, as illustrated in Figure 1.2.13. Similar to the previous finding, increasing the AAm concentration from 1 to 3 M resulted in a denser DN gel, arising from the increased amount of hydrogen bonds as evidenced from the HRMAS NMR spectroscopy. Finally, microhardness measurements revealed that increasing AAm monomer concentration in the second network led to increased values of microhardness, and, in particular, these values increased from 256 MPa for the DN hydrogel prepared at a 1 M AAm concentration to 347 MPa for the DN hydrogel prepared using the highest AAm concentration, of 3 M. This increase was accompanied with a decrease in the values of the equilibrium swelling ratio of the DN hydrogels, as expected.

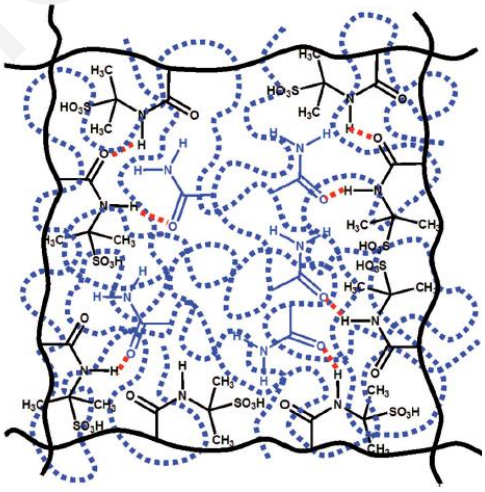

Figure 1.2.13. Schematic representation of the formation of hydrogen bonds between the N–H groups in the PAAm network (blue dashed line) as hydrogen donors, and the C=O groups in the PAMPS network (black solid line) as the hydrogen acceptors.[41]

1.2.5 Toughening Mechanism of the DN and the Multiple Network Hydrogels

In 2007, Brown[42] proposed a model concerning the fracture of the conventional PAMPS/PAAm DN hydrogels when subjected to a tearing test. The author assumed that the fracture process of the DN hydrogels is realized in two stages. In the first stage, a critical stress value, corresponding to the stress required to form a crack in the first brittle network, must be applied to the DN gel in order to create the first bond scission in the structure of the first network. The first network is brittle and breaks up easily as it consists of a relatively highly cross-linked polymer network that becomes highly swollen in the aqueous solution of the second monomer during the swelling equilibrium step required for the preparation of the second network, and, consequently, the final DN hydrogel. Upon the formation of the first crack, many multiple cracks begin to form leading to the formation of a damaged zone around the primary crack ahead of the crack tip, as shown in Figure 1.2.14. This damaged zone possesses an elastic modulus lower than that of the undamaged zone, and a value similar to that of the second ductile network which is the main component in the damaged zone. In the second stage, the crack begins to propagate along the polymer chains of the second polymer network, creating a damaged zone with a particular thickness, *h*, possessing a low cross-linking density, and, hence, a low elastic modulus. In order for the complete failure of the DN hydrogel to occur, the thickness of this zone must increase so that the total elastic energy becomes equal to the toughness of the second network, and thus, to the fracture energy, *G*.

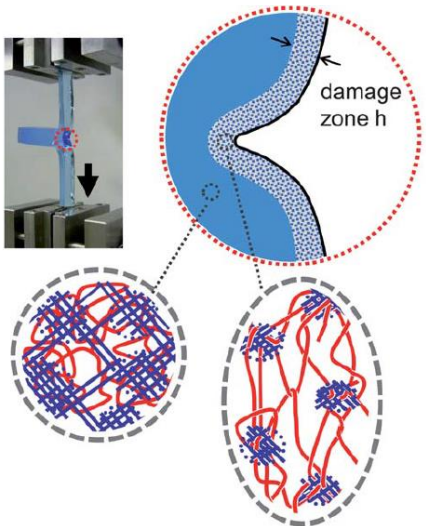

Figure 1.2.14. Structure of the damaged zone created near the crack tip during the tearing test of the PAMPS/PAAm DN hydrogel.[20]

Using this model, the calculation of the maximum thickness, h_{max}, of the damaged zone required for the complete failure of the sample, and the fracture energy of the DN hydrogel, G_{DN}, was possible using the following equations:

$$h_{\max} = \frac{2\,G_2}{(\lambda_m - 1)^2\,E_2} \qquad \textbf{Equation 1.1}$$

$$G_{DN} = \frac{4G_1G_2}{(\lambda_m - 1)E_2\,\Delta b} \qquad \textbf{Equation 1.2}$$

where G_1 (= 0.5 J m^{-2}) and G_2 (= 10 J m^{-2}) correspond to the toughness of the first and the second network, respectively, λ_m (~11) is the stretch ratio of the DN hydrogel, E_2 (=1.5 kPa) is the elastic modulus of the second network alone, and Δb (=3 μm) is the thickness of the crack opening. The h_{max} value was calculated to be equal to 130 μm, whereas the G_{DN} value was estimated to be around 400 J m^{-2}, a value consistent with that obtained for the conventional PAMPS/PAAm DN hydrogels. This improvement in G corresponds to a 40-fold enhancement in the toughness of the DN in comparison with the toughness of the second network alone.

In the same year, Tanaka[43] proposed a similar model for the fracture of the DN hydrogels by taking into account the experimental values obtained from the tensile measurements on the PAMPS/PAAm DN hydrogel. The model assumed that the highly stretched zone around the crack becomes soft with a fracture energy of G_0, as illustrated in Figure 1.2.15.

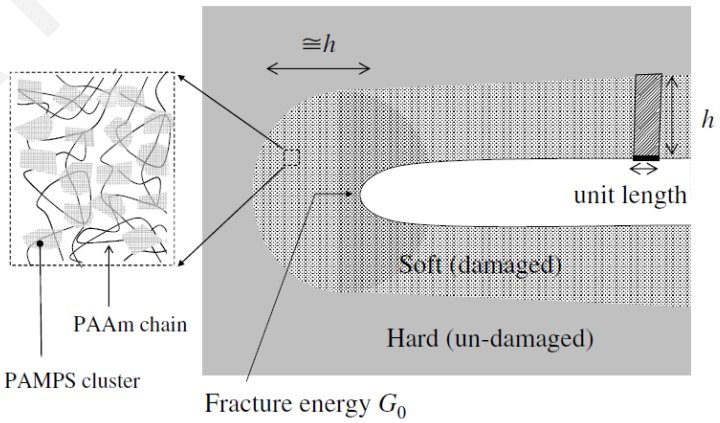

Figure 1.2.15. Structure of the crack formed during the fracture process of the DN hydrogels. Due to the fracture of the first brittle PAMPS network, the damaged zone becomes soft, and the PAMPS clusters act as cross-linking points for the PAAm chains in the second network.[43]

Using the energy balance concept of fracture mechanics, the following equation was obtained:

$$G = G_0 + \sigma_c \, \varepsilon_c \, h \qquad \textbf{Equation 1.3}$$

where G corresponds to the fracture energy of the DN hydrogel, G_0 (= 10 J m^{-2}) corresponds to the fracture energy of the second PAAm network, σ_c (= 0.2 MPa) is the stress and ε_c (~10) is the elongation, both calculated from the point at which the yielding/softening of the DN hydrogel occurs, and h is the thickness of the damaged zone. Using this equation, h was calculated to be equal to 100 μm, whereas G was equal to ~100 J m^{-2}, values similar to the ones calculated using the model developed by Brown.[42]

From these models, it appears that the first highly cross-linked and highly stretched polymer network acts by providing sacrificial bonds, while the second loosely cross-linked (or linear, non cross-linked) nonionic polymer network serves as a soft matrix that can efficiently dissipate the energy released from the fracture of the bonds in the first network, thereby preventing the sample from failure. Hence, even in the case of the TN and QN hydrogels, consisting of nonionic first and nonionic higher polymer networks, a similar fracture mechanism must be taking place during the fracture of the sample. Increasing the number of loosely cross-linked polymer networks increases the polymer volume fraction, and, consequently, the polymer density of the soft component. The increased polymer density of the higher networks results in increased protection of the hydrogel towards fracture and contributes to the enhancement of the mechanical properties.

1.3 Linear Polymers and Polymer Networks Based on *N*-Dodecylacrylamide (DDAAm)

In this section, we will review the limited literature available on the hydrophobic monomer we used in the investigation, DDAAm. The first synthesis and polymerization of DDAAm monomer was reported in 1988 by the research group of McCormick,[44] who prepared random copolymers with various compositions of AAm and various *N*-alkylacrylamides, and, in particular, *N*-octylacrylamide, *N*-decylacrylamide, and DDAAm. The random copolymers were synthesized in water using micellar free radical polymerization in the presence of sodium dodecyl sulfate (SDS) as surfactant and KPS as initiator. After their

preparation, various amounts of the random copolymers were dissolved in water to obtain aqueous solutions of different concentrations, and these solutions were then characterized using rheology for the determination of their viscosity. It was found initially that all the random copolymers exhibited higher values of solution viscosity in comparison with the values obtained for the solution of the PAAm homopolymer. This was attributed to the presence of the hydrophobic domains which formed intermolecular hydrophobic associations resulting in increased values of solution viscosity. It was also found that the solution viscosity had a great dependence on polymer concentration in the solution, as increasing concentration resulted in higher values of solution viscosity due to increased interchain hydrophobic associations. In addition, increasing the length of the alkyl substituent led to a greater dependence of solution viscosity on polymer concentration, as the random copolymer prepared with DDAAm exhibited higher values of solution viscosity with increasing concentration. The solution viscosity was also found to increase with increasing hydrophobic content and molecular weight. On the other hand, the hydrophobic associations were found to be disrupted in the presence of the SDS surfactant, leading to reduced values of the solution viscosity, whereas the presence of sodium chloride enhanced the hydrophobic associations, and, consequently, the solution viscosity. Finally, it was found that increasing the temperature from 25 to 55 ^{o}C resulted in more intense hydrophobic associations, thereby leading to increased values of the solution viscosity.

In 2014, again McCormick's research group[45] synthesized random copolymers of AMPS and DDAAm with various DDAAm contents, ranging between 10 and 60 mol%, using RAFT polymerization. DLS was used to investigate the self-assembly of the resulting random copolymers in water with various polymer concentrations. The DLS measurements indicated that the random copolymers containing 10-30 mol% DDAAm exhibited an increase in their diameters (50-600 nm) with increasing polymer concentration in the solution, a finding which is consistent with the formation of multimolecular micelles. On the other hand, the random copolymers with 40-60 mol% DDAAm exhibited a rather constant diameter (10-20 nm) over the whole concentration range investigated, indicating the formation of stable, compact, unimolecular micelles. In order to evaluate the efficacy of the random copolymers to internalize hydrophobic molecules, a pyrene solution in

acetone was added in the aqueous solution of the copolymer, and the solutions were characterized using fluorescence and ultraviolet/visible (UV/Vis) spectroscopy. It was found from fluorescence spectroscopy that all the random copolymers internalized pyrene into their hydrophobic cores, with the random copolymer with 30 mol% DDAAm presenting the highest value of pyrene uptake, and the random copolymers with 40-60 mol% DDAAm exhibiting high values of pyrene uptake (~0.85) even at low concentrations (0.065 mg mL^{-1}). Furthermore, from the UV absorbance measurements, it was found that the unimolecular micelles formed using the random copolymers with higher DDAAm contents exhibited a much higher pyrene absorbance than the multimolecular micelles formed using the random copolymers with lower DDAAm contents, as the former micelles were more compact. Finally, it was found that the random copolymers possessed a lower cytotoxicity towards KB (HeLa) cells than SDS. The low cytotoxicity of the random copolymers and their increased capability to internalize hydrophobic molecules such as pyrene indicate their potential application in environmental remediation.

The first study on the preparation and characterization of polymer networks using DDAAm was reported from the research group of Creton and Hourdet,[46,47] who prepared hydrophobically modified hydrogels of PAAc. The hydrophobically modified hydrogels were prepared after the partial modification of linear PAAc with allylamine to introduce a particular amount of double bonds (10 mol%), and 1-dodecylamine (3-5 mol%) to confer hydrophobicity to the hydrogel, followed by cross-linking of the obtained double bonds using dithioerythritol. Prior to the addition of the KPS initiator and dithioerythritol for the formation of the hydrogels, the unmodified and modified PAAc were dissolved in water at varying concentrations, and then these solutions were characterized using rheology for the determination of their viscosity. It was found that the solutions of the modified PAAc at low polymer concentrations exhibited higher values of solution viscosity than the solution of the unmodified PAAc (0 mol% DDAAm), which were found to increase with increasing DDAAm content from 3 to 5 mol%. This finding was attributed to the formation of hydrophobic associations between the hydrophobic DDAAm monomer repeating units, resulting in increased values of solution viscosity. Subsequently, dithioerythritol was added to the copolymer solutions, and the formation of the hydrogels was followed using rheology. It was found that the value of the loss modulus (G'') was highly dependent on the

DDAAm content in the hydrogels, as increasing the DDAAm content led to increased values of *G″*. This was attributed to the presence of the hydrophobic monomer repeating units which form reversible hydrophobic associations, leading to increased values of *G″*. In contrast, the value of the storage modulus (*G′*) was independent of the hydrophobic content, but dependent on the chemical cross-links in the hydrogels. The gel formation time, taken as the time when the *G″* value becomes equal to the *G′* value, was found to decrease with increasing DDAAm content in the hydrogels or increasing polymer concentration. Furthermore, the hydrogels were characterized using dynamic sweep experiments and it was found that they exhibited high values of *G′* due to the presence of chemical cross-links, which is consistent with the formation of an elastic material, and relatively high values of *G″*, consistent with the presence of the reversible hydrophobic associations between the DDAAm monomer repeating units in the hydrogels. Finally, both the aqueous solutions and the final hydrogels were characterized using SANS, and it was found that both the solutions and the hydrogels exhibited a self-assembly ability in water with the formation of micelles. However, the micelles formed from the hydrogels exhibited a long-range order arising from the presence of hydrophobic scattering centers with their position depending on DDAAm content and polymer concentration.

In 2017, Luo et al.[48] prepared in dimethylsulfoxide (DMSO) a randomly cross-linked copolymer network of AAm, DDAAm, and MBAAm cross-linker using free radical copolymerization in the presence of nickel nitrate hexahydrate. After its preparation, the gel was swollen in water and characterized using DLS for the determination of the R_h. In order to investigate its thermal transition behavior, the DLS measurements were performed in the temperature range of 25 to 55 ^oC. It was found that the radius of the gel was dependent on the temperature, with a maximum radius value being observed at 43 ^oC. When the temperature was below 43 ^oC, the radius was small, and this was attributed to the decreased mobility of the pendant dodecyl chains in the DDAAm monomer repeating units, whereas at temperatures higher than 43 ^oC, the pendant dodecyl chains possessed increased hydrophobicity leading to a small radius. Figure 1.3.1 illustrates the suggested possible mechanism for the thermal transition behavior of the randomly cross-linked copolymer network. Subsequently, the shape-memory effect of the water-swollen gel was investigated. The water-swollen gel with a rod-like shape was heated up to 50 ^oC in order

to change its shape, followed by its immediate cooling down to 25 °C to fix the permanent shape, and heating to 50 °C in order to recover its initial rod-like shape. Finally, the gel was characterized in terms of its catalytic properties for the reduction of methylene blue with sodium borohydride ($NaBH_4$) at three different temperatures, 30, 43, and 50 °C. It was found that the catalytic activity of the gel exhibited a maximum at the temperature of 43 °C, whereas below and above this temperature the catalytic activity was weak, indicating an "off-on-off" catalytic switching. This behavior was also attributed to the decreased mobility of the pendant dodecyl chains in DDAAm monomer repeating units at 30 °C, whereas at 50 °C the hydrophobicity of the gels was significantly increased. These findings indicate the potential application of this system in controlled catalytic procedures.

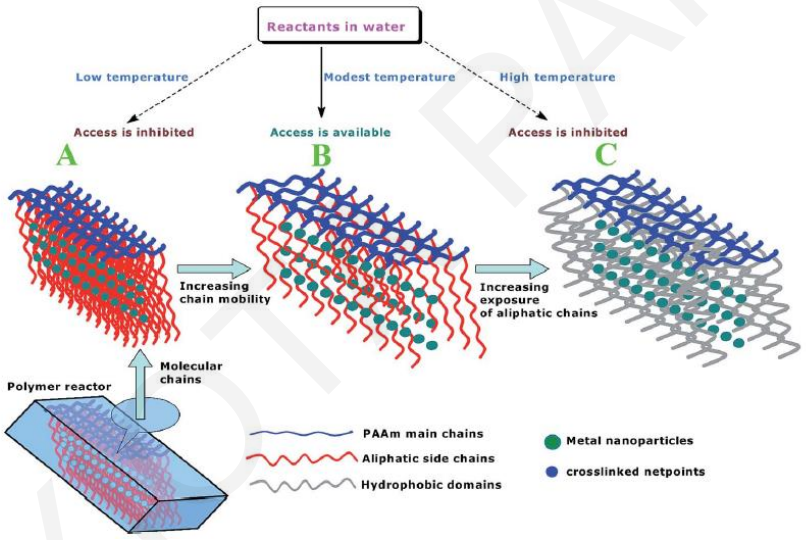

Figure 1.3.1. The possible mechanism for the thermal transition behavior of the randomly cross-linked copolymer network of AAm, DDAAm, MBAAm, also containing nickel nanoparticles.[48]

1.4 Reversible Covalent Bonds Used in the Preparation of Polymer Networks

This section reviews the literature on reversible (dynamic) covalent bonds which are chemical bonds that are cleaved under certain conditions and are reformed in others. These dynamic bonds have a behavior intermediate between those of covalent bonds and non-covalent interactions. Each of these three types of bonds or interactions can be used alone or in combination for the cross-linking and formation of polymer networks. Examples of reversible covalent bonds include the imine, hydrazone, and oxime groups, formed from the condensation reaction of a carbonyl compound, such as an aldehyde or a ketone, with a

primary amine or an amine derivative,[49] which attract an increased interest from the scientific community. These reactions are usually fast in slightly acidic conditions and with high yields, with water being the only byproduct. However, the formation of all these bonds can be reversed upon the application of the appropriate conditions, such as pH or/and temperature. Other dynamic covalent bonds include boronic acids/boronate esters, Diels-Alder adducts, and disulfides, whereas non-covalent interactions include hydrogen-bonds, ion-pairs and metal-ligand interactions.

1.4.1 Imine Bond

The imine bond (or Schiff base) is obtained from the condensation reaction of a carbonyl group, an aldehyde or a ketone, and a primary amine.[49] This reaction is highly reversible in aqueous solutions owing to the presence of water, leading to the hydrolysis of the imine bond and the reformation of the initial reactants. Thus, dynamic covalent bonds with an increased stability towards hydrolysis are usually preferred to be used for the preparation of polymeric materials for particular applications such as bioconjugation.[50]

1.4.2 Hydrazone Bond

Similar to the imine bond, the hydrazone bond is obtained from the condensation reaction of a carbonyl compound, but using a compound with a hydrazine group such as an aryl- or an acyl-substituted hydrazine instead of a simple amine.[49] The rate of this reaction is highly dependent on the pH of the aqueous buffer solution, as the reaction proceeds faster in slightly acidic conditions and slower in neutral or slightly basic conditions.[50,51] However, the reaction in nonionic or slightly basic conditions can be significantly accelerated upon the addition of aniline.[51] The hydrazone bond exhibits increased stability towards hydrolysis over the imine bond.[52] This increased stability is attributed to the presence of the extra nitrogen atom (α-effect) leading to the formation of many resonance forms of the hydrazone bond, while, at the same time, this extra nitrogen atom confers upon the carbon atom of the C=N bond an increased negative charge density, and, therefore, decreased electrophilicity, rendering it less susceptible to attack by a water molecule.[52]

1.4.3 Oxime Bond

While the hydrazone bond remains a very popular dynamic covalent bond, the oxime bond begins to also attract the interest of the scientific community due to its increased stability towards hydrolysis. The oxime bond is obtained from the condensation reaction of a carbonyl group, an aldehyde or a ketone, with an *O*-alkoxyamine, leading to the formation of an aldoxime or a ketoxime, respectively. Similar to the reaction for the formation of the imine and the hydrazone bonds, the reaction for the formation of the oxime bond is well-known to be favored in slightly acidic conditions, whereas in neutral or slightly basic conditions a catalyst, such as aniline, is required.[50,51] However, the oxime bond exhibits increased stability towards hydrolysis over the hydrazone and the imine bonds.[52] This is attributed to the presence of the oxygen atom (α-effect) which exhibits a higher electronegativity than a nitrogen atom, resulting in increased negative charge density on the carbon of the C=N bond, and, thus, decreased electrophilicity, conferring upon the oxime bond a high stability.[52]

The mechanism for the formation of the oxime bond is presented in Figure 1.4.1. In the first stage, the *O*-alkoxyamine nucleophile attacks the electrophilic carbon atom of the carbonyl group through a proton-catalyzed addition, leading to the formation of a tetrahedral intermediate, a hemiaminal, after a proton transfer. In the second stage and upon a new proton transfer, the hydroxyl group is protonated, facilitating the elimination of a water molecule and resulting in the formation of a protonated intermediate. This step is the rate-determining step, as the dehydration of the tetrahedral intermediate is very slow when the pH ranges between 3 and 7. In contrast, when the pH is lower than 3, the amine becomes protonated leading to the formation of the *O*-alkoxyammonium ion which reacts very slowly, and, thus, the first step becomes the rate-determining one. In the final stage, the desired oxime bond is obtained after deprotonation.[50]

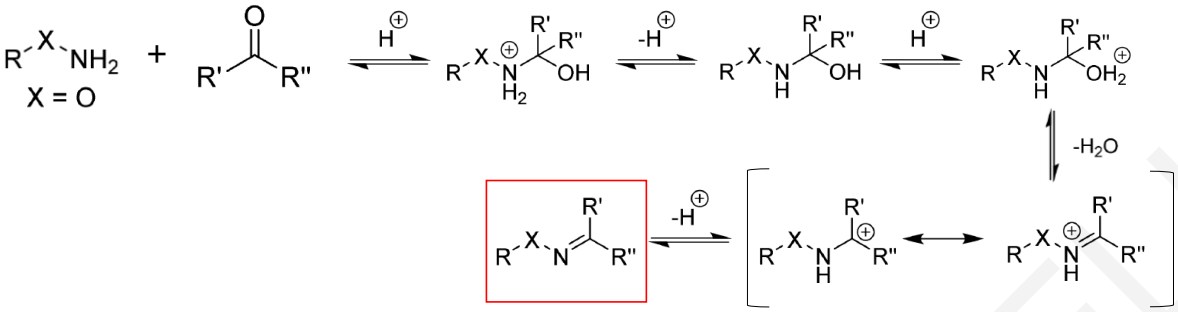

Figure 1.4.1. The mechanism for the formation of the oxime bond obtained from the reaction of a carbonyl compound with an *O*-alkoxyamine.[50]

Finally, it has been shown[50] that the aldehyde reacts faster with the *O*-alkoxyamine in comparison with the ketone, and the ketoxime bond exhibits increased stability towards hydrolysis than the aldoxime bond. However, when an aromatic aldehyde is used, the final aldoxime bond exhibits increased stability, higher than the ketoxime bond. Hence, one can fine-tune the stability of the oxime bond by choosing the appropriate substituents on both the electrophilic and the nucleophilic compounds. For example, when the substituents on the nucleophile are electron-withdrawing groups, the oxime bond will be hydrolyzed more easily. Finally, to avoid any undesirable hydrolysis, reducing the oxime bond with sodium cyanoborohydride will result in the formation of the highly stable carbon-nitrogen single bond.[50]

1.4.4 Polymer Networks Cross-linked via the Oxime Bond

In 2014, the research group of Sumerlin[53] employed the oxime bond to form dynamic macromolecular stars based on amphiphilic diblock copolymers. The amphiphilic diblock copolymers were synthesized in two steps using a controlled polymerization method, and, in particular, RAFT polymerization. These diblock copolymers consisted of DMAAm monomer repeating units as the hydrophilic and inactive block and diacetone acrylamide (DAAm) monomer repeating units as the hydrophobic and reactive block. The DAAm monomer contained a ketone group in the pendant, able to react with an *O*-alkoxyamine group to generate a functionalized compound via the ketoxime bond. After their preparation, the amphiphilic diblock copolymers were allowed to self-assemble in aqueous phosphate-buffered saline (PBS) of pH 7.4, leading to the formation of aggregated micelles. Then, in order to investigate the post-functionalization modification of the aggregated micelles, these were reacted with model *O*-alkoxyamines such as *O*-allyl

hydroxylamine and *O*-(tetrahydro-2*H*-pyran-2-yl) hydroxylamine, and the reactions were followed using ^{1}H NMR spectroscopy. In both reactions, the degree of functionalization was >95%, and thus, the aggregated micelles were subjected to reaction with an *O*-alkoxyamine cross-linker, the *O,O´*-propanediylbishydroxylamine hydrochloride (PDH). This led to the formation of core cross-linked stars, as the ketone group was located in the micellar core. Finally, the dissociation of the core cross-linked stars was performed by competitive oxime exchange reaction with a monofunctional aminooxy- or carbonyl-containing compound in the presence of trifluoroacetic acid (TFA) as catalyst and at high temperatures (60 °C), resulting in the initial but functionalized diblock copolymers.

One year later, the same research group[54] prepared self-healing copolymer networks randomly cross-linked via oxime bonds based on random copolymers of DMAAm and DAAm. The random copolymers were prepared in a single step using free radical polymerization, while the monomers were combined in various ratios to prepare random copolymers with different compositions. After their preparation, the random copolymers were cross-linked through the reaction with PDH in aqueous buffer solution of pH 7.0 in order to obtain the randomly oxime cross-linked hydrogels. In order to investigate the effect of concentration and stoichiometry of the reaction on the hydrogel formation time, the reaction was performed using three different concentrations and two different stoichiometries, while the gel formation time was obtained both from rheology measurements and vial inversion. It was found that in contrast to the stoichiometry of the reaction, concentration had a significant effect on the hydrogel formation time, as increasing concentration resulted in faster gel formation. Furthermore, the gel formation time dependence on the DAAm content in the random copolymers was investigated, and it was found that increasing the DAAm content led to faster gel formation. Finally, the hydrogels exhibited the ability to self-heal within two hours after cut in two separate pieces, and to transform into solution in the presence of an excess amount of a monofunctional aminooxy compound and TFA catalyst within 24 hours (Figure 1.4.2); both abilities were attributed to the dynamic nature of the oxime bonds.

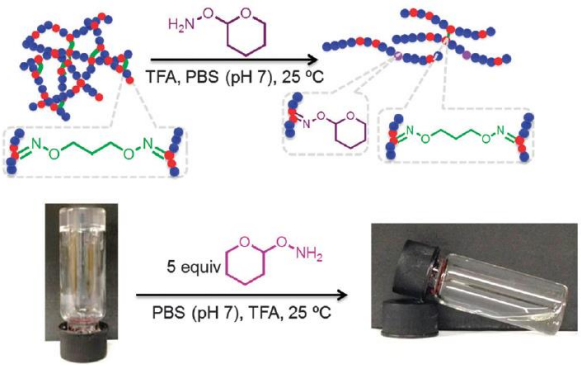

Figure 1.4.2. Gel-to-sol transition of the randomly oxime cross-linked copolymer network upon the addition of an excess amount of *O*-(tetrahydro-2*H*-pyran-2-yl) hydroxylamine and TFA catalyst.[54]

In addition to the previous studies, reports on the preparation of oxime cross-linked polymer networks include model networks based on multiarm poly(ethylene glycol) (PEG) star polymers terminated with aldehyde or ketone groups and *O*-alkoxyamine groups. For example, Grover et al.[55] prepared PEG-based hydrogels cross-linked via oxime bonds from the reaction of an eight-arm PEG star polymer terminated with an *O*-alkoxyamine group and glutaraldehyde. In order to encapsulate mouse mesenchymal stem cells (MSCs) in the hydrogels, the aminooxy-terminated 8-arm PEG star polymer was partially functionalized with a ketone-terminated arginine-glycine-aspartic acid (RGD) peptide via the formation of the ketoxime bond. The functionalized RGD-PEG star polymer was reacted with glutaraldehyde in the presence of the MSCs for the formation of the hydrogels. The obtained hydrogels exhibited high stability and cell viability and proliferation, indicating their potential application as tissue engineering scaffolds.

In another study reported from the research group of Christman,[56] injectable PEG-based hydrogels cross-linked via oxime bonds were prepared from the reaction of functionalized four-arm PEG star polymers, one with a ketone group, and one with an *O*-alkoxyamine group. The formation of the hydrogels was performed in aqueous buffer solutions of various pH values, from 4.0 to 7.4, and it was found that increasing pH resulted in slower gel formation, with the times ranging between 30 minutes and 50 hours, respectively. However, when the two components were mixed together in buffer solutions with varying pH and injected *in vivo* into the subcutaneous space, gelation occurred within 20 minutes for all pH values, due to the complex environment of the tissue. Finally, the oxime reaction

was also tested *in vivo* using partially oxidized hyaluronic acid and partially oxidized alginate through the reaction with the *O*-alkoxyamine-terminated PEG star polymer, and both types of hydrogels were formed after 20 minutes, consistent with the PEG-based hydrogels. These results indicate the potential application of these injectable materials in catheter delivery.

The research group of Becker[57] prepared oxime cross-linked hydrogels from the reaction of a four-arm *O*-alkoxyamine-terminated PEG star polymer and a linear PEG functionalized with two aromatic aldehyde groups on its terminus. The reaction was performed in aqueous buffer solutions of various pH values, from 1.5 to 7.6, while the reactions were also performed in the presence of a catalytic amount of aniline. The gel formation time was determined using rheology measurements. Increasing the pH of the aqueous buffer solution from 1.5 to 7.6 resulted in slower gel formation, and, consequently, in increased gel formation times. However, when the pH was very low, 1.5-2.5, the obtained hydrogels exhibited a brittle behavior due to the fast gelation which leads to increased inhomogeneity in the hydrogel structure. On the other extreme, gel formation was not observed at pH 7.6, while the hydrogel formed at pH 7.4 was a very viscous fluid. Thus, the optimum pH value of the aqueous buffer solution was found to be 4.5, and the particular hydrogel possessed the highest value of storage modulus, *G′*. Finally, when the reaction was performed in buffer solution of pH 6.6-7.6 in the presence of aniline, the gel formation was much faster, and the hydrogels exhibited increased values of *G′*.

Thus, the DN hydrogels approach provides a facile and efficient method to significantly improve the mechanical properties of polymeric hydrogels. This approach has been recently extended to triple, even quadruple network hydrogels with even better results. A major objective of this PhD Thesis is to further extend the concept to 5-fold quintuple polymer network hydrogels to obtain even mechanically more robust materials. In addition to this, network amphiphilicity and cross-link dynamic nature are to be employed to further improve the network mechanical properties.

1.5 Theoretical Background

1.5.1 Polymerization Methods

1.5.1.1 Free Radical Polymerization

One of the most common polymerization methods for the preparation of linear polymers and polymer networks is the free radical polymerization, based on the presence of a free-radical active center. This method belongs to the non-controlled/non-living methods as it produces polymers with a wide distribution of molecular weights. Furthermore, the synthesized polymers cannot be chain extended with other monomers. In the first step, the free-radical active center is formed after the cleavage of the initiator, followed by the addition of the produced free radical to the double bond of a monomer molecule. The second stage involves the propagation of the free radical, in which the free radical is added to monomer molecules, leading to the growth of the polymer chain, and, eventually to the synthesis of the polymer. The final stage of the polymerization involves the termination step in which the polymeric chain cannot grow further, because the free radical is combined with another free radical, leading to the termination of the polymerization. Finally, according to the type of the initiator used in the free radical polymerization, different sources can be employed for the cleavage of the initiator for the formation of the free radical, such as ultra-violet light (photopolymerization), heating (thermal polymerization), or oxidation (redox polymerization).[58]

1.5.1.2 Reversible Addition-Fragmentation Chain Transfer (RAFT) Polymerization

RAFT polymerization, originally developed in 1998 by Moad and co-workers[59] belongs to the controlled/living polymerization methods, and it is one of the most commonly used methods for the preparation of polymers with a controlled degree of polymerization and molecular weight, and narrow distribution of molecular weights with molecular weight dispersities which typically range between 1.1 and 1.2. Control over the molecular weight is achieved *via* the use of the chain transfer agent (CTA). Most CTA compounds contain a dithioester or a trithiocarbonate moiety, and are used according to the type of the monomer employed in RAFT polymerization. Owing to its livingness, the method allows for the polymers to be chain extended with other monomers for the preparation of block

copolymers. Due to the simple and facile nature of RAFT polymerization, a great variety of monomers can be polymerized, and in the presence of various solvents, even water, rendering RAFT polymerization a versatile method. Similar to free radical polymerization, the first stage involves the generation of the free radical from the cleavage (usually thermal) of the initiator, followed by the addition of the produced radical to a monomer molecule. Then, the free radical propagates and is successively added to monomer molecules, resulting in the growth of the polymer chain, which is then added to a R–C=S–Z group present in the CTA molecule. This process leads to the formation of an inactive polymer chain, but, as this process is reversible, the addition of another free radical results in the reactivation of the polymer chain and its subsequent growth. In the final stage, the active polymer chain reacts with another active polymer chain, leading to the termination of the polymerization.

1.5.2 Methods for the Verification of Polymer Structure

In order to determine the average molecular weights and the molecular weight dispersity of the linear polymer precursors, gel permeation chromatography (GPC) was employed, while the structure and composition of the linear polymer precursors were evaluated using proton nuclear magnetic resonance (NMR) spectroscopy; both methods are described below.

1.5.2.1 Gel Permeation Chromatography (GPC)

GPC is employed for the recording of the full molecular weight distribution of the polymers, and, from that, the determination of the average molecular weights and molecular weight dispersities of the linear polymers. In this method, a dilute polymer solution is injected into the mobile phase of the system, and transferred into a column packed with polymer beads of several pore sizes, ranging usually between 50 and 10^6 Å. Depending on the molecular weight and size of the polymer molecules, these molecules elute in different volumes, with the elution volume decreasing with increasing molecular weight. In particular, the small molecules are able to pass nearly through all pores, and thus exhibit a long flow-path in the column, leading to a large elution volume, whereas the large molecules are only able to pass through the beads with a large porosity, leading to a small flow-path in the column, and a small elution volume (size exclusion chromatography). The molar mass distribution, obtained using the plot of concentration against the elution

volume, is then used for the determination of the molecular weights, such as the number-average molecular weight, M_n, and the weight-average molecular weight, M_w, and the dispersity of molecular weight, $Đ$ (= M_w / M_n). However, GPC is not an absolute method for the calculation of the molecular weights, as a calibration must be performed using polymer standards with narrow molecular weight distributions, which are usually poly(methyl methacrylate) (PMMA) or polystyrene (PSty) samples.[60]

1.5.2.2 Nuclear Magnetic Resonance (NMR) Spectroscopy

NMR spectroscopy is utilized for the determination of monomer conversion to polymer, the verification of polymer structure, the calculation of the number-average molar mass of a homopolymer, and the calculation of the chemical composition in a copolymer. These values are calculated using the integrals of the proton peaks in the ^{1}H NMR spectrum, as the integrals are proportional to the number of proton nuclei. The chemical shifts and splitting of the proton peaks depend on the electronic environment and the adjacent nuclei, leading to the presence of several types of proton peaks in the spectrum.[60]

1.5.3 Scattering Methods

In this section, the scattering methods used for the characterization of the linear amphiphilic diblock copolymers and multiblock copolymers, as well as their networks, are described. In particular, two scattering methods were used, DLS and SANS.

1.5.3.1 Dynamic Light Scattering (DLS)

DLS, or photon correlation spectroscopy, PCS, or quasi-elastic light scattering, QELS, [60,61] is a well-established method for the characterization of polymer solutions in order to determine R_h. In this method, the intensity of the total number of photons of the scattered light is recorded at various times using a digital correlator, and then the autocorrelation function is calculated using equation 1.4:[60,61]

$$G^1_{(\tau)} = \lim_{\tau\to\infty}\left[\frac{1}{\tau}\int_0^{\tau} i_\theta(t) i_\theta(t+\tau)dt\right] \qquad \textbf{Equation 1.4}$$

where i_θ is the intensity of the scattered light at an angle θ, and τ is the correlation time, *i.e.*, the time between photon countings. The autocorrelation function, $G^1_{(\tau)}$, is then used for

the calculation of the decay rate, Γ, and, subsequently, the diffusion coefficient, D, after a regularized inverse Laplace transformation. The final R_h is obtained using the Stokes-Einstein equation assuming a spherical shape for the scattering particles (micelles):[60,61]

$$R_h = \frac{k_B T}{6\pi\eta D} \qquad \textbf{Equation 1.5}$$

where k_B is the Boltzmann constant, T is the temperature, η is the solvent viscosity, and D is the diffusion coefficient.[60,61]

1.5.3.2 Small-Angle Neutron Scattering (SANS)

SANS is employed for the determination of the structure (shape, size, interactions) of polymers in solution, or the distance between scattering centers in polymer networks, or the dimensions (chain conformation) of the constituent blocks in microphase separated systems such as block copolymers in the bulk state. Herein, the intensity of the scattered neutrons is based on the difference (*i.e.*, contrast) between the neutron scattering length densities of polymer and solvent. This is due to the presence of hydrogen (^{1}H) atoms in the polymer, and deuterium (^{2}H) atoms in the solvent, leading to a large difference in the scattering length densities.[60] For polymer solutions, the SANS method allows for the determination of R_g and molecular weight (MW) of the obtained structures. The R_g is determined using the Guinier approximation, but this calculation is valid only for small scattering angles, in which $q\,R_g << 1$:[60,61]

$$I(q) = I(0)\exp(-q^2 R_g^2/3) \qquad \textbf{Equation 1.6}$$

where q is the scattering vector, equal to:

$$q = \frac{4\pi}{\lambda}\sin(\frac{\theta}{2}) \qquad \textbf{Equation 1.7}$$

where λ is the wavelength of neutrons, equal to 0.2 - 2 nm.

Thus, R_g can be calculated from the slope of the linear portion of the ln(I) *vs.* q^2 graph, while $I_{(0)}$, obtained from the intercept of the linear portion, can be utilized for the determination of the MW[60,61] using the equation:

$$MW = \frac{I_{(0)}\, d\ N_A}{\varphi\ \Delta SLD^2} \qquad \textbf{Equation 1.8}$$

where d is the polymer density, N_A is the Avogadro number, φ is the polymer volume fraction, and ΔSLD is the difference of the scattering length density between polymer ($SLD_{polymer}$) and solvent (SLD_{D2O}). $SLD_{polymer}$ is calculated using the equation:

$$SLD_{polymer} = \frac{SLD_{core}\,\varphi_{core} + SLD_{shell}\,\varphi_{shell}}{\varphi_{core} + \varphi_{shell}} \qquad \textbf{Equation 1.9}$$

Finally, the aggregation number, N_{agg}, can be determined by dividing MW by the theoretical molecular weight of the linear block copolymer (unimer).

1.5.4 Atomic Force Microscopy (AFM)

Atomic force microscopy (AFM) is used for the investigation of the morphology of polymers formed in their solutions, or for the investigation of the morphology of nanoscale structures at the surface of polymer films. AFM is based on the measurement of forces that are established between a sharp tip and the sample. The sharp tip is mounted on the edge of a cantilever which is used as a force sensor. During the scanning of the surface from the tip, attractive or repulsive interactions between the tip and the surface are formed, resulting in the variation of the static deflection or the dynamic properties (oscillation frequency, oscillation amplitude) of the cantilever. Depending on the type of measurement, the operational modes of AFM can be divided into non-contact, contact, and tapping mode. In the tapping mode, the oscillation of the cantilever is excited close to its resonance frequency using a piezoactuator. During the scanning of the surface, the oscillation frequency of the cantilever is reduced due to the small bending of the cantilever from the forces between the tip and the sample, resulting in the variation of the oscillation amplitude. The oscillation amplitude is monitored using the beam-deflection method, in which a laser beam is reflected at the rear side of the cantilever and deflects onto a position-sensitive four-segment photodiode detector. Finally, a lock-in amplifier is used to detect the electrostatic interaction between the tip and the surface using the variation of the oscillation amplitude, resulting in the visualization of the structure of the surface.[61,62]

1.5.5 Mechanical Properties

Two of the most well-known methods to characterize materials in terms of their mechanical performance are the compressive and tensile tests. In a tensile measurement, the specimen is subjected to the application of two opposite and equal forces, resulting in the elongation of the specimen. When the elongation of the specimen reaches a particular value, the specimen fractures. The same behavior is observed in a compression experiment, but, in this case, the force applied to the specimen has the opposite direction than that in a tension experiment. Once again, the specimen fractures when the deformation of the specimen reaches a particular value.[63]

In a mechanical tester and in both methods, the specimen is deformed at a constant strain rate, and the values of stress and strain applied to the specimen are recorded, leading to the creation of the graph of stress *vs.* strain.[63] The stress, σ, is calculated according to the equation:

$$\sigma = \frac{F}{A} \qquad \textbf{Equation 1.10}$$

where F is equal to the force applied to the specimen, and A is the cross-sectional area of the specimen.[63-65]

The strain, ε, is calculated by dividing the deformation of the specimen by its initial length, according to the equation:

$$\varepsilon = \frac{l - l_0}{l_0} = \frac{\Delta l}{l_0} \qquad \textbf{Equation 1.11}$$

where l is the length of the sample for a particular stress value, and l_o is the initial length of the sample at a zero stress.[63-65] In the case of the tensile experiment, $l > l_o$, whereas in the compression experiment, $l_o > l$.

The slope of the elastic region of the plot of stress *vs.* strain, which corresponds to low values of strain, usually 5-15%, is equal to the elastic/Young's modulus, E. The elastic modulus corresponds to the resistance of the material upon deformation. The linear portion of the stress-strain curve (elastic region) follows Hooke's law according to the equation:

$$E = \frac{\sigma}{\varepsilon}$$ **Equation 1.12**

Finally, the area under the stress-strain curve, until the fracture point of the specimen, is equal to the toughness of the material, *G*, and corresponds to the total energy density per unit volume of the material, sufficient to cause the fracture of the sample.[63-65]

1.5.6 Nanoindentation Testing

Nanoindentation is a relatively modern and facile method for the characterization of the mechanical properties of materials, which involves the indentation of the material using a rigid tip of a specified geometry (conical, spherical, etc.) at the nanoscale. Materials, including metals, polymers, and ceramics, can be studied using this method, which can yield their mechanical properties, mainly their hardness and elastic modulus. Hardness is the resistance of the material against the permanent deformation of the local surface,[65] and it can be calculated from the nanoindentation load-displacement curves using the equation: [66,67]

$$H = \frac{P_{\max}}{A}$$ **Equation 1.13**

where P_{max} is the maximum applied load, and A is the projected contact area at maximum load. The reduced elastic moduli, E_r, of the material can also be extracted from the same nanoindentation load-displacement curves as above, using the expression: [66,67]

$$E_r = \frac{\pi^{1/2} S}{2A^{1/2}}$$ **Equation 1.14**

where *S* is the contact stiffness found from the slope of the unloading portion, d*P*/d*h*, of the load-displacement curve at P_{max}. The reduced elastic modulus, E_r, is a *harmonic* average between the elastic modulus of the sample and that of the indenter (usually made of diamond), defined as: [66,67]

$$\frac{1}{E_r} = \frac{1-\nu_s{}^2}{E_s} + \frac{1-\nu_i{}^2}{E_i}$$ **Equation 1.15**

where E_s and E_i are the elastic moduli for the sample and the indenter, respectively, and ν_s and ν_i are the Poisson's ratios for the sample and the indenter, respectively. The values of E_i and ν_i for the indenter are those corresponding to diamond, and are equal to 1141 GPa and 0.07, respectively.

Finally, the (total) area under the load, *P*, *vs.* displacement, *h*, curve during loading, can be used for the determination of the total work of nanoindentation provided to the system, W_{total}, whereas the elastic recoverable energy (elastic work), $W_{elastic}$, can be determined from the area under the load *vs.* displacement curve during unloading. The dissipated energy during the nanoindentation process (plastic work), $W_{plastic}$, can be calculated from the difference of W_{total} minus $W_{elastic}$. [66,67]

1.5.7 Rheology

The dynamic mechanical properties of polymeric materials can be evaluated using rheology measurements, which investigate the flow and deformation of materials upon the application of particular forces. According to the response of the materials upon the application of stress or strain, these can be classified as elastic solids (such as elastomers, *e.g.*, natural rubber), viscous fluids or viscoelastic solids, with the latter being the combination of the first two types of materials. In particular, the response of an elastic solid upon the application of stress or strain is purely elastic and time-independent, whereas the response of a viscous fluid upon the application of stress or strain is time-dependent. The behavior of a purely elastic material follows Hooke's law (Equation 1.12), whereas the behavior of a purely viscous fluid can be described using Newton's law, according to the equation:[64,68]

$$\sigma = \eta \frac{d\varepsilon}{dt} \qquad \textbf{Equation 1.16}$$

where σ is the stress, $\frac{d\varepsilon}{dt}$ is the strain-rate, and η is the viscosity of the material.

A viscoelastic material, however, exhibits both behaviors; it behaves as an elastic solid and a viscous fluid, as it consists of both elastic and viscous components, and appropriate models describing the behavior of these materials must be used. The time-dependent

dynamic behavior for a viscoelastic material can be determined using the Maxwell model or the Voigt model, according to equations 1.17 and 1.18, respectively.[64,68]

$$\frac{d\varepsilon}{dt} = \frac{1}{E}\frac{d\sigma}{dt} + \frac{\sigma}{\eta} \qquad \textbf{Equation 1.17}$$

$$\frac{d\varepsilon}{dt} = \frac{\sigma}{\eta} - \frac{E\,\varepsilon}{\eta} \qquad \textbf{Equation 1.18}$$

where σ is the stress, $\frac{d\sigma}{dt}$ is the stress-rate, and E is the elastic modulus of the material. The first term in equation 1.17 corresponds to the elastic behavior which is obtained using Hooke's law, whereas the second term corresponds to the viscous behavior of the viscoelastic material, which is described using Newton's law. Similarly, the first term in equation 1.18 corresponds to the viscous behavior, whereas the second term corresponds to the elastic behavior of the viscoelastic material.[64,68]

An important method for the investigation of the viscoelastic properties of these materials in the linear viscoelastic region is the dynamic mechanical testing. In this experiment, an oscillating sinusoidal shear loading (stress or strain) with a particular angular frequency, ω, is applied to the material. The sinusoidal shear strain, γ, is defined as:

$$\gamma = \gamma_0 \sin \omega t \qquad \textbf{Equation 1.19}$$

For a viscoelastic material the response of the shear stress, σ, is also sinusoidal, but out of phase at a phase angle, δ, in comparison with the sinusoidal shear strain. The sinusoidal shear stress is defined as:

$$\sigma = \sigma_0 \ \sin(\omega t + \delta) \qquad \textbf{Equation 1.20}$$

The sinusoidal shear stress converts into the following equation:

$$\sigma = (\sigma_0 \cos \delta)\ \sin \omega t + \ (\sigma_0 \sin \delta)\ \cos \omega t \qquad \textbf{Equation 1.21}$$

Therefore, the shear stress consists of two parameters: the $\sigma_0 \cos \delta$ which is in phase with the shear strain, and the $\sigma_0 \sin \delta$ which is $\pi/2$ out of phase. Combining the equations of shear stress and shear strain, the following equation is obtained:

$$\sigma = \gamma_0(G' \sin \omega t + G'' \cos \omega t) \qquad \textbf{Equation 1.22}$$

The parameter G' is equal to $\frac{\sigma_0}{\gamma_0} \cos \delta$ and the parameter G'' is equal to $\frac{\sigma_0}{\gamma_0} \sin \delta$. The G' is defined as the storage modulus and is in phase with the shear strain, whereas G'' is defined as the loss modulus and is $\pi/2$ out of phase with the shear strain. Therefore, G' and G'' represent the elastic or the viscous behavior of viscoelastic materials, respectively.[64,68]

The evolution of G' and G'' as a function of the angular frequency is monitored using a frequency-dependent experiment, in which a constant shear strain is applied to the material while the oscillatory angular frequency is varied. A viscoelastic material behaves like a viscous fluid and exhibits large values of G'' at low oscillatory frequencies, whereas at high oscillatory frequencies it behaves like an elastic solid and exhibits large values of G'. In the case of chemically cross-linked polymer networks, the polymer chains lack the mobility of viscoelastic fluids, and, consequently, these materials behave like viscoelastic solids over the whole frequency range used and possess large values of G' and low values of G''. On the other hand, when the polymer networks are cross-linked using reversible bonds, they behave as elastic solids (large values of G') or as viscous fluids (large values of G''), depending on the angular frequency. The value of angular frequency at which the value of G' becomes equal to the value of G'' can be used to determine the lifetime of the reversible bond. Usually these values become equal at low values of the angular frequency, where the polymer chains have the appropriate time to move. However, if the reversible bonds are relatively stable, these materials behave as viscoelastic solids over the whole frequency range used, similarly with the chemically cross-linked polymer networks.[68]

Another type of rheology testing is the time-dependent experiment, in which the applied oscillatory frequency is constant, and the values of G' and G'' are recorded as a function of time. This type of experiment can be employed for the identification of the sol-to-gel transition. The gel formation time corresponding to the sol-to-gel transition, is taken as the time when the value of G' becomes equal to the value of G''.[69-71]

1.6 References

1. Alexandridis, P. Amphiphilic copolymers and their applications. *Current Opinion in Colloid & Interface Sci.* **1996**, *1*, 490-501.
2. Riess, G. Micellization of block copolymers. *Prog. Polym. Sci.* **2003**, *28*, 1107-1170.
3. Letchford, K.; Burt, H. A review of the formation and classification of amphiphilic block copolymer nanoparticulate structures: Micelles, nanospheres, nanocapsules and polymersomes. *Eur. J. Pharm. Biopharm.* **2007**, *65*, 259-269.
4. Owen, S. C.; Chan, D. P. Y.; Shoichet, M. S. Polymeric micelle stability. *Nano Today* **2012**, *7*, 53-65.
5. Mai, Y.; Eisenberg, A. Self-assembly of block copolymers. *Chem. Soc. Rev.* **2012**, *41*, 5969-5985.
6. Rösler, A.; Vandermeulen, W. M.; Klok, H. Advanced drug delivery devices via self-assembly of amphiphilic block copolymers. *Adv. Drug. Deliv. Rev.* **2012**, *64*, 270-279.
7. Karayianni, M.; Pispas, S. Self-assembly of amphiphilic block copolymers in selective solvents. *Fluorescence Studies of Polymer Containing Systems* **2016**, *16*, 27-63.
8. Holder, S. J.; Sommerdijk, N. A. J. M. New micellar morphologies from amphiphilic block copolymers and bicontinuous micelles. *Polym. Chem.* **2011**, *12*, 1018-1028.
9. Caccavo, D.; Cascone, S.; Lamberti, G.; Barba, A. A. Hydrogels: Experimental characterization and mathematical modelling of their mechanical and diffusive behaviour. *Chem. Soc. Rev.* **2018**, *47*, 2357-2373.
10. Hoffman, A. S. Hydrogels for biomedical applications. *Adv. Drug Deliv. Rev.* **2002**, *54*, 3-12.
11. Peppas, N. A.; Hilt; J. Z.; Khademhosseini, A.; Langer, R. Hydrogels in biology and medicine: From molecular principles to bionanotechnology. *Adv. Mater.* **2006**, *18*, 1345-1360.
12. Koetting, M. C.; Peters, J. T.; Steichen, S. D.; Peppas, N. A. Stimulus-responsive hydrogels: Theory, modern advances, and applications. *Mater. Sci. Eng. R* **2015**, *93*, 1-49.
13. Caló, E.; Khutoryanskiy, V. V. Biomedical applications of hydrogels: A review of patents and commercial products. *Eur. Polym. J.* **2015**, *65*, 252-267.

14. Patrickios, C. S.; Georgiou, T. K. Covalent amphiphilic polymer networks. *Curr. Opin. Colloid Inter. Sci.* **2003**, *8*, 76-85.
15. Erdodi, G.; Kennedy, J. P. Amphiphilic conetworks: Definition, synthesis, applications. *Prog. Polym. Sci.* **2006**, *31*, 1-18.
16. Patrickios, C. S. Polymer networks: Recent developments. *Macromol. Symp.* **2010**, *291-292*, 1-11.
17. Okumura Y.; Ito K. The polyrotaxane gel: A topological gel by figure-of-eight cross-links. *Adv. Mater.* **2001**, *7*, 485-487.
18. Haraguchi K.; Takehisa T. Nanocomposite hydrogels: A unique organic–inorganic network structure with extraordinary mechanical, optical, and swelling/de-swelling properties. *Adv. Mater.* **2002**, 14, 1120-1124.
19. Gong, J. P.; Katsuyama, Y.; Kurokawa, T.; Osada, Y. Double-network hydrogels with extremely high mechanical strength. *Adv. Mater.* **2003**, *15*, 1155-1158.
20. Gong, J. P. Why are double networks so tough? *Soft Matter* **2010**, *6*, 2583-2890.
21. Gong, J. P. Materials both tough and strong. *Science* **2014**, *344*, 161-162.
22. Kaneko, D.; Tada, T.; Kurokawa, T.; Gong, J. P.; Osada, Y. Mechanically strong hydrogels with ultra-low frictional coefficients. *Adv. Mater.* **2005**, *17*, 535-538.
23. Chen, Y. M.; Gong, J. P.; Tanaka, M.; Yasuda, K.; Yamamoto, S.; Shinomura, M.; Osada Y. Tuning of cell proliferation on tough gels by critical charge effect. *J. Biom. Mater. Research Part A* **2008**, *88*, 74-83.
24. Zhang, H.; Qadeer, A.; Mynarcik, D.; Chen, W. Delivery of rosiglitazone from an injectable triple interpenetrating network hydrogel composed of naturally derived materials. *Biomaterials* **2011**, *32*, 890-898.
25. Zhang, H.; Betz, A.; Qadeer, A.; Attinger, D.; Chen, W. Microfluid formation of monodispersed spherical microgels composed of triple-network crosslinking. *J. Appl. Polym. Sci.* **2011**, *121*, 3093-3100.
26. Argun, A.; Can, V.; Altun, U.; Okay, O. Nonionic double and triple network hydrogels of high mechanical strength. *Macromolecules* **2014**, *47*, 6430-6440.
27. Ducrot, E.; Chen, Y.; Bulters, M.; Sijbesma, R. P.; Creton, C. Toughening elastomers with sacrificial bonds and watching them break. *Science* **2014**, *344*, 186-189.
28. Tavsanli, B.; Can, V.; Okay, O. Mechanically strong triple network hydrogels based on hyaluronan and poly(*N*,*N*-dimethylacrylamide). *Soft Matter* **2015**, *11*, 8517-8524.

29. Hu, J.; Hiwatashi, K.; Kurokawa, T.; Liang, S. M.; Wu, Z. L.; Gong, J. P. Microgel-reinforced hydrogel films with high mechanical strength and their visible mesoscale fracture structure. *Macromolecules* **2011**, *44*, 7775-7781.
30. Hu, J.; Kurokawa, T.; Hiwatashi, K.; Nakajima, T.; Wu, Z. L.; Liang, S. M.; Gong, J. P. Structure optimization and mechanical model for microgel-reinforced hydrogels with high strength and toughness. *Macromolecules* **2012**, *45*, 5218-5228.
31. Nakajima, T.; Sato, H.; Zhao, Y.; Kawahara, S.; Kurokawa, T.; Sugahara, K.; Gong, J. P. A universal molecular stent method to toughen any hydrogels based on double network concept. *Adv. Funct. Mater.* **2012**, *22*, 4426-4432.
32. Nakajima, T.; Fukuda, Y.; Kurokawa, T.; Chung, U.; Gong, J. P. Synthesis and fracture process analysis of double network hydrogels with a well-defined first network. *ACS Macro Lett.*, **2013**, *2*, 518-521.
33. Nakajima, T.; Takedomi, N.; Kurokawa, T.; Furukawa, H.; Gong, J. P. A facile method for synthesizing free-shaped and tough double network hydrogels using physically crosslinked poly(vinyl alcohol) as an internal mold. *Polym. Chem.* **2010**, *1*, 693-697.
34. Dai, T.; Qing, X.; Lu, Y.; Xia, Y. Conducting hydrogels with enhanced mechanical strength. *Polymer* **2009**, *50*, 5236-5241.
35. Kishi, R.; Hiroki, K.; Tominafa T.; Sano, K.; Okuzaki, H.; Martinez, J. G.; Otero, T. F.; Osada, Y. Electro-conductive double-network hydrogels. *J. Polym. Sci., Part B: Polym. Phys*. **2012**, *50*, 790-796.
36. Kishi, R.; Kubota, K.; Miura, T.; Yamaguchi, T.; Okuzaki, H.; Osada, Y. Mechanically tough double-network hydrogels with high electronic conductivity. *J. Mater Chem. C* **2014**, *2*, 736-743.
37. Naficy, S.; Razal, J. M.; Spinks, G. M.; Wallace, G. G.; Whitten, P. G. Electrically conductive, tough hydrogels with pH sensitivity. *Chem. Mater.* **2012**, *24*, 3425-3433.
38. Shams Es-haghi, S.; Weiss, R. A. Fabrication of tough hydrogels from chemically cross-linked multiple nonionic networks. *Macromolecules* **2016**, *49*, 8980-8987.
39. Nakajima, T.; Furukawa, H.; Tanaka, Y.; Kurokawa, T.; Osada, Y.; Gong, J. P. True chemical structure of double-network hydrogels. *Macromolecules* **2009**, *42*, 2184-2189.

40. Shams Es-haghi, S.; Leonov, A. I.; Weiss, R. A. Deconstructing the double-network hydrogels: The importance of grafted chains for achieving toughness. *Macromolecules* **2014**, *47*, 4769-4777.
41. Shestakova, P.; Willem, R.; Vassileva, E. Elucidation of the chemical and morphological structure of double-network (DN) hydrogels by high-resolution magic angle spinning (HRMAS) NMR spectroscopy. *Chem. Eur. J.* **2011**, *17*, 14867-14877.
42. Brown H. R. A model of the fracture of double network gels. *Macromolecules* **2007**, *40*, 3815-3818.
43. Tanaka, Y. A local damage model for anomalous high toughness of double-network gels. *EPL* **2007**, *78*, 56005.
44. McCormick, C. L.; Nonaka, T.; Johnson, C. B. Water-soluble copolymers: 27. Synthesis and aqueous solution behaviour of associative acrylamide/*N*-alkylacrylamide copolymers. *Polymer* **1988**, *29*, 731-739.
45. Wan, W.; Pickett, P. D.; Savin, D. A.; McCormick, C. L. Structurally controlled "polysoaps" *via* RAFT copolymerization of AMPS and *n*-dodecylacrylamide for environmental remediation. *Polym. Chem.* **2014**, *5*, 819-827.
46. Miquelard-Garnier, G.; Demoures, S.; Creton, C.; Hourdet, D. Synthesis and rheological behavior of new hydrophobically modified hydrogels with tunable properties. *Macromolecules* **2006**, *39*, 8128-8139.
47. Miquelard-Garnier, G.; Creton, C.; Hourdet, D. Synthesis and viscoelastic properties of hydrophobically modified hydrogels. *Macromol. Symp.* **2007**, *256*, 189-194.
48. Luo, R.; Zhu, M.; Yuan, X.; Li, S. An autonomic and "off–on–off"-switchable polymer microreactor. *RSC Adv.* **2015**, *5*, 5598-5603.
49. Corbett, P. T.; Leclaire, J.; Vial, L.; West, K. R.; Wietor, J-L.; Sanders, J. K. M.; Otto, S. Dynamic combinatorial chemistry. *Chem. Rev.* **2006**, *106*, 3652-3711.
50. Kölmel, D. K.; Kool, E. T. Oximes and hydrazones in bioconjugation: Mechanism and catalysis. *Chem. Rev.* **2017**, *117*, 10358-10376.
51. Dirksen, A.; Hackeng, T. M.; Dawson, P. E. Nucleophilic catalysis of oxime ligation. *Angew. Chem. Int. Ed.* **2006**, *118*, 7743-7746.
52. Kalia, J.; Raines, R. T. Hydrolytic stability of hydrazones and oximes. *Angew. Chem. Int. Ed.* **2008**, *47*, 7523-7526.

53. Mukherjee, S.; Bapat, A. P.; Hill, M. R.; Sumerlin, B. S. Oximes as reversible links in polymer chemistry: Dynamic macromolecular stars. *Polym. Chem.* **2014**, *5*, 6923-6931.
54. Mukherjee, S.; Hill, M. R.; Sumerlin, B. S. Self-healing hydrogels containing reversible oxime crosslinks. *Soft Matter* **2015**, *11*, 6512-6161.
55. Grover, G. N.; Lam, J.; Nguyen, T. H.; Segura, T.; Maynard, H. D. Biocompatible hydrogels by oxime click chemistry. *Biomacromolecules* **2012**, *13*, 3013-3017.
56. Grover, G. N.; Braden, R. L.; Christman, K. L. Oxime cross-linked injectable hydrogels for catheter delivery, *Adv. Mater.* **2013**, *25*, 2937-2942.
57. Lin, F.; Yu, J.; Tang, W.; Zheng, J.; Defante, A.; Guo, K.; Wesdemiotis, C.; Becker, M. L. Peptide-functionalized oxime hydrogels with tunable mechanical properties and gelation behavior. *Biomacromolecules* **2013**, *14*, 3749-3758.
58. Young J. R.; Lovell, P. A. *Introduction to Polymers*; 2nd Edition, Chapman και Hall, London, 1991, Ch. 2 43-68.
59. Chiefari, J.; Chong, Y. K.; Ercole, F.; Krstina, J.; Jeffery, J.; Le, T. P. T.; Mayadunne, R. T. A.; Meijs, G. F.; Moad, C. L.; Moad, G.; Rizzardo, E.; Thang, S. H. Living free-radical polymerization by reversible addition–fragmentation chain transfer: The RAFT process. *Macromolecules* **1998**, *31*, 5559-5562.
60. Young J. R.; Lovell, P. A. *Introduction to Polymers*; 2nd Ed., Chapman and Hall, London, 1991, Ch. 3, 138-240.
61. Hamley, I. W. *The Physics of Block Copolymers*; 1st Ed., Oxford University Press, New York, 1998, Ch. 1, 1-23.
62. Meyer, E.; Hug, H. J.; Bennewitz, R. *Scanning Probe Microscopy – The Lab on a Tip;* 1st Ed., Springer-Verlag, Berlin, 2004, Ch. 3, 45-92.
63. Panagiotou, C. *Science and Technology of Polymers*; 2nd Ed., Pegasus, Thessaloniki, 2000, Ch. 12, 397-405.
64. Young J. R.; Lovell, P. A. *Introduction to Polymers*; 2nd Ed., Chapman and Hall, London, 1991, Ch. 5, 310-338.
65. Swallowe, G. M. *Mechanical Properties and Testing of Polymers*; 1st Ed., Springer Science+Business Media, Dordrecht, 1999.
66. Oliver, W. C.; Pharr, G. M. An improved technique for determining hardness and elastic modulus using load and displacement sensing indentation experiments. *J. Mater. Research* **1992**, *7*, 1564-1583.

67. Oliver, W. C.; Pharr, G. M. Measurement of hardness and elastic modulus by instrumented indentation: Advances in understanding and refinements to methodology. *J. Mater. Research* **2004**, *19*, 3-20.
68. Mc Crum, N. G.; Buckley C. P.; Bucknall, C. B. *Principles of Polymer Engineering;* 1st Ed., Oxford University Press, Oxford, 1995, Ch. 4, 117-170.
69. Tung, C.-Y. M.; Dynes, P. J. Relationship between viscoelastic properties and gelation in thermosetting systems. *J. Appl. Polym. Sci.* **1982**, *27*, 569-574.
70. Winter, H. H.; Chambon, F. Analysis of linear viscoelasticity of a cross-linking polymer at the gel point. *J. Rheol.* **1986**, *30*, 367-382.
71. Chambon, F.; Winter, H. H. Linear viscoelasticity at the gel point of a cross-linking PDMS with imbalanced stoichiometry. *J. Rheol.* **1987**, *31*, 683-697.

CHAPTER 2: EXPERIMENTAL SECTION

2.1 Chemical Reagents

Most of the chemical reagents used for this Doctoral Thesis were purchased from Sigma-Aldrich – Merck and used as received unless otherwise noted. The chemical reagents used for the preparation and characterization of the hydrophilic polymer network hydrogels and the amphiphilic polymer networks were: the hydrophilic *N*,*N*-dimethylacrylamide (DMAAm, 99%) monomer, the hydrophobic *N*-dodecylacrylamide (DDAAm) and diacetone acrylamide (DAAm, 99%) monomers, the hydrophilic *N*,*N*′-methylenebisacrylamide (MBAAm, 99%) and the hydrophilic degradable *N*,*N*′-(1,2-dihydroxy-ethylene)bisacrylamide (DHEBA, 97%) cross-linkers, the hydrophobic 1,6-hexanediol diacrylate (HDDA, 80%) cross-linker, the 2,2′-azobis(isobutyronitrile) (AIBN, 95%) thermal initiator, the 2-oxoglutaric acid (OXG ≥99%) and 2,2-dimethoxy-2-phenylacetophenone (DMPAP, 99%) photoinitiators, calcium hydride (CaH_2, 90-95%) drying agent, the 2,2-diphenyl-1-picrylhydrazyl hydrate (DPPH, 95%) radical inhibitor, adipic acid dihydrazide (≥98%), aniline (99%), *O*-benzylhydroxylamine hydrochloride (BzHA, 99%), ethanol (EtOH, 96%), glacial acetic acid (CH_3CO_2H, ≥99%), *O*,*O*′-1,3-propanediylbis(hydroxylamine) dihydrochloride (PDH, 98%), sodium acetate (CH_3CO_2Na, ≥99%), sodium periodate ($NaIO_4$, ≥99.8%), and trifluoroacetic acid (TFA, 99%).

The chemical reagents used for the synthesis of the DDAAm monomer were acryloyl chloride (97%), 1-dodecylamine (98%), acetone (≥99%), tetrahydrofuran (THF, purchased from Scharlau, Spain), and triethylamine (TEA, ≥99%, purchased from Scharlau, Spain).

The chemical reagents used for the synthesis of the two chain transfer agents (CTA) for the reversible addition-fragmentation chain transfer (RAFT) polymerizations were 2-bromo-2-methylpropionic acid (BMPA, 98%), carbon disulfide (CS_2, ≥99%), dichloromethane (DCM, 99%), *N*,*N*′-dicyclohexylcarbodiimide (DCC, ≥99%), 4-dimethylaminopyridine (DMAP, ≥99%), 1,4-dioxane (anhydrous, 99.8%), 1-dodecanethiol (≥98%), ethyl acetate (EtOAc, 99%), *n*-hexane (≥97%), hydrochloric acid (HCl, ≥37%), anhydrous magnesium sulphate ($MgSO_4$, ≥99.5%), methanol (MeOH, ≥99.8%), poly(ethylene glycol) (PEG, M_n =

2050 g mol^{-1}), potassium phosphate tribasic (K_3PO_4, ≥98%), and sodium chloride (NaCl, ≥99.5%).

All the RAFT polymerizations were performed in toluene (anhydrous, 99.8%), while *N*,*N*-dimethylformamide (DMF, 99.8%) and deionized water (Millipore grade) were used as the solvents for the free radical photopolymerizations.

Finally, deuterated chloroform ($CDCl_3$, 99.8%), deuterated dimethyl sulfoxide (d_6-DMSO, 99.8%), and deuterated water (D_2O, 99.9%), were used as solvents for NMR spectroscopy, while THF was used as the solvent for gel permeation chromatography (GPC).

2.2 Purification of Monomers, Solvents, Cross-linkers and Initiators

The DMAAm monomer was passed through a basic alumina (Al_2O_3) column to remove the radical inhibitors and any acidic impurities. To remove any traces of moisture and to prevent any undesired radical polymerization, CaH_2 and DPPH, respectively, were added to acryloyl chloride and DMAAm. Then, the flasks were left under continuous stirring at room temperature for three days and stored in the refrigerator until further use. Acryloyl chloride and DMAAm were vacuum-distilled just prior to use for the removal of the radical inhibitors and any impurities, while the HDDA cross-linker was passed through a basic alumina column just prior to use. The same procedure was also followed for acetone, DCM, THF, toluene and TEA, but without the addition of DPPH. The AIBN thermal initiator and the MBAAm cross-linker were purified by recrystallization from ethanol. Finally, for the removal of any traces of moisture, PEG was freeze-dried from 1,4-dioxane prior to the reaction for the synthesis of PEG DMPA.

2.3 Synthesis of Monomer and Chain Transfer Agents

2.3.1 Synthesis of the *N*-Dodecylacrylamide (DDAAm) Monomer

The synthesis of the DDAAm monomer was performed according to the procedure reported by McCormick et al.,[1] from the acylation of 1-dodecylamine with acryloyl chloride. To this end, 15 g (80.9 mmol, 1 eq.) of 1-dodecylamine and 75 mL of THF (20%

w/v) were transferred into a two-necked round-bottomed flask equipped with a magnetic stirring bar and a dropping funnel. Then, 12.4 mL (9 g, 89 mmol, 1.1 eq.) of TEA was added in the solution and the flask was immersed in an ice bath at 0 ^{o}C under continuous stirring. Afterward, 8.06 g (89 mmol, 1.1 eq.) of acryloyl chloride was placed in the dropping funnel and dissolved in 40 mL of THF (20% w/v), and this solution was added dropwise in the reaction flask over a period of 50 min. When the addition was completed, the flask was removed from the ice bath and was left overnight at room temperature under continuous stirring. The next day, the reaction mixture was filtered in order to remove the TEA hydrochloride salt byproduct of the amidation reaction, and, subsequently, THF was removed from the solution using a rotary evaporator. The 1-dodecylamine conversion to amide was determined using ^{1}H NMR spectroscopy (conversion=100%). The final product was obtained as a white powder after two recrystallizations (final yield=80%) from acetone and drying in a vacuum oven, while ^{1}H and ^{13}C NMR spectroscopy were used for the verification of its purity. Finally, the DDAAm monomer was stored in the refrigerator until further use.

2.3.2 Synthesis of the 2-(Dodecylthiocarbonothioylthio)-2-methylpropanoic Acid (DMPA) Chain Transfer Agent (CTA)

The 2-(dodecylthiocarbonothioylthio)-2-methylpropanoic acid (DMPA) RAFT chain transfer agent (CTA) was synthesized according to the method described by Wan and Zhang.[2] To this end, 8.4 g (39.6 mmol, 1.1 eq.) of K_3PO_4 and 8.0 g (39.6 mmol, 1.1 eq.) of 1-dodecanethiol were first transferred into a round-bottomed flask equipped with a magnetic stirring bar and containing 100 mL of acetone. After 30 min of stirring, 6.5 mL (8.2 g, 108 mmol, 3 eq.) of CS_2 was added in the reaction flask, and, finally, after another 30 min of stirring, 6.0 g (36 mmol, 1 eq.) of BMPA was added. The reaction was left overnight at room temperature under continuous stirring, and then the reaction mixture was analyzed using ^{1}H NMR spectroscopy to verify the structure of the desired product and to calculate the conversion of the reaction (conversion=75%). Then, 100 mL of DCM was added into the reaction flask, together with 50 mL of a 1 M aqueous solution of HCl, in order to solubilize the obtained yellow solid in the organic phase. This mixture was transferred into a separating funnel and the aqueous phase was discarded. Subsequently,

the organic phase was extracted with 1 M HCl (2 × 50 mL), water (3 × 50 mL) and brine (3 × 50 mL). After the dehydration of the organic phase with $MgSO_4$, the mixture was filtered, and DCM was removed using a rotary evaporator. The crude product was purified via column chromatography on silica gel using an *n*-hexane : ethyl acetate mixture at a ratio of 9:1. The pure product was obtained as a yellow powder after drying in a vacuum oven, and it was finally stored in the refrigerator (final yield=60%). The purity of DMPA was verified using ^{1}H and ^{13}C NMR spectroscopy.

2.3.3 Synthesis of the Poly(ethylene glycol) Bis[2-(dodecylthiocarbonothioylthio)-2-methylpropionate] (PEG DMPA) Bifunctional CTA

The poly(ethylene glycol) bis[2-(dodecylthiocarbonothioylthio)-2-methylpropionate] (PEG DMPA) difunctional CTA was synthesized following the procedure reported in the literature,[3] from the bisesterification reaction of PEG diol (M_n = 2050 g mol^{-1}) with DMPA in the presence of DCC activator and DMAP catalyst. To this end, 5.0 g (13.70 mmol, 2.44 eq.) of DMPA, and 0.17 g (1.37 mmol, 0.10 eq. to DMPA) of DMAP were first transferred into a round-bottomed flask equipped with a magnetic stirring bar and dissolved in 20.6 mL of DCM (25% w/v). In a second flask, 11.52 g (5.62 mmol, 1.00 eq.) of the PEG diol was dissolved in 46 mL of DCM (25% w/v), and the resulting solution was added to the flask containing DMPA and DMAP. Then, in another flask, 3.11 g (15.1 mmol, 1.10 eq. to DMPA) of DCC was dissolved in 12.4 mL of DCM (25% w/v), and this solution was added dropwise in the previous solution. The reaction was left overnight at room temperature under continuous stirring, after which the produced dicyclohexylurea byproduct was removed by filtration. Then, DCM was removed using a rotary evaporator and the remaining orange solid was characterized using ^{1}H NMR spectroscopy to verify the structure of the desired product and calculate the conversion of the reaction (conversion=75%). The PEG DMPA was isolated as an orange solid after its purification with column chromatography on silica gel using a DCM : MeOH mixture at a ratio of 95:5. The PEG DMPA was then dried under vacuum (final yield=65%), characterized using ^{1}H and ^{13}C NMR spectroscopy for the verification of its structure and purity, and it was finally stored in the refrigerator until further use.

2.4 Synthesis of the Linear Polymers, the Polymer Network Hydrogels and the Amphiphilic Polymer Networks

2.4.1 Degradable Hydrogels Prepared Using Free Radical Photopolymerization

2.4.1.1 Preparation of the Single Network (SN) Hydrogels

The single network (SN) hydrogels were prepared in one step using free radical photopolymerization. To this end, 0.496 g (5 mmol) of DMAAm was first transferred into a glass vial and dissolved in 5 g of water. Then, 30.8 mg (0.2 mmol, 4 mol% with respect to monomer) of MBAAm, and 0.7 mg (5 μmol, 0.1 mol% with respect to monomer) of OXG photoinitiator were added into the resulting solution. The same procedure was followed for the preparation of the SN hydrogel containing the DHEBA cross-linker, by the addition of 40 mg (0.2 mmol, 4 mol% with respect to monomer) of DHEBA in the monomer/photoinitiator aqueous solution. After the complete dissolution of the reagents, the solutions were degassed via nitrogen bubbling, and, finally, the glass vials were placed under a commercial UV (365 nm) lamp assembly of four UV lamps of total power of 36 W from Vivo Ltd. model NW107RG-T3296, and left to polymerize for 4 h. This procedure led to the preparation of two SN hydrogels, the DMAAm-MBAAm 1-4 and the DMAAm-DHEBA 1-4 hydrogels (1 corresponds to the DMAAm monomer concentration of 1 M, and 4 to the cross-linker mol percentage in the hydrogels with respect to the DMAAm monomer of 4 mol%).

2.4.1.2 Preparation of the DMAAm/DMAAm Double-Network (DN) Hydrogels

The double-network (DN) hydrogels were prepared in two steps using free radical photopolymerization. To this end, the DMAAm-MBAAm 1-4 and DMAAm-DHEBA 1-4 SN hydrogels were prepared using the above-mentioned procedure, and each of these gels was divided into two pieces, each possessing a mass of ~2.5 g. Then, one piece from each gel was immersed in 15 mL of an aqueous solution of 2 M DMAAm, containing 0.1 mol% MBAAm cross-linker, and 0.1 mol% OXG photoinitiator, both with respect to monomer. The other piece was also immersed in 15 mL of an aqueous solution of 2 M DMAAm, but containing 0.1 mol% DHEBA cross-linker and 0.1 mol% OXG, also with respect to

monomer. The systems of the SN gels swollen in the above-mentioned monomer/cross-linker/photoinitiator aqueous solutions were stored in a refrigerator to prevent any thermal radical polymerization and were allowed to reach swelling equilibrium for 4 days. Then, the excess aqueous solution was removed from the swollen hydrogels and the hydrogels were weighed three times. Finally, the swollen hydrogels were placed under the UV lamp assembly and left to polymerize for 4 h, resulting in the formation of the four different DN hydrogels: DMAAm-MBAAm 1-4/DMAAm-MBAAm 2-0.1, DMAAm-MBAAm 1-4/ DMAAm-DHEBA 2-0.1, DMAAm-DHEBA 1-4/DMAAm-MBAAm 2-0.1, and DMAAm-DHEBA 1-4/DMAAm-DHEBA 2-0.1.

2.4.1.3 Preparation of the "Inert" DMAAm/OXG SN and "Deactivated" DMAAm/OXG/ DMAAm DN Hydrogels

The "inert" DMAAm/OXG SN hydrogels were obtained in two steps, while the "deactivated" DMAAm/OXG/DMAAm DN hydrogels were obtained in three steps. To this end, after the preparation of the DMAAm-MBAAm 1-4 and DMAAm-DHEBA 1-4 SN hydrogels using the above-mentioned procedure, each of these gels was again divided into two pieces ($m \approx 2.5$ g) and each immersed in 15 mL of an aqueous solution of 0.1 M OXG photoinitiator. The hydrogel/OXG solution systems were stored in a refrigerator and allowed to reach swelling equilibrium for 4 days. Then, the excess solution was removed from the swollen hydrogels, and the hydrogels were weighed three times and placed under the UV lamp assembly for 4 h. This resulted in the preparation of the "inert" DMAAm/OXG hydrogels, and, in particular, the DMAAm-MBAAm 1-4/OXG and the DMAAm-DHEBA 1-4/OXG SN hydrogels. Afterward, these gels were divided into two pieces and separately immersed in an aqueous solution of 2 M DMAAm, containing either 0.1 mol% MBAAm or DHEBA cross-linkers, and 0.1 mol% OXG photoinitiator, with all percentages again being with respect to monomer. The hydrogel/monomer/cross-linker/photoinitiator systems were again stored in a refrigerator and allowed to reach swelling equilibrium for 4 days. Subsequently, the excess solution was removed, and the swollen hydrogels were weighed three times and were left to polymerize under the UV lamp for 4 h. This procedure resulted in the four "deactivated" DN hydrogels, with the structures DMAAm-MBAAm 1-4/OXG/DMAAm-MBAAm 2-0.1, DMAAm-MBAAm 1-

4/OXG/DMAAm-DHEBA 2-0.1, DMAAm-DHEBA 1-4/OXG/DMAAm-MBAAm 2-0.1, and DMAAm-DHEBA 1-4/OXG/DMAAm-DHEBA 2-0.1.

2.4.2 Multiple Network Hydrogels Prepared Using Free Radical Photopolymerization

The multiple network hydrogels were obtained after five sequential photopolymerization steps. First, the DMAAm-MBAAm 1-4 SN hydrogel was prepared, via the UV polymerization of a 1 M aqueous DMAAm solution, containing 4 mol% MBAAm cross-linker and 0.1 mol% OXG photoinitiator, with the percentage referring to the DMAAm monomer. In particular, 0.991 g (10 mmol) of DMAAm was placed in a glass vial and dissolved in 10 g of water. Then, 61.6 mg (0.4 mmol, 4 mol% with respect to the monomer) of MBAAm cross-linker and 1.5 mg (10 μmol, 0.1 mol% again with respect to the monomer) of OXG photoinitiator were added to the monomer solution. After the complete dissolution of the reagents, the solution was degassed via nitrogen bubbling, and the vial was placed under the UV lamp assembly, and left to polymerize for 4 h. Afterward, the gel was divided in five pieces which were separately immersed in aqueous solutions of DMAAm monomer with different concentrations, 1, 2, 3, 4 and 5 M, containing 0.1 mol% MBAAm cross-linker, and 0.1 mol% OXG photoinitiator. The hydrogels were stored in the refrigerator for 3-4 days until swelling equilibrium was reached. The excess aqueous monomer solution was removed, and the swollen hydrogels were weighed three times. Then, the hydrogels were placed under the UV lamp assembly for 4 h, leading to the formation of the five different DN hydrogels DMAAm-MBAAm 1-4 / DMAAm-MBAAm *x*-*y*, with x = 1, 2, 3, 4 and 5, and y = 0.1. These DN hydrogels were immersed again in aqueous solutions of DMAAm monomer with the same concentration as in the previous step (*i.e.*, the DMAAm-MBAAm 1-4/DMAAm-MBAAm 2-0.1 DN hydrogel was immersed in a 2 M DMAAm solution, etc.) also containing 0.1 mol% MBAAm and 0.1 mol% OXG. Once again, after reaching swelling equilibrium, the aqueous solution was removed from each hydrogel, and the swollen hydrogels were weighed and placed under the UV lamp assembly for 4 h, in order to prepare the triple network (TN) hydrogels. The same procedure was repeated for two more times until the successful synthesis of the quintuple (five-fold) network hydrogels.

2.4.3 Randomly Cross-linked Copolymer Networks Prepared Using Free Radical Photopolymerization

The randomly cross-linked copolymer networks were prepared in one step using free radical photopolymerization. To this end, the appropriate amounts of DMAAm and DDAAm monomers with a total mass of 1 g were combined at various ratios, 100:0, 95:5, 90:10, 80:20, 70:30, 60:40 and 50:50, respectively, and dissolved in 5 mL of DMF to reach a final monomer concentration of 20% w/v. Then, the appropriate amounts of HDDA, 1 or 5 mol%, and DMPAP, 0.1 mol%, both with respect to the total moles of monomers, were transferred into the resulting solution. After the complete dissolution of the reagents and the degassing of the solutions via nitrogen bubbling, the vials were placed under the UV lamp assembly and left to polymerize for 4 h, leading to the formation of a total number of eleven randomly cross-linked copolymer networks. It is worth mentioning that when the HDDA amount was 1 mol% (with respect to the total number of moles of monomers) and the DDAAm content higher than 20 mol%, the gels did not form. The copolymer networks were immersed in a large volume of DMF to remove any soluble species, and DMF was replaced every 3 days for two weeks. The copolymer networks were then completely dried in a vacuum oven at 60 ^{o}C for 48 h, and were finally stored at room temperature until further use. The randomly cross-linked copolymer networks prepared using 1 mol% (with respect to the total number of moles of monomers) of HDDA, were also prepared in cylindrical tubes with a diameter of 5 mm using the afore mentioned procedure at a final monomer concentration of 30% w/v, in order to achieve the formation of gels for all DDAAm contents. After their formation, the gels were removed from the tubes and were allowed to equilibrate in water for one week, while water was replaced on a daily basis to remove any soluble species.

2.4.4 Linear Amphiphilic Diblock Copolymers Prepared Using RAFT Polymerization

2.4.4.1 Synthesis of the $DMAAm_{100}$-*b*-$DDAAm_x$ Diblock Copolymers

The P(DMAAm)-*b*-P(DDAAm) diblock copolymers were obtained after two sequential RAFT polymerization steps. Initially, to prepare the poly(DMAAm) macro-CTA, a solution consisting of 0.50 g (5.04 mmol, 100 eq.) of DMAAm, 18.4 mg (0.050 mmol, 1

eq.) of the DMPA CTA, 5.2 mg (0.032 mmol, 0.625 eq.) of AIBN. and 1.15 g of toluene so as to reach a monomer concentration of 30% w/w, was transferred into a 10 mL Schlenk flask equipped with a magnetic stirring bar and a rubber septum. The polymerization mixture was degassed by three freeze-pump-thaw cycles and placed in an oil bath thermostated at 65 ^{o}C for 18-20 h, after which DMAAm conversion to polymer reached 99-100%. Then, a solution consisting of the appropriate amount of DDAAm, e.g., 0.12 g (0.50 mmol, 10 eq.) for the preparation of the DMAAm$_{100}$-*b*-DDAAm$_{10}$ diblock copolymer, and the necessary amount of toluene, 0.28 g, in order to yield a final total solids concentration of 30% w/w, was transferred into another 10 mL Schlenk flask. The resulting solution was degassed by three freeze-pump-thaw cycles, and it was then transferred, using a glass syringe, into the first 10 mL Schlenk flask containing the poly(DMAAm) macro-CTA. The polymerization of DDAAm was allowed to proceed for 22-24 h, after which its conversion to polymer reached 85-99%. The produced diblock copolymers were diluted with THF, precipitated in *n*-hexane or acetonitrile, dried under vacuum, and stored at room temperature until further use.

2.4.4.2 Synthesis of the DDAAm$_{20}$-*b*-DMAAm$_x$ Diblock Copolymers

The P(DDAAm)-*b*-P(DMAAm) diblock copolymers were again obtained after two sequential RAFT polymerization steps. Initially, for the preparation of the poly(DDAAm) macro-CTA, a solution consisting of 0.50 g (2.09 mmol, 20 eq.) of DDAAm, 38.1 mg (0.104 mmol, 1 eq.) of DMPA, 10.7 mg (0.065 mmol, 0.625 eq.) of AIBN, and 1.15 g of toluene so as to reach a monomer concentration of 30% w/w, was transferred into a 15 mL Schlenk flask. The polymerization mixture was degassed by three freeze-pump-thaw cycles and the Schlenk flask was immersed in an oil bath thermostated at 65 ^{o}C for 18-20 h, after which period the DDAAm conversion to polymer was quantitative. Then, the appropriate amounts of DMAAm, e.g., 0.518 g (5.22 mmol, 50 eq.) for the preparation of the DDAAm$_{20}$-*b*-DMAAm$_{50}$ diblock copolymer, and toluene, 1.2 g, were transferred into a 10 mL Schlenk flask. The DMAAm solution in toluene was again degassed, and transferred using a glass syringe into the 15 mL Schlenk flask containing the poly(DDAAm) macro-CTA. The polymerization of DMAAm was left to proceed for 22-24 h, after which period its conversion to polymer reached 90-100%. The produced diblock

copolymers were diluted with THF, precipitated in acetonitrile or *n*-hexane, dried in a vacuum oven for 24 h, and stored at room temperature until further use.

2.4.5 Amphiphilic Polymer Conetworks (APCNs) Prepared Using RAFT Polymerization

The preparation of the amphiphilic polymer conetworks (APCNs) was accomplished after three sequential RAFT polymerizations. First, in order to prepare the poly(DMAAm)-PEG-poly(DMAAm) macro-CTA, a solution consisting of 1.00 g (10.10 mmol, 100 eq.) of DMAAm, 0.282 g (0.1 mmol, 1 eq.) of PEG DMPA, 10.4 mg (0.063 mmol, 0.625 g) of AIBN, and 1.22 g of toluene so as to reach a monomer concentration of 45% w/w, was transferred into a 15 mL Schlenk flask. After degassing of the polymerization mixture, the Schlenk flask was immersed in an oil bath thermostated at 65 ^{o}C for 17-18 h in order for the DMAAm conversion to reach 99-100%. Then, the appropriate amounts of DDAAm, e.g., 1.06 g (4.44 mmol, 44 eq.) for the DDAAm$_{22}$-*b*-DMAAm$_{50}$-*b*-EG$_{46}$-*b*-DMAAm$_{50}$-*b*-DDAAm$_{22}$ pentablock terpolymer, and toluene, 1.3 g, so as to reach a monomer concentration of 45% w/w, were transferred into a 10 mL Schlenk flask. After degassing the resulting solution, the mixture was transferred through a glass syringe into the 15 mL Schlenk flask containing the DMAAm$_{50}$-*b*-EG$_{46}$-*b*-DMAAm$_{50}$ triblock copolymer. After the complete polymerization of DDAAm that required 23 h, the appropriate amounts of HDDA cross-linker, e.g., 0.20 g (0.87 mmol, 8.6 eq., 6 mol% with respect to the total number of monomer repeating units in the pentablock terpolymers) for the HDDA$_{4.3}$-*b*-DDAAm$_{22}$-*b*-DMAAm$_{50}$-*b*-EG$_{46}$-*b*-DMAAm$_{50}$-*b*-DDAAm$_{22}$-*b*-HDDA$_{4.3}$ polymer conetwork, and toluene, 0.24 g, so as to reach a cross-linker concentration of 45% w/w, were transferred through a glass syringe into the polymerization mixture. The polymerization of HDDA for the formation of polymer networks was allowed to proceed for 24 h. Finally, the gels were immersed in a large volume of toluene in order to remove any soluble species; the toluene was replaced every three days for two weeks. The gels were then dried in a vacuum oven at 50 ^{o}C for 24 h and stored at room temperature until further use.

2.4.6 Oxime Cross-linked APCNs Based on End-linked Pentablock Terpolymers Prepared Using RAFT Polymerization

2.4.6.1 Synthesis of the $DMAAm_{50}$-*b*-EG_{46}-*b*-$DMAAm_{50}$ Triblock Copolymer

A P(DMAAm)-*b*-PEG-*b*-P(DMAAm) triblock copolymer was synthesized using RAFT polymerization. To this end, a solution consisting of 10.0 g (101 mmol) of DMAAm, 2.825 g (1.01 mmol) of PEG DMPA, 103.6 mg (0.63 mmol) of AIBN, and 23.3 g of toluene so as to reach a monomer concentration of 30% w/w, was transferred to a 50 mL Schlenk flask. After degassing the polymerization mixture, the Schlenk flask was immersed in an oil bath thermostated at 65 ^{o}C for 18 h, after which period the DMAAm conversion to polymer reached 100%. The produced $DMAAm_{50}$-*b*-EG_{46}-*b*-$DMAAm_{50}$ triblock copolymer was diluted with THF, precipitated in *n*-hexane, dried under vacuum for 24 h, and stored at room temperature.

2.4.6.2 Synthesis of the $DAAm_x$-*b*-$DMAAm_{50}$-*b*-EG_{46}-*b*-$DMAAm_{50}$-*b*-$DAAm_x$ Pentablock Terpolymers using Stepwise RAFT Polymerization

A solution consisting of 2.0 g (0.157 mmol, 1 eq.) of the $DMAAm_{50}$-*b*-EG_{46}-*b*-$DMAAm_{50}$ triblock copolymer, 16.2 mg (0.098 mmol, 0.625 eq.) of AIBN, and the appropriate amounts of diacetone acrylamide (DAAm), e.g., 0.64 g (3.78 mmol, 24 eq.) for the $DAAm_{12}$-*b*-$DMAAm_{50}$-*b*-EG_{46}-*b*-$DMAAm_{50}$-*b*-$DAAm_{12}$ pentablock terpolymer, and 6.15 g of toluene, so as to reach a final solids concentration of 30% w/w, was transferred into a 25 mL Schlenk flask. After degassing the mixture, the Schlenk flask was placed in an oil bath thermostated at 65 ^{o}C for 18 h, after which period the DAAm conversion to polymer reached 99-100%. The produced pentablock terpolymers were diluted with THF, precipitated in *n*-hexane, dried under vacuum, and stored at room temperature.

2.4.6.3 Synthesis of the $DMAAm_{100}$-*co*-$DAAm_x$ Random Copolymers

The $DMAAm_{100}$-*co*-$DAAm_x$ random copolymers were synthesized in one step using RAFT polymerization. To this end, 2.00 g (20.2 mmol, 100 eq.) of DMAAm, 73.6 mg (0.202 mmol, 1 eq.) of DMPA, 20.7 mg (0.126 mmol, 0.625 eq.) of AIBN, and the

appropriate amounts of DAAm, e.g., 0.34 g (2.02 mmol, 10 eq.) for the $DMAAm_{100}$-*co*-$DAAm_{10}$ random copolymer, and 5.44 g of toluene so as to reach a monomer concentration of 30% w/w, were transferred into a 25 mL Schlenk flask. The polymerization mixture was degassed and the Schlenk flask was immersed in an oil bath thermostated at 65 ^{o}C for 18 h, after which period the conversion to polymer of both DMAAm and DAAm reached 100%. The produced random copolymers were precipitated in *n*-hexane, dried in a vacuum oven for 24 h, and stored at room temperature.

2.4.6.4 Reaction of a Pentablock Terpolymer with a Monofunctional Aminooxy Compound

The post-polymerization modification reaction of the $DAAm_{16}$-*b*-$DMAAm_{50}$-*b*-EG_{46}-*b*-$DMAAm_{50}$-*b*-$DAAm_{16}$ pentablock terpolymer with *O*-benzylhydroxylamine hydrochloride (BzHA) was performed in EtOH at a total solids concentration of 10% w/v in the presence of TEA, according to the procedure reported by Sumerlin's group.[4] To this end, 50.0 mg (2.76 μmol, 1 eq.) of $DAAm_{16}$-*b*-$DMAAm_{50}$-*b*-EG_{46}-*b*-$DMAAm_{50}$-*b*-$DAAm_{16}$ pentablock terpolymer was dissolved in 0.50 mL of EtOH and the resulting solution was transferred into a round-bottomed flask equipped with a magnetic stirrer. Then, 28.2 mg (176.6 μmol, 2 eq. to the DAAm monomer repeating units) of BzHA was separately dissolved in 0.28 mL of EtOH, followed by the addition of 74 μL (53.6 mg, 530 μmol, 3 eq. to BzHA) of TEA. The resulting solution was added dropwise to the polymer-solution and the reaction was left under continuous stirring at room temperature for 4 days. Subsequently, the crude reaction was characterized using ^{1}H NMR spectroscopy for the determination of the degree of functionalization of the pentablock terpolymer.

2.4.6.5 Formation of the Oxime Cross-linked APCNs in Aqueous Buffer Solutions with Varying pH and Varying Stoichiometry of the Reaction

The preparation of the oxime cross-linked APCNs was performed using a constant final total solids concentration of 10% w/v in aqueous buffer solutions of varying pH at a constant stoichiometry of the reaction, or in aqueous buffer solution of pH 4.5 and varying stoichiometry of the reaction, in order to find the optimum experimental conditions. The aqueous buffer solutions were prepared using CH_3CO_2H and CH_3CO_2Na at a combined

concentration of 200 mM. The pH value of the aqueous buffer solutions acquired values of 3.0, 4.0, 4.5, 5.0, 6.0, 6.5, and 7.0, while the molar ratio of the ketone to aminooxy units acquired values of 2:1, 1.2:1, 1:1, 1:1.2, and 1:2. For example, when the pH of the buffer solution was varied and the stoichiometry of the reaction was constant, 1:1, 28 mg (1.9 μmol, 1 eq.) of the $DAAm_6$-*b*-$DMAAm_{50}$-*b*-EG_{46}-*b*-$DMAAm_{50}$-*b*-$DAAm_6$ pentablock terpolymer and 2.0 mg (11.4 μmol, 6 eq.) of the *O*,*O*′-1,3-propanediylbis(hydroxylamine) dihydrochloride (PDH) cross-linker were separately dissolved in 260 and 40 μL of the aqueous buffer, respectively. Then, the two separate solutions were mixed together in a glass vial at room temperature, resulting in the formation of the oxime cross-linked APCNs. The formation time of the gel was determined by the tube inversion method, taken as the time when the solution could no longer flow. The same procedure was also followed when the pH of the aqueous buffer solution was constant, 4.5, and the stoichiometry of the reaction was varied. When the molar ratio of the ketone to hydroxylamine units was equal to 1:1.2, 27.6 mg (1.87 μmol, 1 eq.) of the $DAAm_6$-*b*-$DMAAm_{50}$-*b*-EG_{46}-*b*-$DMAAm_{50}$-*b*-$DAAm_6$ pentablock terpolymer and 2.4 mg (13.5 μmol, 7.2 eq.) of the PDH cross-linker were separately dissolved in 260 and 40 μL of the aqueous buffer of pH 4.5, respectively, and mixed together in a glass vial at room temperature for the formation of the APCN.

2.4.6.6 Preparation of the Oxime Cross-linked APCNs using Different Total Solids Concentrations

All the reactions between the $DAAm_x$-*b*-$DMAAm_{50}$-*b*-EG_{46}-*b*-$DMAAm_{50}$-*b*-$DAAm_x$ pentablock terpolymers and PDH cross-linker were performed using the above-mentioned procedure and using the optimum experiment conditions, *i.e.*, aqueous buffer solution of pH 4.5 and a molar ratio of ketone to hydroxylamine units of 1:1, and at three different final total solids concentrations, 10.0, 12.5, and 15.0% w/v. In contrast, in the case of the $DAAm_{25}$-*b*-$DMAAm_{50}$-*b*-EG_{46}-*b*-$DMAAm_{50}$-*b*-$DAAm_{25}$ pentablock terpolymer, the reaction was performed in a mixture of ethanol and aqueous buffer solution of pH 4.5 (0.4 M) at a 1:2 volume ratio.

2.4.6.7 Preparation of the Randomly Oxime Cross-linked Copolymer Networks

The same procedure was also followed for the preparation of the copolymer networks randomly cross-linked via oxime bonds using the optimum experimental conditions and by varying the final total solids concentration from 10 to 15% w/v. For example, 27.9 mg (2.33 μmol, 1 eq.) of the $DMAAm_{100}$-*co*-$DAAm_{10}$ random copolymer and 2.1 mg (11.7 μmol, 5 eq.) of PDH were separately dissolved in 260 and 40 μL of aqueous buffer solution of pH 4.5, and the solutions were mixed together in a glass vial at room temperature for the formation of the gel.

2.4.6.8 Preparation of the Oxime Cross-linked APCNs in an Organic Solvent

The formation of the oxime cross-linked APCNs was also performed in methanol, but using the pentablock terpolymers with the highest number of DAAm repeating units, 24, 32, and 50, *i.e.*, $DAAm_{12}$-*b*-$DMAAm_{50}$-*b*-EG_{46}-*b*-$DMAAm_{50}$-*b*-$DAAm_{12}$, $DAAm_{16}$-*b*-$DMAAm_{50}$-*b*-EG_{46}-*b*-$DMAAm_{50}$-*b*-$DAAm_{16}$ and $DAAm_{25}$-*b*-$DMAAm_{50}$-*b*-EG_{46}-*b*-$DMAAm_{50}$-*b*-$DAAm_{25}$. To this end, the reactions between the pentablock terpolymers and PDH were performed at a final total solids concentration of 15% w/v at the stoichiometric ratio, and in the presence of 2 equivalents of TEA with respect to PDH to neutralize the aminooxy groups in PDH. In particular, 31.9 mg (1.90 μmol, 1 eq.) of the $DAAm_{12}$-*b*-$DMAAm_{50}$-*b*-EG_{46}-*b*-$DMAAm_{50}$-*b*-$DAAm_{12}$ pentablock terpolymer, and 4.1 mg (22.8 μmol, 12 eq.) of PDH were separately dissolved in 200 and 33.6 μL of methanol, respectively. Then, 6.4 μL (45.7 μmol, 24 eq.) of TEA was added into the PDH-solution and the two separate solutions were mixed together in a glass vial at room temperature, leading to the formation of the gel.

2.4.7 Oxime Cross-linked APCNs Based on End-linked Heptablock Quaterpolymers Consisting of DMAAm, DDAAm, and DAAm, Prepared Using RAFT Polymerization

2.4.7.1 Synthesis of the DDAAm$_x$-*b*-DMAAm$_{50}$-*b*-EG$_{46}$-*b*-DMAAm$_{50}$-*b*-DDAAm$_x$ Pentablock Terpolymers Using Stepwise RAFT Polymerization

A solution consisting of 2.00 g (0.157 mmol, 1 eq.) of DMAAm$_{50}$-*b*-EG$_{46}$-*b*-DMAAm$_{50}$ triblock copolymer, 16.20 mg (0.098 mmol, 0.625 eq.) of AIBN, and the appropriate amounts of DDAAm, e.g., 0.905 g (3.78 mmol, 24 eq.) for the DDAAm$_{12}$-*b*-DMAAm$_{50}$-*b*-EG$_{46}$-*b*-DMAAm$_{50}$-*b*-DDAAm$_{12}$ pentablock terpolymer, and toluene, 6.75 g, so as to reach a final solids concentration of 30% w/w, was transferred into a 25 mL Schlenk flask. After degassing the mixture, the Schlenk flask was immersed in an oil bath thermostated at 65 ^{o}C for 18 h, after which period DDAAm conversion reached 99-100%. The produced pentablock terpolymers were diluted with THF, precipitated in *n*-hexane, dried in a vacuum oven for 24 h, and stored at room temperature until further use.

2.4.7.2 Synthesis of the DAAm$_y$-*b*-DDAAm$_x$-*b*-DMAAm$_{50}$-*b*-EG$_{46}$-*b*-DMAAm$_{50}$-*b*-DDAAm$_x$-*b*-DAAm$_y$ Heptablock Quaterpolymers Using Stepwise RAFT Polymerization

The DAAm$_y$-*b*-DDAAm$_x$-*b*-DMAAm$_{50}$-*b*-EG$_{46}$-*b*-DMAAm$_{50}$-*b*-DDAAm$_x$-*b*-DAAm$_y$ heptablock quaterpolymers were prepared according to the procedure described next. For example, the procedure followed for the synthesis of the DAAm$_{14}$-*b*-DDAAm$_{12}$-*b*-DMAAm$_{50}$-*b*-EG$_{46}$-*b*-DMAAm$_{50}$-*b*-DDAAm$_{12}$-*b*-DAAm$_{14}$ heptablock quaterpolymer was as follows: 2.00 g (0.108 mmol, 1 eq.) of the DDAAm$_{12}$-*b*-DMAAm$_{50}$-*b*-EG$_{46}$-*b*-DMAAm$_{50}$-*b*-DDAAm$_{12}$ pentablock terpolymer, 11.10 mg (0.068 mmol, 0.625 eq.) of AIBN, 0.44 g (2.6 mmol, 24 eq.) of DAAm, and 5.68 g of toluene so as to reach a concentration of 30% w/w, were transferred into a 25 mL Schlenk flask. Then, the resulting solution was degassed and the Schlenk flask was immersed in an oil bath thermostated at 65 ^{o}C for 18 h, after which period the DAAm conversion to polymer reached 99-100%. All the obtained heptablock quaterpolymers were diluted with THF,

precipitated in *n*-hexane, dried under vacuum, and stored at room temperature until further use.

2.4.7.3 Preparation of the Oxime Cross-linked APCNs in Mixtures of Ethanol and Aqueous Buffer Solution at Different Total Solids Concentrations

The preparation of the oxime cross-linked APCNs was performed in mixtures of ethanol and aqueous buffer solution of pH 4.5 of various volume ratios, depending on the structure of the heptablock quaterpolymer. The stoichiometry of the reaction was always constant and equal to 1:1, while the final total solids concentration was varied between 12.5 and 20.0% w/v. The volume ratio of the mixture of ethanol and aqueous buffer solution of pH 4.5 acquired values of 2:3, 3:2, 2:1, 3:1, 4:1, 5:1 and 6:1. This necessitated that the concentrations of the aqueous buffer solution, prepared using CH_3CO_2H and CH_3CO_2Na, were also varied, and, in particular, they acquired values of 0.3, 0.5, 0.6, 0.8, 1.0, 1.2 and 1.4 M, so as the final buffer concentration in the mixture to be equal to 0.2 M. To this end, 32.5 mg (1.40 μmol, 1 eq.) of the $DAAm_{14}$-*b*-$DDAAm_{12}$-*b*-$DMAAm_{50}$-*b*-EG_{46}-*b*-$DMAAm_{50}$-*b*-$DDAAm_{12}$-*b*-$DAAm_{14}$ heptablock quaterpolymer was dissolved in 160 μL of ethanol, while 3.5 mg (19.6 μmol, 14 eq.) of PDH was dissolved in 80 μL of the aqueous buffer at pH 4.5 of a 0.6 M concentration, and at a final total solids concentration of 15% w/w. Then, the two solutions were mixed together in a glass vial at room temperature, resulting in the formation of the oxime cross-linked APCN.

2.4.7.4 Preparation of the Oxime Cross-linked APCNs in Organic Solvents in the Presence or Absence of Aniline as a Catalyst

The formation of the oxime cross-linked APCNs was also performed in organic solvents, and, in particular, in DMF and methanol, following the above-mentioned procedure, and in the presence or absence of aniline (10% v/v) only in the case of DMF. When the reactions were performed in the absence of aniline, 2 eq. of TEA with respect to PDH was added into the reaction. In all cases, the stoichiometry of the reaction was always constant and equal to 1:1, while the final total solids concentration was equal to 20% w/v. In particular, 32.5 mg (1.40 μmol, 1 eq.) of the $DAAm_{14}$-*b*-$DDAAm_{12}$-*b*-$DMAAm_{50}$-*b*-EG_{46}-*b*-$DMAAm_{50}$-*b*-$DDAAm_{12}$-*b*-$DAAm_{14}$ heptablock quaterpolymer was dissolved in 150 μL of

the organic solvent, and 3.5 mg (19.6 μmol, 14 eq.) of PDH was dissolved in 24.5 μL of the organic solvent. Then, 5.5 μL (39.2 μmol, 28 eq.) of TEA was added into the PDH-solution, and the two solutions were mixed together in a glass vial at room temperature, leading to the preparation of the oxime cross-linked APCN. When the reaction was performed in DMF with aniline, the heptablock terpolymer and PDH cross-linker were separately dissolved in 140 μL and 22 μL of DMF, respectively, followed by the addition of 18 μL of aniline to the BzHA-solution, and then the particular solution was mixed together with the polymer solution to form the polymer network.

2.5 Characterization of the Linear Polymers and the Polymer Networks

2.5.1 Linear Polymer Precursors

2.5.1.1 Gel Permeation Chromatography (GPC)

Gel permeation chromatography (GPC) was used to characterize all the linear polymer precursors in terms of their molecular weight and molecular weight distribution. To this end, a single PL Mixed "D" column, packed with polymer beads of 5 μm diameter and pore sizes of 100, 500, 10^3 and 10^4 Å, purchased from Polymer Laboratories, was used. The mobile phase was THF, and it was delivered at a flow rate of 1 mL min^{-1} using a Waters 515 isocratic pump. An ERC-7515A refractive index (RI) detector, also from Polymer Laboratories, was used for the measurement of the RI signal. The calibration curve was based on ten linear poly(methyl methacrylate) (polyMMA) standards having molecular weights equal to 0.8, 2.2, 6.4, 12.6, 23.5, 41.4, 84.3, 201, 342, and 675 kg mol^{-1} and narrow molecular weight distributions, purchased from Polymer Standards Service (PSS) GmbH in Germany. The calibration curve was used to calculate from the recorded GPC traces the following quantities: the number-average molecular weight, M_n, the weight-average molecular weight, M_w, the molecular weight dispersity, $Đ$ (= M_w / M_n), and the peak molecular weight, M_p, that corresponds to the maximum peak value of RI signal in the molecular weight distribution.

2.5.1.2 Nuclear Magnetic Resonance (NMR) Spectroscopy

The NMR spectra were recorded in $CDCl_3$, d_6-DMSO, or D_2O, using a 500 MHz Avance spectrometer equipped with an Ultrashield magnet purchased from Bruker, Massachusetts, USA. All synthesized compounds, the DDAAm monomer and the chain transfer agents, were characterized using ^1H and ^{13}C NMR spectroscopy for the verification of their structure. All linear precursors were characterized using ^1H NMR spectroscopy for the determination of monomer conversion, and also for the determination of their compositions and theoretical molecular weights.

2.5.1.3 Dynamic Light Scattering (DLS)

An ALV CGS3 spectrophotometer system from ALV, Langen, Germany, was used for the dynamic light scattering (DLS) measurements. The spectrophotometer system was equipped with an ALV7004 correlator and a 30 mW red diode laser He-Ne emitting at a wavelength of λ = 632.8 nm. The intensity of the light was measured at a scattering angle of 90^o while the temperature was kept at 23 °C. Each measurement was performed for 10 mins and the results were averaged. The decay rates, Γ, were calculated from the autocorrelation functions, and used by the ALV software to calculate the diffusion coefficient, D. The diffusion coefficient was subsequently employed for the determination of the hydrodynamic radius (R_h) using the Stokes-Einstein-equation [$R_h = k_B\, T / (6\, \pi\, \eta\, D)$]. Finally, the distribution of R_h was obtained using a regularized inverse Laplace transformation algorithm of the correlation function which is included in the ALV software. The DLS measurements were performed using aqueous solutions of the linear amphiphilic diblock copolymers and pentablock terpolymers at three different concentrations, 0.05, 0.10 and 1.00% wt.%. The solutions were prepared using the solvent switch method. In this method, the appropriate amount from each linear amphiphilic copolymer was first dissolved in THF, and then each resulting solution was subsequently added dropwise in a glass vial containing the corresponding amount of water (1:1 volume ratio) under continuous stirring. Then, THF was removed using a rotary evaporator and the polymer solutions were weighed, in order to verify their concentration. Finally, prior to the

measurements, the solutions were filtered through 0.45 μm PTFE syringe filters several times to remove dust or other large impurities.

2.5.1.4 Small-Angle Neutron Scattering (SANS)

The structure of the linear amphiphilic diblock copolymers and pentablock terpolymers in water was investigated using SANS at the V16 beamline in the facilities of the Helmholtz-Zentrum in Berlin (HZB), Germany. The wavelength of the neutron pulse acquired values between 0.25 and 1.8 nm, while the sample-to-detector distance was equal to 11 m, in order to obtain values of the scattering vector, q ($q = 4\,\pi\,\sin(\theta/2) / \lambda$), between 0.002 and 0.100 $Å^{-1}$. The measurements were performed using solutions of the linear amphiphilic diblock copolymers and pentablock terpolymers in D_2O at a concentration of 1% w/w. The solutions were again prepared using the solvent switch method. In this case, the appropriate amount from each linear amphiphilic copolymer was first dissolved in 1,4-dioxane, followed by the dropwise addition of the resulting solution in a round-bottomed flask containing the appropriate amount of D_2O to reach a final 1,4-dioxane : D_2O volume ratio of 2:1. Then, the mixture was lyophilized in order to remove both solvents and the obtained dried polymer was dissolved in the necessary amount of D_2O to reach a final concentration of 1% w/w. Finally, the solutions were placed in quartz cuvettes with 1 mm thickness. In order to obtain the coherent scattering intensity of the samples, the background signal of the pure D_2O sample was subtracted from each sample. The Guinier equation, $\ln(I)=\ln(I_0) - (q^2R_g^2/3)$, was used for the determination of the radius of gyration (R_g) of the obtained structures. To this end, R_g was calculated from the slope of the linear portion of the $\ln(I)$ *vs.* q^2 graph, while the value of $\ln(I_0)$ was calculated from the intercept of this linear portion. The value of $I_{(0)}$ was employed for the determination of the molecular weight of micelle ($M_{w,micelle}$) using the equation of the difference of the scattering length density [$M_{w,micelle} = (I_{(0)} \times d \times N_A) / (\varphi \times \Delta SLD^2)$]. The values of the $M_{w,micelle}$ were then used for the calculation of the aggregation number (N_{agg}) of micelles, and, in particular, these values were obtained after dividing the $M_{w,micelle}$ with the theoretical molecular weight of the linear copolymer or terpolymer (unimer).

2.5.1.5 Atomic Force Microscopy (AFM)

An ES-Cypher atomic force microscope from Asylum Research Inc./ Oxford Instruments, operating in the tapping mode, was used for the investigation of the morphology of the obtained structures of the linear amphiphilic diblock copolymers in water. The microscope was equipped with silicon nitride tips with a force constant of 25-75 N m^{-1} and a resonance frequency of 200-400 kHz. The aqueous solutions of the linear amphiphilic copolymers were again prepared using the solvent switch method (THF), while the final concentration of the aqueous solutions was 0.1% w/w. The AFM samples were prepared by transferring one drop of the aqueous solution onto a mica substrate, followed by complete drying in a vacuum oven. The amplitude and phase images were obtained at room temperature at a scan frequency of 2.44 Hz.

2.5.2 Polymer Networks

2.5.2.1 Degrees of Swelling (DSs) of the Degradable Hydrogels

The degrees of swelling (DSs) at the preparation and equilibrium states of all prepared hydrogels were determined after the complete drying of the as-prepared and the equilibrium swollen hydrogels, respectively. In particular, samples from the as-prepared DMAAm-MBAAm 1-4 and DMAAm-DHEBA 1-4 SN, "inert" DMAAm-MBAAm 1-4/OXG and DMAAm-DHEBA 1-4/OXG SN, DMAAm-x/DMAAm-x DN, and "deactivated" DMAAm-x/OXG/DMAAm-x DN hydrogels were placed in a vacuum oven until reaching a constant weight. In addition, samples from all the as-prepared hydrogels were immersed in water, and, after their equilibrium swelling, the hydrogels were also placed in a vacuum oven until reaching a constant weight. Prior to, and after drying, the masses of the gels were determined gravimetrically, and these values were used for the calculation of the DS both at the preparation and equilibrium states. The calculation of the DS at the preparation or equilibrium state was performed by dividing the as-prepared or the swollen mass, respectively, by the dry polymer (polymerized DMAAm plus cross-linker) mass. The DSs were determined three times and their average values were calculated, together with their standard errors at a confidence interval of 95%.

2.5.2.2 Determination of the Soluble Fraction of the Degradable Hydrogels

The determination of the soluble fraction of all prepared hydrogels was performed by immersing the samples from all the as-prepared DMAAm-MBAAm 1-4 and DMAAm-DHEBA 1-4 SN, "inert" DMAAm-MBAAm 1-4/OXG and DMAAm-DHEBA 1-4/OXG SN, DMAAm-x/DMAAm-x DN, and "deactivated" DMAAm-x/OXG/DMAAm-x DN hydrogels in water. In particular, a piece of each hydrogel ($m \approx 0.5$ g) was immersed in water and the hydrogels were left at room temperature. The next day, the aqueous solution was separated from the hydrogel and collected, and the water was replaced. The next day, the aqueous solution was again separated, and this procedure was repeated for two more times. Finally, all the collected solutions were combined, and water was removed using a rotary evaporator at 60 ^{o}C. The thus-predried samples were thoroughly dried in a vacuum oven at 50 ^{o}C until reaching a constant weight. The dried masses were determined gravimetrically. The soluble fraction was calculated by dividing these values by their theoretical dry masses, thus it was expressed as % w/w of the dry mass.

2.5.2.3 Degradation of the Degradable Hydrogels Using Sodium Periodate

All the as-prepared DMAAm-MBAAm 1-4 and DMAAm-DHEBA 1-4 SN, "inert" DMAAm-MBAAm 1-4/OXG and DMAAm-DHEBA 1-4/OXG SN, DMAAm-x/DMAAm-x DN, and "deactivated" DMAAm-x/OXG/DMAAm-x DN hydrogels were subjected to degradation using sodium periodate ($NaIO_4$). To this end, a piece from each hydrogel ($m \approx 0.5$ g) was immersed in 5 mL of an aqueous solution of $NaIO_4$ (2 mg mL^{-1}) and left at room temperature for about two weeks. Then, each aqueous solution was separated from the hydrogel, collected, and replaced by pure water to remove any other soluble species. The water of the collected solution was removed using a rotary evaporator at 60 ^{o}C, while it was completely removed after drying in a vacuum oven at 50 ^{o}C. The mass of the soluble species was determined gravimetrically, while, after two weeks, the aqueous solutions were again separated from the hydrogels, and this procedure was repeated for two more times. Finally, the remaining hydrogels were placed in a vacuum oven at 50 ^{o}C for the complete removal of water and their dried masses were also determined gravimetrically.

2.5.2.4 Degrees of Swelling of the Multiple Network Hydrogels

For the determination of the DS at the preparation and equilibrium states of the multiple hydrogels, samples from the as-prepared SN, DN, TN, quadruple network (QN) and quintuple network (5×N) hydrogels were weighed and immersed in DMAAm aqueous solutions or pure water and allowed for 4 days to reach swelling equilibrium. The excess aqueous solutions were again removed from the hydrogels, and the swollen hydrogels were weighed three times. The mass of each multiple network hydrogel, both at the preparation and equilibrium swelling states, was subsequently used to calculate the corresponding DS by dividing this value by the theoretical mass of the dry polymer (polymerized DMAAm plus MBAAm) mass. The DSs were determined three times and their average values were calculated, together with their standard errors at a confidence interval of 95%. The relative swelling ratio of the SN within the higher multiple network hydrogel was also calculated by dividing the overall hydrogel swollen mass by the dry mass of the SN, followed by the division of this DS value by the DS of the SN in the as-prepared state.

2.5.2.5 Degrees of Swelling of the APCNs Cross-linked via HDDA or Oxime Bonds

In contrast to the polymer network hydrogels that were only allowed to swell in water, the amphiphilic polymer networks consisting of DMAAm and DDAAm cross-linked using HDDA or oxime bonds were also allowed to reach swelling equilibrium in toluene, EtOH, THF, and $CHCl_3$. The oxime cross-linked APCNs were formed at a total solids concentration of 15 w/v at the stoichiometric ratio using the above-mentioned procedure in mixtures of EtOH and aqueous buffer solution of pH 4.5 with varying volume ratios. Then, all these polymer networks were left to mature for three days and were subsequently immersed in the various solvents and allowed for one week to reach swelling equilibrium. In the case of the oxime cross-linked APCNs consisting only of DMAAm and DAAm, these were prepared in an aqueous buffer solution of pH 4.5 and immersed only in pure water. In all cases, the masses of the polymer networks prior to, and after swelling were determined gravimetrically. These values were then used for the calculation of the equilibrium DSs by dividing these values by the theoretical dry polymer mass. The DSs

were determined three times and their average values were calculated, together with their standard errors at a confidence interval of 95%.

2.5.2.6 Mechanical Properties

Samples from all the as-prepared multiple network hydrogels or the water-swollen amphiphilic polymer (co)networks were characterized in terms of their mechanical properties in compression using a high precision 5944 mechanical testing system from Instron, Norwood, MA, USA. The as-prepared multiple network hydrogels and the water-swollen APCNs cross-linked with HDDA were cut in a cubical shape with dimensions 4 × 4 × 4 mm^3. In contrast, all the oxime cross-linked APCNs were prepared at the stoichiometric ratio at a total solids concentration of 15% w/v using the above-mentioned procedure in glass vials, and, consequently, they possessed a cylindrical shape. The oxime cross-linked polymer networks consisting only of DMAAm and DAAm were formed in pure aqueous buffer solution of pH 4.5 and left to mature for three days. Thus, the compression experiments were performed on as-prepared samples, with a ~9 mm diameter and a ~4 mm height. The only exception was the APCN prepared with the pentablock terpolymer with the highest number of DAAm monomer repeating units (50) that was prepared in a mixture of EtOH and aqueous buffer solution of pH 4.5 and swollen in an aqueous buffer solution of pH 7.4. The oxime cross-linked APCNs consisting of DMAAm, DDAAm and DAAm were prepared at the stoichiometric ratio at a total solids concentration of 20% w/v in DMF in the presence of 10% v/v aniline, and after maturing for three days, the gels were immersed in water for one week. Thus, the dimensions of the equilibrium swollen samples differed according to the degree of swelling of each polymer network. The specimens were placed between two parallel plates, and, prior to the measurements, a minimum load of 0.01 N was applied to each sample to ensure that the sample was in complete contact with the plates. The samples were compressed at a strain rate of 1 mm min^{-1} using a 2 kN load cell until their fracture. The stress, calculated as the force measured on the load cell divided by the initial area of the specimen (*i.e.*, 1st Piola-Kirchhoff stress), was expressed as the nominal stress, while the infinitesimal strain ($\varepsilon = \Delta l / l_0$) was employed as a measure of the deformation. The fracture stress (σ_{max}) and fracture strain (ε_{max}) values were obtained from the fracture point of the gel. The

determination of the Young's modulus, *E*, was performed using the slope of the initial linear portion of the stress-strain curve, at a strain of 5-15%, while the area under the stress-strain curve was equal to the fracture energy density of the sample, *i.e.*, the energy density obtained at the fracture point of the hydrogel. Finally, selected samples of the multiple network hydrogels (TN and 5×N) were also subjected to cyclic compression tests. In these experiments, the compression rate was the same as before, while the maximum strain value was selected to be lower than the fracture strain value. Two types of experiments were performed. In the first type, the same sample was subjected up to five times to the same ultimate strain. In the second type, a sample was subjected to a certain strain, followed, three or four times, by the repetition of the same experiment to a higher ultimate strain but using a fresh sample.

2.5.2.7 Nanoindentation Testing

The hardness of multiple network hydrogels was assessed using a NanoTest Platform from Micromaterials Ltd., UK. A Berkovich type three-sided pyramidal diamond indenter with an angle between its central axis and one of its faces of 65.3° and a nominal tip curvature of about 10 nm was employed. The samples were subjected to a maximum load of 0.5 mN, the loading time was 5 s, the hold time at maximum load was 30 s, and the unloading time was 2 s. During the test, the load, *P*, and the depth of penetration, *h*, were continuously monitored. For each sample, a total of five indentation experiments were performed.

2.5.2.8 Rheology Measurements

The oxime cross-linked amphiphilic polymer conetworks were characterized using rheology experiments, in order to evaluate their storage (G') and loss (G'') moduli. The measurements were performed using a Discovery HR2 rheometer from TA Instruments operating in parallel plate geometry. The bottom plate was a Peltier element equipped with a thermostat in order to maintain the temperature at 20 °C, while the diameter of the top plate was 40 mm. For the oscillatory time experiment, the rheometer was operated with an angular frequency of 10 rad s^{-1}, 1% strain, and a plate separation height of 155 μm, corresponding to a solution volume of 0.70 mL. However, this type of experiment was only performed in the case of the oxime cross-linked polymer networks consisting only of

DMAAm and DAAm, in order to follow the evolution of the G' and G'' values and determine their gel formation times. To this end, the appropriate amounts of the pentablock terpolymers or the random copolymers and PDH were dissolved in the aqueous buffer solution of pH 4.5 at the stoichiometric ratio with varying final total solids concentrations, and, in particular, 10.0, 12.5, and 15.0% w/v. For example, 65.2 mg (4.42 μmol, 1 eq.) of the $DAAm_6$-*b*-$DMAAm_{50}$-*b*-EG_{46}-*b*-$DMAAm_{50}$-*b*-$DAAm_6$ pentablock terpolymer and 4.8 mg (26.5 μmol, 6 eq.) of the PDH cross-linker were separately dissolved in 650 and 50 μL of the aqueous buffer solution of pH 4.5, respectively (total solids concentration = 10% w/v). Then, the two separate solutions were mixed together and transferred onto the Peltier element. The gelation time was determined as the time when the value of G'' became equal to the value of G'. For the frequency-dependent oscillatory rheology measurements, preformed polymer networks were subjected to a 10% strain within the frequency range of 0.01 (or 0.001) and 100 rad s^{-1}. To this end, all the oxime cross-linked APCNs had a diameter of 40 mm and were prepared at a total solids concentration of 15% w/v at the stoichiometric ratio and left to mature for three days. The oxime cross-linked gels consisting only of DMAAm and DAAm were formed in aqueous buffer solutions of pH 4.5, whereas the APCN prepared using the linear precursor with the highest number of DAAm repeating units (50) was prepared in a mixture of EtOH and aqueous buffer solution of pH 4.5 and swollen in an aqueous buffer solution of pH 7.4. The oxime cross-linked APCNs consisting of DMAAm, DDAAm and DAAm were prepared in mixtures of EtOH and aqueous buffer solution of pH 4.5 with varying volume ratios, and, after three days, the gels were immersed in pure water and left there for four days. For example, 365.5 mg (15.8 μmol, 1 eq.) of the $DAAm_{14}$-*b*-$DDAAm_{12}$-*b*-$DMAAm_{50}$-*b*-EG_{46}-*b*-$DMAAm_{50}$-*b*-$DDAAm_{12}$-*b*-$DAAm_{14}$ heptablock quaterpolymer was dissolved in 2000 μL of ethanol, while 39.5 mg (0.22 mmol, 14 eq.) of PDH was dissolved in 700 μL of the aqueous buffer pH 4.5 0.6 M, at a final total solids concentration of 15% w/v. Then, the two solutions were mixed together and the oxime cross-linked APCN was obtained.

2.5.2.9 Self-Healing Experiments

Self-healing experiments were performed using as-prepared oxime cross-linked polymer networks, prepared using the above-mentioned procedure, in aqueous buffer solutions of

pH 4.5 at the stoichiometric ratio at a total solids concentration of 15% w/v. After their preparation, the oxime cross-linked gels were allowed to mature for three days. Then, each gel was cut into two equal distinct pieces, and placed in a Petri dish. In order to induce the self-healing, the cut samples were brought into contact and pressed together for 48 h.

2.5.2.10 Gel-to-Sol Transition

Gel-to-sol transition experiments were performed using the oxime cross-linked APCNs and the randomly oxime cross-linked copolymer networks based on DMAAm and DAAm, which were prepared either in aqueous buffer solutions of pH 4.5, or in a mixture of EtOH and aqueous buffer solution of pH 4.5 (at the stoichiometric ratio). For both types of the oxime cross-linked gels, the final total solids concentration was the lowest possible, *i.e.*, 10.0 or 12.5% w/v. After their preparation, the gels were left to mature for three days, and the appropriate amount of TFA (3 eq. to PDH) was added onto the gel surface in order to induce the transition of the gel to solution.

2.5.2.11 Shape Memory Experiments

The shape memory experiments were performed using the water-swollen randomly cross-linked copolymer networks consisting of DMAAm and DDAAm prepared using free radical photopolymerization. All the copolymer networks were prepared in cylindrical tubes with a diameter of 5 mm, and immersed in water to reach swelling equilibrium. Afterward, each water-swollen sample was first heated up to 50-70 ^{o}C to enable reshaping, and it was then cooled down to 25 ^{o}C to fix the temporary shape. Finally, it was again heated up to 50-70 ^{o}C to recover its initial shape.

2.6 References

1. McCormick, C. L.; Nonaka T.; Johnson, C. B. Water-soluble copolymers: 27. Synthesis and aqueous solution behavior of associative acrylamide/*N*-alkylacrylamide copolymers. *Polymer* **1988**, *29*, 731-739.
2. Chong, D.; Tan, J.; Zhang, J. Zhou, Y.; Wan, X.; Zhang, J. Dual electrical switching permeability of vesicles *via* redox-responsive self-assembly of amphiphilic block copolymers and polyoxometalates. *Chem. Commun.* **2018**, *54*, 7838-7841.
3. Pafiti, K. S.; Patrickios, C. S.; Abetz, C.; Abetz, V. High-molecular weight symmetrical multiblock copolymers: Synthesis by RAFT polymerization and characterization. *J. Polym. Sci., Part A: Polym. Chem.* **2013**, *51*, 4957-4965.
4. Mukherjee, S.; Bapat, A. P.; Hill, M. R.; Sumerlin, B. S. Oximes as reversible links in polymer chemistry: Dynamic macromolecular stars. *Polym. Chem.* **2014**, *5*, 6923-6931.

CHAPTER 3: RESULTS AND DISCUSSION

The primary goal of this PhD thesis was to develop hydrophilic polymer networks of enhanced mechanical properties by introducing the elements of network multiplicity, network amphiphilicity, and network reversibility. To this end, three types of polymer networks were prepared and characterized, and, in particular, multiple hydrophilic polymer networks, amphiphilic polymer networks, and dynamic amphiphilic polymer networks cross-linked using covalent oxime bonds. Figure 3.1 schematically represents the three types of polymer networks synthesized in this PhD Thesis.

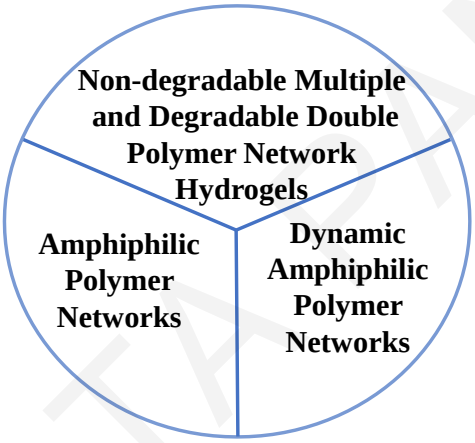

Figure 3.1. Schematic representation of the types of the synthesized polymer networks prepared in this PhD Thesis.

The first specific goal was to prepare and characterize multiple network hydrogels possessing enhanced mechanical properties consisting only of nonionic components, and, in particular, the *N*,*N*-dimethylacrylamide (DMAAm) monomer and the *N*,*N*′-methylenebisacrylamide (MBAAm) cross-linker. Previous studies have shown that the mechanical properties can be significantly improved by introducing a number of loosely cross-linked polymer networks or linear non-cross-linked polymer chains, or/and increasing monomer concentration. In the present study, the enhancement of the mechanical properties was explored by the systematic variation not only of network multiplicity but also of monomer concentration.

The second specific goal involved the determination of the degree of interconnection between the two hydrophilic polymer networks forming partially degradable double-network (DN) hydrogels, which were prepared by the combination of both degradable and

non-degradable cross-linkers. These partially degradable DN hydrogels were subjected to degradation, resulting in the degradation of only the degradable component and its conversion to a solution, whereas the non-degradable component stilled remained a network. The degree of interconnection was determined by comparing the experimental masses of the soluble fraction and the gel fraction with the theoretically calculated ones.

The second general aim of this Thesis included the incorporation of the hydrophobic *N*-dodecylacrylamide (DDAAm) monomer in the hydrophilic polymer network hydrogels for the preparation of amphiphilic randomly cross-linked copolymer networks and well-defined amphiphilic polymer conetworks (APCNs). The particular hydrophobic monomer was chosen due to the formation of hydrophobic associations among the dodecyl side groups, leading to microphase separation, and resulting in the enhancement of the mechanical properties of the produced polymer networks. Furthermore, these polymer networks can exhibit a thermoreversible transition behavior (shape memory), due to the presence of the relatively long side chain in the DDAAm monomer repeating units, which confers semi-crystallinity in the materials containing it.

The final general aim of this Thesis was the preparation of well-defined APCNs containing the hydrophilic DMAAm and the hydrophobic DDAAm monomers cross-linked using dynamic covalent oxime bonds. The oxime bond belongs to the dynamic/reversible covalent bonds, formed through the reaction of a carbonyl group and an aminooxy group. Thus, the obtained oxime cross-linked APCNs may possess self-healing ability due to the presence of the dynamic oxime bonds, in addition to the enhanced mechanical properties and shape memory expected to result from the presence of DDAAm.

The preparation of the polymer networks was achieved using both controlled and non-controlled polymerization methods. In particular, the multiply interpenetrated polymer network hydrogels, the degradable DN hydrogels, and the randomly cross-linked copolymer networks were prepared using conventional free radical photopolymerization, while all APCNs and their linear precursors were synthesized using RAFT polymerization. Finally, the synthesis of the linear amphiphilic polymer precursors for the preparation of the oxime cross-linked APCNs was also accomplished using RAFT polymerization.

After their preparation, all these polymer precursors and polymer networks were characterized using various characterization methods. Initially, all the linear diblock and multiblock copolymer precursors were characterized using GPC and ^{1}H NMR spectroscopy for the determination of their molecular weights and molecular weight distributions, and their compositions, respectively. Afterward, due to the amphiphilic nature of these linear precursors arising from the presence of a hydrophobic monomer, these were also investigated in terms of their self-assembly ability in water, using DLS and SANS. AFM was also employed in some cases for the characterization of the linear amphiphilic polymers, in order to visualize the morphology of the obtained organized structures. All the synthesized polymer networks were evaluated in terms of their degrees of swelling and their mechanical performance using compression experiments, in order to elucidate the dependence of these parameters on the structure and composition of the polymer networks. Furthermore, the thermal transition ability of the pendant hydrophobic dodecyl group in the DDAAm repeating units was demonstrated using shape memory experiments on water-swollen amphiphilic copolymer networks. Finally, the dynamic nature of the APCNs cross-linked via oxime bonds was investigated using self-healing and gel-to-sol transition experiments.

The hydrophilic monomer employed in the preparation of all polymers and polymer networks was DMAAm, while DDAAm served as the hydrophobic monomer. Both DMAAm and DDAAm are nonionic acrylamide monomers and serve as excellent candidates in the preparation of linear amphiphilic polymers and amphiphilic polymer networks, which can be prepared using free radical and RAFT polymerizations. The hydrophilic MBAAm and *N*,*N*′-(1,2-dihydroxy-ethylene)bisacrylamide (DHEBA) cross-linkers were used in the preparation of the hydrophilic polymer network hydrogels, while the hydrophobic 1,6-hexanediol diacrylate (HDDA) cross-linker was employed in the preparation of the amphiphilic polymer networks. 2-Oxoglutatic acid (OXG) and 2,2-dimethoxy-2-phenylacetophenone (DMPAP) served as the water-soluble and the organosoluble photoinitiators, respectively, while 2,2′-azobis(isobutyronitrile) (AIBN) was used as a thermal initiator in the RAFT polymerizations. The synthesized 2-(dodecylthiocarbonothioylthio)-2-methylpropionic acid (DMPA) and poly(ethylene glycol) bis[2-(dodecylthiocarbonothioylthio)-2-methylpropionate] (PEG DMPA) served as the monofunctional and difunctional CTAs, respectively, in the RAFT polymerizations.

Figure 3.2 displays the chemical structures, names, and abbreviations of the main chemical reagents employed in the preparation of the polymer network hydrogels, the linear amphiphilic block copolymer precursors, and the amphiphilic polymer networks. The synthesis and characterization of each of these polymer types will be discussed in the following sections.

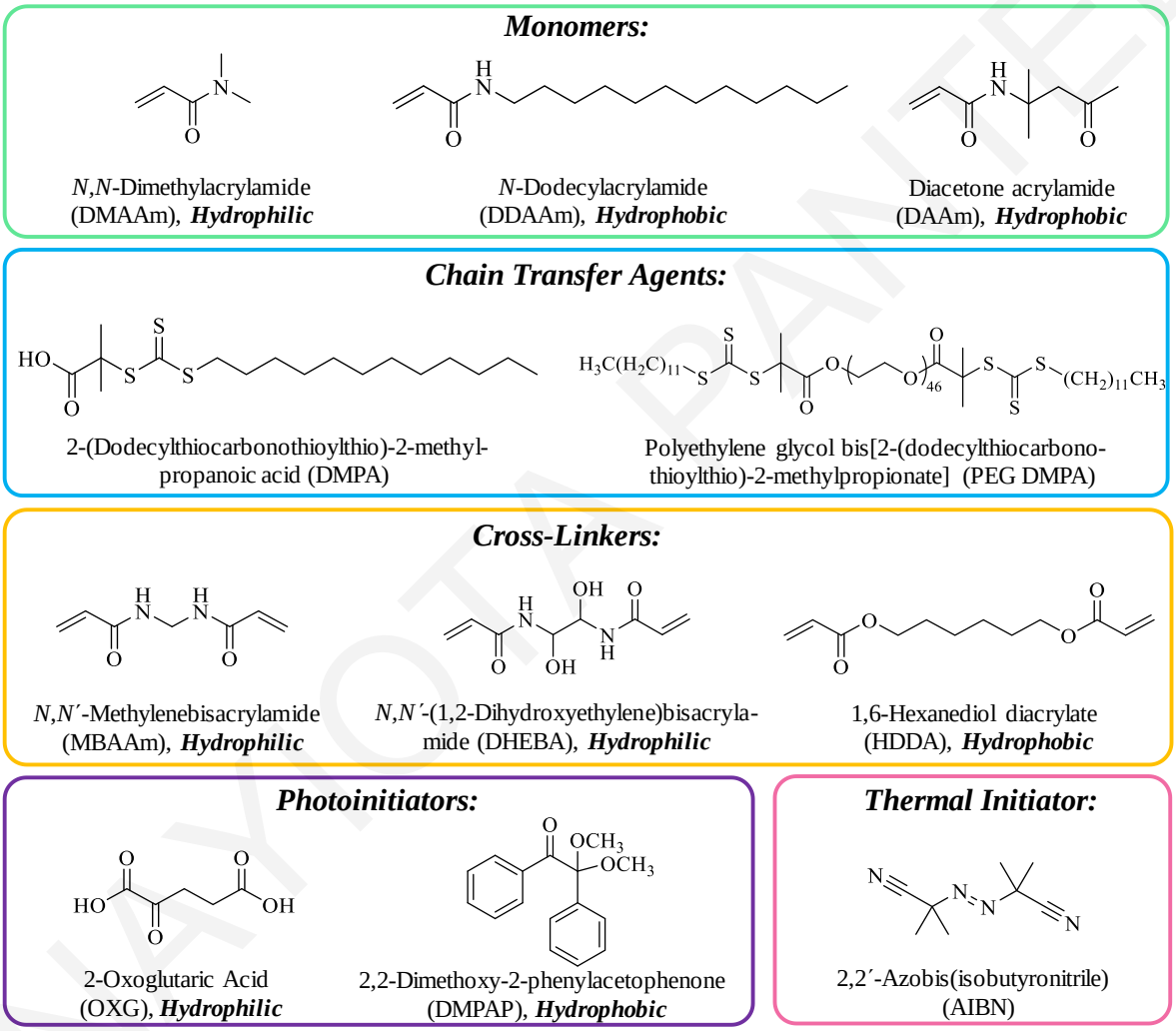

Figure 3.2. The chemical structures, names, and abbreviations of the main chemical reagents employed in this Thesis for the preparation of the polymer network hydrogels, the linear amphiphilic block copolymers, and the amphiphilic polymer networks.

3.1 Synthesis of the DDAAm Monomer, and the DMPA and PEG DMPA CTAs

3.1.1 DDAAm Monomer

The synthesis of DDAAm was achieved in one step from the acylation of 1-dodecylamine with acryloyl chloride in the presence of TEA base, as shown in Figure 3.1.1.

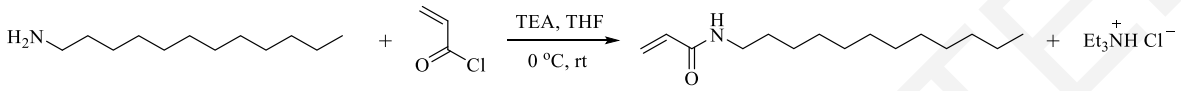

Figure 3.1.1. The reaction between 1-dodecylamine and acryloyl chloride for the preparation of the DDAAm monomer.

After the complete addition of acryloyl chloride, the reaction was left overnight at room temperature under continuous stirring. The next day, the side-product of the acylation, the hydrochloric acid salt of TEA was removed by filtration, and DCM was evaporated. The crude mixture was characterized using ^{1}H NMR spectroscopy, which indicated that the amine was completely consumed (conversion = 100%) and verified the formation of the desired product, DDAAm. However, another set of peaks with a percentage of 5 mol% with respect to DDAAm was also present in the ^{1}H NMR spectrum. Those peaks belonged to the byproduct of the reaction which was identified as *N*,*N*-dodecylbis(acrylamide). The crude mixture was purified by two recrystallizations from acetone, and DDAAm was obtained as a white powder at 80% yield. The structure and purity of the final product was identified using ^{1}H and ^{13}C NMR spectroscopy in $CDCl_3$. The recorded spectra are shown in Figure 3.1.2.

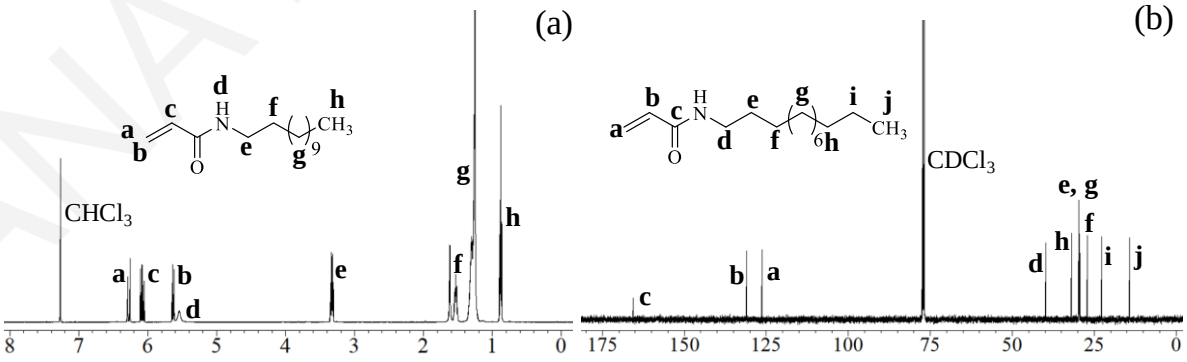

Figure 3.1.2. (a) ^{1}H NMR and (b) ^{13}C NMR spectra in $CDCl_3$ of the pure DDAAm monomer.

3.1.2 DMPA CTA

The DMPA RAFT chain transfer agent was synthesized in one step from the reaction of 1-dodecanethiol, BMPA, and carbon disulfide in the presence of potassium phosphate base, as shown in Figure 3.1.3.

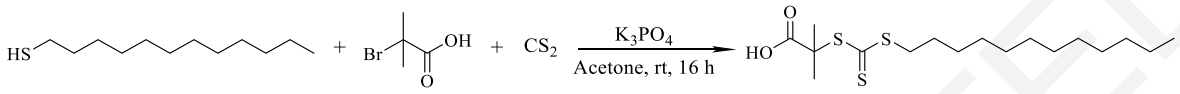

Figure 3.1.3. The reaction of 1-dodecanethiol, BMPA, and CS_2 for the synthesis of the DMPA CTA.

The reaction was performed in acetone, where 1-dodecanethiol and carbon disulfide were allowed to react for 30 min, prior to the addition of the next reagent. When BMPA was finally added in the suspension, the reaction was left overnight at room temperature under continuous stirring. Afterward, the yellow solid that was formed was characterized using ^{1}H NMR spectroscopy, which verified the formation of the desired product at a yield of 75%. Pure DMPA was obtained as a yellow powder after column chromatography on silica gel using a *n*-hexane : ethyl acetate mixture at a ratio of 9:1 at 60% yield. Figure 3.1.4 displays the ^{1}H and ^{13}C NMR spectra of the desired purified product in $CDCl_3$.

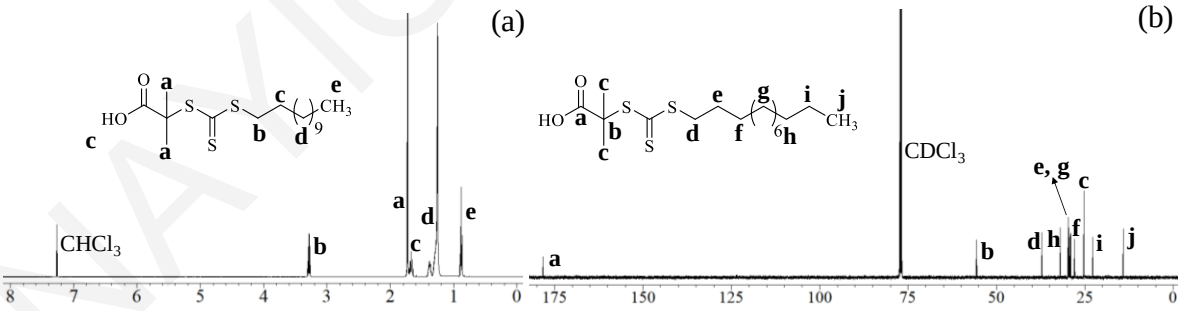

Figure 3.1.4. (a) ^{1}H NMR and (b) ^{13}C NMR spectra in $CDCl_3$ of the DMPA CTA after purification.

3.1.3 PEG DMPA CTA

The synthesis of the PEG DMPA difunctional CTA was accomplished from the bisesterification of PEG diol with DMPA, using DCC as the activator and DMAP as the accelerator, as shown in Figure 3.1.5.

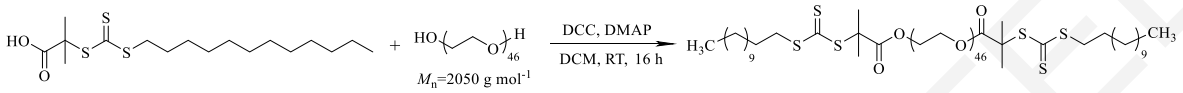

Figure 3.1.5. Esterification of PEG diol with DMPA for the preparation of the PEG DMPA CTA.

After the addition of all reagents, the reaction was left overnight at room temperature under continuous stirring. The next day, the reaction was filtered in order to remove the dicyclohexylurea byproduct, while DCM was removed using a rotary evaporator. The crude orange solid was characterized using ^{1}H NMR spectroscopy, which verified the formation of the desired product at a yield of 75%. Pure PEG DMPA was obtained after column chromatography on silica gel using a *n*-hexane : ethyl acetate mixture at a ratio of 9:1 to remove the DMPA starting material, and then a DCM : methanol mixture at a ratio of 95:5. PEG DMPA was obtained as an orange solid at 65% yield, and was characterized using ^{1}H and ^{13}C NMR spectroscopy in $CDCl_3$. The recorded spectra are shown in Figure 3.1.6.

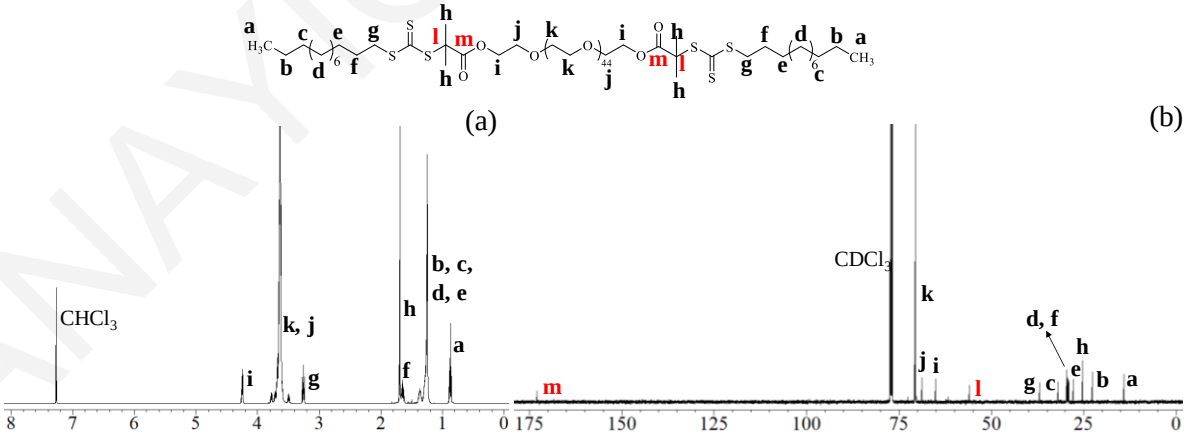

Figure 3.1.6. (a) ^{1}H NMR and (b) ^{13}C NMR spectra in $CDCl_3$ of pure PEG DMPA.

3.2 Degradable Hydrogels Based on the Hydrophilic DMAAm Monomer, the Non-Degradable Hydrophilic MBAAm Cross-linker and the Degradable Hydrophilic DHEBA Cross-Linker, Prepared Using Free Radical Photopolymerization

3.2.1 Preparation of the Single Network (SN) and Double-Network (DN) Hydrogels

The preparation of the two DMAAm-MBAAm 1-4 and DMAAm-DHEBA 1-4 single network (SN) hydrogels, and the four DMAAm/DMAAm DN hydrogels was accomplished in one or two steps, respectively, using free radical photopolymerization. The hydrophilic DMAAm monomer, the hydrophilic MBAAm and DHEBA cross-linkers, and the water-soluble OXG photoinitiator were employed in the preparation of the hydrogels. The hydrophilic DHEBA was chosen as the degradable cross-linker as it is a commercially available acrylamide cross-linker compatible with both the DMAAm monomer and the MBAAm cross-linker due to their similar structures. Both the non-degradable MBAAm and the degradable DHEBA cross-linkers were combined for the preparation of the SN and the DN hydrogels. The preparation of the DN hydrogels was accomplished according to the procedure reported by Gong et al.[1] Thus, the two constituent polymer networks were prepared to possess different cross-linking densities. In particular, the first network consisted of a relatively densely cross-linked polyDMAAm network, prepared using a monomer concentration of 1 M and a MBAAm or DHEBA cross-linker concentration of 4 mol% with respect to monomer, whereas the second polyDMAAm network was prepared at a monomer concentration of 2 M and a much lower MBAAm or DHEBA cross-linker concentration, namely, 0.1 mol% with respect to monomer. After the preparation of the two SN hydrogels, DMAAm-MBAAm 1-4 and DMAAm-DHEBA 1-4, these hydrogels were used as matrices for the synthesis of the second polymer networks, resulting in the preparation of the DN hydrogels. Due to the combination of both cross-linkers, four DN hydrogels with different structures were obtained: the totally non-degradable DMAAm-MBAAm 1-4/DMAAm-MBAAm 2-0.1, the partially degradable DMAAm-MBAAm 1-4/DMAAm-DHEBA 2-0.1 and DMAAm-DHEBA 1-4/DMAAm-MBAAm 2-0.1, and the fully degradable DMAAm-DHEBA 1-4/DMAAm-DHEBA 2-0.1.

3.2.2 Preparation of More SN and DN Hydrogels via Deactivation of the Pendant Double Bonds in the SN Hydrogels

The research groups of Gong,[2] Weiss,[3] and Shestakova,[4] have established that a particular percentage of double bonds of MBAAm cross-linker remains unreacted after the UV irradiation process for the preparation of the SN hydrogels. These double bonds can act as bridges between the two constituent polymer networks of the DN hydrogels, as the polymer chains of the loosely cross-linked second network are grafted onto the double bonds of the first network. In order to deactivate these double bonds, we followed the procedure reported by Gong and co-workers,[2] which involved equilibrium swelling of the as-prepared SN hydrogels in a relatively concentrated aqueous solution of OXG photoinitiator (0.1 M), and then UV irradiating them. This resulted in the preparation of the two "inert" DMAAm-MBAAm 1-4/OXG and DMAAm-DHEBA 1-4/OXG SN hydrogels, which were then divided into two pieces and each piece was separately immersed in an aqueous solution of 2 M DMAAm, containing either MBAAm or DHEBA cross-linker and OXG photoinitiator, all at a percentage of 0.1 mol% with respect to monomer. After their equilibrium swelling and removal of excess solution, the swollen hydrogels were again irradiated by UV light, resulting in the preparation of the four "deactivated" DN hydrogels: the totally non-degradable DMAAm-MBAAm 1-4/OXG/DMAAm-MBAAm 2-0.1, the partially degradable DMAAm-MBAAm 1-4/OXG/DMAAm-DHEBA 2-0.1 and DMAAm-DHEBA 1-4/OXG/DMAAm-MBAAm 2-0.1, and the fully degradable DMAAm-DHEBA 1-4/OXG/DMAAm-DHEBA 2-0.1.

3.2.3 Degrees of Swelling

All the prepared SN, "inert" SN, DN, and "deactivated" DN hydrogels were characterized in terms of their degrees of swelling (DSs) at the preparation and swelling equilibrium states, and the results are listed in Table 3.2.1. The values of the DSs at preparation were calculated by dividing the as-prepared mass of the hydrogel by its dry polymer mass (polymerized DMAAm plus cross-linker), obtained after the complete drying of the gels in a vacuum oven. Similarly, the values of the DSs at equilibrium were determined by dividing the equilibrium swollen hydrogel mass by its dry polymer mass, after their complete drying in a vacuum oven.

Table 3.2.1. Degrees of swelling and soluble fraction (% w/w) of the prepared hydrogels.

No.	Network Structure	Degree of Swelling		Soluble Fraction (% w/w)
		Prep.	Equil.	
	Single Networks			
1	DMAAm-MBAAm 1-4	9.5	10.0	1.5
2	DMAAm-MBAAm 1-4/OXG	10.4	11.5	1.5
3	DMAAm-DHEBA 1-4	9.2	12.8	0.2
4	DMAAm-DHEBA 1-4/OXG	13.0	18.4	6.3
	Double Networks			
5	DMAAm-MBAAm 1-4/DMAAm-MBAAm 2-0.1	3.6	7.8	0.5
6	DMAAm-MBAAm 1-4/OXG/DMAAm-MBAAm 2-0.1	3.7	8.4	0.5
7	DMAAm-MBAAm 1-4/DMAAm-DHEBA 2-0.1	3.6	7.5	1.0
8	DMAAm-MBAAm 1-4/OXG/DMAAm-DHEBA 2-0.1	3.7	7.7	3.2
9	DMAAm-DHEBA 1-4/DMAAm-MBAAm 2-0.1	4.2	16.0	0.6
10	DMAAm-DHEBA 1-4/OXG/DMAAm-MBAAm 2-0.1	3.8	12.2	0.5
11	DMAAm-DHEBA 1-4/DMAAm-DHEBA 2-0.1	4.3	16.1	3.9
12	DMAAm-DHEBA 1-4/OXG/DMAAm-DHEBA 2-0.1	4.0	12.2	3.7

The table shows that the values of the DSs at preparation of the DMAAm-MBAAm 1-4 and DMAAm-DHEBA 1-4 SN hydrogels were the same or very close to the theoretically calculated values of the DSs at preparation of 9.5 and 9.3, respectively, calculated on the basis of monomer and cross-linker loadings. Despite the very similar structures of the MBAAm and DHEBA cross-linkers, the DMAAm-DHEBA 1-4 SN hydrogel exhibited a slightly higher value of the DS at equilibrium than the corresponding value of the DMAAm-MBAAm 1-4 SN hydrogel (relative DS for the DHEBA-containing hydrogel = 1.10, relative DS for the MBAAm-containing hydrogel = 1.05). As a result, the value of the preparation DS of the "inert" DMAAm-DHEBA 1-4 SN hydrogel was higher than the corresponding value of the "inert" MBAAm-containing SN hydrogel.

The table shows that all the values of the preparation DSs of the DN hydrogels were lower than their SN hydrogel-counterparts. For example, the preparation DS of the DMAAm-MBAAm 1-4 SN hydrogel is equal to 9.5, while this value is equal to 3.6 for the DMAAm-MBAAm 1-4/DMAAm-MBAAm 2-0.1 DN hydrogel. This is attributed to the increased polymer volume fraction in the DN hydrogels compared to that in the SN hydrogel-

counterparts, owing to the incorporation of the second polymer network upon the swelling step in the monomer/cross-linker/photoinitiator solution, followed by its photopolymerization. Furthermore, this increase in the polymer volume fraction of the DN hydrogels can be attributed to the concentration of the DMAAm monomer in the second polymer network which is higher than that in the first network. Thus, the polymer volume fraction is significantly increased, and, consequently, the values of the preparation DSs are significantly decreased.

3.2.4 Determination of the Soluble Fraction of the SN and DN Hydrogels

In order to determine the soluble fraction of the SN, "inert" SN, DN, and "deactivated" DN hydrogels, samples from all these hydrogels were allowed to reach swelling equilibrium in water to release any soluble species. After the complete removal of water by vacuum drying at 50 ^{o}C, the dried soluble species were weighed, and these values were subsequently used for the determination of the soluble fraction. The soluble fraction of each hydrogel was calculated by dividing the dry mass of the soluble species by its theoretical dry mass and multiplying it by 100, to be expressed as % w/w. The obtained results are also shown in Table 3.2.1. The table shows that in all cases the values of the soluble fraction were very low, and, in particular, acquiring values between 0.2 and 6.3% w/w. These results indicate both the complete polymerization of the DMAAm monomer and the MBAAm and DHEBA cross-linkers in the case of the SN hydrogels, and, at the same time, the complete incorporation of the loosely cross-linked second polyDMAAm network in the DN hydrogels. The highest amount of soluble fraction was observed in the case of the "inert" DMAAm-DHEBA 1-4/OXG SN hydrogel, and this may be attributed to the increased absorbed amount of OXG photoinitiator in the particular hydrogel that is released upon the immersion of the hydrogel in water. This finding is consistent with the relatively higher value of the equilibrium DS of the DMAAm-DHEBA 1-4 SN hydrogel than the MBAAm-containing hydrogel, and, consequently, the higher value of the preparation DS of the "inert" DMAAm-DHEBA 1-4/OXG SN hydrogel. In contrast, the soluble fraction of the "inert" DMAAm-MBAAm 1-4/OXG SN hydrogel was the same as the value for the corresponding plain hydrogel, due to the low swelling of the hydrogel precursor in the aqueous solution of the OXG photoinitiator. The table also shows that the DN and the "deactivated" DN hydrogels containing DHEBA cross-linker in both polymer

networks exhibited increased amounts of soluble fraction, possibly owing to the slightly decreased cross-linking efficiency of the DHEBA cross-linker. In contrast, the values of the soluble fraction of the corresponding DN and "deactivated" DN hydrogels based on the DMAAm-MBAAm 1-4 SN hydrogel were lower, due to the high cross-linking efficiency of the MBAAm cross-linker.

3.2.5 Degradation of the Fully Degradable Hydrogels and Identification of the Structure and Composition of the Degradation Products

Sodium periodate ($NaIO_4$) is a reagent known to cleave vicinal diols, leading to the formation of the corresponding aldehyde or ketone.[5-8] This reagent was chosen for the cleavage of the vicinal diol moiety in the DHEBA cross-linker units. To this end, samples of the degradable DMAAm-DHEBA 1-4 SN hydrogel, the "inert" degradable DMAAm-DHEBA 1-4/OXG SN hydrogel, the fully degradable DMAAm-DHEBA 1-4/DMAAm-DHEBA 2-0.1 DN hydrogel, and the "deactivated" fully degradable DMAAm-DHEBA 1-4/OXG/DMAAm-DHEBA 2-0.1 DN hydrogel were subjected to degradation by immersing them in an aqueous solution of $NaIO_4$ (2 mg mL^{-1}). The amount of the added $NaIO_4$ was calculated by taking into account the total amount of the degradable DHEBA cross-linker in the SN and DN hydrogels. The molar ratio of the $NaIO_4$ to the DHEBA cross-linker repeating units was equal to 2:1, to ensure the complete cleavage of the vicinal diol groups in the DHEBA cross-linker units in the hydrogels, according to Nayak et al.[7] After the addition of the aqueous solution of $NaIO_4$, the hydrogels were left undisturbed at room temperature for 10-15 days in order to allow the hydrogels to be transformed into a clear transparent solution. Subsequently, the water was completely removed using a rotary evaporator at 60 ^oC and a vacuum oven at 50 ^oC, and a certain amount of the obtained soluble species was dissolved in deuterated water (D_2O) and characterized using ^1H NMR spectroscopy to identify the structure of the soluble species and calculate their composition. Figure 3.2.1 depicts the ^1H NMR spectra of the samples obtained after the degradation using $NaIO_4$ of the DMAAm-DHEBA 1-4 SN hydrogel (part (a)) and the DMAAm-DHEBA 1-4/DMAAm-DHEBA 2-0.1 DN hydrogel (part (b)).

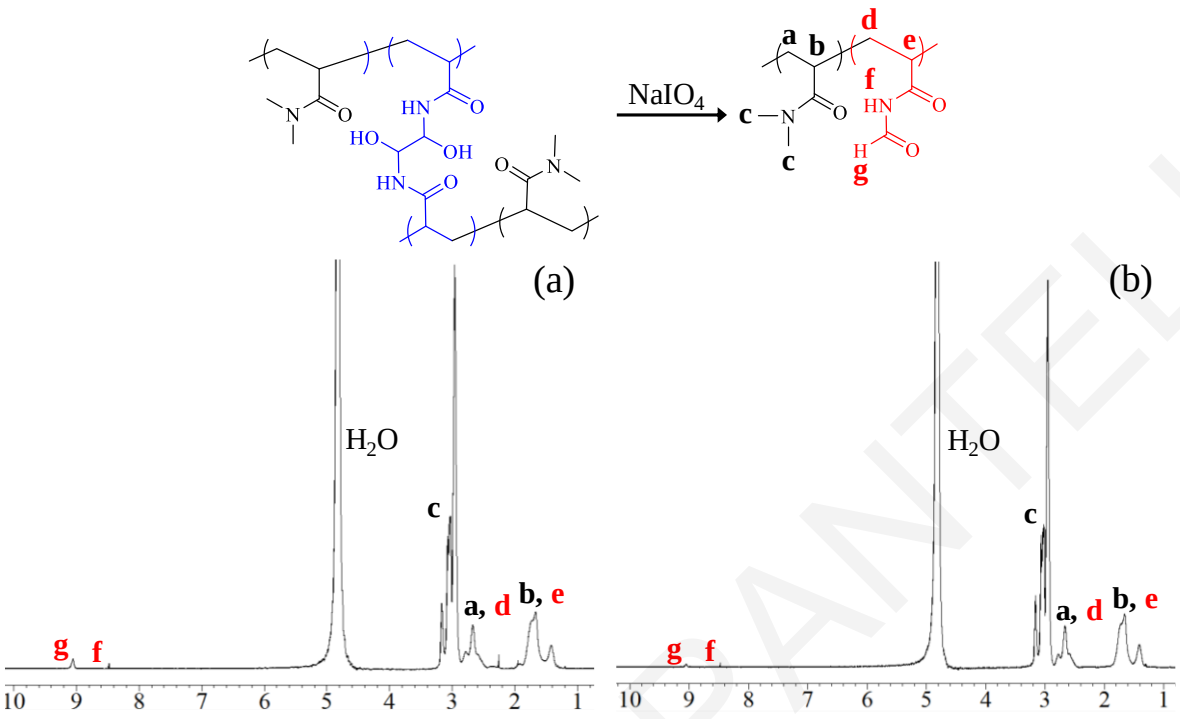

Figure 3.2.1. ^{1}H NMR spectra in D_2O of the hydrogels after their treatment with $NaIO_4$. (a) DMAAm-DHEBA 1-4 SN hydrogel, and (b) DMAAm-DHEBA 1-4/DMAAm-DHEBA 2-0.1 DN hydrogel.

Both parts of Figure 3.2.1 show that only a new peak, *g*, at δ = 9.10 ppm appeared in the ^{1}H NMR spectrum of both the SN and DN hydrogels, arising from the cleavage of the vicinal diol group in the DHEBA cross-linker repeating units in the hydrogels. It was expected that after the treatment of the vicinal diol group in the DHEBA cross-linker units with $NaIO_4$, the hydroxyl groups would be oxidized, resulting in the formation of two equivalents of the corresponding aldehyde, as the DHEBA cross-linker is a symmetrical molecule. Thus, the degradation products are linear random copolymers consisting of DMAAm monomer repeating units and *N*-formylacrylamide (FAAm) monomer repeating units bearing an aldehyde group. The *g* peak at δ = 9.10 ppm corresponds to the aldehyde proton, –(C=O)–*H*, in the FAAm monomer repeating units in the random copolymers, verifying the formation of the expected degradation products.

However, the *g* peak was found to be more intense in the case of the SN hydrogel. This was due to the lower total content of the DHEBA cross-linker in the DN hydrogel arising from the increased DMAAm polymer volume fraction in the DN hydrogel in comparison with that in the SN hydrogel-counterpart, which was also accompanied by a sufficiently

low amount of DHEBA cross-linker (0.1 mol%) incorporated during the preparation step of the second network.

Subsequently, the ^{1}H NMR spectra were used for the determination of the composition of the degradation products, and, in particular, the determination of the FAAm content in the obtained linear DMAAm-*co*-FAAm random copolymers. The FAAm content was determined by comparing the area under the *g* peak corresponding to the aldehyde proton in the FAAm monomer repeating units (–(C=O)–*H*, δ = 9.10 ppm) to the area under the peak corresponding to the methyl protons on the nitrogen atom (–(C=O)–N(C*H*$_3$)$_2$, δ = 2.85-3.20 ppm) in the DMAAm monomer repeating units. These values, together with the theoretical values calculated from the amount of DHEBA cross-linker in the polymerization feed, are presented in Table 3.2.2. The values of the FAAm content calculated from the ^{1}H NMR spectra were in good agreement with the theoretical values in both cases, although the agreement was better in the case of the SN hydrogel where the FAAm content was higher and, therefore, the accuracy of the experimental measurement was also higher.

Table 3.2.2. Theoretical and experimental values for the FAAm content in the linear random copolymers obtained after the degradation of the SN and DN hydrogels using $NaIO_4$.

No.	Network Structure	FAAm content (mol %)	
		Theoretical	**^{1}H NMR**
1	DMAAm-DHEBA 1-4	7.60	7.40
2	DMAAm-DHEBA 1-4/DMAAm-DHEBA 2-0.1	2.86	2.15

3.2.6 Degradation of the Partially Degradable Hydrogels

Having established the successful degradation of the DMAAm-DHEBA 1-4 SN and the "inert" DMAAm-DHEBA 1-4/OXG SN hydrogels, and the DMAAm-DHEBA 1-4/DMAAm-DHEBA 2-0.1 DN and the "deactivated" DMAAm-DHEBA 1-4/OXG/DMAAm-DHEBA 2-0.1 DN hydrogels using $NaIO_4$, and that the degradation products are soluble, linear DMAAm-*co*-FAAm random copolymers, the partially degradable hydrogels were also subjected to degradation using $NaIO_4$. Similar to the afore mentioned procedure, the amount of the added $NaIO_4$ was again calculated by taking into account the amount of the DHEBA cross-linker in the fully degradable DMAAm-DHEBA

1-4/DMAAm-DHEBA 2-0.1 DN hydrogel, which was the highest. Thus, the added amount of $NaIO_4$ was always constant and the same for all the DN hydrogels subjected to degradation, to ensure the availability of sufficient $NaIO_4$ molecules in the hydrogels to facilitate their degradation. The samples were again left undisturbed at room temperature for two weeks, after which period a network structure was still present in the cases of the DMAAm-MBAAm 1-4/DMAAm-DHEBA 2-0.1 DN, DMAAm-MBAAm 1-4/OXG/DMAAm-DHEBA 2-0.1 "deactivated" DN, DMAAm-DHEBA 1-4/DMAAm-MBAAm 2-0.1 DN and DMAAm-DHEBA 1-4/OXG/DMAAm-MBAAm 2-0.1 "deactivated" DN hydrogels.

3.2.7 Identification of the Possible Structures of the Degradation Products of the Partially Degradable DN Hydrogels

The partially degradable DMAAm-MBAAm 1-4/DMAAm-DHEBA 2-0.1 DN, DMAAm-MBAAm 1-4/OXG/DMAAm-DHEBA 2-0.1 "deactivated" DN, DMAAm-DHEBA 1-4/DMAAm-MBAAm 2-0.1 DN, and DMAAm-DHEBA 1-4/OXG/DMAAm-MBAAm 2-0.1 "deactivated" DN hydrogels consist of the non-degradable DMAAm-MBAAm polymer network and the degradable DMAAm-DHEBA polymer network. Thus, we expected that, $NaIO_4$ treatment would transform their degradable DMAAm-DHEBA component into a solution, whereas their non-degradable DMAAm-MBAAm component would still remain a network. To achieve the hydrolysis of the degradable component, the appropriate amount of $NaIO_4$ was added to the hydrogels, and, after two weeks, the supernatant aqueous solution was removed from each hydrogel, and the water was replaced for three more times in order to allow the soluble species to be completely released. Then, the collected aqueous solutions were combined, the water was removed using a rotary evaporator at 60 ^oC and a vacuum oven at 50 ^oC, and the remaining dried (soluble) species, was weighed in order to evaluate their dry masses.

Due to the successful degradation of the fully degradable DN hydrogels using $NaIO_4$, we expected that the degradation of the degradable component in the partially degradable DN hydrogels would also be successful, and, consequently, the masses of the soluble fraction (degradable component) and the gel fraction (non-degradable component) will be equal to the calculated theoretical dry masses of the corresponding polymer network prior to

degradation. For example, in the case of the DMAAm-MBAAm 1-4/DMAAm-DHEBA 2-0.1 DN hydrogel, the theoretical dry mass of the first non-degradable DMAAm-MBAAm network prior to the degradation should be equal to the mass of the gel fraction after the degradation, whereas the theoretical dry mass of the degradable second DMAAm-DHEBA network should be equal to the mass of the soluble fraction. In contrast, in the case of the DMAAm-DHEBA 1-4/DMAAm-MBAAm 2-0.1 DN hydrogel, the theoretical dry mass of the first degradable DMAAm-DHEBA network prior to the degradation should be equal to the mass of the soluble fraction after the degradation, whereas the theoretical dry mass of the non-degradable second DMAAm-MBAAm network should be equal to the mass of the gel fraction.

The possible structures of the DN hydrogels before and after $NaIO_4$ treatment are schematically illustrated in Figure 3.2.2. In our system, we believe that the loosely cross-linked polymer chains of the second polyDMAAm network, containing either MBAAm or DHEBA cross-linker, are connected onto the active double bonds of the MBAAm or DHEBA cross-linker remaining in the SN hydrogel. In order to deactivate these remaining double bonds, the SN hydrogels were subjected to a photo-induced deactivation prior to the preparation of the DN hydrogels.

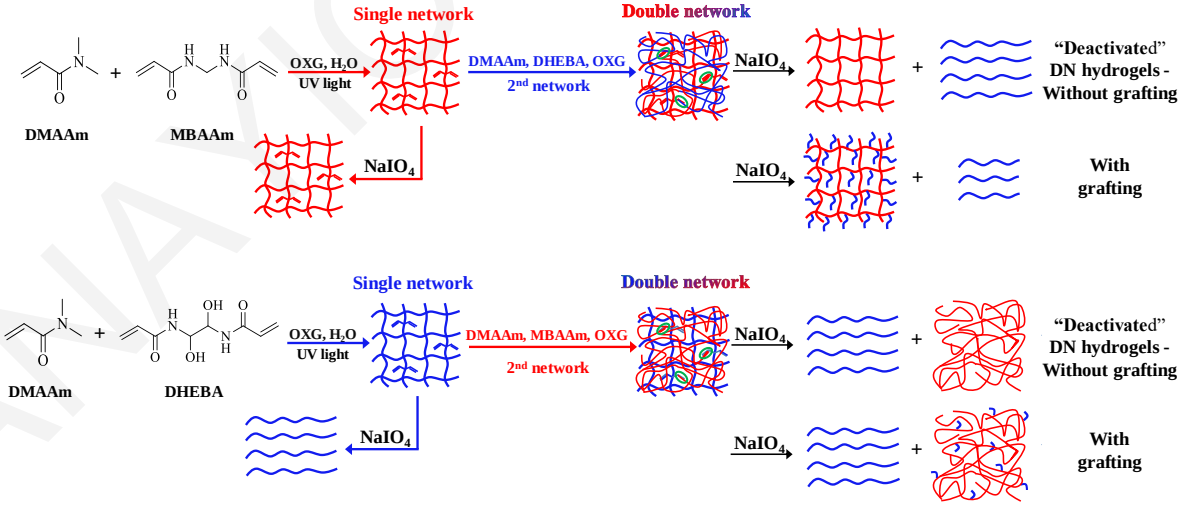

Figure 3.2.2. Preparation and degradation of the partially degradable DN hydrogels based on DMAAm and cross-linked using both DHEBA and MBAAm, with or without deactivation of the remaining pendant cross-linker double bonds right after the preparation of the first network.

Figure 3.2.2 shows that four possible structures can be obtained for the partially degradable DN hydrogels containing both the MBAAm and DHEBA cross-linkers. In the first case,

the double bonds of the cross-linker in the SN hydrogel are completely polymerized or deactivated using OXG photoinitiator, leading to the preparation of a DN hydrogel consisting of two independent polymer networks. Degradation of this DN hydrogel using $NaIO_4$ results in the degradation of the degradable DMAAm-DHEBA second network, whose degradation product, a DMAAm-*co*-FAAm random copolymer, is dissolved in water and is completely released from the non-degradable DMAAm-MBAAm first hydrogel. Thus, it is expected that, the dry masses of the soluble fraction and the gel fraction will be equal to the theoretical dry mass of the corresponding polymer network prior to degradation.

In the second case, the double bonds of the cross-linker in the SN hydrogel are not completely polymerized, and a certain percentage remains active after the preparation of the SN hydrogel. During the preparation of the second network, polyDMAAm chains are grafted onto these double bonds. Subjecting the resulting DN hydrogels to hydrolysis using $NaIO_4$ results in the degradation of the degradable DMAAm-DHEBA network, but the degradation product, a DMAAm-*co*-FAAm random copolymer, is not completely released from the non-degradable DMAAm-MBAAm hydrogel as the degradation product and the DMAAm-MBAAm network are partially covalently interconnected. Thus, it is expected that, the experimental dry masses of the soluble fraction and the gel fraction will not correspond to the theoretical dry masses of the corresponding polymer network prior to degradation. For example, in the case of the DMAAm-MBAAm 1-4/DMAAm-DHEBA 2-0.1 DN hydrogel, the dry mass of the soluble fraction will be smaller than the theoretical dry mass, as the grafted polyDMAAm chains of the second network are connected onto the double bonds of the non-degradable MBAAm cross-linker in the first network, creating permanent intercross-linking points. These interconnections would reduce the amount of the linear DMAAm-*co*-FAAm random copolymer which is available to be released from the degraded second network. This difference in the experimental and the theoretical dry masses was used to determine the degree of interconnection within the DN hydrogels.

3.2.8 Determination of the Degree of Interconnection Within the DN Hydrogels

Table 3.2.3 lists the theoretical and experimental dry masses for both the soluble fraction and the gel fraction for the partially degradable DN and "deactivated" DN hydrogels, which were employed in the determination of the grafting percentage between the two constituent polymer networks, which are also listed in the table. The grafting percentage was calculated by deducting the experimental dry mass from the theoretically calculated dry mass, followed by the division of the result by the total experimental dry mass (soluble and gel fractions) and multiplication by 100. It is worth mentioning that the non-degradable DMAAm-MBAAm 1-4/DMAAm-MBAAm 2-0.1 DN hydrogel and DMAAm-MBAAm 1-4/OXG/DMAAm-MBAAm 2-0.1 "deactivated" DN hydrogel were used as controls and were also subjected to degradation, but the experimental masses of the soluble fractions were found to be equal to the mass of the added $NaIO_4$, ~10 mg, indicating the absence of any degradation of the initial DN hydrogels, as the particular hydrogels did not contain the degradable DHEBA cross-linker.

Table 3.2.3. Experimental dry masses of the gel fraction and the soluble fraction, and the grafting percentage obtained after the degradation of the partially degradable DN hydrogels using $NaIO_4$, and the theoretically calculated dry masses of the partially degradable DN hydrogels prior to degradation.

No.	Double Network Structure	Theor. Dry Mass (g)		Exper. Dry Mass (g)		Grafting (%)
		Gel Fraction	Soluble Fraction	Gel Fraction	Soluble Fraction[a]	
1	DMAAm-DHEBA 1-4/ DMAAm-MBAAm 2-0.1	0.0580	0.0486	0.0501	0.0565	7.3 ± 0.1
2	DMAAm-DHEBA 1-4/OXG/ DMAAm-MBAAm 2-0.1	0.0637	0.0373	0.0658	0.0352	2.5 ± 0.5
3	DMAAm-MBAAm 1-4/ DMAAm-DHEBA 2-0.1	0.0564	0.0445	0.0809	0.0200	20.2 ± 4.0
4	DMAAm-MBAAm 1-4/OXG/ DMAAm-DHEBA 2-0.1	0.0432	0.0784	0.0590	0.0626	13.0 ± 2.1

[a] The final values of the experimental dry masses of the soluble fraction were obtained after the deduction of the mass of the $NaIO_4$ added to the DN hydrogels, which was equal to 0.0100 g.

Table 3.2.3 shows that the highest value of grafting percentage was observed in the case of the DMAAm-MBAAm 1-4/DMAAm-DHEBA 2-0.1 DN hydrogel, 20.2%, whereas the lowest value was obtained in the case of the DMAAm-DHEBA 1-4/OXG/DMAAm-MBAAm 2-0.1 "deactivated" DN hydrogel, 2.5%. Both the "active" DN hydrogels

exhibited a higher value of grafting percentage than the corresponding "deactivated" DN hydrogels. This decrease is attributed to the swelling step of the SN hydrogel-precursor in the aqueous solution of the OXG photoinitiator and its irradiation with UV light prior to the preparation step to obtain the DN hydrogels. This photo-induced deactivation results in the neutralization of the pendant double bonds of the MBAAm and DHEBA cross-linkers in the corresponding SN hydrogel, leading to the preparation of a DN hydrogel comprising two independent polymer networks.

In the case of the DMAAm-DHEBA 1-4/DMAAm-MBAAm 2-0.1 DN hydrogel, the grafting percentage was small, 7.3%, lower than 10%, indicating the almost quantitative polymerization of the DHEBA cross-linker. On the other hand, when the DMAAm-DHEBA SN hydrogel was first allowed to reach swelling equilibrium in the aqueous solution of the OXG photoinitiator and later irradiated by UV light, the grafting percentage was found to decrease by a factor of 3.5. However, the grafting percentage was not found to be 0.0% but rather 2.5 ± 0.5%, indicating that the neutralization was not quantitative, as a very small amount of double bonds of the DHEBA cross-linker still remained active in the SN hydrogel.

In the case of the DMAAm-MBAAm 1-4/DMAAm-DHEBA 2-0.1 DN hydrogel, the grafting percentage was higher, 20.2 ± 4.0%, indicating that a relatively higher amount of double bonds of the MBAAm cross-linker than the double bonds of the DHEBA cross-linker in the SN hydrogel remained active. However, this value was found to decrease by almost a factor of two when the SN hydrogel-precursor was first allowed to reach swelling equilibrium in the aqueous solution of the OXG photoinitiator and later UV irradiated prior to the preparation step for the DN hydrogel.

3.2.9 Conclusions

In the present study, the DMAAm monomer, the non-degradable MBAAm cross-linker and the degradable DHEBA cross-linker were employed for the preparation of SN and DN hydrogels. Due to the combination of both cross-linkers, two different SN hydrogels: a non-degradable and a degradable, and, consequently, four different DN hydrogels were obtained: a totally non-degradable, a fully degradable, and two partially degradable. Prior to the degradation of the partially degradable DN hydrogels using $NaIO_4$, preliminary degradation experiments were performed using the degradable SN hydrogel and the fully degradable DN hydrogel. The characterization of the degradation products using ^1H NMR spectroscopy verified the formation of DMAAm-*co*-FAAm random copolymers, arising from the oxidation of the two neighboring hydroxyl groups in DHEBA cross-linker, as expected. In addition, this method allowed for the determination of the FAAm content in the random copolymers, with the experimental values being in good agreement with the theoretically calculated values, and particularly in the case of the SN hydrogel. In the cases of the partially degradable DN hydrogels, we expected that the degradation using $NaIO_4$ would lead to the degradation of only the degradable DMAAm-DHEBA component, whereas the non-degradable DMAAm-MBAAm component would still remain a network. Thus, both the soluble fraction (degradable component) and the gel fraction (non-degradable component) were collected, completely dried, and weighed. Comparison of the experimental dry masses with the theoretically calculated dry mass of the soluble and the gel fractions resulted in the determination of the grafting percentage within the DN hydrogels, which was relatively low, ranging between 7.3 and 20.2%. Finally, this grafting percentage was found to significantly decrease and become 2.5 and 13.0%, respectively, when the remaining double bonds of the cross-linker in the SN hydrogel were neutralized through a photo-induced deactivation prior to the preparation of the corresponding DN hydrogel.

3.3 Multiple Network Hydrogels Based on the DMAAm Monomer and the MBAAm Cross-Linker Prepared Using Free Radical Photopolymerization[a]

3.3.1 Preparation of the Multiple Network Hydrogels

The multiple network hydrogels of this study were prepared *via* successive aqueous photopolymerizations of monomer and cross-linker within the previous network hydrogel having the immediately lower multiplicity, as is schematically illustrated in Figure 3.3.1. Unlike the previous studies on the conventional PAMPS/PAAm DN hydrogels,[1] and PAMPS/PAAm/PAMPS TN hydrogels,[9] the present system comprised only nonionic components, thereby avoiding any possibly undesired effects arising from electrostatic interactions. Thus, DMAAm and MBAAm were used as the hydrophilic nonionic monomer and cross-linker, respectively, whereas OXG served as the photoinitiator. The employment of five successive photopolymerizations resulted in the preparation of SN, DN, TN, QN, and quintuple (5×N) hydrogels, *i.e.*, networks possessing multiplicity from 1 to 5.

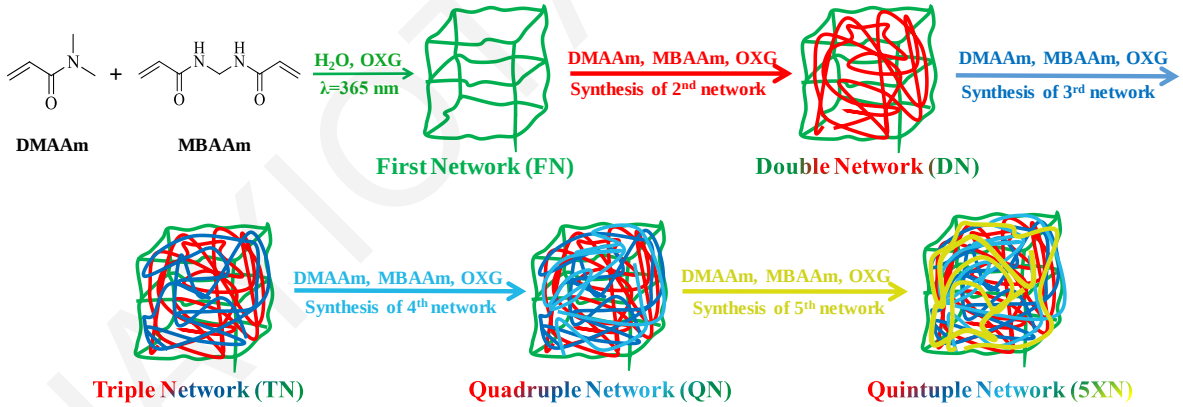

Figure 3.3.1. Synthetic procedure followed for the preparation of the multiple network hydrogels using successive free radical photopolymerizations.

In addition to varying network multiplicity, DMAAm monomer concentration was also varied, acquiring values of 1, 2, 3, 4, and 5 M. The first network was common for all multiple networks and contained DMAAm at a 1 M concentration and a rather high concentration of MBAAm cross-linker, 4 mol% with respect to DMAAm, *i.e.*, 0.04 M. In

[a] Reprinted with permission from *Macromolecules* **2018**, *51*, 7533-7545.

the subsequent networks, the MBAAm concentration was much lower, 0.1 mol% with respect to DMAAm, *i.e.*, 0.001 to 0.005 M, depending on monomer concentration. For a particular network multiplicity, the same DMAAm concentration was employed for the preparation of the second network and upward. For example, a particular quintuple network, whose higher networks comprised a 3 M DMAAm concentration, possessed successive networks in which the DMAAm concentrations were 1 M, 3 M, 3 M, 3 M and again 3 M. In total, twenty-one networks were prepared, and their structures are depicted in Scheme 3.3.1 using concentric circles of different colors (same color coding as in Figure 3.3.1, *i.e.*, green, red, blue, cyan and yellow for the first, second, third, fourth and fifth networks, respectively) and different line thicknesses (thicker lines for the higher DMAAm concentrations).

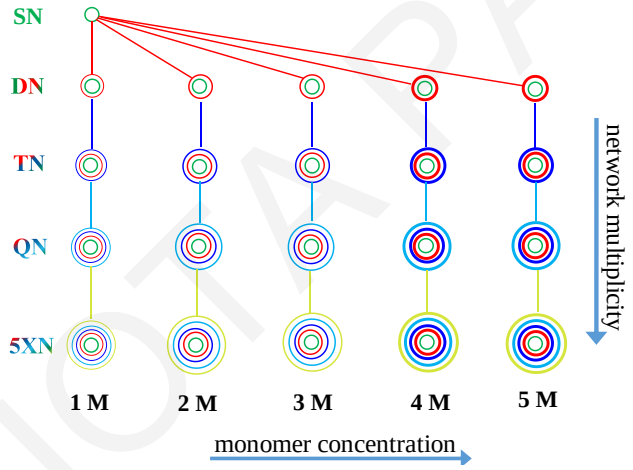

Scheme 3.3.1. "Family tree" for the prepared multiple network hydrogels. Networks are represented *via* concentric circles whose color and line thickness indicate network multiplicity and monomer concentration, respectively. Green, red, blue, cyan and yellow colors indicate the first, second, third, fourth and fifth networks, while thicker lines indicate higher monomer concentration.

3.3.2 Degrees of Swelling (DSs) of the Multiple Network Hydrogels

The effects of network multiplicity and monomer concentration on the DS at the preparation state for the multiple network hydrogels are depicted in Figure 3.3.2. Part (a) of Figure 3.3.2 is the three-dimensional (3-D) representation of the dependence of the DS at the preparation state on network multiplicity and monomer concentration, whereas parts (b) and (c) are the two-dimensional (2-D) projections focusing on the effects of the two parameters separately. The maximum value of the DS at preparation plotted in Figure 3.3.2 was 5.5 and was exhibited by the DN with 1 M monomer concentrations, while the

minimum DS value was 1.4 and was displayed by the 5×N network with 5 M monomer concentrations. Due to its much higher value than its homologues, the DS at preparation of the single network of 9.5 was not plotted in Figure 3.3.2. The figure shows that an increase in monomer concentration or network multiplicity led to a reduction in the DSs at preparation. The DSs at preparation decreased almost linearly with network multiplicity (Figure 3.3.2 (c)), especially from double to quadruple networks, whereas the DSs at preparation decreased more abruptly upon increasing monomer concentration from 1 to 2 M (Figure 3.3.2 (b)), and less abruptly when increasing to higher monomer concentrations.

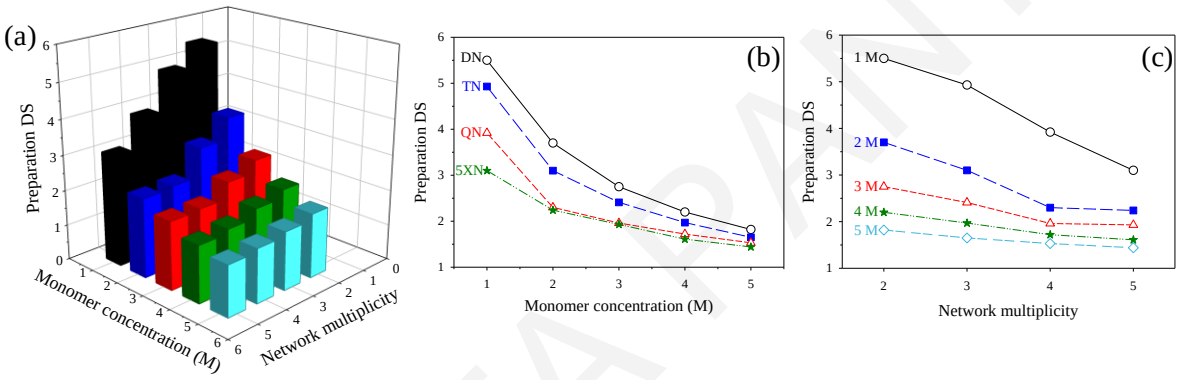

Figure 3.3.2. Effects of monomer concentration and network multiplicity on the aqueous degrees of swelling at preparation for the multiple networks. (a) Three-dimensional plot showing the effects of both monomer concentration and network multiplicity on the degrees of swelling at preparation. Two-dimensional plots separately presenting the dependence of the degrees of swelling at preparation on (b) monomer concentration and (c) network multiplicity of the multiple network hydrogels.

To explain the trend of the DSs at preparation *vs.* network multiplicity (Figure 3.3.2(c)), we consider the experimental sequence followed to make the multiple hydrogels: starting from the SN hydrogel with a value of DS at preparation of 9.5, this network was subsequently equilibrium swollen in aqueous solutions of DMAAm monomer with five different concentrations, from 1 to 5 M, also containing a small amount of MBAAm cross-linker. Figure 3.3.3 plots the dependence of the values of the DSs at the preparation and swelling equilibrium states on network multiplicity of the hydrogels after their equilibrium swelling in the aqueous solutions of 1 M (part (a)), 2 M (part (b)), 3 M (part (c)), 4 M (part (d)), and 5 M (part (e)) DMAAm, also containing 0.1 mol% MBAAm cross-linker. In all five cases, the DSs at swelling equilibrium were moderately higher than the initial DS at preparation, as indicated in the five plots in Figure 3.3.3. Upon their photopolymerization, these DMAAm-MBAAm solutions were converted to the second networks, which,

together with the SN would constitute the DNs, and would necessarily possess a higher (global, taking into account polyDMAAm from both networks) polymer volume fraction, and, consequently, a lower DS than its SN at preparation. This was also the case for the subsequent polymerization steps for the preparation of the higher networks. It appears that, in all cases, the gain in polymer volume fraction upon polymerization was greater than the reduction in polymer volume fraction during equilibration in the monomer/cross-linker mixture, which led to a gradual increase in polymer volume fraction and a corresponding reduction in the DS at preparation with network multiplicity.

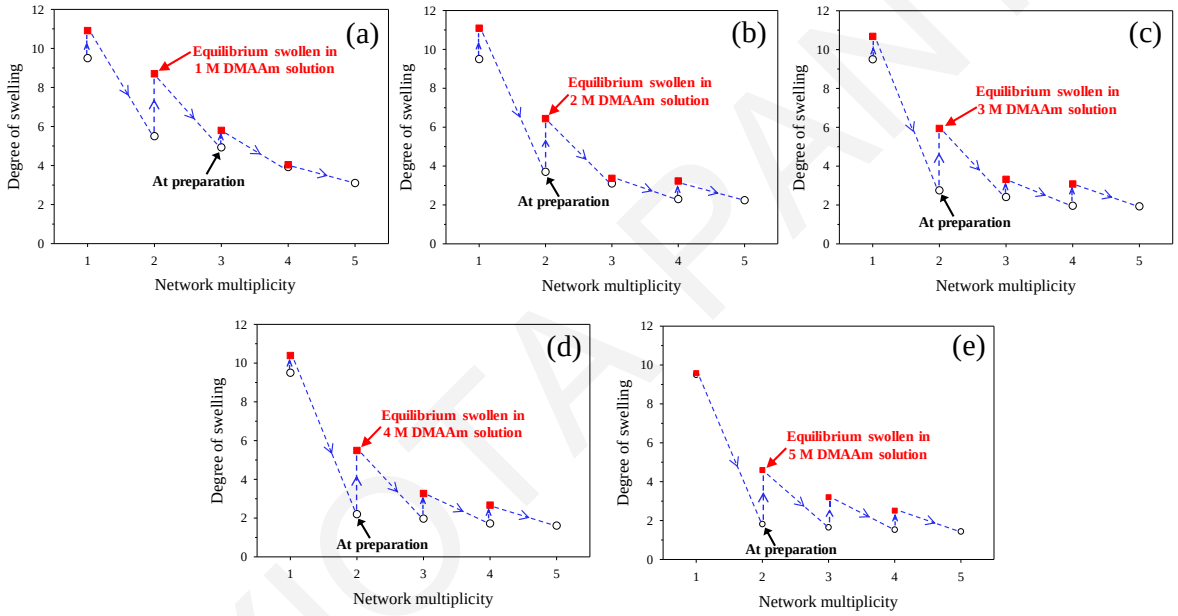

Figure 3.3.3. Effect of network multiplicity on the degrees of swelling at preparation and after equilibrium swelling in (a) 1 M, (b) 2 M, (c) 3 M, (d) 4 M, and (e) 5 M DMAAm aqueous solutions also containing 0.1 mol% MBAAm cross-linker relative to monomer.

Figure 3.3.3 can also be used to explain the trend of the DS at preparation *vs.* monomer concentration (Figure 3.3.2(b)). We first observed that the equilibrium DS in the various DMAAm concentrations of a network with a particular multiplicity was nearly independent of monomer concentration, as it differed only by 16% from 1 to 5 M for the SNs, as indicated in parts (a) and (e) of Figure 3.3.3. Given this, upon their photopolymerization, solutions with a higher DMAAm concentration in the incoming network would be expected to lead to multiple network hydrogels with a higher polymer volume fraction, and, consequently, a lower DSs at preparation, which is indeed the experimental observation. For example, assuming a DS of the SN equilibrated in 1 M and

5 M DMAAm monomer concentrations to be the same and equal to 10 (they actually were 11 and 9.5, respectively), a DS at preparation for the DN can be calculated to be equal to 5.3 and 1.8, respectively, for the two above cases, which is very close to the values actually measured and presented in Figure 3.3.2(b).

Another important parameter is the prestretch ratio of the SN within the multiple network hydrogels.[10] The prestretch ratio is equal to the cube root of the ratio of the DS of the first network alone (inverse of the polymer volume fraction of the first network) within the complex hydrogel system divided by the DS of the first network (SN) in its as-prepared state. Figure 3.3.4 shows the dependence of the prestretch ratio on monomer concentration and network multiplicity. Increasing monomer concentration or network multiplicity resulted in an increase in the prestretch ratio. However, this increase was linear only when network multiplicity was increased, and when DMAAm monomer concentration was equal to 3 M and above.

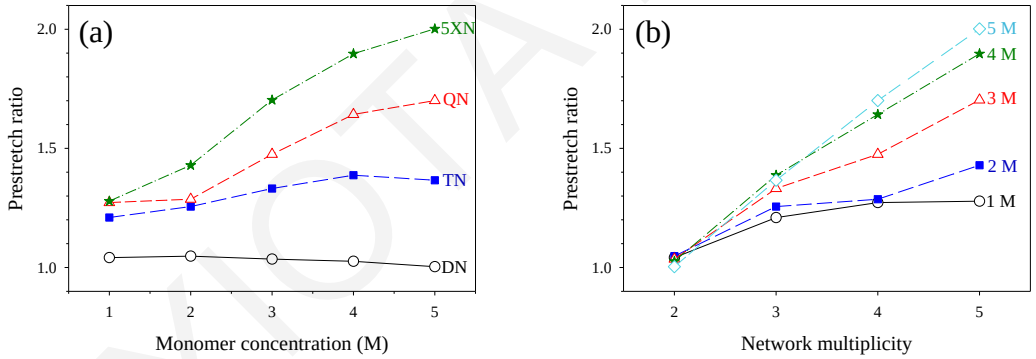

Figure 3.3.4. Prestretch ratio of the SN (first network) within the complex multiple network hydrogels at their as-prepared state, calculated as the cube root of the ratio of the polymer volume fraction in the SN divided by the polymer volume fraction from the first network within the final multiple network. (a) Effect of monomer concentration, and (b) Effect of network multiplicity.

Related to the DSs in water in the as-prepared state are the corresponding water content and polymer volume fraction in the hydrogels. These quantities are plotted in Figures 3.3.5 and 3.3.6. Similar to Figure 3.3.2, part (a) of Figure 3.3.5 is the 3-D plot showing the effects of both monomer concentration and network multiplicity on water content, whereas parts (b) and (c) are the 2-D projections of part (a), separately illustrating the effect of these parameters on water content. The values of the water content span a range between 30.6% for the 5×N hydrogel prepared using a 5 M DMAAm concentration, and 82.0% for the DN prepared using a 1 M DMAAm concentration. Similarly, Figure 3.3.6 shows the

variation of the polymer volume fraction in the hydrogels with respect to monomer concentration and network multiplicity, in a 3-D and two 2-D plots. Polymer volume fractions vary from 0.18 for the DN prepared using a 1 M DMAAm concentration, all the way to 0.69 for the 5×N hydrogel prepared using a 5 M DMAAm concentration.

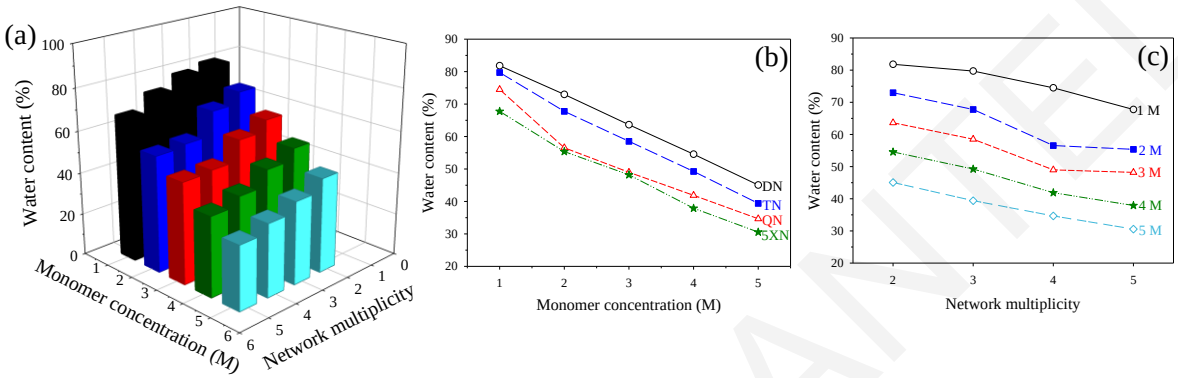

Figure 3.3.5. Water content in the as-prepared multiple network hydrogels. (a) Three-dimensional plot showing the effects of both monomer concentration and network multiplicity. Separate effects of (b) monomer concentration, and (c) network multiplicity.

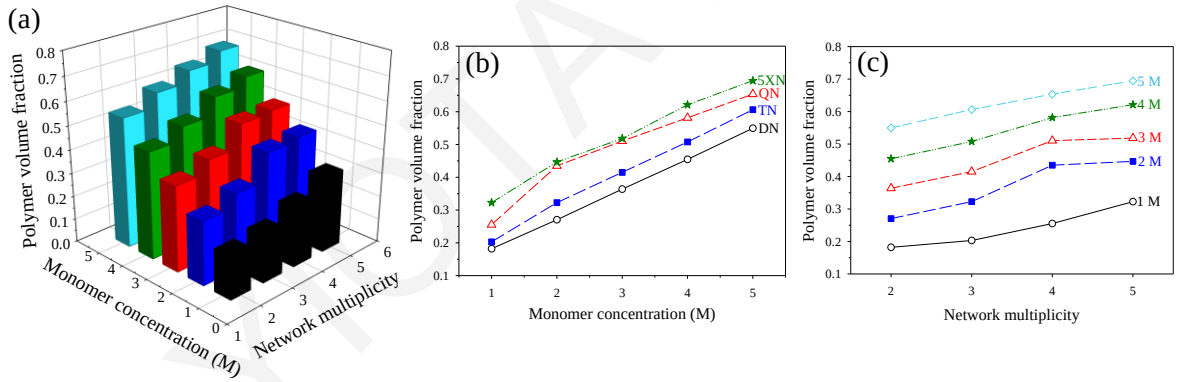

Figure 3.3.6. Polymer volume fraction in the as-prepared multiple network hydrogels. (a) Three-dimensional plot showing the effects of both monomer concentration and network multiplicity. Separate effects of (b) monomer concentration, and (c) network multiplicity.

Figure 3.3.7 presents the equilibrium DSs of the hydrogels in monomer/cross-linker solutions as a function of the DMAAm monomer concentration and network multiplicity. Similar to the previous figures, part (a) of Figure 3.3.7 is the 3-D plot showing the effects of both monomer concentration and network multiplicity on the equilibrium DS, whereas parts (b) and (c) are the 2-D projections of part (a), separately illustrating the effects of monomer concentration and network multiplicity, respectively, on the equilibrium DSs. The figure indicates that the equilibrium DSs decreased both with the DMAAm monomer

concentration and network multiplicity, thereby presenting the same trends as the DSs at preparation illustrated in Figure 3.3.2. Thus, the same explanations may be given here for the behavior presented in Figure 3.3.2.

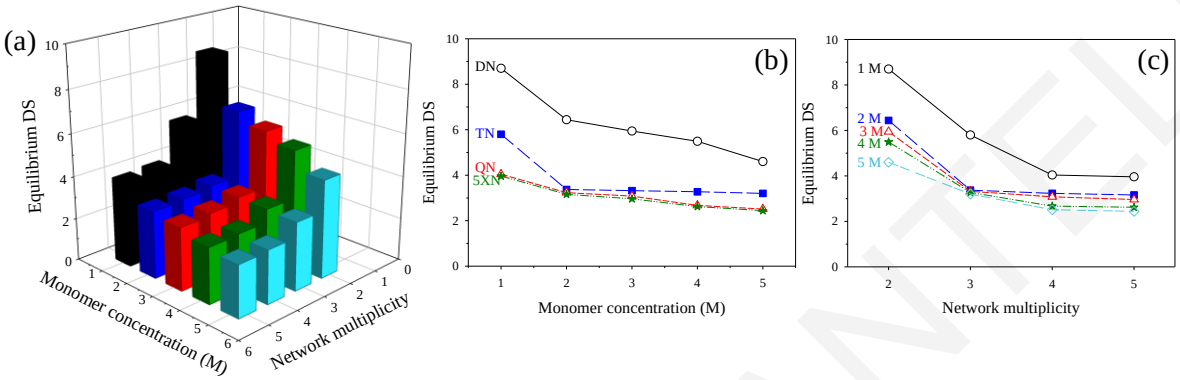

Figure 3.3.7. Aqueous degrees of swelling at equilibrium in monomer / cross-linker solutions for the multiple networks, and their dependence on monomer concentration and network multiplicity. (a) 3-D plot showing the effects of both monomer concentration and network multiplicity on the equilibrium degrees of swelling. 2-D plots separately presenting the effects of (b) monomer concentration and (c) network multiplicity on the degrees of swelling at equilibrium for the multiple networks.

3.3.3 Mechanical Behavior of the Multiple Network Hydrogels

3.3.3.1 Stress-Strain Curves

Figure 3.3.8 presents some original mechanical property data, and in particular, the representative stress-strain curves chosen to be the ones nearest to the average curve from the repetitions. While the stress-strain curves in part (a) of the figure for the multiple network hydrogels at a 1 M monomer concentration have a smooth shape, some curves for hydrogels of higher multiplicity and at higher monomer concentrations, e.g., for the 5×N at monomer concentrations of 2, 3 and 4 M (parts (b), (c) and (d) of the figure), and the QN at a 3 M monomer concentration (part (c)), possess an irregular shape with strain localization, manifesting the presence of network heterogeneities.

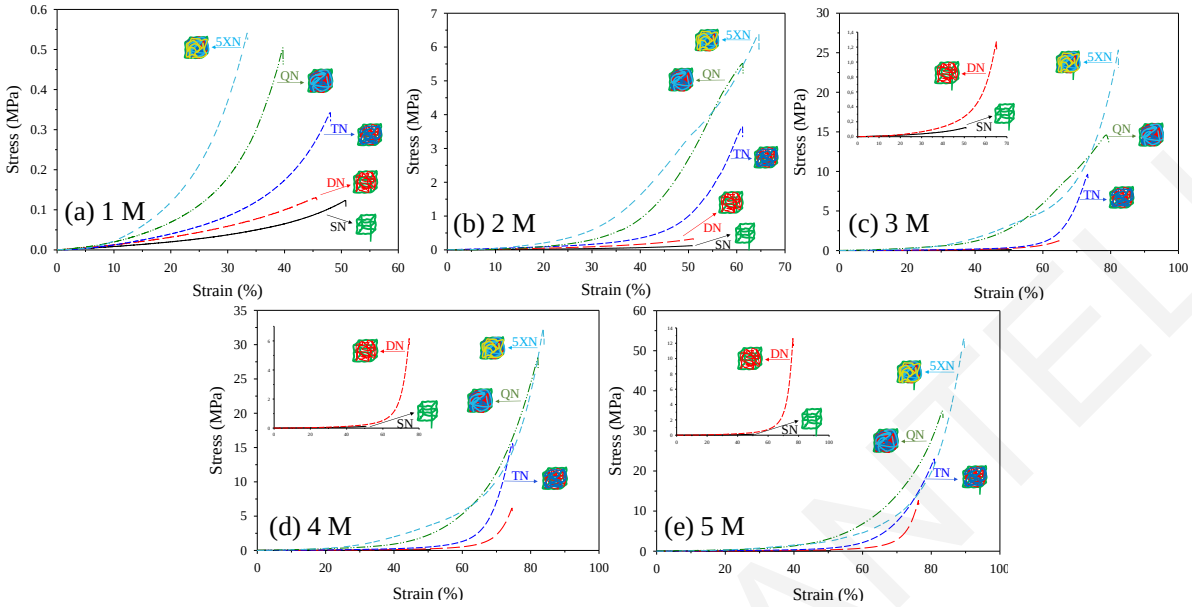

Figure 3.3.8. Overlay of stress-strain curves of the multiple network hydrogels prepared using (a) 1 M, (b) 2 M, (c) 3 M, (d) 4 M, and (e) 5 M DMAAm concentration.

The effects of network multiplicity and monomer concentration on the mechanical properties of the networks are shown in Figures 3.3.9 to 3.3.16. The determined mechanical properties included the compressive fracture stress, fracture strain, fracture energy density, and Young's modulus. Furthermore, we also calculated the network mechanical properties normalized with respect to the DS at preparation, hereafter to be called "normalized mechanical properties". This involved the multiplication of the original mechanical property times the degree of swelling at the measurement (DS at preparation), so as to be fairer with the networks containing more water which would be expected to be softer (less stiff) and weaker (less tough). We expect this normalization procedure to be most appropriate for the Young's moduli, satisfactory for the fracture stress and fracture energy density, and possibly less appropriate for the fracture strain. Finally, we investigated the behavior of selected multiple network hydrogels to cyclic compression and the results are presented in Figure 3.3.17.

3.3.3.2 Fracture Stress

Figure 3.3.9 presents the fracture stress of all the networks in compression, which is a measure of the strength of the materials. Part (a) of Figure 3.3.9 is the 3-D representation of the dependence of the fracture stress on network multiplicity and monomer

concentration, whereas parts (b) and (c) are the 2-D projections focusing on the effects of the two parameters separately. It appears from Figure 3.3.9(a) that an increase in both monomer concentration and network multiplicity led to an increase in the fracture stress of the networks. The 5×N hydrogel made at the maximum monomer concentration, 5 M, was the strongest sample, exhibiting a record of fracture stress of 51 MPa, whereas the weakest sample was the SN (made at a monomer concentration of 1 M) displaying a fracture stress of 0.12 MPa. This 425-fold improvement of the stress at break of the final quintuple network compared to its parent SN shows the great beneficial effect of the four sequential network interpenetrations and demonstrates the power and generality of the double-network concept. This fracture stress of 51 MPa compares favorably with the values of 17 and 26 MPa, reported by Gong[1] and Okay[11] for their DN and TN, respectively, although the values of the DSs were different for the three cases.

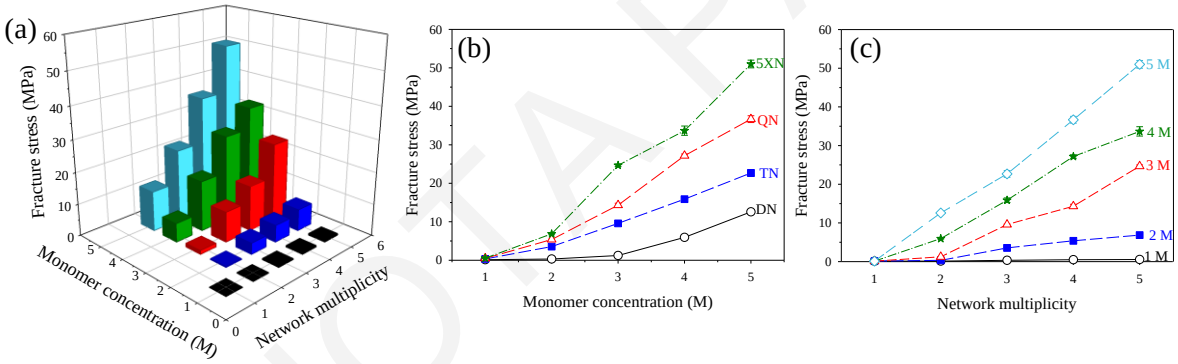

Figure 3.3.9. Compressive fracture stress for the as-prepared multiple network hydrogels, and its dependence on monomer concentration and network multiplicity. (a) Three-dimensional plot showing the effects of both monomer concentration and network multiplicity on the fracture stress. Two-dimensional plots separately presenting the effects of (b) monomer concentration and (c) network multiplicity on the fracture stress of the multiple network hydrogels.

Part (b) of Figure 3.3.9 shows that an increase in monomer concentration caused an almost linear increase in fracture stress, similar to the also almost linear decrease in the DS at preparation observed in Figure 3.3.2(b). For each network multiplicity, the fracture stress points formed an almost perfect straight line if monomer concentrations above 2 M are taken. The slopes of these straight lines were calculated and are listed in Table 3.3.1 (right-hand-side part of the table), and appear to increase with network multiplicity.

Part (c) of Figure 3.3.9 indicates that an increase in network multiplicity resulted in a linear increase in fracture stress, similar to the also linear decrease in the DS at preparation

observed in Figure 3.3.2(c). For each monomer concentration, the fracture stress points formed an almost perfect straight line if network multiplicities equal to 2 and above are taken. The slopes of these straight lines were also calculated and are listed in Table 3.3.1 too (left-hand-side part of the table), and appear to increase linearly with monomer concentration.

Table 3.3.1. Slopes of fracture stress against network multiplicity and monomer concentration calculated from Figure 3.3.9.

***Vs.* Network Multiplicity**		***Vs.* Monomer Concentration**	
Monomer Concentration (M)	**Slope**	**Network Multiplicity**	**Slope**
1	0.12	-	-
2	1.80	DN	5.70
3	6.20	TN	6.60
4	8.80	QN	11.20
5	12.60	5×N	13.20

Thus, a greater fracture stress is attained by increasing either monomer concentration or network multiplicity. However, higher monomer concentration and higher network multiplicity also result in lower DSs, *i.e.*, higher polymer volume fractions, which are expected to favor higher values of fracture stress. To take into account the effect of lower DS, we normalized the values of fracture stress by multiplying them by the corresponding values of the DS at preparation (because characterization of the mechanical properties was performed on as-prepared rather than water-equilibrated samples). These normalized values of fracture stress are presented in Figure 3.3.10, whose three parts correspond to the three parts of Figure 3.3.9. Despite this normalization using the DSs at preparation, the normalized fracture stress again increased with both monomer concentration and network multiplicity. This indicates that there is a net gain for the fracture stress when monomer concentration or network multiplicity are increased. The improvement in normalized fracture stress between the 5×N network prepared at a 5 M monomer concentration and its SN precursor was equal to 66, sufficiently high but much lower than 425, the corresponding improvement of the fracture stress before normalization. The data in parts (b) and (c) of Figure 3.3.10 fell on almost straight lines whose slopes were calculated and

are listed in Table 3.3.2. These slopes are greater than the corresponding values listed in Table 3.3.1, exactly due to the performed normalization.

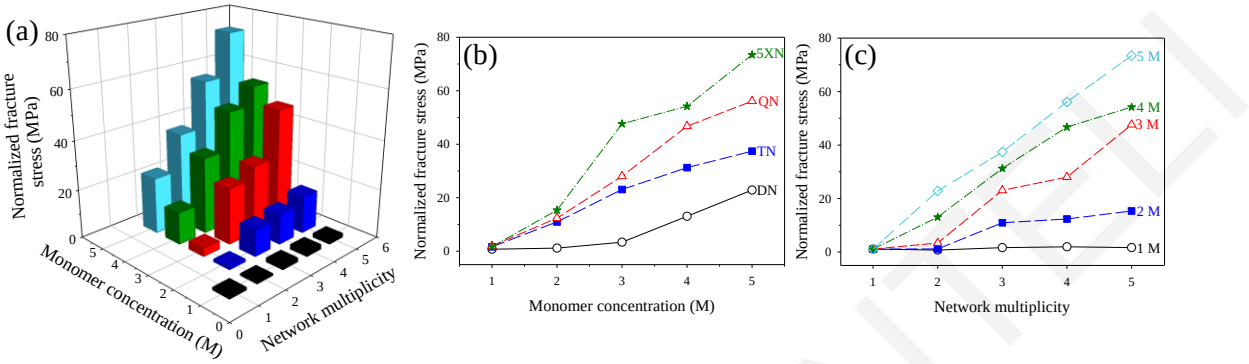

Figure 3.3.10. Normalized fracture stress [= (fracture stress) × (DS at preparation)] in compression for the as-prepared multiple network hydrogels. (a) Three-dimensional plot showing the effects of both monomer concentration and network multiplicity. Separate effects of (b) monomer concentration, and (c) network multiplicity.

Table 3.3.2. Slopes of normalized fracture stress against network multiplicity and monomer concentration calculated from Figure 3.3.10.

***Vs.* Network Multiplicity**		***Vs.* Monomer Concentration**	
Monomer Concentration (M)	**Slope**	**Network Multiplicity**	**Slope**
1	0.20	-	-
2	4.40	DN	9.80
3	13.80	TN	10.10
4	13.90	QN	14.30
5	17.80	5×N	18.20

3.3.3.3 Fracture Strain

Figure 3.3.11 exhibits the fracture strain of the networks in compression, which indicates the percent deformation at break. Part (a) of Figure 3.3.11 is the 3-D representation of the dependence of fracture strain on network multiplicity and monomer concentration, whereas parts (b) and (c) are the 2-D projections focusing on the effects of the two parameters separately. Figure 3.3.11(a) shows that the 5×N prepared at the maximum monomer concentration, 5 M, exhibited the highest fracture strain of ~88%, comparable with 92 and 91%, reported by Gong[1] and Okay[11] for their DN and TN, respectively. On the other extreme, the lowest fracture strain was 33% and was also presented by a 5×N, and, in

particular, the one made at a 1 M monomer concentration. These two observations suggest that, unlike fracture stress, which always increases with network multiplicity, fracture strain decreases with network multiplicity for low monomer concentrations. Further examination of Figure 3.3.11(a) reveals that a minimum monomer concentration of 2 M is required for network multiplicity to always have a favorable effect on fracture strain.

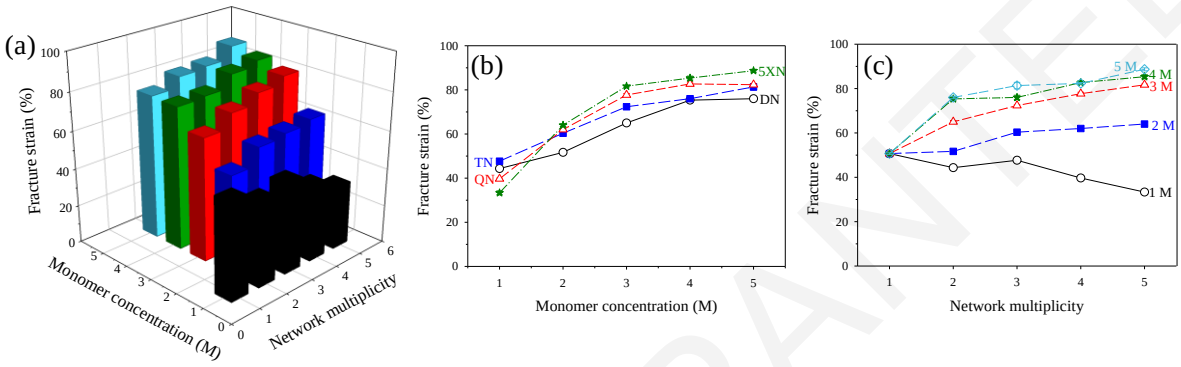

Figure 3.3.11. Fracture strain in compression for the as-prepared multiple networks, and its dependence on monomer concentration and network multiplicity. (a) Three-dimensional plot showing the effects of both monomer concentration and network multiplicity on the compressive fracture strain. Two-dimensional plots separately presenting the effects of (b) monomer concentration and (c) network multiplicity on the compressive fracture strain of the multiple networks.

Part (b) of Figure 3.3.11 plots the dependence of the fracture strain on monomer concentration for the various network multiplicities. The figure shows that an increase in monomer concentration caused an increase in fracture strain for all network multiplicities. However, the curves for the different network multiplicities are almost identical, largely coinciding with each other. Furthermore, the increase in fracture strain levels off at a 3 M monomer concentration for all network multiplicities. Nonetheless, the dependence of fracture strain on monomer concentration was always the same for all network multiplicities, which was not the case for the dependence of fracture strain on network multiplicity, discussed next.

Part (c) of Figure 3.3.11 displays the dependence of the fracture strain on network multiplicity for the various monomer concentrations. The figure shows that the fracture strain dependence on network multiplicity is different for the different monomer concentrations, as already mentioned above. At the lowest monomer concentration, 1 M DMAAm, the compressive fracture strain decreases with network multiplicity. This may be attributed to the values of the DSs of the networks with this monomer concentration for

all network multiplicities. Although the DSs for the networks with this monomer concentration decrease with network multiplicity, the values of these DSs remain relatively high, from 3.1 to 5.5, thereby not helping the network withstand a large deformation (not enough material to prevent crack propagation). At the higher monomer concentrations, 3 to 5 M DMAAm, the compressive fracture strain increases with network multiplicity, with most increase attained when going from the SN to the DN, or from the DN to the TN, and it subsequently levels off for higher multiplicities. For these monomer concentrations, the DS values are lower, from 1.4 to 2.8, and the networks can consequently sustain a greater network deformation before fracture (more effective prevention of crack propagation). Finally, for the intermediate monomer concentration of 2 M, the fracture strain is almost independent of network multiplicity, ranging between 52 and 64% for the double and quintuple networks, respectively.

Thus, fracture strain is slightly favored by a higher monomer concentration for all network multiplicities, and by a higher network multiplicity only at the higher monomer concentrations. However, to also take into consideration in a simple way the effect of lower DS at the higher monomer concentrations and at higher network multiplicities, we again normalized the values of the fracture strain by multiplying them by the corresponding values of the DS at preparation. These normalized values of fracture strain are presented in Figure 3.3.12, whose three parts correspond to the three parts of Figure 3.3.11. One can observe from part (a) of Figure 3.3.12 that the highest normalized fracture strain is exhibited by the DN prepared at a 1 M monomer concentration, whereas the lowest by the 5×N also prepared at a 1 M monomer concentration. These observations indicate the great effect of network multiplicity on the normalized fracture strain for this low monomer concentration.

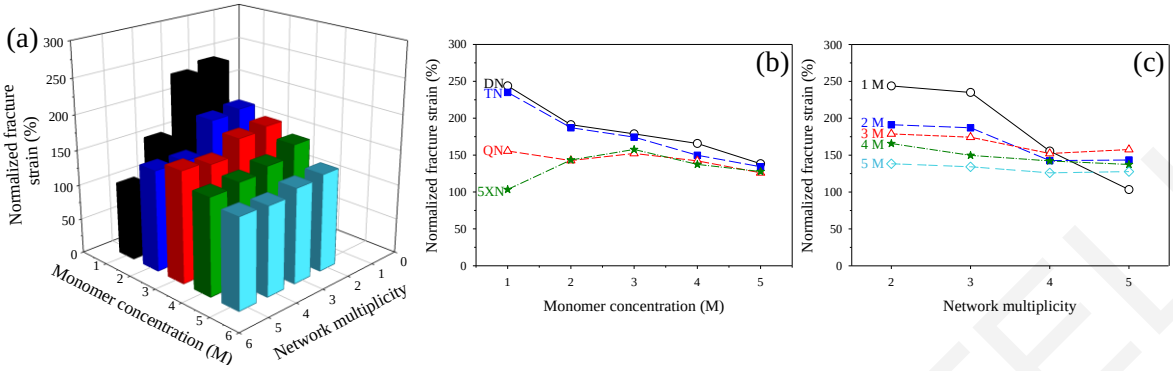

Figure 3.3.12. Normalized compressive fracture strain [= (fracture strain) × (DS at preparation)] for the as-prepared multiple networks. (a) Three-dimensional plot showing the effects of both monomer concentration and network multiplicity. Separate effects of (b) monomer concentration, and (c) network multiplicity.

Figure 3.3.12(b) shows that the normalized fracture strain is almost independent of monomer concentration for monomer concentrations equal to or above 2 M, for all network multiplicities. At the lower network multiplicities, *i.e.*, for the DNs and the TNs, an increase in monomer concentration from 1 to 2 M results in the lowering of the normalized fracture strain. In contrast, the networks with the highest multiplicity, *i.e.*, the quintuple networks, present higher values of normalized fracture strain as monomer concentration increases from 1 to 2 M. Finally, the normalized fracture strain for quadruple networks is almost independent of monomer concentration.

Figure 3.3.12(c) shows the dependence of the normalized fracture strain on network multiplicity for the various monomer concentrations. For the lower monomer concentrations, 1 and 2 M DMAAm, the values of the normalized fracture strain decrease as network multiplicity increases from 3 upwards. In contrast, for the highest monomer concentrations, 3 M and higher, the values of the normalized fracture strain remain constant and independent of network multiplicity. It appears, therefore, that, in contrast to the behavior of the normalized fracture stress, the normalized fracture strain does not always improve as network multiplicity or monomer concentration increases. Thus, when the targeted enhancement in mechanical properties concerns the (normalized) fracture strain, a lower network multiplicity may sometimes be preferable. However, when an optimized (normalized) fracture stress is desirable, a higher network multiplicity is always beneficial. Fracture energy density is another important materials' mechanical property,

bearing features of both the fracture stress and fracture strain, and is discussed next, both in its absolute and normalized forms.

3.3.3.4 Fracture Energy Density

Figure 3.3.13 displays the fracture energy density of the networks in compression (work of compression to fracture) which is a measure of the toughness of the material, calculated as the area under the stress-strain curve, and it is, therefore, expected to exhibit trends intermediate between those of fracture stress and fracture strain. Part (a) of the figure is a 3-D illustration of the fracture energy density with respect to both network multiplicity and monomer concentration, whereas parts (b) and (c) are the 2-D projections showing the effects of these two parameters separately. Figure 3.3.13(a) indicates that an increase in both monomer concentration and network multiplicity resulted in an increase in the fracture energy density of the networks. Thus, fracture energy density qualitatively behaves for the present system similarly to fracture stress rather than to fracture strain. The quintuple network made at the maximum monomer concentration, 5 M, was the toughest sample, exhibiting a record of fracture energy density of 5.5 MJ m^{-3}, whereas the weakest sample was the SN (made at a monomer concentration of 1 M) displaying a fracture energy density of 19 kJ m^{-3}. These values reflect a 290-fold improvement of the fracture energy density of the final quintuple network compared to its parent SN, the result of the tremendous reinforcement of the SN all the way to the quintuple network. This fracture energy density of 5.5 MJ m^{-3} compares favorably with the values of 3.0 and 3.1 MJ m^{-3}, corresponding to the DNs and TNs of Gong[1] and Okay,[11] respectively, although the values of the DSs were different for the three cases.

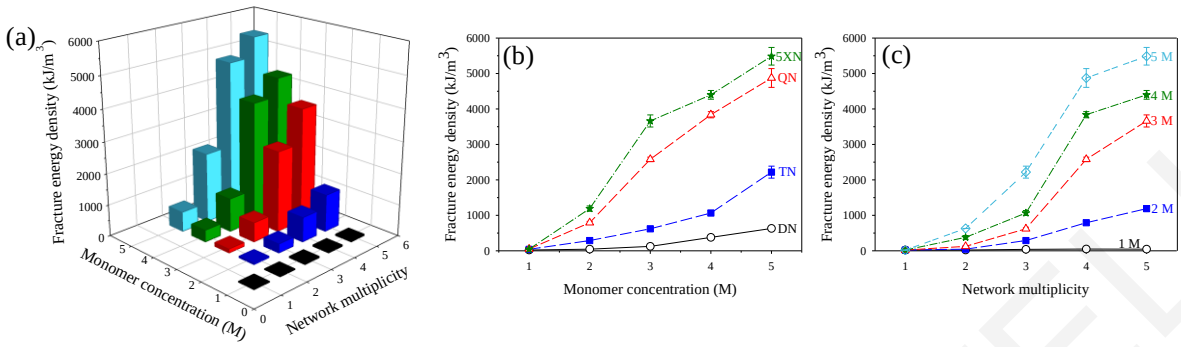

Figure 3.3.13. Fracture energy density in compression for the as-prepared multiple networks, and its dependence on monomer concentration and network multiplicity. (a) Three-dimensional plot showing the effects of both monomer concentration and network multiplicity on the compressive fracture energy density. Two-dimensional plots separately presenting the effects of (b) monomer concentration and (c) network multiplicity on the compressive fracture energy density of the multiple networks.

Part (b) of Figure 3.3.13 shows the dependence of fracture energy density on monomer concentration for the various network multiplicities. For all network multiplicities, fracture energy density increases with monomer concentration. Furthermore, the fracture energy density curves corresponding to higher network multiplicities are shifted upwards, signifying that fracture energy density also increases with network multiplicities. The increase in fracture energy density is linear with monomer concentration for the DNs. This is also the case for the TNs, if the 5 M monomer concentration point were disregarded from the TN-fracture energy density curve. On the other hand, the increase in fracture energy density with monomer concentration presents a concave down shape for the quadruple and quintuple networks, indicating a reduced benefit as monomer concentration increases for these more complex networks. The trends in Figure 3.3.13 (b) (linear and concave down trends) are expectedly intermediate between those in Figures 3.3.9 (b) and 3.3.11 (b), corresponding to fracture stress and fracture strain, which presented linear and concave down trends, respectively.

Part (c) of Figure 3.3.13 presents the dependence of fracture energy density on network multiplicity for the various monomer concentrations. For all monomer concentrations, fracture energy density increases with network multiplicity. Furthermore, the fracture energy density curves corresponding to higher monomer concentrations are located higher than those corresponding to lower monomer concentrations, indicating that fracture energy density also increases with monomer concentration, as already observed before. The

increase in fracture energy density with network multiplicity is linear for monomer concentrations of 1 and 2 M, whereas it is concave down for the three higher monomer concentrations. These trends again reflect those in Figures 3.3.9 (c) and 3.3.11 (c), corresponding to fracture strain and fracture stress, which presented linear and (mostly) concave down trends, respectively.

To check if the trends in fracture energy density against monomer concentration and network multiplicity are preserved when the swelling state of each sample is taken into account, Figure 3.3.14 plots the normalized fracture energy density values against the two above-mentioned parameters. The three parts of this figure correspond to the three parts of Figure 3.3.13. The values of fracture energy density normalized using the DSs at preparation again increase with both monomer concentration and network multiplicity. This indicates that there is a net gain for the fracture energy density when monomer concentration and network multiplicity are increased, even when the DS variation is taken into account. The curves of normalized fracture energy density *vs.* monomer concentration for the lower network multiplicities are linear, as are those of normalized fracture energy density *vs.* network multiplicity for the lower monomer concentrations, whereas the other curves are concave down. Thus, the trends of normalized fracture energy density with respect to the two parameters investigated are the same as those of the original fracture energy density.

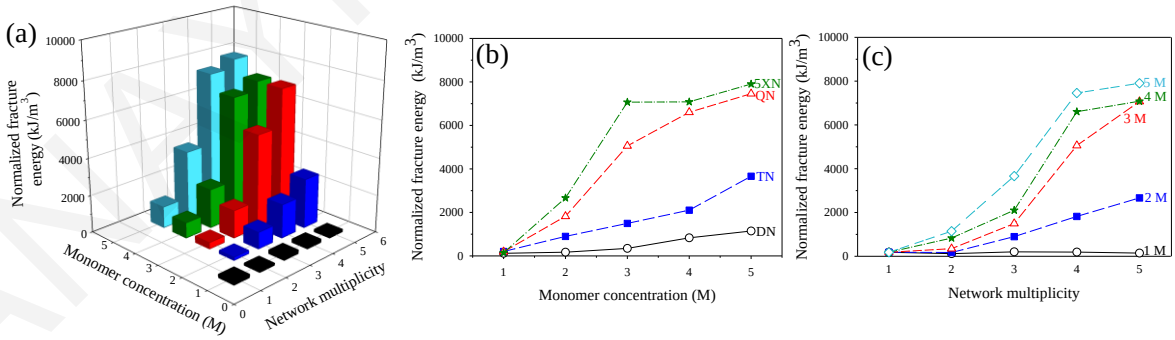

Figure 3.3.14. Normalized fracture energy density [= (fracture energy density) × (DS at preparation)] in compression for the as-prepared multiple networks. (a) Three-dimensional plot showing the effects of both monomer concentration and network multiplicity. Separate effects of (b) monomer concentration, and (c) network multiplicity.

3.3.3.5 Young's Modulus

Figure 3.3.15 exhibits the Young's modulus of the networks in compression, which is a measure of the stiffness of the material, giving the force (per unit area) required to be applied in order to attain a desired (relative) deformation. Part (a) of the figure is a 3-D illustration of the dependence of the Young's modulus on both network multiplicity and monomer concentration, whereas parts (b) and (c) are the 2-D projections showing the effects of these two parameters separately. Figure 3.3.15 (a) shows that an increase in both monomer concentration and network multiplicity resulted in an increase in the compressive Young's modulus of the networks. The quintuple network made at the maximum monomer concentration, 5 M, was the stiffest sample, exhibiting a Young's modulus of about 2.1 MPa, whereas the softest sample was the SN (made at a monomer concentration of 1 M) displaying a Young's modulus of about 0.1 MPa. This 21-fold improvement in the Young's modulus of the final quintuple network compared to its parent SN was the result of the four sequential network interpenetrations conferring upon the quintuple network the double-network enhancement effect four times over. Below we will demonstrate that this enhancement is due, at least partially, to an increase in the concentration of trapped entanglements with network multiplicity. This Young's modulus value of 2.1 MPa compares favorably with the values of 0.47 and 2 MPa, reported by Gong[1] and Okay[11] for their DN and TN, respectively, although the values of the DSs were different for the three cases.

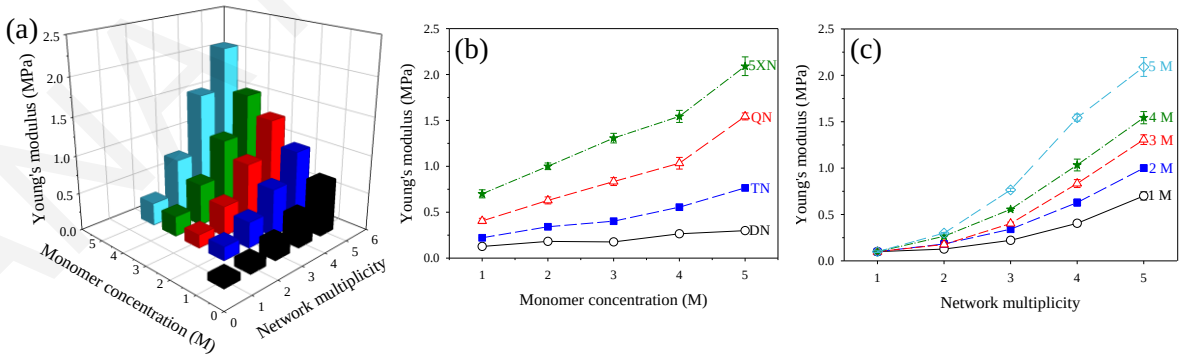

Figure 3.3.15. Young's modulus in compression for the as-prepared multiple networks, and its dependence on monomer concentration and network multiplicity. (a) Three-dimensional plot showing the effects of both monomer concentration and network multiplicity on the compressive Young's modulus. Two-dimensional plots separately presenting the effects of (b) monomer concentration and (c) network multiplicity on the compressive Young's modulus of the multiple networks.

Part (b) of Figure 3.3.15 shows that an increase in monomer concentration from 1 to 4 M caused a very linear increase in Young's modulus for each network multiplicity, whereas the increase in monomer concentration from 4 to 5 M was more abrupt. The modulus increase with monomer concentration may be attributed mainly to the corresponding reduction in the DSs at preparation (Figure 3.3.2).

Part (c) of Figure 3.3.15 shows that an increase in network multiplicity caused an increase in the Young's modulus in a concave up fashion. This modulus increase with network multiplicity may have three origins. First, each subsequent network introduction is accompanied by the entrapment of more entanglements, particularly given the relatively high polymer concentrations in the system (see subsequent section on the normalization of the Young's moduli). Second, with the introduction of a new network, all previous networks, the single network in particular (see Figure 3.3.4), are further stretched out because all as-prepared networks undergo more swelling as they are imbibed in the aqueous solutions of the monomer/cross-linker mixtures (see Figure 3.3.3). This high stretching may lead to strain hardening behavior of the early (first and second) networks, thereby resulting in a higher than expected modulus. Finally third, the introduction of the extra network also brings in some more cross-linker, thereby slightly increasing cross-linking density.

Similarly to the other network mechanical properties, the values of the Young's modulus were also normalized by multiplication by the values of the DSs at preparation. The results of this operation are shown in Figure 3.3.16. Examining first part (a) of the figure, we can see that the highest normalized Young's modulus value was exhibited by the quintuple network prepared at a 5 M monomer concentration. The same network also displayed the highest Young's modulus in an absolute sense (Figure 3.3.15). Thus, the performed normalization using the DS did not change the identity of the stiffest network. However, the lowest normalized Young's modulus was presented by the DN made at a 3 M monomer concentration, rather than the SN (made at a 1 M monomer concentration), indicating that there was a change in the identity of the softest material.

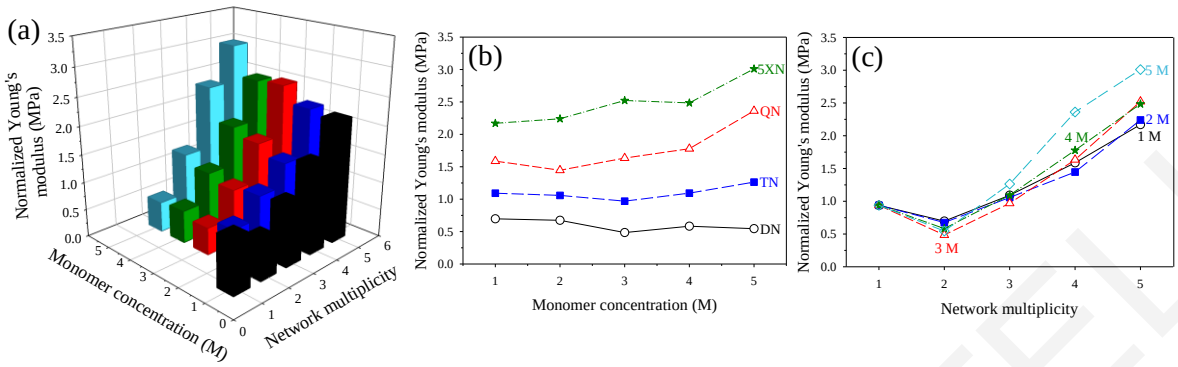

Figure 3.3.16. Normalized Young's modulus [= (Young's modulus) × (DS at preparation)] in compression for the as-prepared multiple networks. (a) Three-dimensional plot showing the effects of both monomer concentration and network multiplicity. Separate effects of (b) monomer concentration, and (c) network multiplicity.

Turning now our attention to part (b) of Figure 3.3.16, we may observe that, for a given network multiplicity, the cross-linking density-normalized Young's modulus ($E \times DS$) is constant with respect to most monomer concentrations, from 1 to 4 M. The same figure shows that these constant values of cross-linking density-normalized Young's moduli increase almost linearly with network multiplicity. This can be better seen in part (c) of Figure 3.3.16, which plots the cross-linking density-normalized Young's modulus *vs.* network multiplicity. This figure shows that, with the exception of the data points corresponding to the higher multiplicity samples at a 5 M monomer concentration, all other data points of the cross-linking density-normalized Young's modulus with respect to network multiplicity collapse on a single master straight line for all other monomer concentrations, exhibiting no dependence on monomer concentration. This is an important finding, which we will analyze in the following paragraph and show that it is due to an overall bulk concentration of elastic chains which remains constant at each monomer concentration, but increases linearly with network multiplicity.

We begin our analysis by mentioning that the shear modulus, S, which is equal to the Young's modulus, E, divided by 3 ($S = E/3$), is proportional to the concentration (per unit swollen gel volume) of the elastically effective chains, ν_e. In particular, the equation connecting these two quantities within the phantom network model is:[12]

$$S = 0.5\, \nu_e\, R\, T \qquad \textbf{Equation 3.1}$$

On the other hand, the degree of swelling, *DS*, is gel volume divided by (dry) polymer volume. Thus, the product of DS times v_e should be equal to the concentration of the elastically effective chains per unit dry gel volume, $v_{e,bulk}$ (bulk concentration of elastic chains):

$$v_{e,bulk} = v_e\, DS \qquad \textbf{Equation 3.2}$$

Combining the above two equations may lead to the calculation of $v_{e,bulk}$ as:

$$v_{e,bulk} = 2\frac{E\, DS}{3\, R\, T} \qquad \textbf{Equation 3.3}$$

which implies that the normalized (with the DS) Young's modulus plotted in the *y*-axis of Figure 3.3.16 is directly proportional to $v_{e,bulk}$. Using average values (for monomer concentrations from 1 to 4 M) for the normalized Young's moduli in Figure 3.3.16(c), we calculated, *via* equation 3.3, the corresponding $v_{e,bulk}$ values which are listed in Table 3.3.3. The same table also presents the bulk concentration of elastic chains calculated from the MBAAm cross-linker loading (estimated as twice the bulk concentration of MBAAm, given the fact that this is a divinyl cross-linker interconnecting four network chains, only half of which belong to its unit cell) in the gels (just those with DMAAm concentrations of 1 and 4 M), taking into account the relevant DSs exhibited by the system at the various stages of the preparation.

Table 3.3.3. Bulk concentration of the elastic chains calculated from the modulus measurements and the cross-linker loading onto the various multiple hydrogels.

No.	Network	Bulk Concentration of Elastic Chains (M)		
		Calculated from modulus measurement	Calculated from MBAAm loading	
			for 1 M DMAAm	for 4 M DMAAm
1	Single	0.252	0.760	
2	Double	0.161	0.380	0.144
3	Triple	0.283	0.214	0.058
4	Quadruple	0.433	0.144	0.030
5	Quintuple	0.633	0.110	0.018

A first observation from the table is that the experimental bulk modulus concentration of elastic chains in the SN calculated from the modulus measurement is smaller than that calculated from the cross-linker loading, possibly due to loop formation. In contrast, the

elastic chain bulk concentration for the triple and higher networks calculated from the modulus measurements are higher than those obtained from the cross-linker concentration. This difference increases primarily with network multiplicity and secondarily with monomer concentration. We propose that this difference is primarily due to an increased concentration of entrapped entanglements which are known to greatly contribute to the Young's modulus,[12-16] and less so to strain hardening and the increase in cross-linker concentration. Regarding strain hardening, a Mooney representation[17] of the stress-strain curves for all multiple networks prepared at 1 and 4 M monomer concentrations indicated strain hardening which increased with monomer concentration. However, this dependence is not consistent with the trend observed in Figure 3.3.16(b), and it may suggest that, whereas strain hardening would also have some contribution to the calculated bulk modulus increase, this contribution might not be the dominant. Regarding the increase in cross-linker concentration, the amount of extra MBAAm cross-linker introduced for the higher networks is minimal compared to that introduced for the preparation of the first network (SN). Indeed, one should expect that the polymer chains should be highly entangled in the present system, especially since the first network is interpenetrated from one (double networks) to four times (quintuple networks), and also since the polymer volume fractions reach the value of 0.7 in some cases. However, at this point, an explanation should be provided as to why the concentration of trapped entanglements is not largely dependent on the monomer concentration in the networks. This may be due to one or more of the following reasons: (a) the constancy of the ratio of monomer to cross-linker concentration used for network preparation, (b) the constancy of monomer concentration in each multiple network sequence (after the first network), and (c) the small contribution of double or multiple entanglements to the modulus increase. The proportionality of the concentration of trapped entanglements to network multiplicity may be attributed to the formation of new types of entanglements between the polymer chains of the new network with all prior networks.

3.3.3.6 Mechanism of Mechanical Property Enhancement

Given Figures 3.3.9 and 3.3.13, showing that fracture stress and fracture energy density increase with both monomer concentration and network multiplicity, it appears that both polymer density and multiple penetration contribute to the enhancement of these two

mechanical properties. First, a higher polymer density in the higher (after the first) networks increases protection of the hydrogel towards fracture *via* inhibition of crack formation and propagation in the first network, as is the case with the conventional AMPS/AAm DN hydrogels. Second, a higher network multiplicity helps in two different ways: one is *via* the protection from fracture of the previous networks by the later networks (multiple DN effect), and the other is *via* the more entanglements formed which cause a corresponding increase in the overall cross-linking density, thereby increasing the stiffness of the hydrogel which also enhances fracture stress and fracture energy density. One may use the normalization procedure and separate the contributions from polymer density and network multiplicity on the mechanical property enhancement. For example, given that the enhancement factor in fracture stress between the 5×N network prepared at a 5 M DMAAm concentration and its parent SN is 425, whereas the corresponding enhancement factor after normalization with the DSs is 66, this may imply that the enhancement in fracture stress arising from polymer density alone is equal only to 6.4 (= 425/66), whereas that from multiplicity alone is equal to 66, *i.e.*, 10.3 times greater than the enhancement coming from polymer density. This may imply that the enhancement in these two mechanical properties mainly originates from multiple penetration, and warrants further investigation.

3.3.3.7 Cyclic Compression

Finally, selected multiple network hydrogels from this study were subjected to cyclic compression testing to assess the reversibility of the materials. Two types of experiments were performed. In the first type, the same sample was repeatedly compressed to the same ultimate strain, whereas in the second type, a fresh sample was compressed, each time, to an increasing ultimate strain. The results are shown in Figure 3.3.17, with the stress-strain curves of the first type of experiments being displayed in parts (a) and (b) of the figure, whereas parts (c) and (d) exhibiting the stress-strain curves from the second type of experiments.

Figure 3.3.17 (a) shows three successive loading-unloading stress-strain curves for the TN hydrogel prepared using a 4 M DMAAm concentration up to a maximum strain of 75%, whereas part (b) of the same figure shows the corresponding curves for the 5×N hydrogel

prepared using a 5 M DMAAm concentration up to a maximum strain of 85%. For both samples, there was hysteresis and energy dissipation mainly in the first cycle, indicating bond fracture and damage in the first network during the first loading, similar to the case of DNs[1] and TNs.[11] However, the hysteresis displayed by the 5×N hydrogel (calculated hysteresis energies were 2.50, 0.38 and 0.39 MJ m^{-3} for the first, second and third compression cycles, respectively) were much larger than the ones presented by the TN (hysteresis energies here were calculated to be 0.310, 0.061 and 0.060 MJ m^{-3} for the first, second and third compression cycles, respectively), probably arising from the greater prestretch ratio[10] of the first network in the former sample than in the latter, and also the accumulation of a higher concentration of heterogeneities in the former sample.[11]

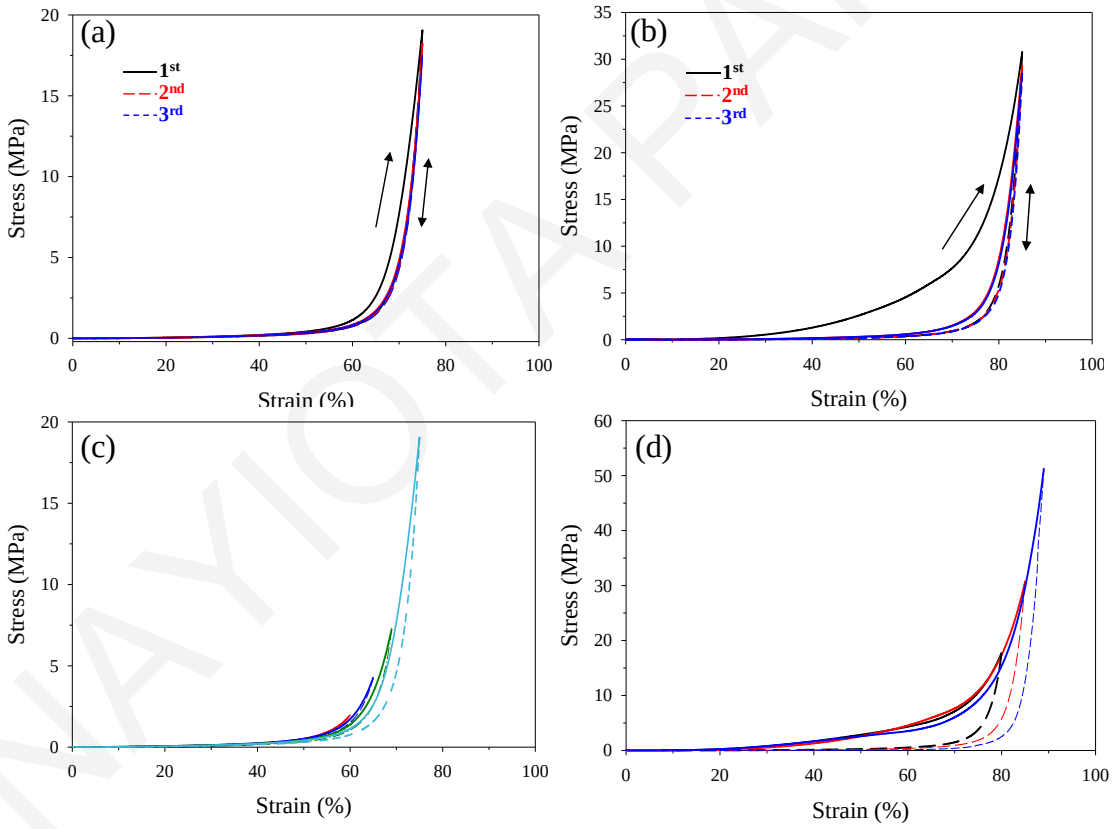

Figure 3.3.17. Cyclic compressive testing of TN and 5×N hydrogels. Three successive loading / unloading cycles for (a) the TN hydrogel prepared using a 4 M DMAAm concentration up to a maximum strain of 75%, and (b) the 5×N hydrogel prepared using a 5 M DMAAm concentration up to a maximum strain of 85%. Successive loading / unloading cycles, with each subsequent cycle reaching a higher strain. (c) Five successive loading / unloading cycles for the TN hydrogel prepared using a 4 M DMAAm concentration with increasing maximum strain values of 50, 60, 65, 70 and 75%. (d) Three successive loading / unloading cycles for the 5×N hydrogel prepared using a 5 M DMAAm concentration with increasing maximum strain values of 80, 85 and 89%. Loading stress-strain curves are illustrated using solid lines, while unloading curves are depicted using dashed lines.

Figure 3.3.17(c) shows five successive loading-unloading stress-strain curves for the TN hydrogel prepared using a 4 M DMAAm concentration with increasing compressive strain values of 50, 60, 65, 70 and 75%, while part (d) of the figure shows three successive loading and unloading stress-strain curves for the 5×N hydrogel prepared using a 5 M DMAAm concentration with increasing compressive strain values of 80, 85 and 89%. All cycles for both samples exhibited hysteresis, with this hysteresis increasing with increasing the ultimate strain (note that here a fresh sample was used for each new cycle). Again, the calculated dissipated energies were much greater for the 5×N (calculated dissipated energies were 1.72, 2.51 and 3.18 MJ m^{-3} for ultimate strain values of 80 85 and 89%, respectively) than the TN (dissipated energies were calculated here to be 0.004, 0.011, 0.035, 0.093, 0.310 MJ m^{-3} for ultimate strain values of 50, 60, 65, 70 and 75%, respectively) samples for the same reasons as those given in parts (a) and (b) of the figure.

3.3.4 Nanoindentation Testing

Finally, some multiple network hydrogels, those prepared using a DMAAm concentration of 1 M, were characterized using a nanoindenter for the determination of their hardness, elastic modulus, and recoverable energy. Prior to presenting the characterization results, Figure 3.3.18 provides the experimental geometry (hydrogel and indenter), the loading profile, and typical load-indentation displacement curves for all five multiple network hydrogels from which the nanoindentation results were extracted.

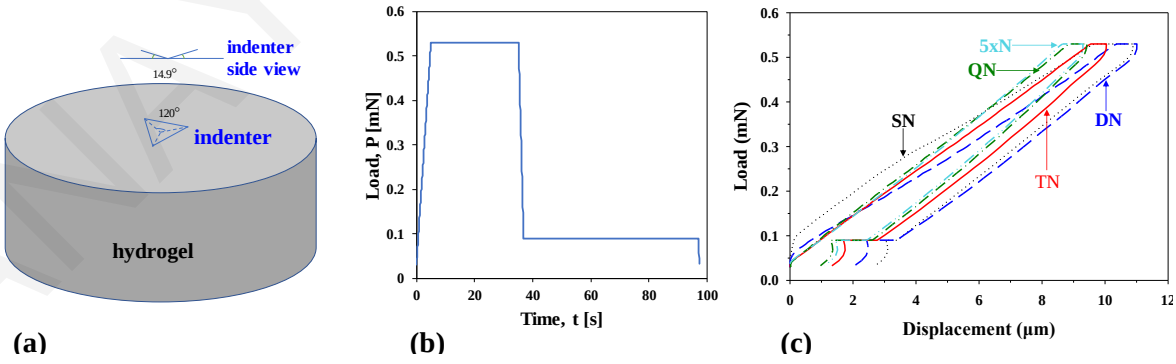

Figure 3.3.18. (a) Experimental geometry, (b) loading profile, and (c) typical load-indentation displacement curves for all five multiple network hydrogels.

Figures 3.3.19, 3.3.20, and 3.3.21 present all the characterization results obtained from the nanoindentation on the multiple network hydrogels prepared using a DMAAm

concentration of 1 M. Figure 3.3.19 shows the effect of network multiplicity on the nanoindentation hardness (in blue) and the elastic modulus determined from the nanoindentation reduced elastic modulus (in black). For comparison, the same figure also plots the network multiplicity dependence of the Young's modulus (in red) determined from the uniaxial compression experiments. All three quantities increased with network multiplicity, consistent with the increase in network compaction with network multiplicity, as indicated by the degrees of swelling depicted in Figure 3.3.2. For all values of network multiplicity, the hardness (resistance to penetration) values were always intermediate between those of the nanoindentation elastic modulus and the elastic modulus from uniaxial compression. The values of the elastic moduli from nanoindentation were always higher than those from the uniaxial compression, because the samples were in their non-linear regime (~30% strain) in the former type of test, thereby being subjected to significant strain stiffening.[18] In contrast, the elastic moduli from uniaxial compressive testing were determined in the linear elastic regime (5-15% strain).

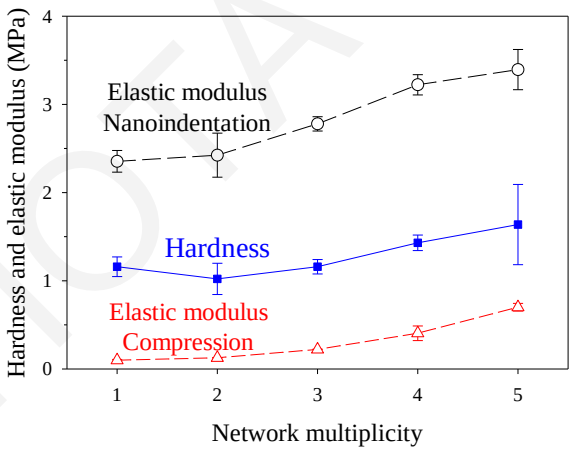

Figure 3.3.19. Dependence of the nanoindentation hardness and elastic modulus on network multiplicity, and comparison with the elastic modulus determined from uniaxial compression.

As it is not possible to calculate the elastic moduli at a lower strain from the present nanoindentation curves collected using a sharp indenter (strain is independent of applied load and penetration depth, and fixed at 25-30%), instead we calculated the elastic moduli from the uniaxial compression tests at a higher strain, 30%, so as to compare these latter values with those from nanoindentation collected at a comparable strain. The thus-calculated values of elastic moduli at 30% strain were indeed higher than those determined from the same compression curves in the linear regime (5-15% strain), thereby confirming

strain stiffening. The particular values for the elastic moduli determined at 30% strain were 0.26, 0.42, 0.56, 1.93 and 4.67 MPa for the SN, DN, TN, QN and 5×N, respectively, in comparison with the values of 0.099, 0.13, 0.22, 0.40 and 0.70 MPa determined for the same network hydrogels at 5-15% strain. Furthermore, these former values approached those determined from the nanoindentation experiments, which were 2.35, 2.42, 2.78, 3.22 and 3.39 MPa, for the SN, DN, TN, QN and 5×N, respectively, with a near-quantitative agreement observed for the higher networks, the QN and the 5×N, in particular.

To separate the effect of network compaction from that of network multiplicity, the three families of data presented in Figure 3.3.19 were normalized by multiplication by the aqueous degrees of swelling at preparation and are replotted in this normalized form in Figure 3.3.20. It is apparent from this figure that, for network multiplicities of two and higher, the normalized values of the nanoindentation hardness and elastic modulus were almost independent of network multiplicity, as they exhibited reductions of 10 and 21%, respectively. This may suggest that the trend in these two quantities presented in the previous figure, Figure 3.3.19, was mainly due to the effect network compactness (cross-linking density) rather than network multiplicity itself. On the other hand, the normalized values of the compressive elastic modulus exhibited an increase of 210% with network multiplicity, as already presented and discussed earlier.

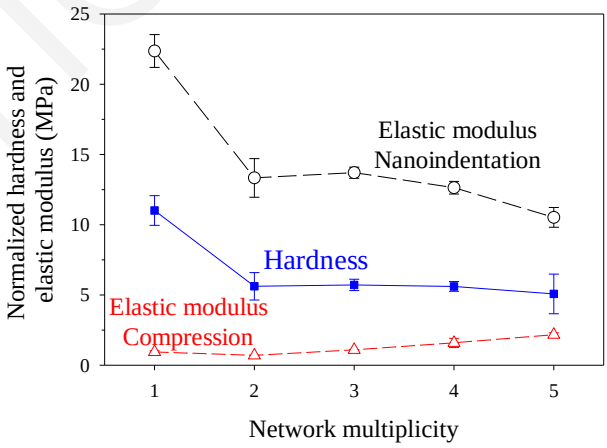

Figure 3.3.20. Dependence of the normalized values of the nanoindentation hardness and elastic modulus, and the compressive elastic modulus of the networks on their multiplicity.

Figure 3.3.21 shows the dependence of the elastic and plastic work (part (a)), and the percentage of the elastic work (part (b)) on network multiplicity. For all network

multiplicities, the elastic work was higher than the plastic work, indicating that most of the energy involved in the nanoindentation process was recoverable. The difference between the elastic and plastic works was between a factor of 2 and a factor of 4, with the difference increasing with network multiplicity, and the percentage of elastic work, also shown in the figure, increasing from *ca.* 65% for the SN upto 80% for the 5×N. These observations indicated that more energy was recoverable for networks of higher multiplicity. These trends were in place, despite the slight decrease in both the elastic and plastic works with network multiplicity, indicating that smaller work was necessary to be provided to the indenter to penetrate the system as multiplicity increased.

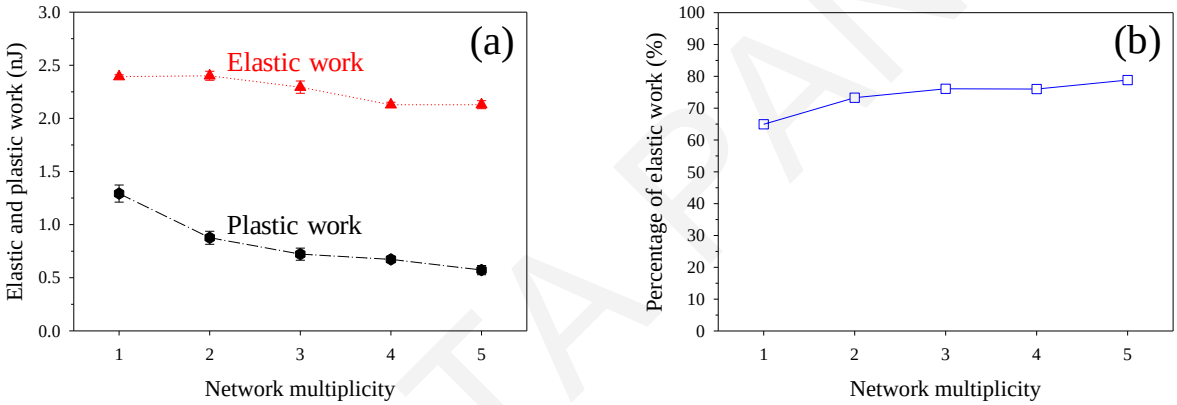

Figure 3.3.21. Effect of network multiplicity on the (a) elastic and plastic works, and (b) the percentage of the elastic work, involved in the nanoindentation process.

3.3.5 Conclusions

A large number (twenty-one) of multiple network hydrogels were prepared in this study using free radical photopolymerization of the DMAAm monomer and the MBAAm cross-linker. The preparations were designed so that the DMAAm monomer concentration was systematically varied from 1 to 5 M, and the hydrogel multiplicity was also systematically varied from one (single) to five (quintuple). The resulting materials were characterized in terms of their mechanical properties in uniaxial compression, which included the stress and strain at break, the fracture energy density, and the Young's modulus. Our measurements showed that fracture stress and fracture energy density increased with both monomer concentration and network multiplicity. Importantly, the values of fracture stress and fracture energy density normalized with respect to hydrogel swelling degrees also increased with monomer concentration and network multiplicity, indicating that there is a net gain in these mechanical properties from increasing monomer concentration and network multiplicity, even when the trends in the degrees of swelling are taken into account. It was estimated, however, that the contribution from network multiplicity to the increase in the fracture stress was greater than that from monomer concentration. In most cases, fracture strain also benefited from increases in monomer concentration and network multiplicity, but the enhancements were smaller than the ones measured for fracture stress and fracture energy density. The Young's modulus of all the hydrogels increased with network multiplicity and monomer concentration; however, their bulk Young's modulus values, calculated by normalization with the degree of swelling, were independent of monomer concentration and increased linearly with network multiplicity beyond the expected values, possibly indicating the formation of new types of entanglements between the polymer chains of the new network with all prior networks. Finally, our results from the characterization of some multiple network hydrogels in terms of their hardness using nanoindentation indicated that hardness and elastic modulus increased with network multiplicity, consistent with the increase in the Young's modulus with network multiplicity determined in the above-mentioned uniaxial compression tests. In addition, the nanoindentation experiments showed that the fraction of elastic work was always high, and also increased with network multiplicity, indicating that more energy is recoverable for the higher networks.

3.4 Randomly Cross-Linked Copolymer Networks Based on DMAAm and DDAAm Prepared Using Free Radical Photopolymerization

3.4.1 Preparation of the Randomly Cross-Linked Copolymer Networks

The preparation of the randomly cross-linked copolymer networks was accomplished in one step using free radical photopolymerization, employing the hydrophobic DDAAm and the hydrophilic DMAAm monomers. DMF was used as the polymerization solvent, as it is a non-selective solvent suitable for the homogeneous polymerization of both monomers and their homopolymers. The hydrophobic HDDA served as the cross-linker and the organosoluble DMPAP as the photoinitiator. Eleven copolymer networks were prepared with a range of compositions, with the DDAAm content varying between 0 and 50 mol%. In addition, in order to elucidate the effect of cross-linking density on the degrees of swelling and the mechanical properties of the randomly cross-linked copolymer networks, two series of gels were prepared, with 1 and 5 mol% with respect to the total moles of HDDA cross-linker. The DDAAm content in the prepared randomly cross-linked copolymer networks is listed in Table 3.4.1.

Table 3.4.1. Structure and composition of the randomly cross-linked polymer conetworks prepared using free radical photopolymerization.

No.	Gel Structure	DDAAm content (mol %)
1	$DMAAm_{100}$-*co*-$HDDA_1$	0
2	($DMAAm_{95}$-*co*-$DDAAm_5$)-*co*-$HDDA_1$	5
3	($DMAAm_{90}$-*co*-$DDAAm_{10}$)-*co*-$HDDA_1$	10
4	($DMAAm_{80}$-*co*-$DDAAm_{20}$)-*co*-$HDDA_1$	20
5	$DMAAm_{100}$-*co*-$HDDA_5$	0
6	($DMAAm_{95}$-*co*-$DDAAm_5$)-*co*-$HDDA_5$	5
7	($DMAAm_{90}$-*co*-$DDAAm_{10}$)-*co*-$HDDA_5$	10
8	($DMAAm_{80}$-*co*-$DDAAm_{20}$)-*co*-$HDDA_5$	20
9	($DMAAm_{70}$-*co*-$DDAAm_{30}$)-*co*-$HDDA_5$	30
10	($DMAAm_{60}$-*co*-$DDAAm_{40}$)-*co*-$HDDA_5$	40
11	($DMAAm_{50}$-*co*-$DDAAm_{50}$)-*co*-$HDDA_5$	50

3.4.2 Degrees of Swelling of the Copolymer Networks in Water and Organic Solvents

In order to investigate the effect of the DDAAm content and the cross-linking density in the randomly cross-linked copolymer networks on their equilibrium degrees of swelling, all gels were immersed in water and in various organic solvents (EtOH, THF, $CHCl_3$, and

toluene), and allowed to reach swelling equilibrium. The dependence of the equilibrium degrees of swelling in water and in the previously mentioned organic solvents on the DDAAm content of the randomly cross-linked copolymer networks cross-linked using 1 mol% (part (a)) and 5 mol% of HDDA cross-linker (part (b)) are plotted in Figure 3.4.1. It is worth mentioning that the copolymer networks prepared using 1 mol% of HDDA cross-linker containing 30 mol% DDAAm or higher did not form a gel, and, therefore, Figure 3.4.1 presents only the values of equilibrium degrees of swelling for the randomly cross-linked copolymer networks containing only 0-20 mol% DDAAm cross-linked using 1 and 5 mol% HDDA.

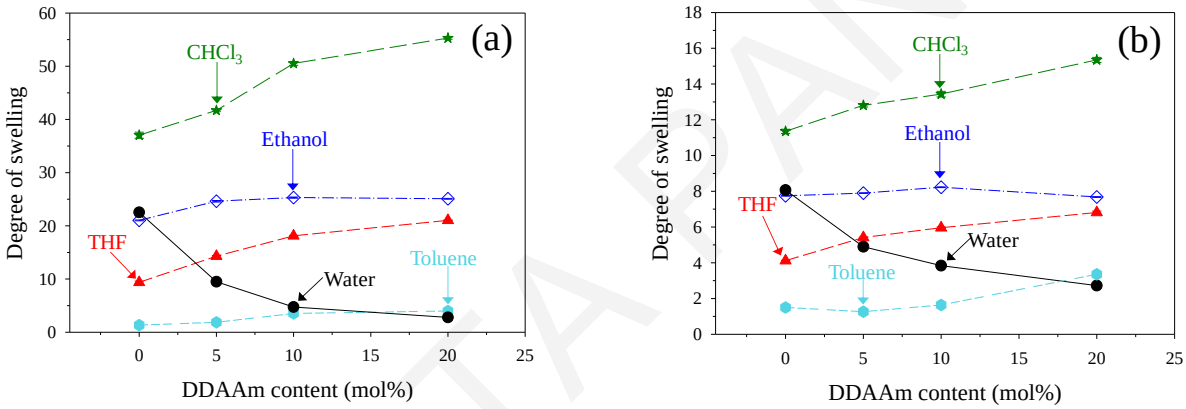

Figure 3.4.1. Effect of the DDAAm content on the equilibrium degrees of swelling of the randomly cross-linked copolymer networks cross-linked using (a) 1 mol% and (b) 5 mol% HDDA.

Figure 3.4.1 shows that the values of the equilibrium DSs depended on the type of solvent, the DDAAm content, and the cross-linking density in the copolymer networks. Increasing the DDAAm content in the copolymer networks resulted in a decrease in the values of the equilibrium DSs in water and an increase in the corresponding values in the organic solvents, as expected. Furthermore, copolymer networks with higher cross-linking density (5 mol%) exhibited lower DSs in all solvents and for all DDAAm contents than the corresponding copolymer networks with lower cross-linking density (1 mol%), also as was expected. The values of the equilibrium DSs increased in the order: toluene < water < THF < EtOH < $CHCl_3$, and this is attributed to the selectivity of each solvent for the particular system.

Both parts of the figure show that the equilibrium aqueous DSs decreased upon increasing the DDAAm content in the copolymer networks, as expected, arising from the increase in

the hydrophobicity of the gels. The highest values of the equilibrium aqueous DSs were obtained in the cases of gels consisting only of DMAAm and HDDA, which were equal to 22.5 and 8.1 for the gels cross-linked using 1 and 5 mol% of HDDA cross-linker, respectively, whereas, in both cases, the lowest values were obtained when the DDAAm content was the highest, 20 mol%.

Regarding the values of the equilibrium DSs in the organic solvents, it was found that these values were significantly affected by the selectivity of each solvent for the randomly cross-linked copolymer networks. In particular, the gels swollen in $CHCl_3$ exhibited the highest values of equilibrium DSs, as this solvent is non-selective and compatible with both the hydrophilic DMAAm and hydrophobic DDAAm monomers and their corresponding homopolymers. In contrast, the lowest values of equilibrium DSs were observed in the case of the gels swollen in toluene, as toluene is also compatible with both monomers, but more suitable for the hydrophobic DDAAm monomer and its homopolymer. Finally, the randomly cross-linked copolymer networks swollen in EtOH and THF exhibited intermediate values of equilibrium DSs in both cases, while these values were found to be almost independent of DDAAm content in the case of the gels swollen in EtOH.

3.4.3 Mechanical Properties of the Water-Swollen Randomly Cross-linked Copolymer Networks

3.4.3.1 Stress-Strain Curves

Figures 3.4.2 and 3.4.3 present the original data obtained from the compression experiments performed on the water-swollen randomly cross-linked copolymer networks. In particular, Figure 3.4.2 displays repetitions of the three stress-strain curves for each of the four water-swollen copolymer networks cross-linked using 1 mol% of HDDA cross-linker, while Figure 3.4.3 presents the corresponding curves for the three water-swollen copolymer networks containing low amounts of DDAAm, 0-10 mol%, and cross-linked using 5 mol% of HDDA cross-linker.

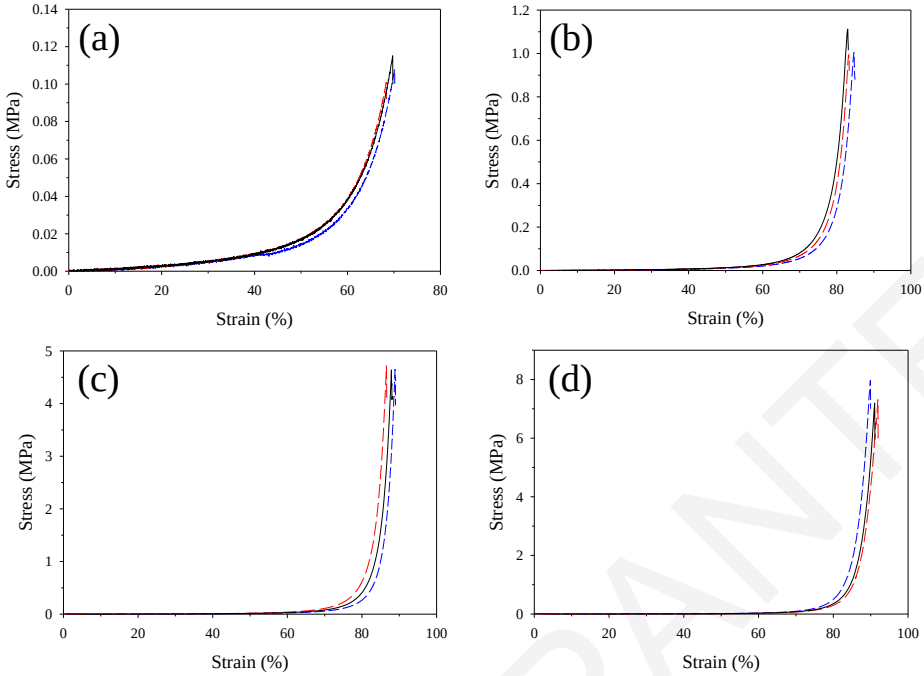

Figure 3.4.2. Compressive stress-strain curves (three repetitions) for the randomly cross-linked copolymer networks cross-linked using 1 mol% of HDDA cross-linker. (a) $DMAAm_{100}$-*co*-$HDDA_1$, (b) ($DMAAm_{95}$-*co*-$DDAAm_5$)-*co*-$HDDA_1$, (c) ($DMAAm_{90}$-*co*-$DDAAm_{10}$)-*co*-$HDDA_1$, and (d) ($DMAAm_{80}$-*co*-$DDAAm_{20}$)-*co*-$HDDA_1$.

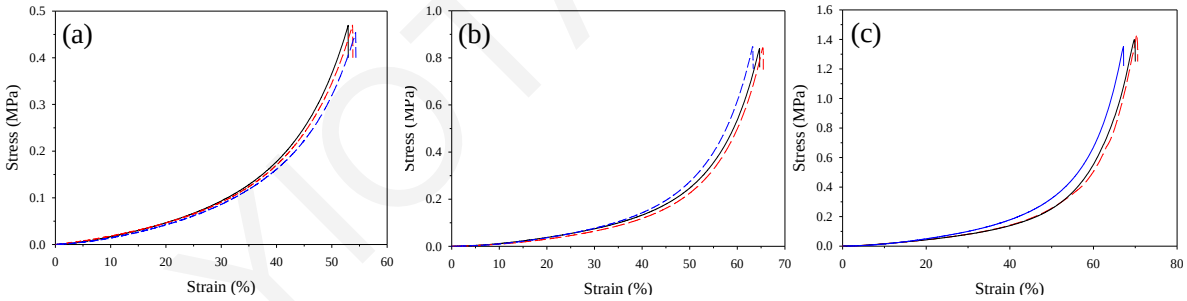

Figure 3.4.3. Compressive stress-strain curves (three repetitions) for the randomly cross-linked copolymer networks cross-linked using 5 mol% of HDDA cross-linker. (a) $DMAAm_{100}$-*co*-$HDDA_5$, (b) ($DMAAm_{95}$-*co*-$DDAAm_5$)-*co*-$HDDA_5$, and (c) ($DMAAm_{90}$-*co*-$DDAAm_{10}$)-*co*-$HDDA_5$.

All stress-strain curves in both figures had a smooth shape without any signs of strain hardening. The randomly cross-linked copolymer networks cross-linked using 5 mol% HDDA and containing 20 mol% DDAAm or higher, upon their immersion and equilibration in water, exhibited a fragile behavior and collapsed, thereby precluding the characterization of their mechanical behavior. In particular, these copolymer networks were highly inhomogeneous, possessing two distinct macrophases. The inner part of the gel was very tough, whereas the outer part of the gel was fragile. This can be attributed to

macrophase separation during gel formation.[19] On the other hand, the samples randomly cross-linked using 1 mol% HDDA and consisting of 30-50 mol% DDAAm did not form a gel at all.

These curves were used for the determination of the fracture stress, fracture strain, Young's modulus, and fracture energy density.

3.4.3.2 Fracture Stress and Fracture Strain

Figure 3.4.4 displays the dependence of the fracture stress values (part (a)) and the fracture strain values (part (b)) on the DDAAm content for the water-swollen randomly cross-linked copolymer networks prepared using 1 and 5 mol% of HDDA cross-linker. Both the fracture stress and fracture strain values increased with increasing the DDAAm content in the copolymer networks. The ($DMAAm_{80}$-*co*-$DDAAm_{20}$)-*co*-$HDDA_1$ randomly cross-linked copolymer network, containing the highest DDAAm content, exhibited the highest values of fracture stress, 7.4 MPa, and fracture strain, 91%. On the other extreme, the $DMAAm_{100}$-*co*-$HDDA_1$ gel exhibited the lowest value of fracture stress, 0.1 MPa, while the $DMAAm_{100}$-*co*-$HDDA_5$ copolymer network possessed the lowest value of fracture strain, 54%, as both copolymer networks were prepared in the absence of the DDAAm monomer.

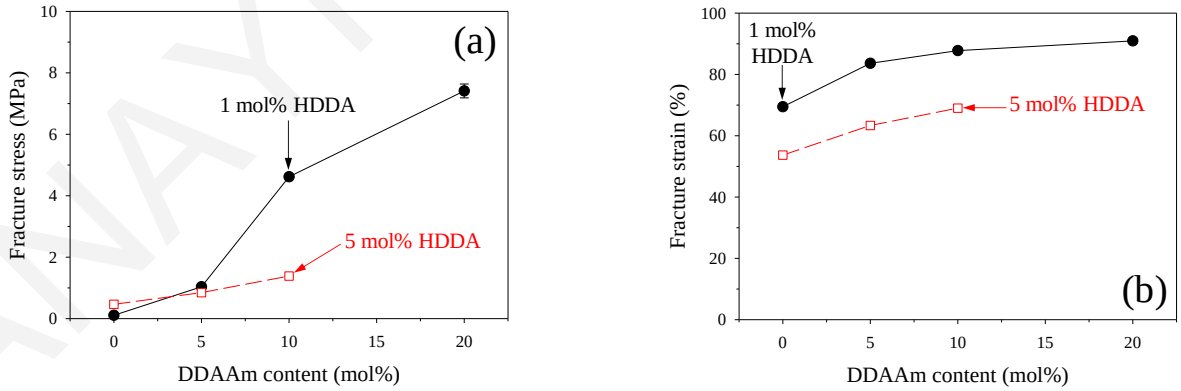

Figure 3.4.4. Dependence of (a) the fracture stress and (b) the fracture strain on the DDAAm content for the water-swollen randomly cross-linked copolymer networks prepared using 1 and 5 mol% of HDDA cross-linker.

Part (a) of the figure shows that increasing the DDAAm content in the randomly cross-linked copolymer networks led to an increase in the fracture stress values for both cross-

linker loadings. This behavior can be attributed to the effect of the DDAAm monomer repeating units on the gel aqueous DS and structure, and also on the formation of semi-crystalline hydrophobic domains among the DDAAm monomer repeating units. When the DDAAm content is low, the values of the equilibrium aqueous DSs are higher, resulting in lower polymer volume fractions, and leading to decreased fracture stress values as the gel cannot sustain a high deformation and fractures more easily. Furthermore, increasing the DDAAm content in the copolymer networks results in enhanced formation of extra physical cross-linking points arising from the presence of crystallites in the gel structure.

In addition, the figure shows that the fracture stress values of the copolymer networks containing 10 mol% DDAAm or higher decreased upon increasing the cross-linking density in the polymer networks. A higher cross-linking density renders the gels more fragile, leading to lower fracture stress values than the corresponding values of the gels containing a lower cross-linking density.

Part (b) shows that the fracture strain values slightly increased with increasing DDAAm content in the copolymer networks for both cross-linking loadings, again due to decreased DS and structure formation. Increasing the cross-linking density in the randomly cross-linked copolymer networks resulted in a large decrease in the fracture strain values, for all DDAAm contents. This can be attributed to the higher flexibility of the polymer chains in the copolymer networks with a lower cross-linking density, which can sustain a greater deformation before they break.

3.4.3.3 Young's Modulus and Fracture Energy Density

Figure 3.4.5 shows the effect of DDAAm content on the Young's modulus values (part (a)) and the fracture energy density values (part (b)). The ($DMAAm_{90}$-*co*-$DDAAm_{10}$)-*co*-$HDDA_5$ gel exhibited the highest value of Young's modulus, 240 kPa, whereas the lowest value, 9.1 kPa, was exhibited by the ($DMAAm_{95}$-*co*-$DDAAm_5$)-*co*-$HDDA_1$ copolymer network. Increasing the cross-linking density in the copolymer networks resulted in increased Young's modulus values, as expected.

The highest value of fracture energy density, 265 kJ m^{-3}, was presented by the ($DMAAm_{80}$-*co*-$DDAAm_{20}$)-*co*-$HDDA_1$ copolymer network, whereas the lowest value, 11

kJ m^{-3}, was exhibited by the $DMAAm_{100}$-*co*-$HDDA_1$ gel. This can be again attributed to the DDAAm content in the copolymer networks; a higher content leads to increased fracture stress and fracture strain values, and, consequently, increased fracture energy density values, as this mechanical property is calculated from the area under the stress-strain curve.

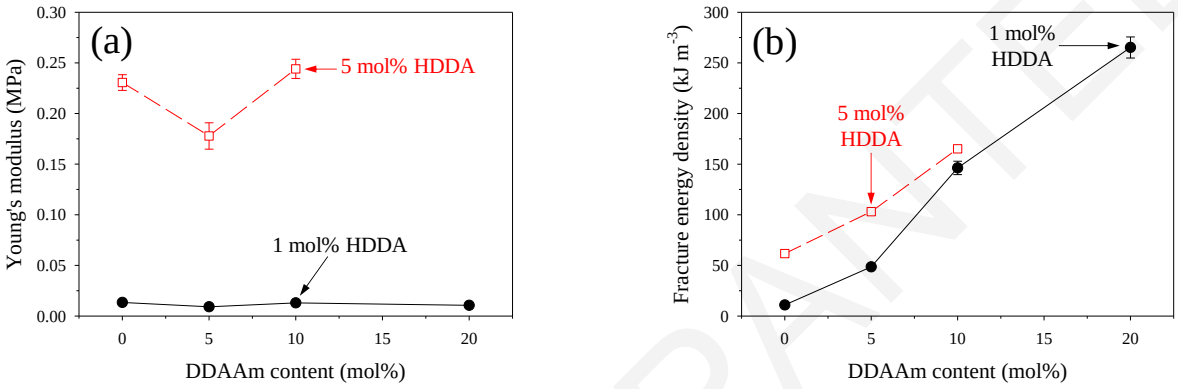

Figure 3.4.5. Dependence of (a) the Young's modulus and (b) the fracture energy density on the DDAAm content for the water-swollen randomly cross-linked copolymer networks prepared using 1 and 5 mol% of HDDA cross-linker.

Part (a) of the figure shows that the values of the Young's modulus mainly depended on the cross-linking density, rather than on the DDAAm content in the randomly cross-linked copolymer networks. In particular, these values increased from 9.1-13.4 kPa to 180-240 kPa when the cross-linking density was increased from 1 to 5 mol% in the copolymer networks. This behavior can be explained by considering the cross-linking density in the gels; a higher cross-linking density results in a tighter cross-linked gel which possesses a higher Young's modulus value, whereas a loosely cross-linked gel exhibits a lower Young's modulus value.

For both types of copolymer networks, the Young's moduli values were found to be nearly independent of the DDAAm content, as they remained almost constant with increasing this value. Thus, there is no measurable effect of the DDAAm content on Young's modulus, indicating that this mechanical property is dominated by the concentration of the chemical rather than the physical cross-links.

Part (b) of the figure shows that increasing the DDAAm content in the randomly cross-linked copolymer networks resulted in an increase in the values of the fracture energy

density for both cross-linking densities. However, in contrast to the fracture stress and fracture strain values, and, similar to the Young's modulus values, the copolymer networks cross-linked using 5 mol% HDDA exhibited higher values of fracture energy density than the corresponding values of the copolymer networks cross-linked using 1 mol% HDDA. This is expected, as the stress values for low strain values were very low in the case of the copolymer networks cross-linked using 1 mol% HDDA, resulting in low fracture energy density values.

3.4.4 Thermal Transition Property

The research groups of Osada,[20] Okay,[21,22] and Furukawa[23] have reported the preparation of amphiphilic randomly cross-linked copolymer networks consisting of the hydrophilic AAc and DMAAm monomers and the hydrophobic *n*-dodecyl acrylate and *n*-octadecyl/stearyl acrylate monomers, bearing a long side chain group that exhibits a melting temperature (T_m). Upon their immersion and equilibration in water, these copolymer networks exhibited shape memory when they were heated up to a temperature near the T_m of the pendant alkyl groups in the hydrophobic monomer repeating units. Very recently, the research group of Li[24] reported the preparation of a thermoresponsive randomly cross-linked copolymer network consisting of AAm and DDAAm monomers, MBAAm cross-linker and nickel nanoparticles. This gel also exhibited a thermoreversible shape memory effect when it was heated up to 50 ^oC, owing to the presence of the pendant dodecyl groups in the DDAAm monomer repeating units that possess T_m around 55-57 ^oC.[25]

Following this work, all randomly cross-linked copolymer networks of this study cross-linked using 1 mol% HDDA and prepared in cylindrical tubes (concentration = 30% w/v) were investigated in terms of their thermal transition property by heating the water-swollen gels up to 50-70 ^oC. In the first step, the water-swollen gels were heated at a temperature near the T_m of the pendant dodecyl groups in the DDAAm monomer repeating units, in order to enable the reshaping of the initial cylindrical shape for the formation of a knot. In the second step, the knot-shaped gel was cooled down to 25 ^oC, leading to the fixation of this temporary shape. In the final step, the knot-shaped water-swollen gel was reheated to 50 ^oC, resulting in the recovery of the gel to its initial shape within a particular time period,

which was found to depend on the composition of the copolymer networks and the temperature. Figures 3.4.6 and 3.4.7 present the photographs obtained for the (DMAAm$_{80}$-*co*-DDAAm$_{20}$)-*co*-HDDA$_1$ and (DMAAm$_{70}$-*co*-DDAAm$_{30}$)-*co*-HDDA$_1$ randomly cross-linked copolymer networks, respectively. Part (a) of Figure 3.4.6 displays the initial shape of the water-swollen (DMAAm$_{80}$-*co*-DDAAm$_{20}$)-*co*-HDDA$_1$ gel, part (b) displays the temporary shape of the copolymer network after its heating and cooling, and, finally, part (c) displays the recovered shape of the copolymer network after its heating. Similarly, part (a) of Figure 3.4.7 displays the initial shape of the water-swollen (DMAAm$_{70}$-*co*-DDAAm$_{30}$)-*co*-HDDA$_1$ gel, part (b) displays the fixed shape after its heating, part (c) shows the temporary shape of the water-swollen gel after its cooling, and, finally, part (d) displays the recovered shape of the polymer network after its heating. It is worth mentioning that the DMAAm$_{100}$-*co*-HDDA$_1$ randomly cross-linked copolymer network, which was used as a control, did not exhibit shape memory behavior, owing to the absence of DDAAm monomer repeating units.

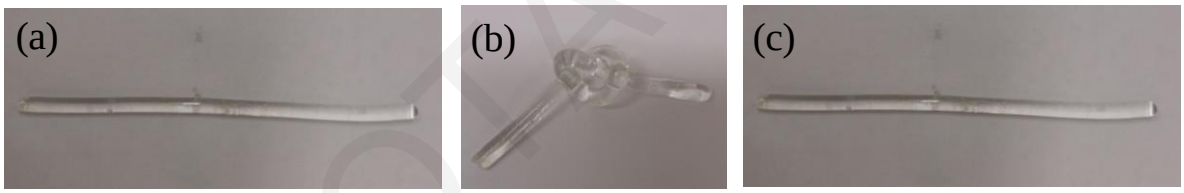

Figure 3.4.6. Shape memory effect for the water-swollen (DMAAm$_{80}$-*co*-DDAAm$_{20}$)-*co*-HDDA$_1$ randomly cross-linked copolymer network. (a) Initial shape at 25 ^{o}C, (b) fixed knot shape after heating the gel up to 50 ^{o}C and cooling down to 25 ^{o}C, (c) recovered shape after heating the gel up to 50 ^{o}C.

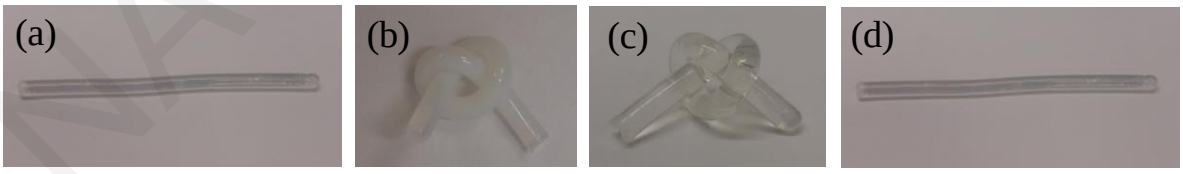

Figure 3.4.7. Shape memory effect for the water-swollen (DMAAm$_{70}$-*co*-DDAAm$_{30}$)-*co*-HDDA$_1$ randomly cross-linked copolymer network. (a) Initial shape at 25 ^{o}C, (b) fixed knot shape after heating the gel up to 50 ^{o}C, (c) temporary shape after cooling down to 25 ^{o}C, (d) recovered shape after heating the gel up to 50 ^{o}C.

The thermal transition behavior of the water-swollen randomly cross-linked copolymer networks was highly dependent on the DDAAm content and the transition temperature. In particular, it was found that increasing the DDAAm content in the copolymer networks

resulted in longer recovery times for the gel to assume its initial rod-like shape. This was also the case for the dependence of the temperature on the DDAAm content, as higher DDAAm contents required higher temperatures to induce the recovery of the initial shape within the same time period as for the gels with a lower DDAAm content that recovered at a lower temperature. Table 3.4.2 lists the times required for the randomly cross-linked copolymer networks to regain their initial shape after their heating to various temperatures.

Table 3.4.2. Recovery times for the randomly cross-linked copolymer networks to resume their initial shape after heating to various temperatures.

No.	Gel Structure	T (°C)	Recovery time (s)
1	(DMAAm$_{90}$-*co*-DDAAm$_{10}$)-*co*-HDDA$_1$	50	5
2	(DMAAm$_{80}$-*co*-DDAAm$_{20}$)-*co*-HDDA$_1$	50	60
		55	18
3	(DMAAm$_{70}$-*co*-DDAAm$_{30}$)-*co*-HDDA$_1$	50	180
		55	75
		60	33
4	(DMAAm$_{60}$-*co*-DDAAm$_{40}$)-*co*-HDDA$_1$	50	320
		60	280

The table shows that the (DMAAm$_{90}$-*co*-DDAAm$_{10}$)-*co*-HDDA$_1$ copolymer network required the shortest time to recover, 5 s, when the gel was heated to 50 °C, whereas the (DMAAm$_{60}$-*co*-DDAAm$_{40}$)-*co*-HDDA$_1$ gel required 320 s to recover its initial shape at the same temperature. It is also worth mentioning that increasing the DDAAm content resulted in decreased transparency of the water-swollen gel when it was heated to 50 °C or higher. When the (DMAAm$_{70}$-*co*-DDAAm$_{30}$)-*co*-HDDA$_1$ copolymer network was heated up to 50, 55 and 60 °C, the gel required 180, 75, and 33 s, respectively, to recover its initial shape. In contrast, the water-swollen copolymer network containing the highest DDAAm content, 50 mol%, failed to recover its initial cylindrical shape even after 15 min of heating at a relatively high temperature, 70 °C. Apparently, the high DDAAm content in this sample leads to very strong hydrophobic associations among the pendant dodecyl groups in the DDAAm monomer repeating units which cannot be easily reversed at a higher temperature.

3.4.5 Conclusions

We employed free radical photopolymerization for the preparation of randomly cross-linked copolymer networks consisting of the hydrophobic DDAAm and the hydrophilic DMAAm monomers. A total number of 11 gels were prepared, varying in their hydrophobic monomer and cross-linker contents. The obtained polymer networks were characterized in terms of their equilibrium degrees of swelling in water and organic solvents and their mechanical properties in water. Increasing the DDAAm content in the gels resulted in a decrease in the values of the degrees of swelling in water, and an increase of these values in the organic solvents, as expected. Increasing the cross-linking density in the polymer networks resulted in a decrease in the values of the equilibrium degrees of swelling in all solvents. The compressive fracture stress and strain values increased upon increasing the DDAAm content, but decreased with increasing the cross-linking density. On the other hand, the values of the Young's modulus were found to be almost independent of the DDAAm content, but highly dependent on the cross-linking density, with the values of the Young's modulus greatly increasing with cross-linking density. In contrast, the values of the fracture energy density were found to increase with both the DDAAm content and the cross-linking density. Finally, the water-swollen randomly cross-linked copolymer networks cross-linked using 1 mol% HDDA were characterized in terms of their thermal transition property using shape memory experiments. Most water-swollen gels containing DDAAm monomer repeating units were found to exhibit shape memory, as they were able to recover their initial cylindrical shape within seconds or minutes depending on the composition of the gels or the temperature. Increasing the DDAAm content in the gels resulted in an increase in the recovery time of the gels, whereas this time was found to significantly decrease when the transition temperature was increased.

3.5 Linear Amphiphilic Diblock Copolymers Based on the Hydrophilic DMAAm Monomer and the Hydrophobic DDAAm Monomer

3.5.1 Synthesis of the Homopolymers and the Diblock Copolymers

The preparation of the homopolymers and the diblock copolymers was accomplished in one or two steps, respectively, using sequential RAFT polymerization, employing the hydrophilic DMAAm and the hydrophobic DDAAm monomers. To this end, after the successful synthesis of the homopolymer precursor, the second monomer was directly added in the polymerization mixture and allowed to polymerize, in order to prepare the diblock copolymer. Two series of diblock copolymers were prepared, in which the degree of polymerization (DP) of the first block was kept constant, while the DP of the second block was varied in order to prepare diblock copolymers with different compositions and molecular weights. The synthetic route for the preparation of the diblock copolymers is illustrated in Figure 3.5.1. The first series of the diblock copolymers consisted of the hydrophilic polyDMAAm as the first block with a DP equal to 100 and the hydrophobic polyDDAAm as the second block with varying DPs, while the second series consisted of a polyDDAAm segment as the first block with a DP equal to 20, and a polyDMAAm segment as the second block with varying DPs. In total, six polyDMAAm-*b*-polyDDAAm and six polyDDAAm-*b*-polyDMAAm diblock copolymers were prepared, in which the DP in the second block was varied between 5 and 100, and 10 and 100, respectively.

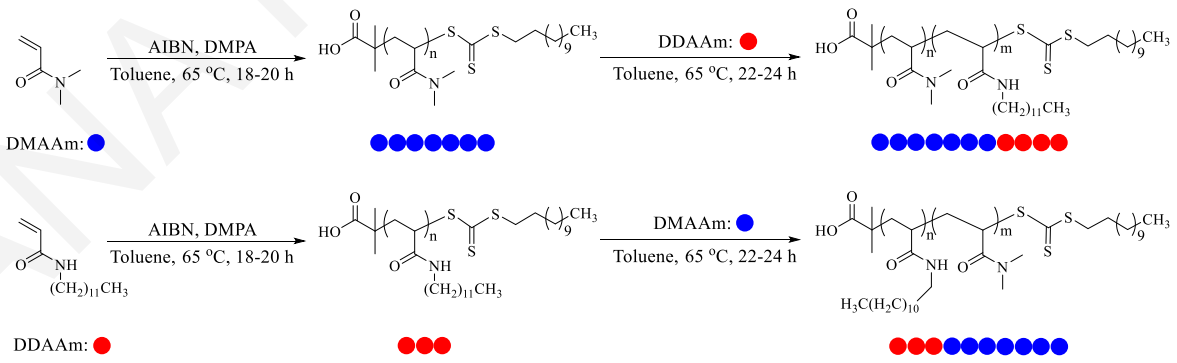

Figure 3.5.1. Synthetic routes followed for the preparation of the desired homopolymers and the DMAAm-*b*-DDAAm and DDAAm-*b*-DMAAm diblock copolymers using RAFT polymerization.

The polymerizations were all performed in toluene, as toluene can dissolve both the DMAAm and DDAAm monomers, both the polyDMAAm and polyDDAAm homopolymers, and, consequently, all the resulting diblock copolymers of polyDMAAm and polyDDAAm. Finally, DMPA was chosen as the chain transfer agent due to its compatibility with acrylamide monomers, and AIBN was chosen as the thermally activated radical source.

3.5.2 Molecular Weights and Compositions of the Homopolymers and the Diblock Copolymers

Table 3.5.1 lists the characterization results of all the prepared homopolymers and diblock copolymers. In particular, the table lists the conversion to polymer of the DMAAm or DDAAm monomers at each step, the molecular weights (M_p and M_n), and the molecular weight dispersity values ($Đ = M_w/M_n$) obtained using GPC, and the copolymer compositions obtained using ^{1}H NMR spectroscopy. Furthermore, the table lists the theoretical values of the molecular weight and DDAAm content, calculated from the ^{1}H NMR spectra and the polymerization feed ratio, respectively.

Table 3.5.1. Monomer to polymer conversion, and experimental and theoretical molecular weights and compositions.

No.	Polymer Structure[a,b]	Monomer conversion (%)	Theory MW[c] (kg mol^{-1})	GPC Results			DDAAm (mol%)	
				M_p (kg mol^{-1})	M_n (kg mol^{-1})	$Đ$	Theory[d]	NMR[e]
1	$DMAAm_{100}$	100	10.3	10.4	7.8	1.4	-	-
	DM_{100}-*b*-DD_5	85	8.8	9.9	8.4	1.5	4.1	4.0
2	$DMAAm_{100}$	100	10.3	8.0	6.0	1.4	-	-
	DM_{100}-*b*-DD_{10}	90	8.1	11.8	7.0	1.6	8.3	8.4
3	$DMAAm_{100}$	100	10.3	9.8	7.3	1.4	-	-
	DM_{100}-*b*-DD_{30}	95	14.1	22.0	17.0	1.4	22	24
4	$DMAAm_{100}$	100	10.3	11.0	7.6	1.4	-	-
	DM_{100}-*b*-DD_{50}	99	19.4	22.7	18.4	1.4	33	32
5	$DMAAm_{100}$	100	10.3	13.6	8.9	1.5	-	-
	DM_{100}-*b*-DD_{75}	98	26.5	40.9	32.0	1.5	42	44
6	$DMAAm_{100}$	100	10.3	13.8	9.8	1.4	-	-
	DM_{100}-*b*-DD_{100}	95	32.5	48.9	34.5	1.5	49	52
7	$DDAAm_{20}$	99	5.2	6.8	6.3	1.2	-	-
	DD_{20}-*b*-DM_{10}	99	7.3	8.1	7.3	1.2	67	66
8	$DDAAm_{20}$	100	5.2	6.6	6.1	1.2	-	-
	DD_{20}-*b*-DM_{15}	100	7.6	7.4	6.8	1.2	57	58
9	$DDAAm_{20}$	100	5.2	6.6	6.1	1.2	-	-
	DD_{20}-*b*-DM_{20}	99	8.1	8.1	7.0	1.2	50	50
10	$DDAAm_{20}$	99	5.2	9.9	8.7	1.3	-	-
	DD_{20}-*b*-DM_{30}	90	11.4	13.7	10.4	1.4	43	40
11	$DDAAm_{20}$	100	5.2	7.2	6.5	1.2	-	-
	DD_{20}-*b*-DM_{70}	100	13.4	18.4	13.7	1.4	22	21
12	$DDAAm_{20}$	100	5.2	9.4	8.5	1.2	-	-
	DD_{20}-*b*-DM_{100}	100	18.4	19.0	9.9	1.6	17	16

[a] DM, DD: further abbreviations for DMAAm and DDAAm, respectively. [b, d] Calculated from the polymerization feed ratio. [c, e] Calculated from the ^{1}H NMR spectra.

The table shows that the DMAAm or DDAAm conversion to homopolymer was quantitative, 99-100%, after 18-20 h of polymerization, allowing the subsequent addition of the second monomer without first isolating the homopolymer. However, the conversion to polymer of the second monomer, DDAAm or DMAAm at the preparation of the second block in the diblock copolymers, was not always quantitative, as these values ranged between 85 and 100%. The experimental molecular weights, M_p and M_n, of the produced (co)polymers were in good agreement with the expected molecular weights in all cases. The molecular weight dispersity values ranged between 1.2 and 1.6, and found to increase with the degree of polymerization, and, therefore, the molecular weight of the diblock copolymers. Figure 3.5.2 presents the GPC traces of the homopolymer precursors and the diblock copolymers $DMAAm_{100}$-*b*-$DDAAm_x$ (part (a)) and $DDAAm_{20}$-*b*-$DMAAm_x$ (part (b)). The figure shows that the elution time of the diblock copolymers decreased upon increasing the degree of polymerization of the second block, as expected. Furthermore, the

GPC traces of the diblock copolymers were unimodal without any shoulders, indicating the successful polymerization of the second monomer in all cases. All these results clearly indicate the suitability of RAFT polymerization for the controlled polymerization of both the hydrophilic DMAAm monomer and the hydrophobic DDAAm monomer.

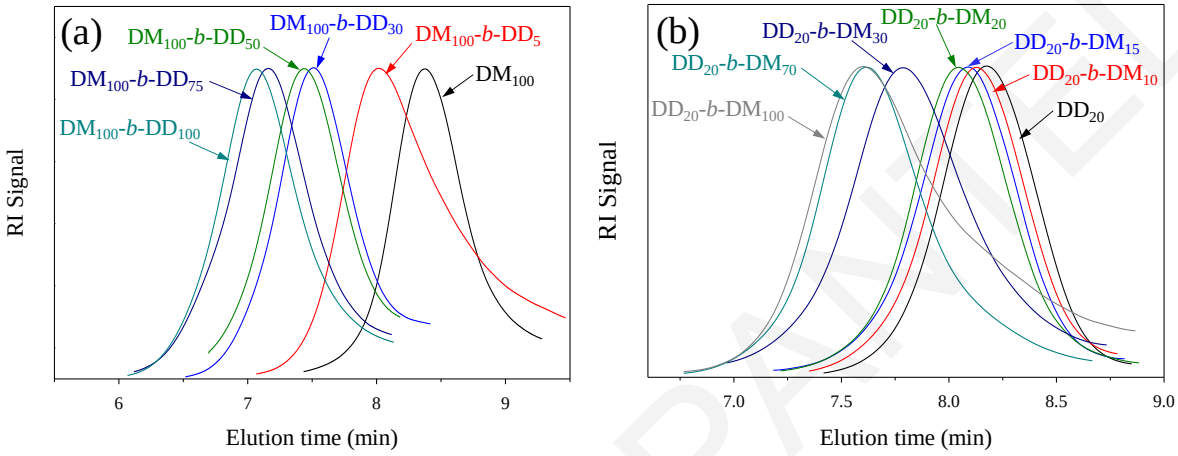

Figure 3.5.2. GPC traces of all the synthesized amphiphilic diblock copolymers and their precursors. (a) $DMAAm_{100}$-*b*-$DDAAm_x$ and (b) $DDAAm_{20}$-*b*-$DMAAm_x$.

Figure 3.5.3 presents the ^1H NMR spectra of the $DMAAm_{100}$ precursor and the $DMAAm_{100}$-*b*-$DDAAm_{30}$ diblock copolymer. The calculation of the experimental DDAAm content in the diblock copolymers was accomplished by comparing the area under the peak corresponding to the terminal methyl protons ($-(CH_2)_{11}-CH_3$, δ = 0.87 ppm) in the DDAAm monomer repeating units to the area under the peak corresponding to the methyl protons on the nitrogen atom ($-(C=O)-N(CH_3)_2$, δ = 2.75-3.25 ppm) in the DMAAm monomer repeating units. The thus-determined experimental values of the DDAAm content were in very good agreement with the corresponding theoretical values calculated from the polymerization feed ratios. The lowest DDAAm content value, 4 mol%, was measured in the case of the $DMAAm_{100}$-*b*-$DDAAm_5$ diblock copolymer, whereas the highest, 66 mol%, was determined in the case of the $DDAAm_{20}$-*b*-$DMAAm_{10}$ diblock copolymer.

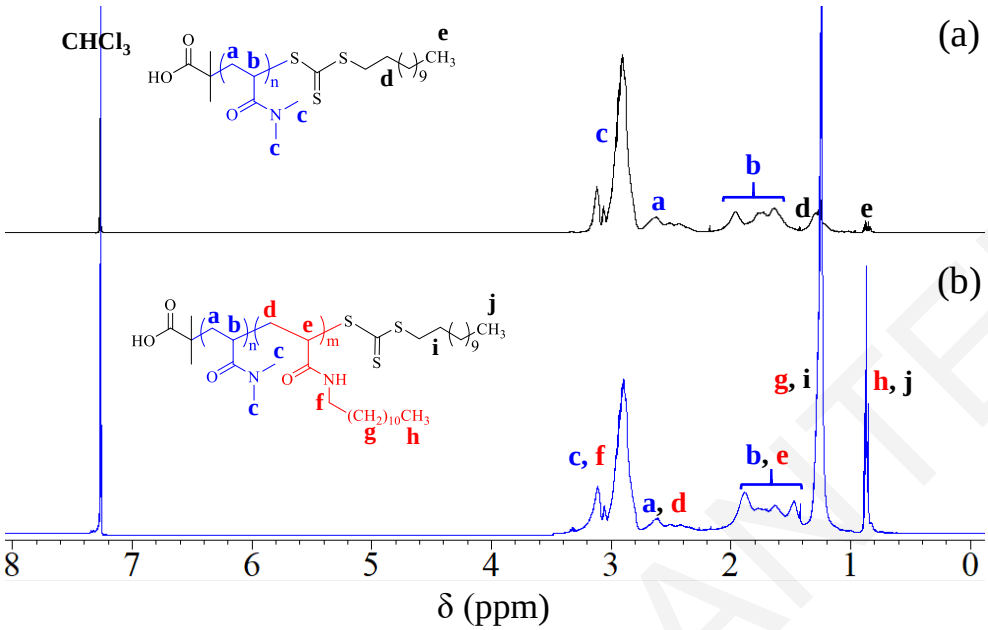

Figure 3.5.3. ^{1}H NMR spectra in $CDCl_3$ of (a) the $DMAAm_{100}$ homopolymer precursor and (b) the $DMAAm_{100}$-*b*-$DDAAm_{30}$ diblock copolymer.

3.5.3 Investigation of the Self-Assembly of the Diblock Copolymers in Water Using DLS, SANS, and AFM

The self-assembly of all synthesized diblock copolymers in water was investigated using DLS, SANS, and AFM. Water was chosen because it is a selective solvent; it is highly polar and readily dissolves the hydrophilic polyDMAAm block, whereas it is a non-solvent for the hydrophobic polyDDAAm block. Thus, dissolving the diblock copolymers in water should be accompanied by their self-assembly with the formation of micelles, consisting of a polyDDAAm-based core and a polyDMAAm-based shell. In preliminary initial experiments, the preparation of the aqueous solutions of the diblock copolymers for the DLS measurements was performed by the direct dissolution of each copolymer in water, at concentrations of 0.1 and 1% w/w. However, this led to the successful dissolution of only the diblock copolymers with low DDAAm contents, whereas the diblock copolymers with higher DDAAm contents failed to dissolve, resulting in solutions of lower concentrations. This problem was solved using the "solvent switch method", by first dissolving the diblock copolymers into a non-selective solvent, THF, followed by the addition of these solutions to water and subsequent evaporation of THF. The R_h values obtained using DLS on the aqueous copolymer solutions of 0.1 and 1% w/w are presented in Table 3.5.2.

The "solvent switch method" was also followed for the preparation of the copolymer solutions for the SANS measurements, but using 1,4-dioxane instead of THF as the non-selective solvent. In particular, the appropriate amount from each diblock copolymer was dissolved in 1,4-dioxane, followed by the dropwise addition of the resulting solution to the necessary D_2O amount so as to obtain a final 1,4-dioxane : D_2O volume ratio of 2:1. Then, both solvents were removed by freeze-drying, and the resulting dried diblock copolymer was dissolved in the appropriate amount of D_2O, so as to produce a solution of final concentration of 1% w/w.

Figure 3.5.4 presents the SANS profiles for the six DMAAm$_{100}$-*b*-DDAAm$_x$ (part (a)) and three DDAAm$_{20}$-*b*-DMAAm$_x$ diblock copolymers (part (b)) dissolved in 1% w/w solutions in D_2O. Part (a) shows that increasing the number of DDAAm monomer repeating units in the DMAAm$_{100}$-*b*-DDAAm$_x$ diblock copolymers led to increased scattering intensities within the low q range. The least hydrophobic DMAAm$_{100}$-*b*-DDAAm$_5$ diblock copolymer exhibited the lowest values of scattered intensity, while the most hydrophobic DMAAm$_{100}$-*b*-DDAAm$_{100}$ diblock copolymer exhibited the highest values of scattered intensity. This is due to the increase in the number of the hydrophobic DDAAm monomer repeating units in the copolymers, leading to larger and denser cores with increased scattering capabilities.

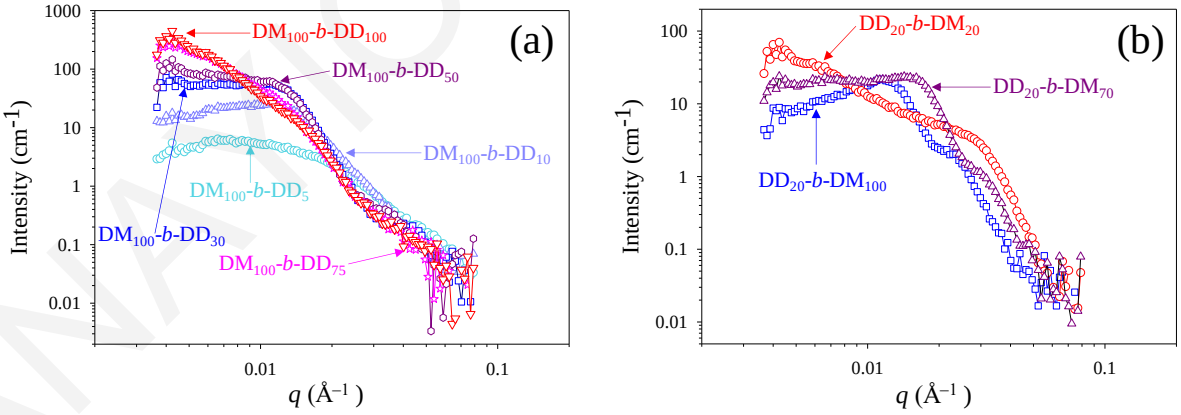

Figure 3.5.4. SANS profiles for the (a) DMAAm$_{100}$-*b*-DDAAm$_x$ and (b) DMAAm$_{20}$-*b*-DMAAm$_x$ diblock copolymers in 1% w/w solutions in D_2O.

Part (b) of the figure shows that increasing the number of DMAAm monomer repeating units in the DDAAm$_{20}$-*b*-DMAAm$_x$ diblock copolymers led to reduced scattering intensities. The DDAAm$_{20}$-*b*-DMAAm$_{100}$ diblock copolymer exhibited the lowest value of

scattered intensity within the low q range, while the DDAAm$_{20}$-*b*-DMAAm$_{20}$ diblock copolymer exhibited the highest scattered intensity values within the same q range.

Subsequently, the SANS profiles were used for the determination of the radius of gyration (R_g), the molecular weight of the micelles ($M_{w,micelle}$), and the aggregation number of the micelles (N_{agg}), by fitting the Guinier model ln(I) *vs.* q^2 to the SANS data in the low-q range. In particular, the calculation of the R_g values was achieved taking into account the slope of the linear portion of the particular graph, while the $I_{(0)}$ values were calculated from the intercept of the linear portion. Then, the $I_{(0)}$ values were employed for the determination of the $M_{w,micelle}$ values, which were then used for the calculation of the N_{agg} values. In the calculations, the interactions between the micelles were considered to be negligible (structure factor, S(q) = 1), as the acrylamide monomers are nonionic and since the SANS profiles were obtained on 1% w/w copolymer solutions, which are relatively dilute. The experimental R_g values, the $M_{w,micelle}$ and their N_{agg} obtained using SANS, and the ratio of R_g to R_h, are also listed in Table 3.5.2.

Furthermore, the micellar size of the DMAAm$_{100}$-*b*-DDAAm$_x$ diblock copolymers was determined from AFM measurements on 0.1% w/w aqueous copolymer solutions, that were also prepared using the "solvent switch method", employing THF as the non-selective solvent. Table 3.5.2 includes the experimental average R_{AFM} values obtained using AFM, that were calculated from the diameter histogram of each diblock copolymer.

Finally, the table lists the theoretically calculated minimum radius of gyration for unimers (R_{min}^{unimer}) and the theoretically calculated maximum radius for spherical micelles ($R_{max}^{micelle}$) corresponding to each diblock copolymer. The theoretical R_{min}^{unimer} values were calculated as the root mean-square radius of gyration for unimers using random-flight statistics *via* the equation $\langle r_g^2 \rangle^{1/2} = (2 \times 1.96 \times DP/3)^{1/2} \times 0.154$, where 1.96 is the stiffness factor of poly(acrylic acid) (PAAc), DP is the overall diblock copolymer degree of polymerization, and 0.154 nm is the length of one C–C bond.[26] The theoretical $R_{max}^{micelle}$ values were obtained as the maximum radius for spherical micelles comprising fully stretched diblock copolymer chains calculated by multiplying the overall diblock copolymer DP by the contribution of one monomer repeating unit of 0.252 nm.[26]

Figure 3.5.5 shows the dependence of all the theoretically calculated and experimentally determined radii (R_{min}^{unimer}, $R_{max}^{micelle}$, R_h, R_g, and R_{AFM}) on the DDAAm content in the diblock copolymers. In particular, part (a) plots the dependence of the radii on the DDAAm content in the $DMAAm_{100}$-*b*-$DDAAm_x$ diblock copolymers using a logarithmic *y*-axis, while part (b) plots the dependence of the radii on the $DDAAm_{20}$-*b*-$DMAAm_x$ diblock copolymers in double-linear axes. Figure 3.5.6 displays the effect of the DDAAm content on N_{agg}.

Table 3.5.2. Theoretical and experimental values of the various radii, the R_g / R_h ratio, and the $M_{w,micelle}$ and N_{agg} values.

No.	Polymer Structure	Theory R_{min}^{unimer} (nm)[a]	Theory $R_{max}^{micelle}$ (nm)[b]	DLS R_h (nm)		SANS R_g (nm)	SANS R_g / R_h	SANS $M_{w,micelle}$ (kg mol^{-1})	SANS N_{agg}[c]	AFM R (nm)
				0.1%	1%					
1	DM_{100}-*b*-DD_5	1.80	26	23	17	8.9	0.52	100	9	17.0
2	DM_{100}-*b*-DD_{10}	1.85	28	28	21	13.5	0.64	870	69	18.5
3	DM_{100}-*b*-DD_{30}	2.01	33	31	41	17.6	0.43	3470	200	15.0
4	DM_{100}-*b*-DD_{50}	2.16	38	36	55	18.3	0.33	4100	180	210
5	DM_{100}-*b*-DD_{75}	2.33	44	39	43	17.8	0.41	2100	75	180
6	DM_{100}-*b*-DD_{100}	2.49	50	26	40	16.0	0.40	1200	35	230
7	DD_{20}-*b*-DM_{10}	0.96	8	25	31	-	-	-	-	-
8	DD_{20}-*b*-DM_{15}	1.04	9	27	45	-	-	-	-	-
9	DD_{20}-*b*-DM_{20}	1.11	10	29	51	22.0	0.43	190	26	-
10	DD_{20}-*b*-DM_{30}	1.24	13	20	43	18.8	0.44	940	120	-
11	DD_{20}-*b*-DM_{70}	1.67	23	23	28	8.0	0.29	110	9	-
12	DD_{20}-*b*-DM_{100}	1.93	30	25	38	9.5	0.25	130	9	-

[a] The theoretical values for R_{min}^{unimer} were calculated as the root mean-square radius of gyration for unimers using random flight statistics corrected for the carbon tetrahedral angle, using the stiffness factor of PAAc, equal to 1.96, and using the equation $\langle r_g^2 \rangle^{1/2} = (2 \times 1.96 \times DP/3)^{1/2} \times 0.154$, where DP is the overall degree of polymerization and 0.154 nm is the length of one C–C bond.[26] [b] The theoretical values for $R_{max}^{micelle}$ were taken as the maximum radius for spherical micelles comprising fully stretched diblock copolymer chains calculated by multiplying the overall diblock copolymer DP by the contribution of one monomer repeating unit of 0.252 nm.[26] [c] Calculated as the ratio of the M_w of the micelle divided by the theoretical molecular weight of the diblock copolymer (unimer).

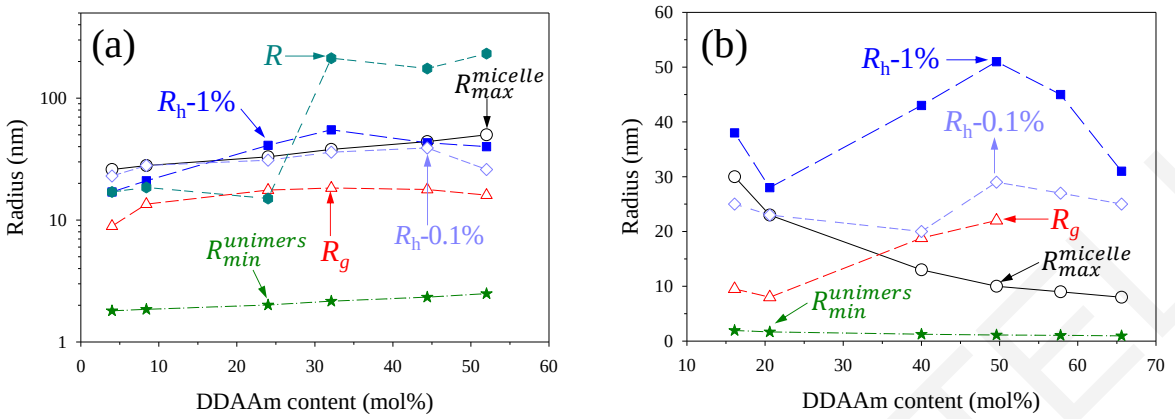

Figure 3.5.5. Dependence of the radii on the DDAAm content in the diblock copolymers with structure (a) $DMAAm_{100}$-*b*-$DDAAm_x$ in semi-logarithmic axes and (b) $DDAAm_{20}$-*b*-$DMAAm_x$ in double-linear axes.

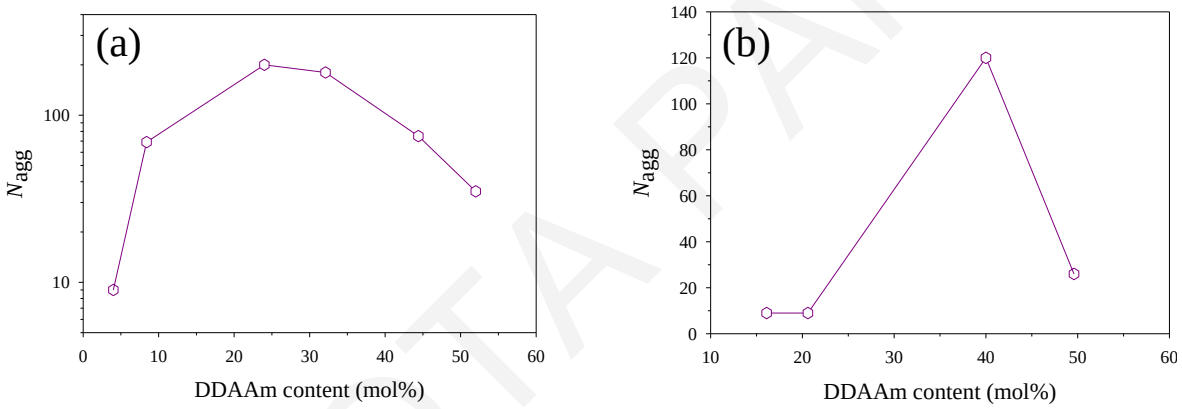

Figure 3.5.6. Dependence of N_{agg} on the DDAAm content in the diblock copolymers with structure (a) $DMAAm_{100}$-*b*-$DDAAm_x$, and (b) $DDAAm_{20}$-*b*-$DMAAm_x$.

Table 3.5.2 and part (a) of Figure 3.5.5 show that the $R_{min}^{unimers}$ and $R_{max}^{micelle}$ values increased with increasing the DDAAm content in the $DMAAm_{100}$-*b*-$DDAAm_x$ diblock copolymers, as the overall DP increases with the DP of the second polyDDAAm block, and, consequently, the DDAAm content. All the experimental radii were higher to much higher than the corresponding $R_{min}^{unimers}$ values, indicating the formation of spherical micelles or multimicellar aggregates, respectively, but definitely not unimers. The R_g values of the $DMAAm_{100}$-*b*-$DDAAm_x$ diblock copolymers were lower than the corresponding $R_{max}^{micelle}$ values by a factor of 2-3, suggesting the formation of spherical micelles. The R_{AFM} values obtained using AFM for the three most hydrophilic DMAAm-DDAAm diblock copolymers with DDAAm contents of 4.0-24.0 mol% were lower than the $R_{max}^{micelle}$ values by a factor of 1.5-2, indicating the formation of spherical micelles. In contrast, when the DDAAm content was higher than 24 mol%, these diblock copolymers

exhibited very high radii, with values ranging between 180 and 230 nm, much higher than the $R_{max}^{micelle}$ values, suggesting the formation of multimicellar aggregates. The formation of these micellar aggregates is probably driven by the increased hydrophobicity of these samples, and materialized through hydrophobic associations between the methyl groups in the DMAAm monomer repeating units (shell), and between the pendant dodecyl groups in the DDAAm monomer repeating units (core), leading to reduced micelle stability and aggregation.

On the other hand, the experimental R_h values were found to be lower than the $R_{max}^{micelle}$ values only when the concentration of the copolymer solution was low, 0.1% w/w, or in the cases of the DMAAm$_{100}$-*b*-DDAAm$_5$, DMAAm$_{100}$-*b*-DDAAm$_{10}$, DMAAm$_{100}$-*b*-DDAAm$_{75}$, and DMAAm$_{100}$-*b*-DDAAm$_{100}$ diblock copolymers obtained on 1% w/w copolymer solutions. In contrast, the aqueous copolymer solutions of 1% w/w of the DMAAm$_{100}$-*b*-DDAAm$_{30}$ and the DMAAm$_{100}$-*b*-DDAAm$_{50}$ diblock copolymers exhibited R_h values higher than the $R_{max}^{micelle}$ values, indicating the formation of multimicellar aggregates. Finally, it is worth mentioning that the R_h values obtained using DLS on 1% w/w copolymer solutions presented a maximum at a DDAAm content equal to 32 mol%, close to the transition in the R_{AFM} values obtained using AFM at a 24 mol% DDAAm content, suggesting that the multimicellar aggregates, rather than the spherical micelles, are the dominant species in the aqueous solutions of diblock copolymers of higher hydrophobe contents. In fact, the DLS measurements on the 1% w/w copolymer solutions indicated a bimodal distribution of radii, and, in particular, the formation of multimicellar aggregates with large radii, ranging between 100 and 300 nm, but, possessing a lower peak intensity (~20-30%) than the peak corresponding to the spherical micelles.

Part (b) of Figure 3.5.5 shows that increasing the DP of the second polyDMAAm block in the DDAAm$_{20}$-*b*-DMAAm$_x$ diblock copolymers resulted in a decrease in the DDAAm content values, and, consequently, the theoretical $R_{min}^{unimers}$ and $R_{max}^{micelle}$ values decreased with increasing the DDAAm content. Similar to the DMAAm$_{100}$-*b*-DDAAm$_x$ diblock copolymers, all the experimental radii were higher to much higher than the $R_{min}^{unimers}$ values, indicating the formation of spherical micelles or multimicellar aggregates, but not unimers. In the case of the DDAAm$_{20}$-*b*-DMAAm$_{100}$ diblock copolymer which possesses the lowest DDAAm content, its R_g and R_h values obtained using DLS on 0.1% w/w

copolymer solutions were lower than the $R_{max}^{micelle}$ values, indicating the formation of spherical micelles. On the other hand, the diblock copolymers with DDAAm contents higher than 21 mol% exhibited R_g and R_h values (0.1% w/w) higher than the $R_{max}^{micelle}$ values, indicating the formation of multimicellar aggregates. The R_h values obtained on 1% w/w copolymer solutions were higher than the $R_{max}^{micelle}$ values in all cases, indicating once again the formation of multimicellar aggregates. Finally, both R_h values presented a maximum when the DDAAm content was equal to 50 mol%, while the R_h values obtained on the 1% w/w copolymer solutions exhibited a minimum when the DDAAm content was equal to 21 mol%. In contrast, the R_h values obtained on 0.1% w/w copolymer solutions were found to be nearly independent of the DDAAm content, as these values remained almost constant, ranging between 20 and 29 nm. This can be attributed to the constant degree of polymerization of DDAAm in the hydrophobic block (DP = 20), indicating that the micelle formation process is mainly dictated by the number of the DDAAm repeating units in the diblock copolymers.

In addition, Table 3.5.2 shows that the values of $M_{w,micelle}$ ranged between 100 and 4100 kg mol^{-1}, while N_{agg} (Figure 3.5.6) acquired values between 9 and 200. The diblock copolymers containing the lowest DDAAm content values, *i.e.*, DMAAm$_{100}$-*b*-DDAAm$_5$, DDAAm$_{20}$-*b*-DMAAm$_{70}$, and DDAAm$_{20}$-*b*-DMAAm$_{100}$, exhibited the lowest N_{agg} values, indicating the formation of spherical micelles rather than multimicellar aggregates, possessing smaller cores and, consequently, lower R_h values. These N_{agg} values were also found to increase upon increasing the DDAAm content in the diblock copolymers and reaching a maximum when the DDAAm content reached 24 mol% for the DMAAm$_{100}$-*b*-DDAAm$_x$ diblock copolymers or 40 mol% for the DDAAm$_{20}$-*b*-DMAAm$_x$ diblock copolymers. These results are consistent with the previous results, as the occurrence of strong hydrophobic associations leads to a higher number of aggregated micelles.

Finally, the table shows that the R_g/R_h ratio acquired values between 0.25 and 0.64, indicating that the diblock copolymers possessed a loose rather than a compact structure. Note than the theoretical R_g/R_h ratio for a hard sphere is equal to 0.78. The DMAAm$_{100}$-*b*-DDAAm$_{10}$ diblock copolymer exhibited the most compact structure, whereas the DDAAm$_{20}$-*b*-DMAAm$_{100}$ diblock copolymer exhibited the loosest structure.

3.5.4 Micellar Size and Morphology

The size and morphology of the obtained micelles formed by the diblock copolymers (concentration = 0.1% w/w) was examined using AFM. Figures 3.5.7, 3.5.8, and 3.5.9 display the amplitude (part (a)) and phase (part (b)) images as well as the diameter analysis histogram (part (c)) obtained using AFM on aqueous solutions of the $DMAAm_{100}$-*b*-$DDAAm_5$, $DMAAm_{100}$-*b*-$DDAAm_{10}$, and $DMAAm_{100}$-*b*-$DDAAm_{30}$ diblock copolymers, respectively. Figure 3.5.10 presents the amplitude (part (a)) and phase (part (b)) images obtained on the aqueous solution of the $DMAAm_{100}$-*b*-$DDAAm_{75}$ diblock copolymer, while Figure 3.5.11 presents the amplitude images obtained for the $DMAAm_{100}$-*b*-$DDAAm_{50}$ (part (a)) and $DMAAm_{100}$-*b*-$DDAAm_{75}$ diblock copolymers (part (b)).

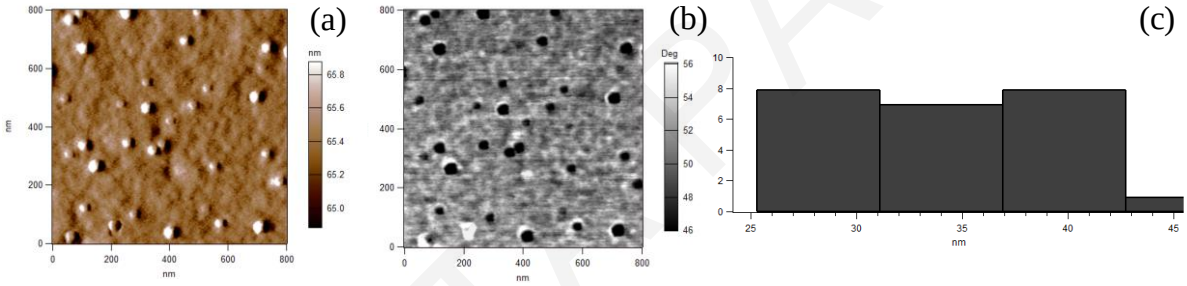

Figure 3.5.7. (a) Amplitude image (0.80 μm × 0.80 μm), (b) phase image (0.80 μm × 0.80 μm), and (c) diameter analysis histogram obtained using AFM for the $DMAAm_{100}$-*b*-$DDAAm_5$ diblock copolymer.

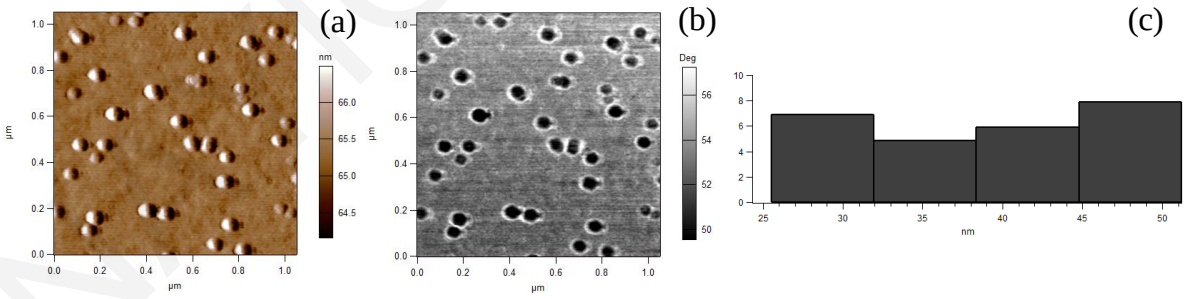

Figure 3.5.8. (a) Amplitude image (1.05 μm × 1.05 μm), (b) phase image (1.05 μm × 1.05 μm), and (c) diameter analysis histogram obtained using AFM for the $DMAAm_{100}$-*b*-$DDAAm_{10}$ diblock copolymer.

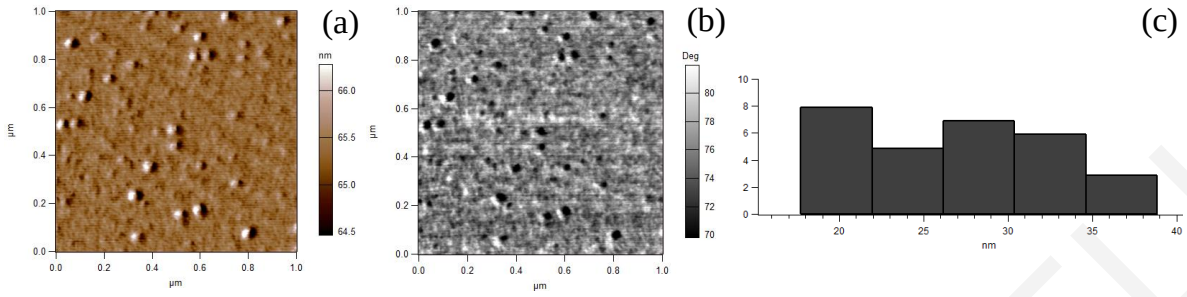

Figure 3.5.9. (a) Amplitude image (1 μm × 1 μm), (b) phase image (1 μm × 1 μm), and (c) diameter analysis histogram obtained using AFM for the $DMAAm_{100}$-*b*-$DDAAm_{30}$ diblock copolymer.

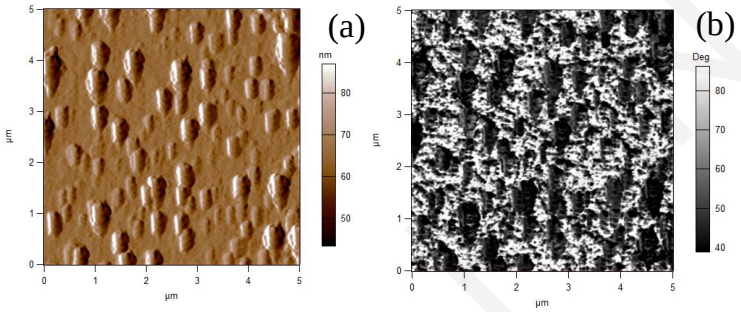

Figure 3.5.10. (a) Amplitude image (5 μm × 5 μm) and (b) phase image (5 μm × 5 μm) obtained using AFM for the $DMAAm_{100}$-*b*-$DDAAm_{75}$ diblock copolymer.

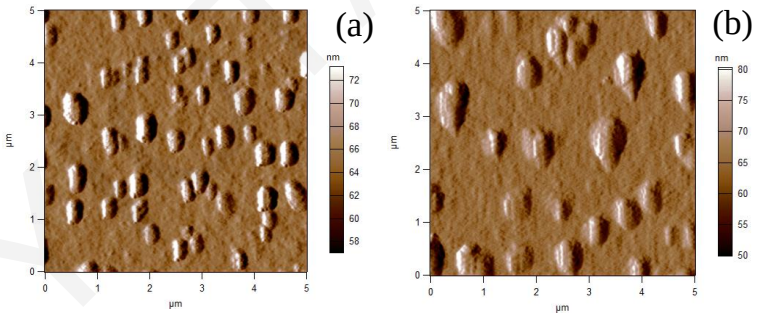

Figure 3.5.11. (a) Amplitude images (5 μm × 5 μm) obtained using AFM for the (a) $DMAAm_{100}$-*b*-$DDAAm_{50}$ and (b) $DMAAm_{100}$-*b*-$DDAAm_{100}$ diblock copolymers.

Figures 3.5.7, 3.5.8, and 3.5.9 show that the micelles formed by the $DMAAm_{100}$-*b*-$DDAAm_5$, $DMAAm_{100}$-*b*-$DDAAm_{10}$, and $DMAAm_{100}$-*b*-$DDAAm_{30}$ diblock copolymers were spherical, whereas Figures 3.5.10 and 3.5.11 show that the micelles formed by the $DMAAm_{100}$-*b*-$DDAAm_{50}$, $DMAAm_{100}$-*b*-$DDAAm_{75}$, and $DMAAm_{100}$-*b*-$DDAAm_{100}$ diblock copolymers were much larger with a broader size distribution, and possessing an ellipsoidal shape.

In particular, Figure 3.5.7 shows that the formed micelles were spherical, exhibiting a nearly monomodal diameter distribution, as the diameters ranged between 25 and 42 nm. This implies micelle radii between 12 and 21 nm. These values are in very good agreement with the corresponding R_h values of 23 nm (0.1% w/w) and 17 nm (1% w/w) obtained using DLS. Furthermore, part (b) of the figure clearly shows that the spherical micelles comprised a core, depicted in black, and a shell, depicted in white. Thus, these micelles possessed a core-shell structure, probably consisting of hydrophobic DDAAm monomer repeating units in the core, and hydrophilic DMAAm monomer repeating units in the shell. This was also the case for the $DMAAm_{100}$-*b*-$DDAAm_{10}$ and $DMAAm_{100}$-*b*-$DDAAm_{30}$ diblock copolymers, as the formed micelles also possessed a spherical shape and a core-shell structure. In particular, the micelles formed by the $DMAAm_{100}$-*b*-$DDAAm_{10}$ diblock copolymer exhibited micelle diameter values between 25 and 50 nm, and, therefore, micelle radii values between 12 and 25 nm. These values are also in very good agreement with the corresponding R_h values of 28 nm (0.1% w/w) and 21 nm (1% w/w). On the other hand, the micelles formed by the $DMAAm_{100}$-*b*-$DDAAm_{30}$ diblock copolymer possessed micelle diameter values between 20 and 40 nm, indicating a slightly broader diameter distribution than the other two diblock copolymers. These micelle radii values range between 10 and 20 nm, which are smaller than the corresponding R_h values of 31 nm (0.1% w/w) and 41 nm (1% w/w) obtained using DLS.

In contrast, Figure 3.5.10 shows that the micelles formed by the $DMAAm_{100}$-*b*-$DDAAm_{75}$ diblock copolymer were not spherical but possessed an ellipsoidal shape with large diameters and broad diameter distribution. This is expected, as the particular diblock copolymer possessed the highest R_h value obtained using DLS on 0.1% w/w copolymer solution. Part (b) of the figure clearly indicates the formation of multimicellar aggregates. This behavior was also observed in the cases of the DDAAm-richer diblock copolymers, with the micelles formed by the $DMAAm_{100}$-*b*-$DDAAm_{100}$ diblock copolymer exhibiting the largest diameter.

3.5.5 Conclusions

We presented the synthesis and characterization of two series of amphiphilic diblock copolymers with the two possible block sequences, of various compositions and molecular weights, based on the hydrophilic DMAAm and the hydrophobic DDAAm monomers, prepared by sequential RAFT polymerization. In all cases, the degree of polymerization of the first block was kept constant, while the degree of polymerization of the second block was systematically varied. Characterization of the linear homopolymer precursors and the final amphiphilic diblock copolymers in terms of their molecular weights and compositions indicated small differences between the experimental and the theoretically calculated molecular weights, and experimental compositions very close to the theoretical ones. Investigation of the self-assembly behavior of the diblock copolymers in water using DLS and SANS indicated the formation of micelles and not unimers. For both series of the diblock copolymers, the R_g values determined from SANS were lower than both the R_h values obtained using DLS on 0.1 and 1% w/w copolymer solutions. In most cases, increasing the copolymer concentration in the aqueous solutions resulted in an increase in the R_h values. In the case of the DMAAm$_{100}$-*b*-DDAAm$_x$ diblock copolymers, the R_h values obtained on 0.1% w/w copolymer solutions were lower than the theoretical $R_{max}^{micelle}$values, indicating the formation of (regular) spherical micelles. The values of R_h obtained on 1% w/w copolymer solutions exhibited a maximum at 32 mol% DDAAm, whereas this maximum was obtained at a higher DDAAm content, 44 mol%, in the case of the 0.1% w/w copolymer solutions. On the other hand, in the case of the DDAAm$_{20}$-*b*-DMAAm$_x$ diblock copolymers, the R_h values obtained on 1% w/w copolymer solutions were higher than the theoretical $R_{max}^{micelle}$values, indicating the formation of aggregated micelles. The R_g values and both the R_h values exhibited a minimum at 21 mol% DDAAm, while the R_h values exhibited a maximum at 50 mol% DDAAm. Finally, AFM measurements revealed the formation of spherical micelles with a core-shell structure in the cases of the most hydrophilic DMAAm$_{100}$-*b*-DDAAm$_x$ diblock copolymers (DDAAm < 24 mol%), with lower R values than the R_h values, and the formation of ellipsoidal micelles in the cases of the DDAAm-rich diblock copolymers.

3.6 Amphiphilic Polymer Conetworks (APCNs) Based on PEG, DMAAm and DDAAm Prepared Using Sequential RAFT Polymerization

3.6.1 Synthesis of the DDAAm$_x$-*b*-DMAAm$_{50}$-*b*-EG$_{46}$-*b*-DMAAm$_{50}$-*b*-DDAAm$_x$ Pentablock Terpolymers and Their End-linking for the Preparation of the Polymer Conetworks

The preparation of the APCNs was accomplished through three sequential RAFT polymerization steps. The preparation procedure is schematically illustrated in Figure 3.6.1. All the produced polymers and the resulting polymer conetworks contained a PEG midblock comprising approximately 46 ethylene glycol monomer repeating units, originating from the PEG DMPA bifunctional chain transfer agent. First, the RAFT polymerization of the hydrophilic DMAAm monomer was performed, yielding the DMAAm$_{50}$-*b*-EG$_{46}$-*b*-DMAAm$_{50}$ (ABA) triblock copolymer. Subsequently, the hydrophobic DDAAm monomer was again RAFT polymerized off the ends of the ABA triblock copolymer, yielding the DDAAm$_x$-*b*-DMAAm$_{50}$-*b*-EG$_{46}$-*b*-DMAAm$_{50}$-*b*-DDAAm$_x$ (ABCBA) pentablock terpolymer. Finally, the commercially available HDDA cross-linker was added to end-link the linear ABCBA pentablock terpolymers and form the APCNs.

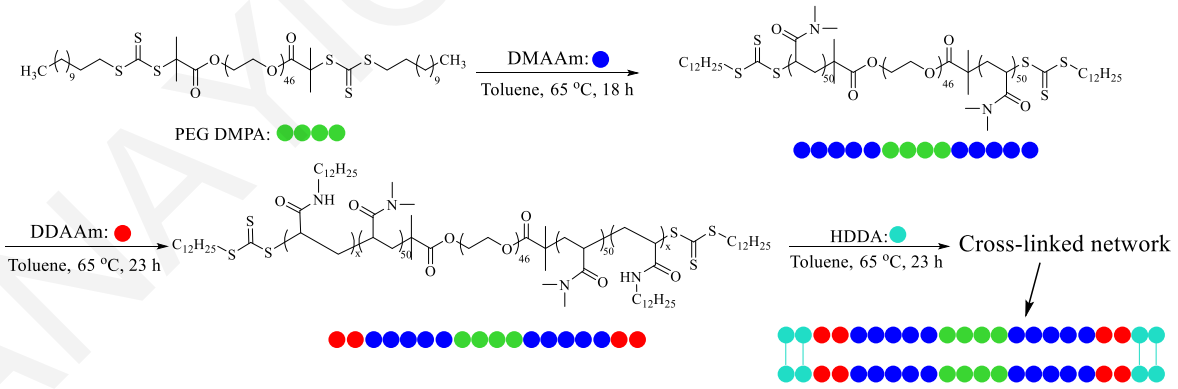

Figure 3.6.1. Procedure followed for the synthesis of the amphiphilic ABCBA pentablock terpolymers, and their end-linking for the preparation of the amphiphilic polymer conetworks.

The total degree of polymerization of the hydrophilic polyDMAAm block was always constant and equal to 100, whereas the total degree of polymerization of the hydrophobic polyDDAAm block was systematically varied to prepare polymer conetworks of different

compositions. In total, seven polymer conetworks were prepared in which the total degree of polymerization of DDAAm was equal to 12, 18, 24, 34, 44, 68 and 100, while one polymer conetwork consisted only of the hydrophilic component DMAAm. AIBN was employed as the thermally activated radical source and toluene as the polymerization solvent due to its good compatibility with both monomers and both homopolymers. A relatively high concentration of monomers and cross-linker was employed in each polymerization step to ensure their complete polymerization, whereas the loading of the HDDA cross-linker with respect to the overall monomer loading was kept constant at 6 mol%.

3.6.2 Molecular Weights and Compositions of the Linear Precursors

Prior to the addition of the DDAAm monomer to synthesize the linear ABCBA pentablock terpolymers and the HDDA cross-linker to induce the cross-linking of the linear polymer chains and form the final APCNs, all the linear polymers were characterized using ^{1}H NMR spectroscopy and GPC. In particular, ^{1}H NMR spectroscopy was used for the determination of the DDAAm content (relative, with respect to DMAAm) in the ABCBA pentablock terpolymers, while GPC was used for the determination of the molecular weights (M_p and M_n) and molecular weights dispersities ($Đ = M_w/M_n$) of the linear ABA triblock copolymers and the linear ABCBA pentablock terpolymers. The theoretical values of the molecular weight of the triblock copolymers were determined using ^{1}H NMR spectroscopy, by comparing the area under the peak of the methyl protons on the nitrogen atom (–(C=O)–N(CH_3)$_2$, δ = 2.80 – 3.20 ppm) in the DMAAm monomer repeating units to the area under the peak corresponding to the protons of the ethylene glycol monomer repeating units (–OCH_2CH_2O–, δ = 3.60-3.75 ppm). On the other hand, the theoretical values of the molecular weight of the pentablock terpolymers were determined by comparing the area under the peak of the terminal methyl protons (–(CH$_2$)$_{11}$–CH_3, δ = 0.85 ppm) in the DDAAm monomer repeating units to the area under the peak corresponding to the protons of the ethylene glycol monomer repeating units (–OCH_2CH_2O–, δ = 3.60-3.75 ppm). All the characterization results are listed in Table 3.6.1, together with the theoretical molecular weights and theoretical DDAAm content in the pentablock terpolymers, calculated on the basis of monomer feed ratio and monomer conversion.

Table 3.6.1. Theoretical and experimental values of the molecular weights and relative (with respect to DMAAm) DDAAm content in the linear ABA triblock copolymers and ABCBA pentablock terpolymers.

No.	Polymer Structure[a,b]	Theory MW[c] (kg mol^{-1})	GPC			DDAAm (mol%)	
			M_p (kg mol^{-1})	M_n (kg mol^{-1})	$Đ$	Theory[d]	NMR[e]
1	DM_{50}-*b*-EG_{46}-*b*-DM_{50}	12.7	14.2	12.6	1.2	0.0	0.0
2	DM_{50}-*b*-EG_{46}-*b*-DM_{50}	12.7	11.2	9.5	1.2	0.0	0.0
	DD_6-*b*-DM_{50}-*b*-EG_{46}-*b*-DM_{50}-*b*-DD_6	12.4	15.6	12.2	1.4	10.7	10.5
3	DM_{50}-*b*-EG_{46}-*b*-DM_{50}	12.7	10.8	9.5	1.3	0.0	0.0
	DD_9-*b*-DM_{50}-*b*-EG_{46}-*b*-DM_{50}-*b*-DD_9	13.8	16.6	12.8	1.4	15.2	14.5
4	DM_{50}-*b*-EG_{46}-*b*-DM_{50}	12.7	9.9	7.3	1.4	0.0	0.0
	DD_{13}-*b*-DM_{50}-*b*-EG_{46}-*b*-DM_{50}.*b*-DD_{13}	13.5	15.5	11.4	1.6	21.0	22.0
5	DM_{50}-*b*-EG_{46}-*b*-DM_{50}	12.7	11.2	9.5	1.4	0.0	0.0
	DD_{17}-*b*-DM_{50}-*b*-EG_{46}-*b*-DM_{50}-*b*-DD_{17}	17.6	19.9	14.1	1.5	25.0	25.0
6	DM_{50}-*b*-EG_{46}-*b*-DM_{50}	12.7	10.5	6.2	1.3	0.0	0.0
	DD_{22}-*b*-DM_{50}-*b*-EG_{46}-*b*-DM_{50}-*b*-DD_{22}	14.3	21.8	18.0	1.6	32.0	33.0
7	DM_{50}-*b*-EG_{46}-*b*-DM_{50}	12.7	11.2	7.7	1.3	0.0	0.0
	DD_{34}-*b*-DM_{50}-*b*-EG_{46}-*b*-DM_{50}-*b*-DD_{34}	24.5	30.4	21.9	1.7	43.0	47.0
8	DM_{50}-*b*-EG_{46}-*b*-DM_{50}	12.7	11.5	8.0	1.4	0.0	0.0
	DD_{50}-*b*-DM_{50}-*b*-EG_{46}-*b*-DM_{50}-*b*-DD_{50}	31.9	37.6	26.5	1.7	51.0	55.0

[a] DM, DD: further abbreviations for DMAAm and DDAAm, respectively. [b, d] Calculated from the monomer feed ratio. [c, e] Calculated from the ^{1}H NMR spectra.

In all cases, the DMAAm conversion to polymer was quantitative after 17-18 h of polymerization, allowing the subsequent sequential addition of the DDAAm monomer without isolating the $DMAAm_{50}$-*b*-EG_{46}-*b*-$DMAAm_{50}$ triblock copolymer. After 23 h of polymerization, the DDAAm conversion was also quantitative, similarly allowing the addition of the HDDA cross-linker to obtain the final polymer conetworks without the prior isolation of the ABCBA pentablock terpolymer. Regarding the molecular weights of the produced polymers, the experimental values of the molecular weights were reasonably in good agreement with the theoretical molecular weights in all cases. The molecular weight dispersities were found to vary between 1.2 and 1.7 and increased upon increasing the number of the DDAAm monomer repeating units, and, consequently, the molecular

weight of the pentablock terpolymer. Figure 3.6.2 presents the GPC traces of one of the linear ABA triblock copolymers and all the linear ABCBA pentablock terpolymers. The figure shows that the elution time decreased upon increasing the molecular weight of the ABCBA pentablock terpolymer, as expected. In addition, the pentablock terpolymers with lower degrees of polymerization of the DDAAm units exhibited peaks with narrower molecular weight distributions, whereas when the degree of polymerization was higher, the distribution curves became wider. However, all chromatograms were unimodal, without any shoulders, indicating the successful chain extension of the triblock copolymer precursor with the hydrophobic DDAAm monomer.

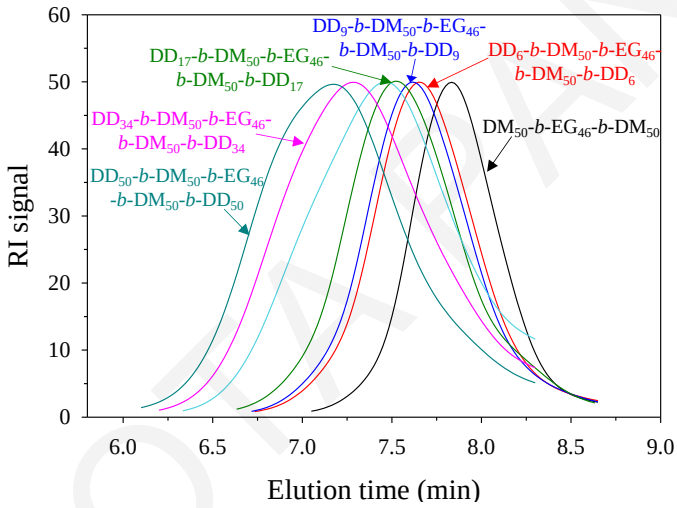

Figure 3.6.2. GPC traces of a $DMAAm_{50}$-*b*-EG_{46}-*b*-$DMAAm_{50}$ ABA triblock copolymer precursor and the $DDAAm_x$-*b*-$DMAAm_{50}$-*b*-EG_{46}-*b*-$DMAAm_{50}$-*b*-$DDAAm_x$ ABCBA pentablock terpolymers.

Figure 3.6.3 presents the ^{1}H NMR spectra of a $DMAAm_{50}$-*b*-EG_{46}-*b*-$DMAAm_{50}$ triblock copolymer (part (a)) and one of the ABCBA pentablock terpolymers, the $DDAAm_{13}$-*b*-$DMAAm_{50}$-*b*-EG_{46}-*b*-$DMAAm_{50}$-*b*-$DDAAm_{13}$ pentablock terpolymer (part (b)). The calculation of the DDAAm content was performed by comparing the area under the peak corresponding to the terminal methyl protons ($-(CH_2)_{11}-CH_3$, δ = 0.85 ppm) in the DDAAm monomer repeating units to the area under the peak corresponding to the methyl protons on the nitrogen atom ($-(C=O)-N(CH_3)_2$, δ = 2.80 – 3.20 ppm) in the DMAAm monomer repeating units. The calculated values of the DDAAm content ranged between 10.5 and 55.0 mol%, and these values were very close to the theoretical values, which fell in the range from 10.7 to 51.0 mol%.

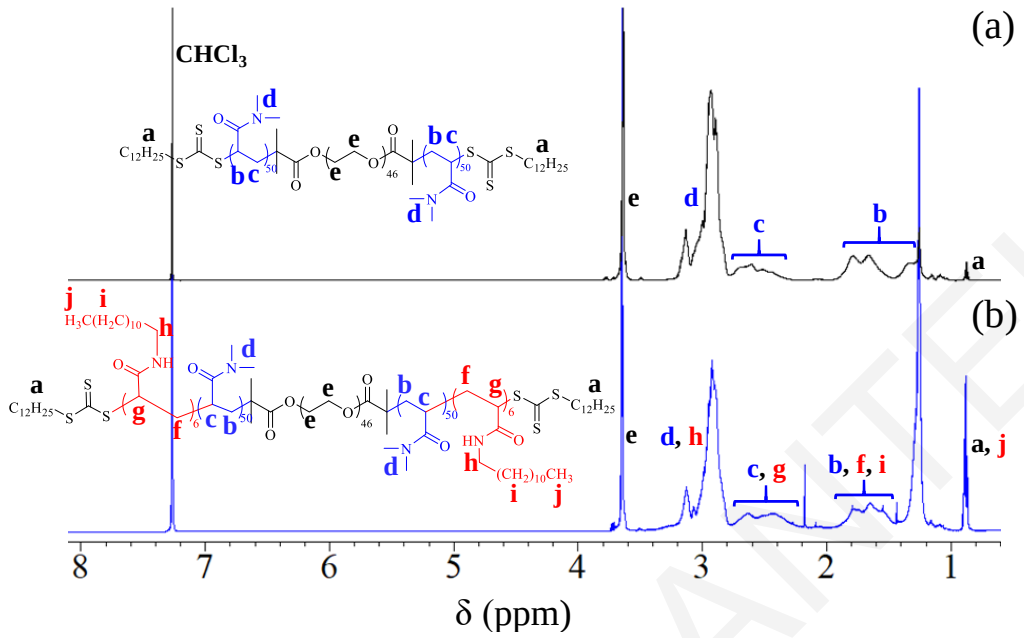

Figure 3.6.3. ^{1}H NMR spectra in $CDCl_3$ for (a) a $DMAAm_{50}$-*b*-EG_{46}-*b*-$DMAAm_{50}$ triblock copolymer precursor and (b) the $DDAAm_{13}$-*b*-$DMAAm_{50}$-*b*-EG_{46}-*b*-$DMAAm_{50}$-*b*-$DDAAm_{13}$ pentablock terpolymer.

3.6.3 Investigation of the Self-Assembly of the Linear ABCBA Pentablock Terpolymers in Water Using DLS and SANS

The self-assembly of the linear ABCBA pentablock terpolymers was examined in water using DLS and SANS. Water is a solvent selective for the polyDMAAm and PEG blocks and a non-solvent for the hydrophobic polyDDAAm blocks. This should lead to the formation of micelles, with a polyDMAAm plus PEG hydrophilic shell, and a polyDDAAm hydrophobic core. Due to the placement of the hydrophobic segments as the end-blocks of the ABCBA pentablock terpolymers, flower-like rather than star-like micelles were expected to form. Preliminary DLS experiments showed that when the precursors were directly dissolved in water, aggregated structures with large sizes were formed. Furthermore, even at lower concentrations, 0.05 and 0.1% w/w, the linear precursors with a relatively high DDAAm content (33-55 mol%) failed to dissolve completely in pure water, leading to polymer solutions with a lower final concentration. To effect full polymer dissolution, the precursors were first dissolved in a non-selective solvent, THF, and then each resulting solution was added dropwise into water, followed by evaporation of THF (solvent switch method). The R_h values obtained using DLS on the aqueous terpolymer solutions of 0.05, 0.1, and 1% w/w are listed in Table 3.6.2.

Similarly to the procedure followed for the preparation of the copolymer solutions for the DLS measurements, the copolymer solutions for the SANS measurements were prepared using the solvent switch method, but using 1,4-dioxane instead of THF. Each diblock copolymer was initially dissolved in 1,4-dioxane and the resulting solution was added dropwise to the necessary D_2O amount so as to obtain a final 1,4-dioxane: D_2O volume ratio of 2:1. Then, both solvents were removed by freeze-drying and the resulting dried diblock copolymer was dissolved in the appropriate amount of D_2O to reach a final concentration of 1% w/w.

Figure 3.6.4 presents the SANS profiles for the DDAAm$_6$-*b*-DMAAm$_{50}$-*b*-EG$_{46}$-*b*-DMAAm$_{50}$-*b*-DDAAm$_6$, DDAAm$_{13}$-*b*-DMAAm$_{50}$-*b*-EG$_{46}$-*b*-DMAAm$_{50}$-*b*-DDAAm$_{13}$ and DDAAm$_{22}$-*b*-DMAAm$_{50}$-*b*-EG$_{46}$-*b*-DMAAm$_{50}$-*b*-DDAAm$_{22}$ pentablock terpolymers obtained in 1% w/w solutions in D_2O. The figure shows that the intensity values at low *q* were found to increase with the number of DDAAm monomer repeating units in the pentablock terpolymers. This can be attributed to the formation of micelles with denser cores that scatter more intensely when the number of the hydrophobic DDAAm monomer repeating units in the pentablock terpolymers is increased.

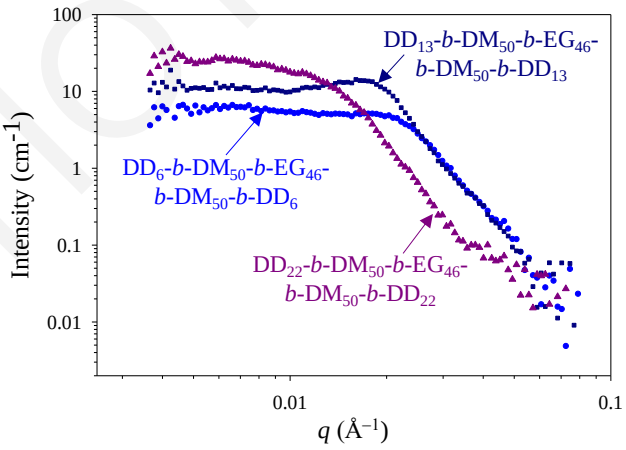

Figure 3.6.4. SANS profiles for the linear DDAAm$_x$-*b*-DMAAm$_{50}$-*b*-EG$_{46}$-*b*-DMAAm$_{50}$-*b*-DDAAm$_x$ pentablock terpolymers with x = 6, 13, 22.

Subsequently, the SANS profiles were used for the determination of the R_g, $M_{w,\ micelle}$, and N_{agg} values, which are also listed in Table 3.6.2. Finally, the table includes the theoretically calculated $R_{max}^{micelle}$ values for the ABCBA pentablock terpolymers. The experimental

micellar radii, R_h, and R_g, and the theoretical $R_{max}^{micelle}$ values of the ABCBA pentablock terpolymers are plotted against their DDAAm content in Figure 3.6.5.

Table 3.6.2. R_h and R_g obtained using DLS and SANS, respectively, $M_{w,\ micelle}$ and N_{agg} obtained using SANS, and theoretically calculated $R_{max}^{micelle}$.

No.	Polymer Structure	Theory $R_{max}^{micelle}$ (nm)[a]	DLS R_h (nm)			SANS R_g (nm)	SANS $M_{w,\ micelle}$ (kg mol^{-1})	SANS N_{agg}[b]
			0.05%	0.1%	1%	1%		
1	DD_6-*b*-DM_{50}-*b*-EG_{46}-*b*-DM_{50}-*b*-DD_6	23	50	90	280	9.3	240	16
2	DD_{13}-*b*-DM_{50}-*b*-EG_{46}-*b*-DM_{50}-*b*-DD_{13}	24	31	46	350	11.9	950	50
3	DD_{17}-*b*-DM_{50}-*b*-EG_{46}-*b*-DM_{50}-*b*-DD_{17}	25	21	37	100	-	-	-
4	DD_{22}-*b*-DM_{50}-*b*-EG_{46}-*b*-DM_{50}-*b*-DD_{22}	27	36	42	110	15.2	710	30
5	DD_{34}-*b*-DM_{50}-*b*-EG_{46}-*b*-DM_{50}-*b*-DD_{34}	30	30	37	100	-	-	-
6	DD_{50}-*b*-DM_{50}-*b*-EG_{46}-*b*-DM_{50}-*b*-DD_{50}	34	23	36	190	-	-	-

[a] Equal to the half chain contour length of the polymer chain, calculated by the multiplication of the total DP of DMAAm and DDAAm monomers times the contribution of one monomer repeating unit, 0.252 nm, plus the product of the multiplication of the DP of the EG repeating units times the contribution of one EG repeating unit, 0.38 nm, divided by 2.[26] [b] Calculated as the ratio of the M_w of the micelle divided by the theoretical molecular weight of the ABCBA pentablock terpolymer (unimer).

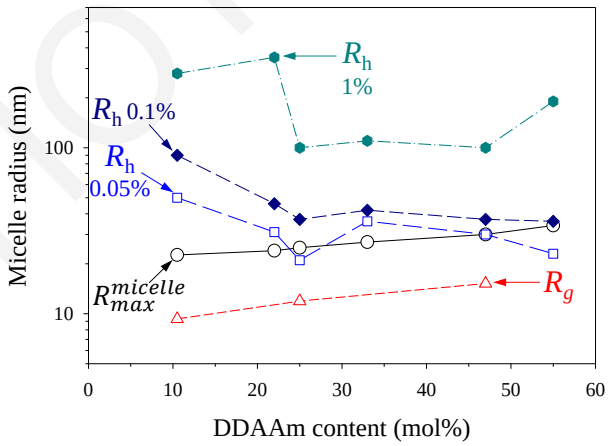

Figure 3.6.5. Dependence of the micellar radii on the DDAAm content in the ABCBA pentablock terpolymers.

Table 3.6.2 and Figure 3.6.5 show that increasing the DDAAm content in the pentablock terpolymers resulted in increased $R_{max}^{micelle}$ values, as expected. The R_g values were lower than the theoretical $R_{max}^{micelle}$ values, suggesting the formation of single flower-like spherical micelles. In contrast, the R_h values obtained at all three terpolymer concentrations, 0.05, 0.1, and 1% w/w, were greater than or close to the theoretical values of $R_{max}^{micelle}$ values,

indicating the formation of multimicellar aggregates rather than single flower-like spherical micelles. There is probably a distribution of spherical micelles and their multimicellar aggregates, with SANS being more appropriate for the detection of the former and DLS being more appropriate for the latter.

Regarding the R_h values obtained using DLS, it was found that increasing the concentration of the terpolymer solution from 0.05 to 0.1% w/w resulted in increased R_h values. However, when the concentration became even higher, 1% w/w, aggregated micelles with much larger radii, ranging between 100 and 350 nm, were formed. This may be attributed to the formation of bridged flower-like micelles, arising from the formation of bridges between neighboring micelles at this relatively high terpolymer concentration (1% w/w), at which the micelles are much closer to each other. On the other hand, the R_h values at this concentration were found to increase from 280 to 350 nm when the DDAAm content was increased from 10 to 20 mol%, and significantly decrease when the DDAAm content was further increased to 25 mol%. When the DDAAm content was further increased, these values remained almost constant and independent of the DDAAm content. A similar trend was also observed for the R_h values calculated using the polymer solutions of lower concentrations, but, in these cases, the R_h values were significantly decreased when the DDAAm content reached 20 mol%. Similarly, when the DDAAm content was further increased, the R_h values were also found to remain constant and independent of the DDAAm content, ranging between 21 and 36 nm in the case of the terpolymer solutions of concentration of 0.05% w/w, and 36-46 nm in the case of terpolymer solutions of concentration of 0.1% w/w.

The formation of aggregated flower-like micelles may be attributed to the formation of hydrophobic associations between the pendant dodecyl groups in the DDAAm monomer repeating units and the methyl groups in the DMAAm repeating units. When the DDAAm content, *i.e.*, the degree of polymerization of the DDAAm monomer repeating units in the pentablock terpolymers is the lowest, 10 mol% (terpolymer concentration = 0.05 and 0.1% w/w) or 20 mol% (terpolymer concentration = 1% w/w), the flower-like micelles tend to aggregate through the formation of hydrophobic associations and form large aggregated structures. When the DDAAm content is increased, the flower-like micelles exhibit lower and rather constant values of R_h, possibly due to the presence of sufficient number of

DDAAm monomer repeating units and, consequently, sufficient hydrophobic associations. This is highly evidenced from the N_{agg} values, calculated using the SANS profiles, which were found to increase when the DDAAm content was increased to 20 mol%, and were found to decrease when the hydrophobe content was further increased to 25 mol%.

Another possible reason for the rather constant R_h values at all terpolymer concentrations for DDAAm contents above 25 mol% is the length of the middle hydrophilic $DMAAm_{50}$-EG_{46}-$DMAAm_{50}$ triblock copolymer segment which constitutes the shell of the aggregates, as it is highly flexible, and affects the structure and size of the obtained flower-like micelles. However, when the length of the hydrophilic block is constant, the radius of the micellar corona of the flower-like micelles is also constant, and, therefore, the radius of the flower-like micelles becomes mainly dependent on the length of the hydrophobic end-blocks which constitute the micellar core. Thus, the DDAAm content and, therefore, the amount of the hydrophobic associations, are believed to mainly affect the values of the R_h of the flower-like micelles, as discussed above.

3.6.4 Preparation of the Amphiphilic End-Linked Polymer Conetworks

In addition to the systematic variation of the degree of polymerization of the hydrophobic polyDDAAm end-blocks, the total degree of polymerization of the HDDA cross-linker part was also varied in direct proportion to the total degree of polymerization of the linear ABCBA pentablock terpolymers. The lowest total degree of polymerization of HDDA was 6 for the $DMAAm_{50}$-*b*-EG_{46}-*b*-$DMAAm_{50}$ triblock copolymer, also containing the lowest total number of DMAAm and DDAAm monomer repeating units, while the highest value was 12 for the $DDAAm_{50}$-*b*-$DMAAm_{50}$-*b*-EG_{46}-*b*-$DMAAm_{50}$-*b*-$DDAAm_{50}$ pentablock terpolymer, also containing the highest total number of DMAAm and DDAAm monomer repeating units. Table 3.6.3 lists the structures of the prepared polymer conetworks and their experimental DDAAm content relative only to the DMAAm comonomer.

Table 3.6.3. Structure of the obtained polymer networks prepared using RAFT polymerization.

No.	Polymer Network Structure	DDAAm content (mol%)
1	$HDDA_3$-*b*-DM_{50}-*b*-EG_{46}-*b*-DM_{50}-*b*-$HDDA_3$	0
2	$HDDA_{3.2}$-*b*-DD_6-*b*-DM_{50}-*b*-EG_{46}-*b*-DM_{50}-*b*-DD_6-*b*-$HDDA_{3.2}$	10.5
3	$HDDA_{3.4}$-*b*-DD_9-*b*-DM_{50}-*b*-EG_{46}-*b*-DM_{50}-*b*-DD_9-*b*-$HDDA_{3.4}$	14.5
4	$HDDA_{3.6}$-*b*-DD_{13}-*b*-DM_{50}-*b*-EG_{46}-*b*-DM_{50}-*b*-DD_{13}-*b*-$HDDA_{3.6}$	22
5	$HDDA_{3.8}$-*b*-DD_{17}-*b*-DM_{50}-*b*-EG_{46}-*b*-DM_{50}-*b*-DD_{17}-*b*-$HDDA_{3.8}$	25
6	$HDDA_4$-*b*-DD_{22}-*b*-DM_{50}-*b*-EG_{46}-*b*-DM_{50}-*b*-DD_{22}-*b*-$HDDA_4$	33
7	$HDDA_5$-*b*-DD_{34}-*b*-DM_{50}-*b*-EG_{46}-*b*-DM_{50}-*b*-DD_{34}-*b*-$HDDA_5$	47
8	$HDDA_6$-*b*-DD_{50}-*b*-DM_{50}-*b*-EG_{46}-*b*-DM_{50}-*b*-DD_{50}-*b*-$HDDA_6$	55

3.6.5 Degrees of Swelling of the Polymer Conetworks in Water and Organic Solvents

The dependence of the equilibrium DSs of the APCNs in five different solvents, THF, EtOH, $CHCl_3$, toluene, and water, on their DDAAm content is plotted in Figure 3.6.6. Part (a) of the figure presents the dependence of the equilibrium DSs of the APCNs on the DDAAm content in double-linear axes, while part (b) presents the same dependence but using a logarithmic *y*-axis.

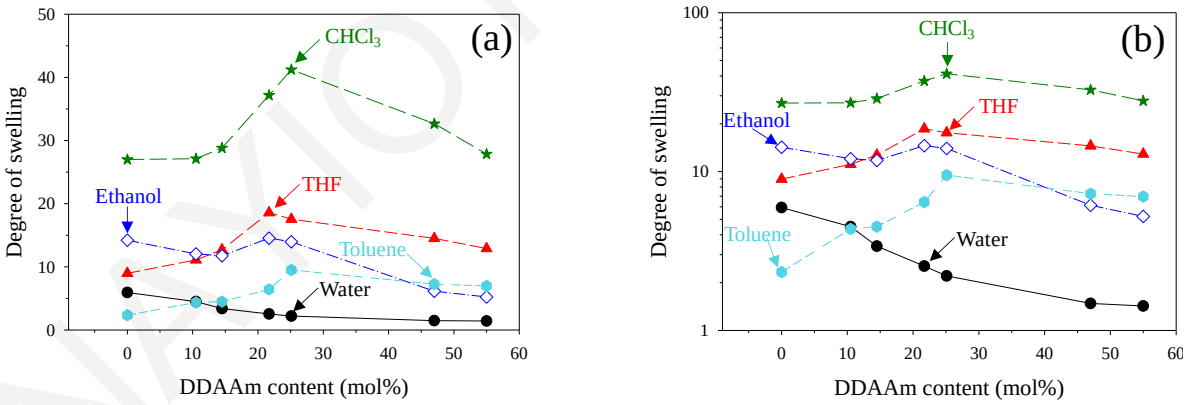

Figure 3.6.6. Dependence of the equilibrium degrees of swelling of the APCNs on their DDAAm content in (a) double-linear axes, and (b) semi-logarithmic axes.

Figure 3.6.6 shows that the equilibrium DSs in the four organic solvents exhibited a maximum with the DDAAm content, at 25 mol%, whereas this maximum was absent in the case of the water-swollen APCNs. The lowest values of the equilibrium DSs were observed in the case of the water-swollen APCNs, whereas the highest values were observed for the APCNs swollen in $CHCl_3$. In particular, the values of the equilibrium DSs

increased in the order: water < toluene < ethanol < THF < $CHCl_3$. This trend can be attributed to the selectivity of each solvent. Water is a solvent selective for the polyDMAAm and PEG blocks and a non-solvent for the polyDDAAm blocks (lowest values of DSs), whereas $CHCl_3$ and THF are both non-selective solvents (higher values of DSs), ethanol is a more suitable solvent for the hydrophilic polyDMAAm block, and toluene is a more suitable solvent for the hydrophobic polyDDAAm block, and, consequently, these last two solvents exhibit intermediate values of equilibrium DSs.

Regarding the water-swollen APCNs, it was found that increasing the number of DDAAm repeating units, *i.e.*, the DDAAm content in the APCNs, resulted in decreased values of the DSs in water, as expected. The maximum value of the equilibrium DS in water, 5.9, was measured in the case of the APCN consisting only of DMAAm and PEG, whereas the minimum value, 1.4, was obtained when the relative DDAAm content was the highest, 55 mol%.

In the case of the organo-swollen APCNs, the initial increase in the equilibrium DSs up to the DDAAm content of 25 mol% can be attributed to the increased number of the hydrophobic DDAAm monomer repeating units in the APCNs, whereas the subsequent decrease for higher DDAAm contents may be due to the relatively high degrees of polymerization for the HDDA cross-linker repeating units.

3.6.6 Mechanical Properties of the Water-Swollen Polymer Conetworks

3.6.6.1 Stress-Strain Curves

Figure 3.6.7 displays the original mechanical property data obtained from the compression experiments on the water-swollen APCNs. In particular, Figure 3.6.7 presents the three stress-strain curves for the four water-swollen APCNs with the lowest number of the DDAAm repeating units, $HDDA_3$-*b*-DM_{50}-*b*-EG_{46}-*b*-DM_{50}-*b*-$HDDA_3$ (part (a)), $HDDA_{3.4}$-*b*-DD_6-*b*-DM_{50}-*b*-EG_{46}-*b*-DM_{50}-*b*-DD_6-*b*-$HDDA_{3.4}$ (part (b)), $HDDA_{3.5}$-*b*-DD_9-*b*-DM_{50}-*b*-EG_{46}-*b*-DM_{50}-*b*-DD_9-*b*-$HDDA_{3.5}$ (part (c)), $HDDA_{3.8}$-*b*-DD_{13}-*b*-D_{50}-*b*-EG_{46}-*b*-D_{50}-*b*-DD_{13}-*b*-$HDDA_{3.6}$ (part (d)), and $HDDA_{3.8}$-*b*-DD_{17}-*b*-D_{50}-*b*-EG_{46}-*b*-D_{50}-*b*-DD_{17}-*b*-$HDDA_{3.8}$ (part (e)). It is worth mentioning that the APCNs with a DDAAm content higher than 25 mol%

could not be characterized in terms of their mechanical properties, because they were extremely fragile, possibly a result of their very low equilibrium water content.

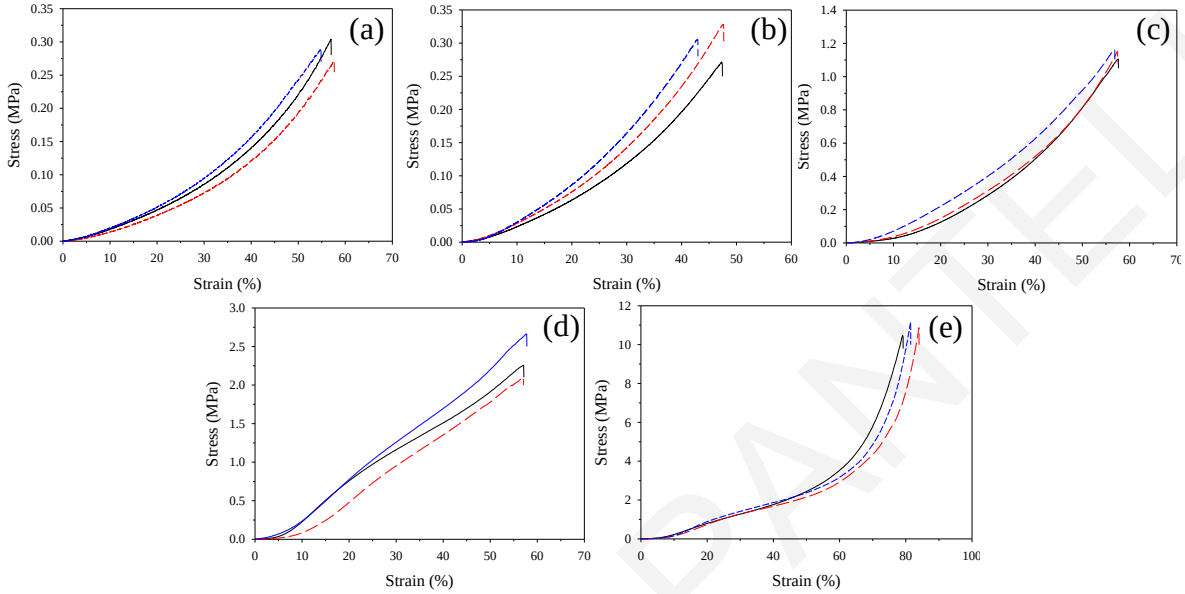

Figure 3.6.7. Compressive stress-strain curves for the water-swollen APCNs. (a) $HDDA_3$-*b*-DM_{50}-*b*-EG_{46}-*b*-DM_{50}-*b*-$HDDA_3$, (b) $HDDA_{3.2}$-*b*-DD_6-*b*-DM_{50}-*b*-EG_{46}-*b*-DM_{50}-*b*-DD_6-*b*-$HDDA_{3.2}$, (c) $HDDA_{3.4}$-*b*-DD_9-*b*-DM_{50}-*b*-EG_{46}-*b*-DM_{50}-*b*-DD_9-*b*-$HDDA_{3.4}$, (d) $HDDA_{3.6}$-*b*-DD_{13}-*b*-D_{50}-*b*-EG_{46}-*b*-D_{50}-*b*-DD_{13}-*b*-$HDDA_{3.6}$, (e) $HDDA_{3.8}$-*b*-DD_{17}-*b*-D_{50}-*b*-EG_{46}-*b*-D_{50}-*b*-DD_{17}-*b*-$HDDA_{3.8}$.

Figure 3.6.7 shows that the stress-strain curves in parts (a), (b), and (c) exhibited a smooth concave-up shape, whereas the curves in part (d) and, particularly in part (e) exhibited strain localization. More importantly, as the DDAAm content increased, the failure stress also increased (see Figure 3.6.8a). This can be attributed to microphase separation driven by the polyDDAAm blocks, leading to the formation of hydrophobic cores, whose size increased with the DDAAm content.

3.6.6.2 Fracture Stress and Fracture Strain

Figure 3.6.8 displays the dependence of the fracture stress values (part (a)) and the fracture strain values (part (b)) on the DDAAm content in the water-swollen APCNs. Increasing the DDAAm content in the APCNs resulted in an increase in both the fracture stress and strain values. The highest values of fracture stress, 10.8 MPa, and fracture strain, 81.3%, were obtained in the case of the APCN containing a relatively high DDAAm content, 25 mol%. The gel that exhibited the lowest fracture stress value of 0.29 MPa was the APCN

consisting only of hydrophilic DMAAm and PEG monomers and HDDA cross-linker repeating units (DDAAm content = 0 mol%). On the other hand, the lowest fracture strain value, 45.7%, was presented by the APCN containing 10.7 mol% DDAAm.

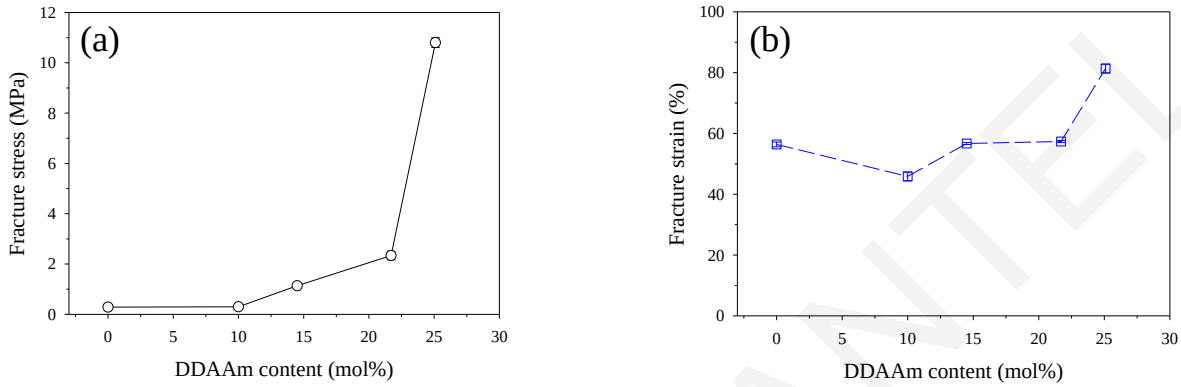

Figure 3.6.8. Dependence of (a) the fracture stress and (b) the fracture strain on the DDAAm content for the water-swollen APCNs.

Part (a) of the figure shows that the fracture stress increased with increasing the DDAAm content. This behavior can be attributed to the lower aqueous equilibrium degrees of swelling of the more hydrophobic gels, but, more importantly, to microphase separation in water, with the size of the hydrophobic domains increasing with the hydrophobe content. The formation of the hydrophobic nanodomains provides an important route for mechanical energy dissipation, resulting in gel strengthening.

Part (b) of the figure shows that increasing the DDAAm content led to a slight increase in the values of fracture strain in most cases. In particular, the fracture strain was reduced from 56.4 to 45.7% when the DDAAm content was increased from 0.0 to 10.7 mol%, increased to 56.7% when the DDAAm content increased to 14.5 mol%, slightly increased to 57.3% when the DDAAm content increased to 22 mol%, and significantly increased to 80.3% when the DDAAm content became equal to 25 mol%.

3.6.6.3 Young's Modulus and Fracture Energy Density

Figure 3.6.9 shows the effect of the DDAAm content in the water-swollen APCNs on the Young's modulus values (part (a)) and the fracture energy density values (part (b)). Increasing the DDAAm content in the APCNs lead to increased values for both Young's modulus and fracture energy density. The APCN prepared at a 25 mol% DDAAm content

exhibited the highest value of Young's modulus, 4.5 MPa, and the highest value of fracture energy density, 2 MJ m^{-3}. On the other hand, the APCN consisting only of DMAAm and PEG monomers and HDDA cross-linker repeating units exhibited the lowest value, 0.24 MPa, while the lowest fracture energy density value, 51 kJ m^{-3}, was presented by the APCN containing 10.7 mol% DDAAm.

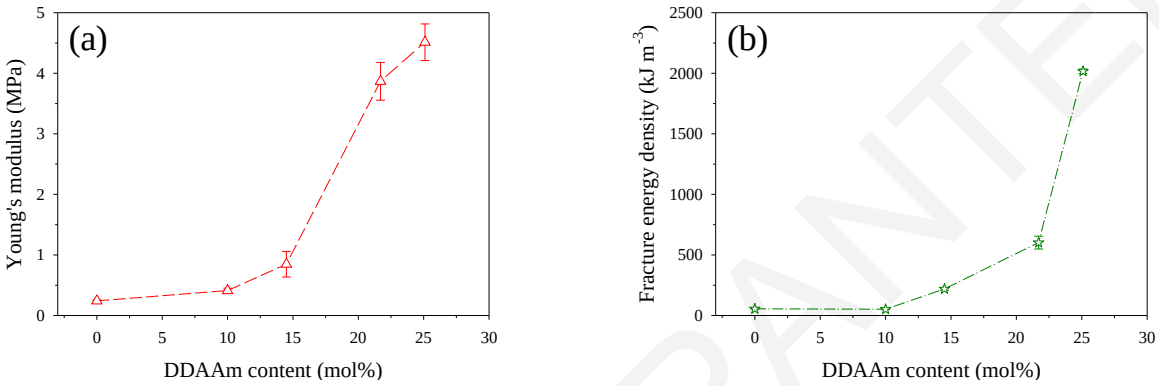

Figure 3.6.9. Dependence of (a) the Young's modulus and (b) the fracture energy density on the DDAAm content for the water-swollen APCNs.

Part (a) of the figure shows that the values of the Young's modulus increased upon increasing the DDAAm content. This behavior can once again be attributed to the equilibrium aqueous DSs of the gels and the formation of hydrophobic nanodomains arising from the establishment of hydrophobic associations among the DDAAm monomer repeating units. Initially, high DDAAm contents lead to reduced values of the equilibrium DS, that favor high polymer volume fractions, resulting in increased Young's modulus values. Furthermore, APCNs with high DDAAm contents contain higher total cross-linking densities, arising from the presence of hydrophobic associations that act as extra cross-links, and, consequently, promote the formation of clusters with a much higher cross-linking density, resulting in an increase in the Young's modulus values.

Part (b) of the figure shows that increasing the DDAAm content in the polymer networks resulted in increased values of the fracture energy density. This behavior can be explained using both the values of fracture stress and fracture strain, as the fracture energy density is calculated from the area under the stress – strain curve. Thus, the particular mechanical property exhibits a behavior intermediate between these two mechanical properties. Since the behavior of the fracture stress can be explained using the equilibrium DSs of the gels and the formation of the hydrophobic domains, the same explanations can be also given for

the fracture energy density. Increased values of DDAAm content in the gels results in low values of the DSs and high values of the polymer volume fraction, thereby leading to increased values of the fracture energy density. In addition, high DDAAm contents contribute to the formation of clusters with a higher cross-linking density, and, therefore, a higher energy must be given to the system to disrupt the hydrophobic associations in the clusters.

3.6.7 Conclusions

We presented the preparation, via sequential RAFT polymerization, of APCNs, consisting of hydrophilic PDMAAm and PEG segments, and hydrophobic PDDAAm segments. APCNs possessing a range of compositions were prepared, with the DDAAm and DMAAm appearing in 8 different molar ratios. Prior to the end-linking for the preparation of the APCNs, the linear ABCBA pentablock terpolymer precursors were characterized in terms of their molecular weights and compositions, which were found to be in good agreement with the values expected on the basis of the monomer feed ratio and monomer conversion. Increasing the DDAAm content in the linear precursors resulted in increased values of molecular weight and molecular weight dispersity. Furthermore, dilute aqueous solutions of the pentablock terpolymers were studied in terms of their self-assembly using DLS and SANS. DLS indicated the formation of aggregated micelles, rather than regular spherical micelles, having values of hydrodynamic radii higher than the maximum possible for single spherical micelles. These values of hydrodynamic radii were found to increase with increasing the concentration of the terpolymer aqueous solution. The subsequently formed polymer conetworks were characterized in terms of their equilibrium DSs in water and organic solvents and their mechanical properties in water. The values of the aqueous equilibrium DSs were found to decrease upon increasing the DDAAm content in the gels, whereas the corresponding values in organic solvents exhibited a maximum at a DDAAm content of 25 mol%. All compressive mechanical properties, fracture stress, fracture strain, Young's modulus and fracture energy density were found to increase upon increasing the DDAAm content, and this enhancement was probably due to microphase separation driven by the hydrophobic polyDDAAm blocks and the formation of hydrophobic nanodomains, rather than the mere reduction in the aqueous equilibrium DSs effected by the presence of these hydrophobic blocks.

3.7 Amphiphilic Polymer Networks Based on Pentablock Terpolymers or Random Copolymers of DMAAm and DAAm Prepared Using RAFT Polymerization and Cross-linked Using Oxime Bonds

3.7.1 Synthesis of the Pentablock Terpolymers and the Random Copolymers

The synthesis of the linear random copolymers and the linear amphiphilic pentablock terpolymers was accomplished in one or two steps, respectively, using RAFT polymerization. Both the random copolymers and the pentablock terpolymers consisted of the inert hydrophilic DMAAm monomer and the reactive hydrophobic diacetone acrylamide (DAAm) monomer, that bears a ketone group in the pendant. The ketone group is known to react with an aminooxy-bearing compound and form a ketoxime dynamic covalent bond. Thus, the reaction between the linear precursors and the difunctional aminooxy-bearing compound *O*,*O*′-1,3-propanediylbis(hydroxylamine) dihydrochloride (PDH) should result in the formation of oxime bonds, which act as covalent, but potentially reversible cross-linking points, and, therefore, in the formation of the corresponding polymer network. It is worth mentioning that before choosing the DAAm monomer, efforts were made to prepare oxime cross-linked polymer networks whose linear precursors contained an aromatic aldehyde group instead of a ketone group. However, when the polymer precursors were reacted with PDH, the gels were formed very quickly, within 60 seconds, which produced rather fragile gels whose formation could not be followed by rheology.

In all cases, the total degree of polymerization of the inert DMAAm monomer repeating units was constant and equal to 100, while the total degree of polymerization of the reactive DAAm monomer repeating units was equal to 5 or 10 in the case of the random copolymers or ranged between 6 and 50 in the case of the pentablock terpolymers. Both the random copolymers and the pentablock terpolymers were prepared using AIBN as the thermal initiator and toluene as the polymerization solvent. However, the random copolymers were prepared using the DMPA monofunctional chain transfer agent, while the pentablock terpolymers were synthesized using the PEG DMPA difunctional chain transfer agent. Thus, all the polymers prepared using PEG DMPA contained a PEG-middle block consisting of 46 ethylene glycol monomer repeating units.

Figure 3.7.1 illustrates the structures and the synthetic route followed for the preparation of the linear pentablock terpolymer precursors, which were subsequently employed in the formation of the oxime cross-linked APCNs. In the first step, the PEG DMPA served as the chain transfer agent for the polymerization of the DMAAm monomer and the formation of the $DMAAm_{50}$-*b*-EG_{46}-*b*-$DMAAm_{50}$ triblock copolymer. After its isolation, the triblock copolymer was used as macro-CTA for the polymerization of the DAAm monomer and the formation of the desired $DAAm_x$-*b*-$DMAAm_{50}$-*b*-EG_{46}-*b*-$DMAAm_{50}$-*b*-$DAAm_x$ pentablock terpolymers. In total, five pentablock terpolymers were prepared, in which the total degree of polymerization of DAAm acquired values of 6, 12, 24, 32, and 50. On the other hand, in the case of the random copolymers, the DMAAm and DAAm monomers were combined at two different molar ratios, leading to the preparation of two different random copolymers, $DMAAm_{100}$-*co*-$DAAm_5$ and $DMAAm_{100}$-*co*-$DAAm_{10}$.

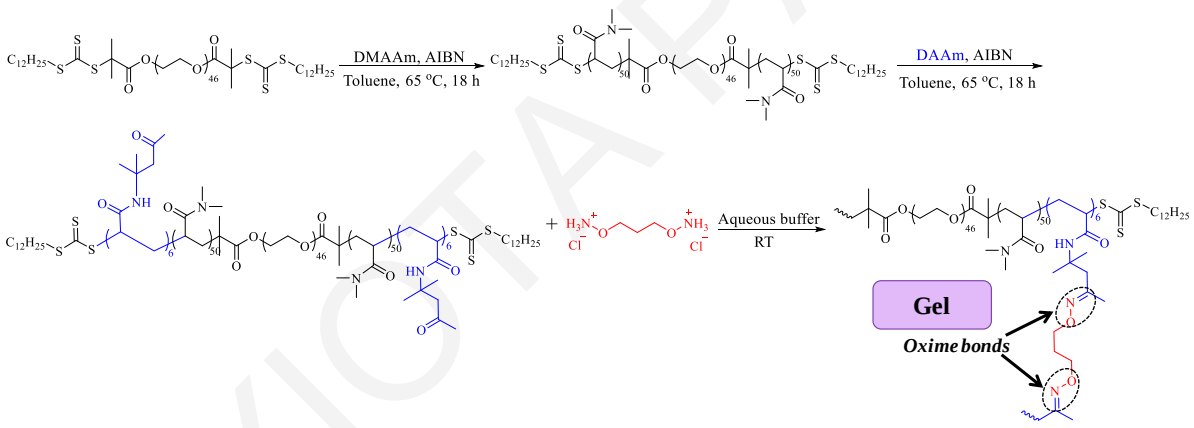

Figure 3.7.1. Synthetic procedure followed for the preparation of the linear amphiphilic ABCBA pentablock terpolymers and their subsequent use for the formation of the oxime cross-linked APCNs.

3.7.2 Molecular Weights and Compositions of the Linear Precursors

All the prepared random copolymers, the triblock copolymer precursor, and the final pentablock terpolymers were characterized in terms of their molecular weights (M_p and M_n) and molecular weights dispersities ($Đ = M_w/M_n$), and compositions using GPC and ^{1}H NMR spectroscopy, respectively. Table 3.7.1 lists all the results obtained from the characterization of the polymers, as well as the theoretical values of molecular weight and composition. In particular, the table lists the expected values of the theoretical molecular weights and the expected DAAm content (relative, with respect to DMAAm), and the

molecular weights and molecular weights dispersities obtained using GPC, and the DAAm content determined from ^{1}H NMR spectroscopy. The determination of the theoretical molecular weight of the triblock copolymer was performed by comparing the area under the peak of the methyl protons on the nitrogen atom (–(C=O)–N(C*H*$_3$)$_2$, δ = 2.80 – 3.20 ppm) in the DMAAm monomer repeating units to the area under the peak corresponding to the protons of the ethylene glycol monomer repeating units (–OC*H*$_2$C*H*$_2$O–, δ = 3.60-3.75 ppm). The determination of the theoretical molecular weight of the pentablock terpolymers was accomplished by comparing the area under the peak corresponding to the terminal methyl protons next to the ketone group (–(C=O)–C*H*$_3$, δ = 2.00 ppm) in the DAAm monomer repeating units to the area under the peak corresponding to the ethylene protons of PEG (–OC*H*$_2$C*H*$_2$O–, δ = 3.60-3.75 ppm), while the theoretical molecular weight of the random copolymers was determined by comparing the area under the peak of the terminal methyl protons in the DAAm monomer repeating units to the area under the peak corresponding to the terminal methyl protons of the DMPA CTA (–(CH$_2$)$_{11}$–C*H*$_3$, δ = 0.87 ppm).

Table 3.7.1. Theoretical, and experimental values of the molecular weights and compositions, obtained using GPC and ^{1}H NMR spectroscopy, respectively.

No.	Polymer Structure [a,b]	Theory MW [c] (kg mol^{-1})	GPC Results			DAAm (mol%)	
			M_p (kg mol^{-1})	M_n (kg mol^{-1})	$Đ$	Theory[d]	NMR[e]
	Random Copolymers						
1	D$_{100}$-*co*-DA$_5$	11.3	7.1	5.1	1.3	5.7	5.9
2	D$_{100}$-*co*-DA$_{10}$	12.3	9.6	7.2	1.3	10.7	10.0
	Triblock Copolymer						
3	D$_{50}$-*b*-EG$_{46}$-*b*-D$_{50}$	12.7	11.2	9.5	1.3	-	-
	Pentablock Terpolymers						
4	DA$_3$-*b*-D$_{50}$-*b*-EG$_{46}$-*b*-D$_{50}$-*b*-DA$_3$	13.7	13.7	10.3	1.3	5.7	7.0
5	DA$_6$-*b*-D$_{50}$-*b*-EG$_{46}$-*b*-D$_{50}$-*b*-DA$_6$	14.7	16.1	12.7	1.4	10.7	12.0
6	DA$_{12}$-*b*-D$_{50}$-*b*-EG$_{46}$-*b*-D$_{50}$-*b*-DA$_{12}$	16.8	17.1	11.9	1.6	20.0	23.0
7	DA$_{16}$-*b*-D$_{50}$-*b*-EG$_{46}$-*b*-D$_{50}$-*b*-DA$_{16}$	18.1	18.7	14.3	1.5	24.0	26.0
8	DA$_{25}$-*b*-D$_{50}$-*b*-EG$_{46}$-*b*-D$_{50}$-*b*-DA$_{25}$	21.2	22.4	14.6	1.6	30.6	34.0

[a] D, DA: Further abbreviations for DMAAm and DAAm, respectively. [b, c, e] Calculated from the ^{1}H NMR spectra.
[d] Calculated from the polymerization feed ratio.

In all cases, the conversions of the DMAAm and DAAm monomers were quantitative after 16-18 h of polymerization, indicating the suitability of the RAFT method for the polymerization of these monomers. The GPC results obtained for the random copolymers indicated much lower values of M_n (by almost a factor of 2) than the corresponding theoretical values of the molecular weights calculated from the ^{1}H NMR spectra, while in the case of the pentablock terpolymers, the values of the M_n were slightly lower than the theoretical values. The molecular weight dispersity values were found to range between 1.3 and 1.6, and slightly increased upon increasing the molecular weight of the pentablock terpolymers. Figure 3.7.2 presents the GPC traces for the DMAAm$_{50}$-*b*-EG$_{46}$-*b*-DMAAm$_{50}$ triblock copolymer precursor and the final amphiphilic DAAm$_x$-*b*-DMAAm$_{50}$-*b*-EG$_{46}$-*b*-DMAAm$_{50}$-*b*-DAAm$_x$ pentablock terpolymers. The figure shows that increasing the molecular weight of the polymers resulted in lower elution times, as expected. In addition, the absence of any shoulders or secondary peaks in the chromatograms indicate the successful chain extension of the triblock copolymer precursor with the DAAm monomer.

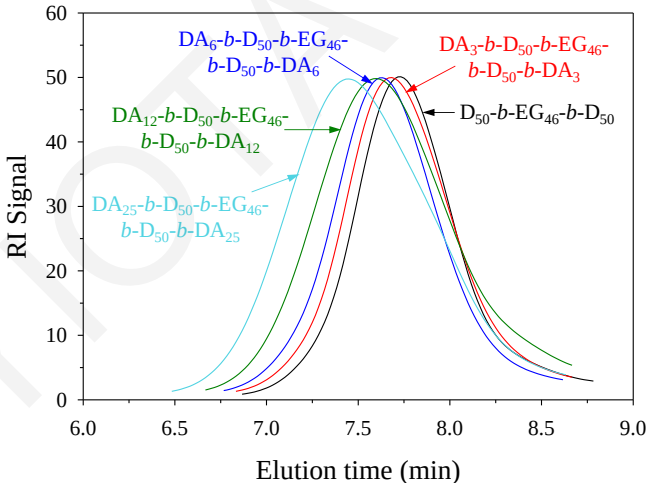

Figure 3.7.2. GPC traces of the DMAAm$_{50}$-*b*-EG$_{46}$-*b*-DMAAm$_{50}$ triblock copolymer precursor, and the amphiphilic DAAm$_x$-*b*-DMAAm$_{50}$-*b*-EG$_{46}$-*b*-DMAAm$_{50}$-*b*-DAAm$_x$ pentablock terpolymers.

Figure 3.7.3 presents the ^{1}H NMR spectra in $CDCl_3$ of the DMAAm$_{50}$-*b*-EG$_{46}$-*b*-DMAAm$_{50}$ triblock copolymer precursor (part (a)) and the DAAm$_6$-*b*-DMAAm$_{50}$-*b*-EG$_{46}$-*b*-DMAAm$_{50}$-*b*-DAAm$_6$ pentablock terpolymer (part (b)). In both cases, the experimental DAAm content was calculated by comparing the area under the peak corresponding to the terminal methyl protons in the DAAm monomer repeating units to the area under the peak

corresponding to the methyl protons on the nitrogen atom (–(C=O)–N(CH_3)$_2$, δ = 2.80-3.20 ppm) in the DMAAm monomer repeating units. The calculated values of DAAm content ranged between 5.9 and 34.0 mol% and in all cases these values were slightly higher, but very close to, the theoretical values, calculated from the polymerization feed ratio.

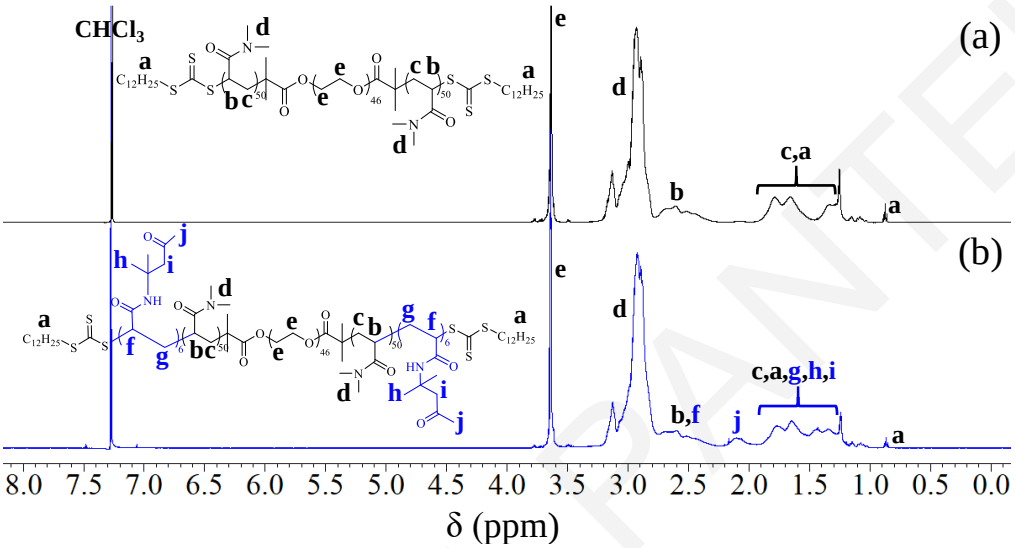

Figure 3.7.3. ^{1}H NMR spectra in $CDCl_3$ of (a) the DMAAm$_{50}$-*b*-EG$_{46}$-*b*-DMAAm$_{50}$ triblock copolymer precursor and (b) the DAAm$_6$-*b*-DMAAm$_{50}$-*b*-EG$_{46}$-*b*-DMAAm$_{50}$-*b*-DAAm$_6$ pentablock terpolymer.

3.7.3 Functionalization of the Pentablock Terpolymers with a Monofunctional Aminooxy Compound

Prior to the investigation studies for the formation of the oxime cross-linked polymer networks through the reaction of the linear precursors with the difunctional aminooxy compound PDH, preliminary experiments on the post-polymerization modification of the pentablock terpolymers were performed. To this end, the DAAm$_{16}$-*b*-DMAAm$_{50}$-*b*-EG$_{46}$-*b*-DMAAm$_{50}$-*b*-DAAm$_{16}$ pentablock terpolymer was subjected to reaction with the monofunctional aminooxy compound *O*-benzylhydroxylamine hydrochloride (BzHA, 2 eq. to the DAAm monomer repeating units) at a concentration of 10% w/v in EtOH in the presence of TEA (3 eq. to BzHA), and the reaction was allowed to proceed for 4 days at room temperature. Then, the reaction mixture was characterized using ^{1}H NMR spectroscopy in order to determine the extent of functionalization. The calculation of the extent of functionalization was performed by comparing the area under the peak of the terminal methyl protons (–(C=O)–CH_3, δ = 2.00 ppm) in the DAAm monomer repeating

units in the initial polymer to the area under the peak corresponding to the same methyl protons, that were downshifted to 1.70 ppm in the final functionalized polymer. It was found that the extent of functionalization was high, 85%, indicating the successful modification of the linear polymer precursor via the oxime bond. This value compares favorably with the extent of functionalization value of 95% reported by Sumerlin's group,[27] for the functionalization of $DMAAm_{100}$-*b*-$DAAm_{40}$ diblock copolymer with *O*-allyl hydroxylamine hydrochloride and *O*-(tetrahydro-2*H*-pyran-2-yl)-hydroxylamine.

3.7.4 Effect of pH and Stoichiometry of the Reaction on the Gel Formation Time of the Oxime Cross-linked Polymer Networks

Having established that the reaction between a ketone group (pentablock terpolymer) and an aminooxy group (BzHA) results in the successful formation of the oxime bond and the functionalization of the pentablock terpolymer, we investigated the formation of polymer networks by reacting the linear precursors with PDH that bears two aminooxy groups in order to induce the cross-linking of the linear polymers. The reactions were all performed in aqueous media, as the particular reaction is known to be favored in aqueous conditions, and particularly in slightly acidic conditions.[28-32] In order to evaluate the dependence of the gel formation time of the polymer networks on the pH of the aqueous buffer solution and the stoichiometry of the reaction, and to find the optimum conditions for their preparation, these parameters were separately investigated. Figure 3.7.4 presents the dependence of the gel formation time on the pH of the aqueous buffer solution (part (a)) and the ratio of the ketone to the aminooxy units (part (b)) through the reaction of the $DAAm_6$-*b*-$DMAAm_{50}$-*b*-EG_{46}-*b*-$DMAAm_{50}$-*b*-$DAAm_6$ pentablock terpolymer and PDH at a total solids concentration of 10% w/v.

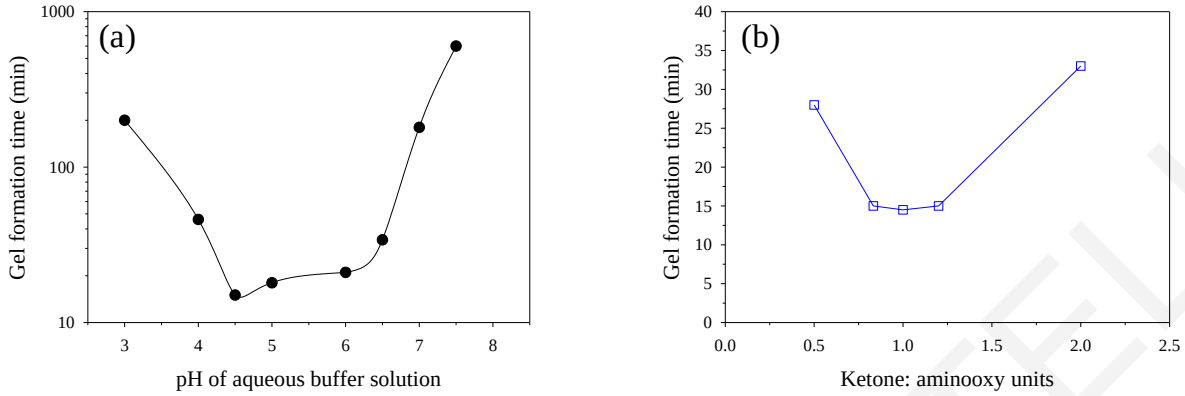

Figure 3.7.4. Effects of (a) pH (using a constant molar ratio of the ketone to the aminooxy units of 1:1), and (b) the ratio of the ketone to the aminooxy units (in aqueous buffer of pH 4.5) on the gel formation time of the polymer networks prepared at a total solids concentration of 10% w/v using the $DAAm_6$-*b*-$DMAAm_{50}$-*b*-EG_{46}-*b*-$DMAAm_{50}$-*b*-$DAAm_6$ pentablock terpolymer and PDH.

Part (a) of the figure shows that the gel formation time exhibited a minimum when the pH of the aqueous buffer solution was equal to 4.5, indicating that at this particular pH, the polymer networks have the shortest formation time, 14.5 min. When the pH of the aqueous buffer solution was low, 3-4, or high, 6.5-7.5, the gel formation was much slower, ranging between 200 and 600 min. In the former case, the longer gel formation times can be attributed to the extensive protonation of the aminooxy group (pK_a value for the CH_3O-NH_3^+ Cl^- = 4.6[33]) of the PDH cross-linker at low pH values, leading to an insufficient amount of (deprotonated) aminooxy groups to participate in the oxime formation reaction, and, therefore, the reaction becomes very slow. On the other hand, increasing the pH of the aqueous buffer solution above 4.5 results in slower gel formation, as a lower proton concentration is present in the aqueous buffer solutions. The protons catalyze the oxime formation reaction by the activation of the carbonyl group, leading to a faster nucleophilic attack of the aminooxy group.[30] Therefore, when the pH is increased, the polymer networks exhibit longer formation times, requiring 34 min at pH 6.5, and 10 h at pH 7.5, with no gel formation observed at pH 8.

The pH value, and, consequently, the proton concentration must be intermediate, as a very high proton concentration (pH 3-3.5) results in the complete protonation of the aminooxy group, leading to a very slow oxime formation reaction, while a very low proton concentration (pH 6.5-7.5) also results in a slower reaction. Finally, it is also worth mentioning that the polymer network formed in the aqueous buffer solution of pH 4.5

exhibited the highest toughness, while the polymer networks prepared in aqueous buffer solutions of pH 6-7.5 exhibited a liquid-like behavior. Our findings are consistent with previous reports[28-32] that demonstrated that the reaction between a carbonyl group and an aminooxy group is highly favored at moderately acidic pH values.

Regarding the effect of the stoichiometry of the reaction on the gel formation time of the polymer networks, part (b) of the figure shows that the gel formation time exhibited a minimum (14.5 mins) when the ratio of the ketone to the aminooxy units was 1:1, *i.e.*, at the stoichiometric ratio. However, the stoichiometry had a weaker effect on the gel formation time than the pH value of the aqueous buffer solution, as the gel formation time significantly increased by two-fold only at the two extreme values of the ratio of the ketone to the aminooxy units, 2:1, *i.e.*, 100% excess of ketone units, or 1:2, *i.e.*, 100% excess of aminooxy units. In contrast, the gel formation time remained almost constant and independent of this ratio, as it was only slightly increased to 15 mins in both cases when this ratio was equal to 1.2:1 and 1:1.2, *i.e.*, 20% excess of the ketone or the aminooxy units.

In conclusion, these findings indicate that the optimum pH value of the aqueous buffer solution for gel formation is 4.5, while the appropriate ratio of the ketone to the aminooxy units is 1:1. Thus, the particular conditions were followed for performing the reaction between the linear polymer precursors and the PDH cross-linker.

3.7.5 Elucidation of the Effect of the DAAm Content on the Gel Formation Time of the Oxime Cross-linked Polymer Networks

The effect of the DAAm content on the gel formation time of the oxime cross-linked polymer networks was investigated by performing the reaction between each linear polymer precursor and the PDH cross-linker using the optimum experimental conditions. Figure 3.7.5 displays the dependence of the gel formation time for the oxime cross-linked polymer networks on the DAAm content in the linear precursors, and, in particular, the $DMAAm_{100}$-*co*-$DAAm_x$ random copolymers (part (a)) and the $DAAm_x$-*b*-$DMAAm_{50}$-*b*-EG_{46}-*b*-$DMAAm_{50}$-*b*-$DAAm_x$ pentablock terpolymers (part (b)). The reactions were performed at a constant total solids concentration of 15% w/v, while the gel formation

times were determined from both tube inversion and rheology measurements. The gel formation times obtained using rheology were determined from the crossover of the elastic, *G′*, and loss, *G″*, moduli.[34-36] It is worth mentioning that all polymers were water-soluble, except for the pentablock terpolymer with the highest number of DAAm monomer repeating units, 50, for which the gel formation reaction was performed in an EtOH : buffer solution of pH 4.5 mixture at 1:2 volume ratio. Thus, the gel formation times for this particular polymer network were not plotted in Figure 3.7.5. The gel formation time for the APCN based on the DAAm$_{16}$-*b*-DMAAm$_{50}$-*b*-EG$_{46}$-*b*-DMAAm$_{50}$-*b*-DAAm$_{16}$ pentablock terpolymer could not be determined from rheology, as the aqueous polymer solution was very viscous and difficult to handle.

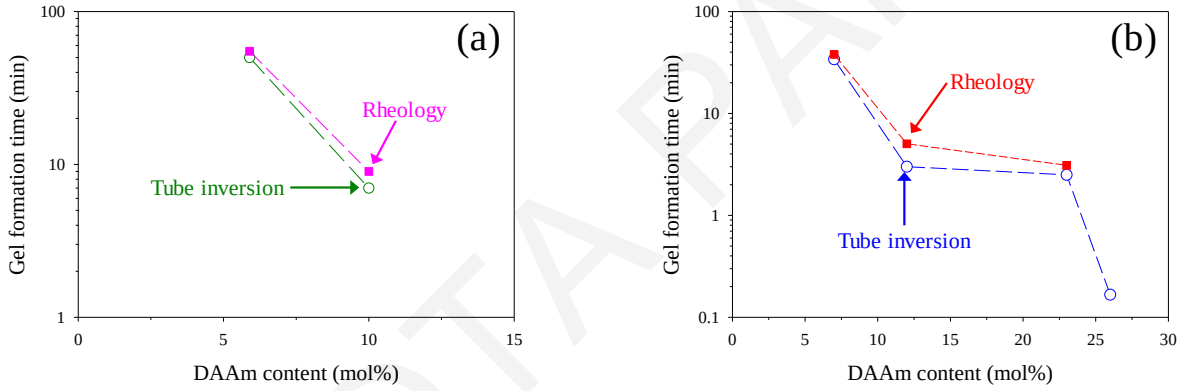

Figure 3.7.5. Effect of DAAm content on the gel formation times for the polymer networks prepared from PDH and (a) the DMAAm$_{100}$-*co*-DAAm$_x$ random copolymers and (b) the DAAm$_x$-*b*-DMAAm$_{50}$-*b*-EG$_{46}$-*b*-DMAAm$_{50}$-*b*-DAAm$_x$ pentablock terpolymers. All the reactions were performed in aqueous buffer solutions of pH 4.5 at the stoichiometric ratio at a total solids concentration of 15% w/v. The gel formation times were determined from both tube inversion (green and blue lines) and rheology measurements (pink and red lines).

Both parts of the figure show that the gel formation time is highly dependent on the DAAm content in the linear polymers, as increasing this value results in reduced gel formation times. Furthermore, the gel formation times determined from the rheology measurements were slightly longer, but in good agreement with, the corresponding times calculated from the tube inversion experiments. This suggests that rheology is a more demanding method than the tube inversion method with regards to the criterion for gel formation.

The DAAm content in the precursors is a measure of the cross-linking density in the final polymer networks, as the oxime bonds serve as cross-linking points. Thus, when the degree of polymerization of DAAm is increased, the cross-linking density is also increased, and,

therefore, gel formation occurs faster. This is expected, as, according to the Flory-Stockmayer equation (equation 3.4)[37,38] about the gel point conversion, increasing the functionality of the polymer, f_{ketone} ($f_{aminooxy}$ is constant and equal to 2, and r is constant and equal to 1), results in a lower conversion required to achieve gelation:

$$\rho = \frac{1}{\sqrt{r\,(f_{ketone}-1)\,(f_{aminooxy}-1)}} \qquad \textbf{Equation 3.4}$$

where ρ is the gel point conversion, r is the molar ratio of the two reacting groups, equal to 1 in our case, and f_{ketone} and $f_{aminooxy}$ are functionalities for the polymer (f_{ketone} = 5-50) and the PDH cross-linker ($f_{aminooxy}$ = 2), respectively.

For example, the conversion required to achieve gelation for the $DMAAm_{100}$-*co*-$DAAm_5$ and $DMAAm_{100}$-*co*-$DAAm_{10}$ random copolymers must be equal to 0.50 and 0.33, respectively. Thus, increasing the DAAm content leads to a lower critical conversion, and, consequently, the random copolymer with 10.0 mol% DAAm is converted faster to gel than the random copolymer with 5.9 mol% DAAm. As shown in the figure, increasing this value led to a decrease in the gel formation time from 50-55 to 7-9 min for the randomly cross-linked copolymer networks prepared using the $DMAAm_{100}$-*co*-$DAAm_5$ and $DMAAm_{100}$-*co*-$DAAm_{10}$ random copolymers, respectively.

In the case of the oxime cross-linked APCNs, the polymer network prepared using the $DAAm_3$-*b*-$DMAAm_{50}$-*b*-EG_{46}-*b*-$DMAAm_{50}$-*b*-$DAAm_3$ pentablock terpolymer with the lowest DAAm content, 7 mol%, required 34-38 min to form, whereas the APCN prepared using the $DAAm_{16}$-*b*-$DMAAm_{50}$-*b*-EG_{46}-*b*-$DMAAm_{50}$-*b*-$DAAm_{16}$ pentablock terpolymer with a relatively high DAAm content, 26 mol%, required 10 s to form. In contrast, the $DAAm_{25}$-*b*-$DMAAm_{50}$-*b*-EG_{46}-*b*-$DMAAm_{50}$-*b*-$DAAm_{25}$ pentablock terpolymer required a longer time to form than the above-mentioned terpolymer, and, particularly, 1.50 min, despite its higher DAAm content, due to the presence of ethanol which results in slower gelation. It is worth noting that when the amount of ethanol in the mixture was increased, the gel formation time was also significantly increased, as the particular gel required 25 min to form when the ethanol : aqueous buffer volume ratio was equal to 2:1, and was further increased when the ratio became equal to 4:1.

3.7.6 Elucidation of the Effect of Total Solids Concentration on the Gel Formation Time of the Oxime Cross-Linked Polymer Networks

For the elucidation of the effect of total solids concentration on the gel formation time of the oxime cross-linked polymer networks, all the linear polymer precursors were subjected to reaction with PDH at three different total solids concentrations, 10.0, 12.5 and 15.0% w/v. Figure 3.7.6 presents the effect of total solids concentration on the gel formation time for the randomly cross-linked copolymer networks based on the $DMAAm_{100}$-*co*-$DAAm_{10}$ random copolymer (part (a)), and for the APCNs based on the $DAAm_6$-*b*-$DMAAm_{50}$-*b*-EG_{46}-*b*-$DMAAm_{50}$-*b*-$DAAm_6$ (part (b)), and the $DAAm_{16}$-*b*-$DMAAm_{50}$-*b*-EG_{46}-*b*-$DMAAm_{50}$-*b*-$DAAm_{16}$ (part (c)) pentablock terpolymers. Once again, the reactions were performed in aqueous buffer solutions of pH 4.5 at the stoichiometric ratio, while the gel formation times were determined both from tube inversion (blue line) and rheology measurements (red line).

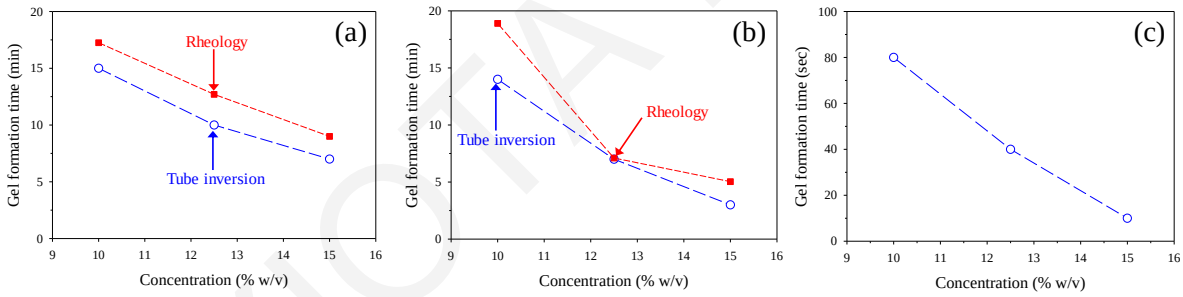

Figure 3.7.6. Dependence of the gel formation time on the total solids concentration employed for the preparation of the polymer networks from the reaction of PDH and (a) the $DMAAm_{100}$-*co*-$DAAm_{10}$ random copolymer, (b) the $DAAm_6$-*b*-$DMAAm_{50}$-*b*-EG_{46}-*b*-$DMAAm_{50}$-*b*-$DAAm_6$, and (c) the $DAAm_{16}$-*b*-$DMAAm_{50}$-*b*-EG_{46}-*b*-$DMAAm_{50}$-*b*-$DAAm_{16}$ pentablock terpolymers. All reactions were performed in aqueous buffer solutions of pH 4.5 at the stoichiometric ratio. The gel formation times were determined both from tube inversion (blue line) and rheology measurements (red line).

Figure 3.7.6 shows that the total solids concentration had a significant effect on the time taken for the formation of the polymer networks. In particular, increasing the total solids concentration results in faster gelation, and this is evidenced in all three cases. Once again, the gel formation times determined from the rheology measurements were close to, but slightly higher than, the times calculated from the tube inversion experiments. The randomly cross-linked copolymer networks based on the $DMAAm_{100}$-*co*-$DAAm_{10}$ random copolymer prepared at 10.0, 12.5, and 15.0% w/v required 15-17, 10-13, and 7-9 min,

respectively, to form, while the APCNs prepared at the same concentrations using the DAAm$_6$-*b*-DMAAm$_{50}$-*b*-EG$_{46}$-*b*-DMAAm$_{50}$-*b*-DAAm$_6$ pentablock terpolymer required 14-19, 7, and 3-5 min, respectively, to form. Finally, part (c) shows that the APCNs based on the DAAm$_{16}$-*b*-DMAAm$_{50}$-*b*-EG$_{46}$-*b*-DMAAm$_{50}$-*b*-DAAm$_{16}$ pentablock terpolymer prepared at the same concentrations required 80, 40, and 10 s, respectively, to form, due to the presence of a higher DAAm content in the particular pentablock terpolymer, resulting in faster gelation.

Figures 3.7.7, 3.7.8, and 3.7.9 present the temporal evolution of the two moduli, *G′* and *G″*, during gel formation as followed by rheology. In particular, Figure 3.7.7 presents the rheology graphs for the randomly cross-linked copolymer networks based on the DMAAm$_{100}$-*co*-DAAm$_5$ random copolymer prepared at a total solids concentration of 15.0% w/v (part (a)), and the DMAAm$_{100}$-*co*-DAAm$_{10}$ random copolymer prepared at total solids concentrations of 10.0 (part (b)), 12.5 (part (c)) and 15.0% w/v (part (d)). Figure 3.7.8 presents the same data for the oxime cross-linked APCNs prepared using the DAAm$_6$-*b*-DMAAm$_{50}$-*b*-EG$_{46}$-*b*-DMAAm$_{50}$-*b*-DAAm$_6$ pentablock terpolymer at total solids concentrations of 10.0 (part (a)), 12.5 (part (b)) and 15.0% w/v (part (c)), while Figure 3.7.9 presents the same data for the oxime cross-linked APCNs prepared using the DAAm$_3$-*b*-DMAAm$_{50}$-*b*-EG$_{46}$-*b*-DMAAm$_{50}$-*b*-DAAm$_3$ (part (a)) and DAAm$_{12}$-*b*-DMAAm$_{50}$-*b*-EG$_{46}$-*b*-DMAAm$_{50}$-*b*-DAAm$_{12}$ (part (b)) pentablock terpolymers, both prepared at a total solids concentration of 15.0% w/v.

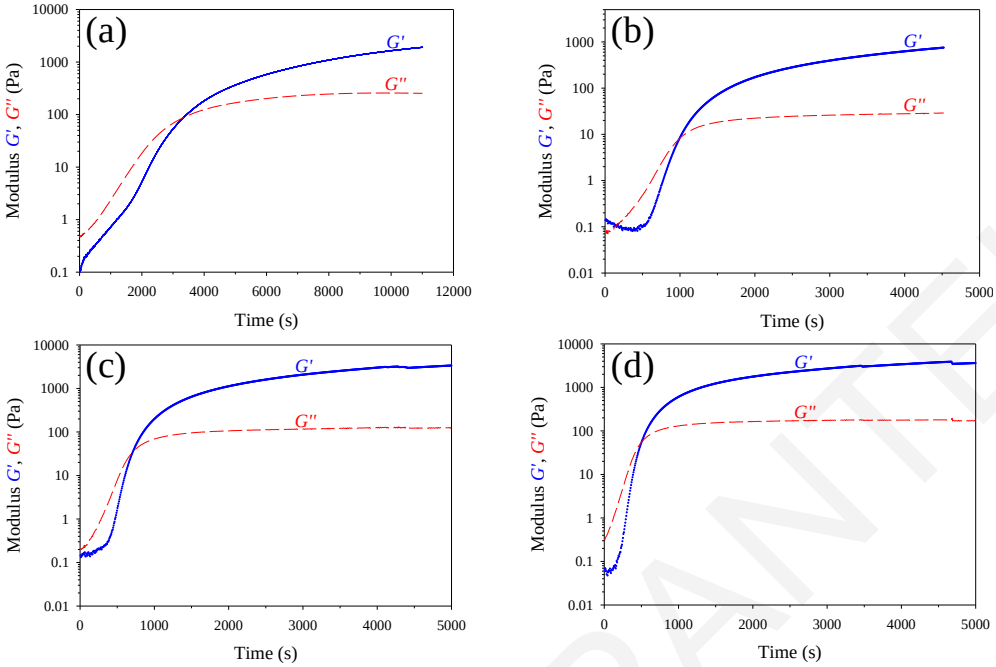

Figure 3.7.7. Evolution of *G′* and *G″* recorded using rheology during the formation of the randomly cross-linked copolymer networks based on PDH and (a) $DMAAm_{100}$-*co*-$DAAm_5$, prepared at the stoichiometric ratio at a total solids concentration of 15% w/v in an aqueous buffer solution of pH 4.5, and (b) $DMAAm_{100}$-*co*-$DAAm_{10}$ cross-linked using PDH and prepared at the stoichiometric ratio at total solids concentrations of (b) 10.0, (c) 12.5, and (d) 15.0% w/v in aqueous buffer solutions of pH 4.5.

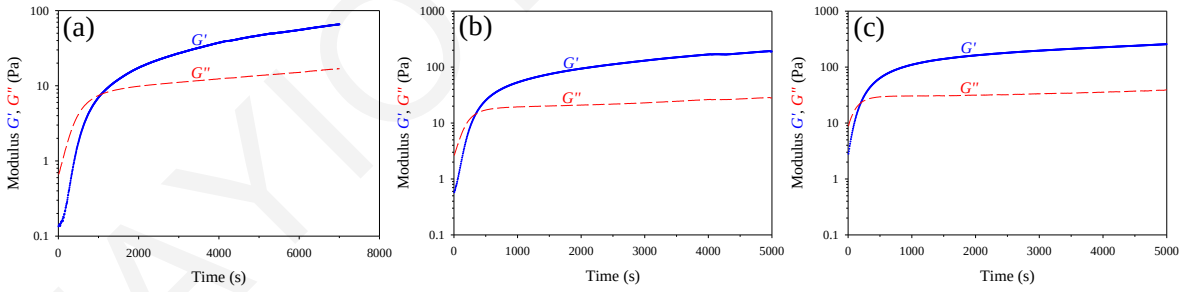

Figure 3.7.8. Evolution of *G′* and *G″* during the formation of the oxime cross-linked APCNs based on $DAAm_6$-*b*-$DMAAm_{50}$-*b*-EG_{46}-*b*-$DMAAm_{50}$-*b*-$DAAm_6$ cross-linked using PDH prepared at total solids concentrations of (a) 10.0, (b) 12.5, and (c) 15.0% w/v at the stoichiometric ratio in aqueous buffer solutions of pH 4.5.

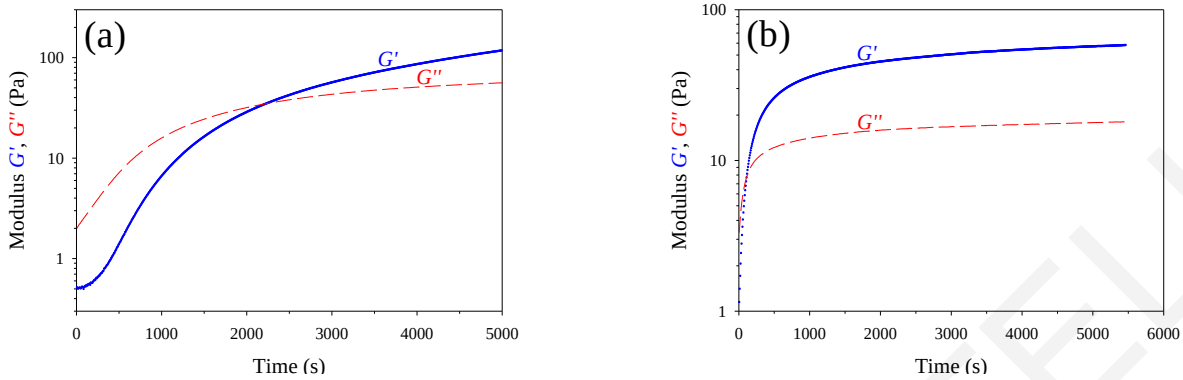

Figure 3.7.9. Evolution of *G′* and *G″* during the formation of the oxime cross-linked APCNs based on (a) the DAAm$_3$-*b*-DMAAm$_{50}$-*b*-EG$_{46}$-*b*-DMAAm$_{50}$-*b*-DAAm$_3$ and (b) the DAAm$_{12}$-*b*-DMAAm$_{50}$-*b*-EG$_{46}$-*b*-DMAAm$_{50}$-*b*-DAAm$_{12}$ pentablock terpolymers cross-linked using PDH and prepared in aqueous buffer solutions of pH 4.5 at the stoichiometric ratio at a total solids concentration of 15.0% w/v.

Finally, the reaction between some selected pentablock terpolymers, those with the highest DAAm content, and PDH was performed in methanol. These reactions were performed at the stoichiometric ratio at a total solids concentration of 15.0% w/v in the presence of 2 eq. of TEA (to PDH cross-linker) for the neutralization (deprotonation) of the aminooxy groups in the PDH cross-linker. It was found that the oxime cross-linked APCNs based on the DAAm$_{12}$-*b*-DMAAm$_{50}$-*b*-EG$_{46}$-*b*-DMAAm$_{50}$-*b*-DAAm$_{12}$, DAAm$_{16}$-*b*-DMAAm$_{50}$-*b*-EG$_{46}$-*b*-DMAAm$_{50}$-*b*-DAAm$_{16}$ and DAAm$_{25}$-*b*-DMAAm$_{50}$-*b*-EG$_{46}$-*b*-DMAAm$_{50}$-*b*-DAAm$_{25}$ pentablock terpolymers required much longer times to form than the corresponding APCNs prepared in aqueous buffer solutions or in an EtOH : aqueous buffer mixture, and, in particular, 150, 120, and 60 min, respectively. These results indicate the formation of the oxime cross-linked APCNs in an organic solvent, but, at the same time, verify that the aqueous media is the most suitable environment for promptly performing this type of reaction.

3.7.7 Investigation of the Dynamic Nature of the Oxime Bonds

For the investigation of the dynamic nature of the oxime bonds, some selected preformed polymer networks were subjected to frequency-dependent oscillatory rheology. The polymer networks were prepared according to the above-mentioned procedure at the stoichiometric ratio at a total solids concentration of 15.0% w/v in aqueous buffer solutions of pH 4.5 or in an EtOH : buffer solution of pH 4.5 at a 1:2 volume ratio, and after their

preparation, they were allowed to mature for three days prior to the measurements. Figures 3.7.10 and 3.7.11 present the rheology profiles obtained from the frequency sweep measurements. In particular, Figure 3.7.10 displays these profiles for the randomly cross-linked copolymer networks based on the $DMAAm_{100}$-*co*-$DAAm_5$ (part (a)) and $DMAAm_{100}$-*co*-$DAAm_{10}$ random copolymers (part (b)), while Figure 3.7.11 presents the same profiles for the oxime cross-linked APCNs prepared using the $DAAm_6$-*b*-$DMAAm_{50}$-*b*-EG_{46}-*b*-$DMAAm_{50}$-*b*-$DAAm_6$ (part (a)) and $DAAm_{25}$-*b*-$DMAAm_{50}$-*b*-EG_{46}-*b*-$DMAAm_{50}$-*b*-$DAAm_{25}$ pentablock terpolymers (part (b)).

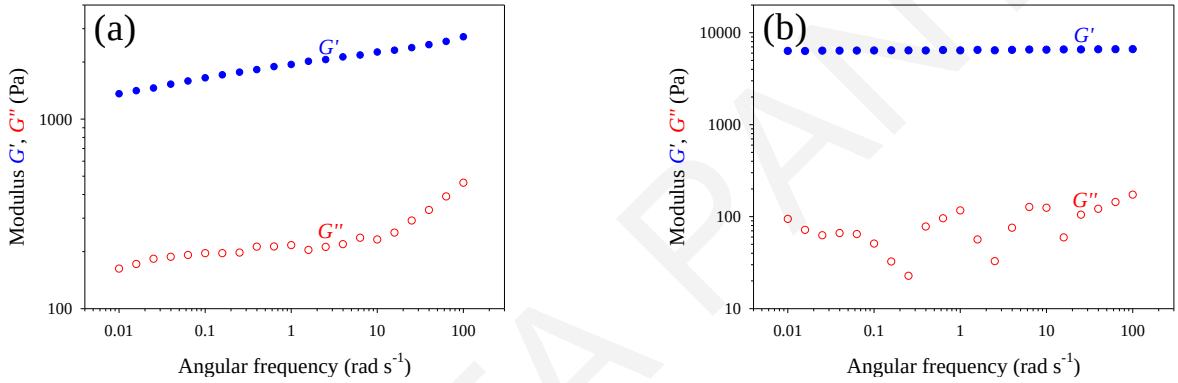

Figure 3.7.10. Dependence of *G′* and *G″* on the angular frequency of the randomly cross-linked copolymer networks cross-linked via oxime bonds formed using PDH and (a) $DMAAm_{100}$-*co*-$DAAm_5$, and (b) $DMAAm_{100}$-*co*-$DAAm_{10}$ prepared at the stoichiometric ratio at a total solids concentration of 15.0% in aqueous buffer solutions of pH 4.5. The experiments were performed at a 10% strain.

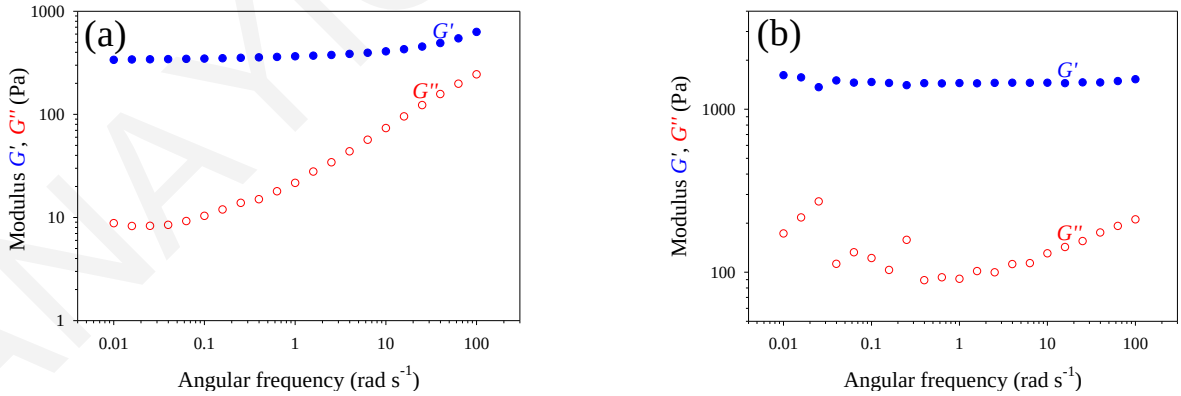

Figure 3.7.11. Dependence of *G′* and *G″* on the angular frequency of the oxime cross-linked APCNs based on (a) the $DAAm_6$-*b*-$DMAAm_{50}$-*b*-EG_{46}-*b*-$DMAAm_{50}$-*b*-$DAAm_6$ and (b) the $DAAm_{25}$-*b*-$DMAAm_{50}$-*b*-EG_{46}-*b*-$DMAAm_{50}$-*b*-$DAAm_{25}$ pentablock terpolymers. The gels were prepared at the stoichiometric ratio at a total solids concentration of 15.0% in an aqueous buffer solution of pH 4.5 and in an EtOH : buffer solution of pH 4.5 at a volume ratio of 1:2, respectively. Both experiments were performed at a 10% strain.

Both figures show that the values of G' were always higher than the values of G'', indicating the successful preformation of the polymer networks in both cases. Increasing the degree of polymerization of the DAAm monomer repeating units in the initial linear precursors resulted in polymer networks with a higher cross-linking density, and, consequently, increased values of G', as evidenced from both figures.

Furthermore, the figures show that the trends in the values of G' and G'' were highly dependent on the cross-linking density of the oxime cross-linked polymer networks. In particular, when the cross-linking density is low, such as in the case of the polymer networks based on the $DMAAm_{100}$-*co*-$DAAm_5$ random copolymer and the $DAAm_6$-*b*-$DMAAm_{50}$-*b*-EG_{46}-*b*-$DMAAm_{50}$-*b*-$DAAm_6$ pentablock terpolymer, the G' values were gradually increased with increasing angular frequency. In addition, in these cases, the G'' values were significantly increased when angular frequency was increased, particularly in the case of the $DAAm_6$-*b*-$DMAAm_{50}$-*b*-EG_{46}-*b*-$DMAAm_{50}$-*b*-$DAAm_6$ pentablock terpolymer. These results indicate that the cross-linking density was very low and the resulting networks possessed both elastic and viscous characteristics. In contrast, when the cross-linking density is higher, such as in the cases of the polymer networks based on the $DMAAm_{100}$-*co*-$DAAm_{10}$ random copolymer and the $DAAm_{25}$-*b*-$DMAAm_{50}$-*b*-EG_{46}-*b*-$DMAAm_{50}$-*b*-$DAAm_{25}$ pentablock terpolymer, the values of G' and G'' over the whole frequency range were almost constant and with very small variations, and always much higher than the values of G''. Thus, these results indicate that the higher degree of polymerization of the DAAm monomer repeating units resulted in the formation of polymer networks with a sufficient cross-linking density, and, consequently, these polymer networks behave much more as elastic solids rather than as viscous fluids. Furthermore, the almost constant values of G'' over the whole frequency range investigated indicate the slow exchange reaction between the oxime bonds, which is slower than 0.01 rad s^{-1} and not detectable from these rheology experiments. Thus, a particular polymer network, the one based on the $DAAm_{25}$-*b*-$DMAAm_{50}$-*b*-EG_{46}-*b*-$DMAAm_{50}$-*b*-$DAAm_{25}$ pentablock terpolymer was subjected to frequency-dependent oscillatory rheology, in which the angular frequency ranged from 0.001 to 100 rad s^{-1}, and the results are presented in Figure 3.7.12.

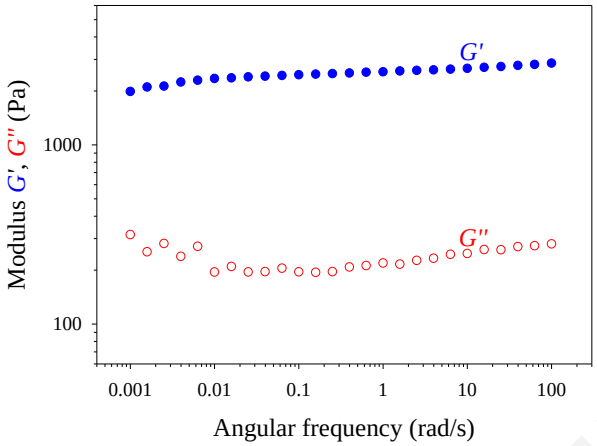

Figure 3.7.12. Dependence of G' and G'' on the angular frequency of the oxime cross-linked APCN prepared from the reaction of the $DAAm_{25}$-*b*-$DMAAm_{50}$-*b*-EG_{46}-*b*-$DMAAm_{50}$-*b*-$DAAm_{25}$ pentablock terpolymer and PDH. The gel was prepared at a total solids concentration of 15.0% at the stoichiometric ratio in an EtOH : buffer solution of pH 4.5 at a volume ratio of 1:2, and it was then equilibrated in an aqueous buffer solution of pH 7.4. The experiment was performed at a 10% strain.

Figure 3.7.12 shows that, once again, G'' exhibited nearly constant values over the whole frequency range used, indicating the very slow exchange reaction between the oxime bonds, which is even slower than 0.001 rad s^{-1}.

3.7.8 Equilibrium Aqueous Degrees of Swelling of the Oxime Cross-linked Polymer Networks

For the determination of the equilibrium aqueous DSs, the thus-prepared oxime cross-linked polymer networks, after their preparation and maturing for three days, were allowed to reach swelling equilibrium in an aqueous buffer solution of pH 7.4. Figure 3.7.13 exhibits the dependence of the equilibrium degrees of swelling on the DAAm content in the linear random copolymers and the pentablock terpolymers.

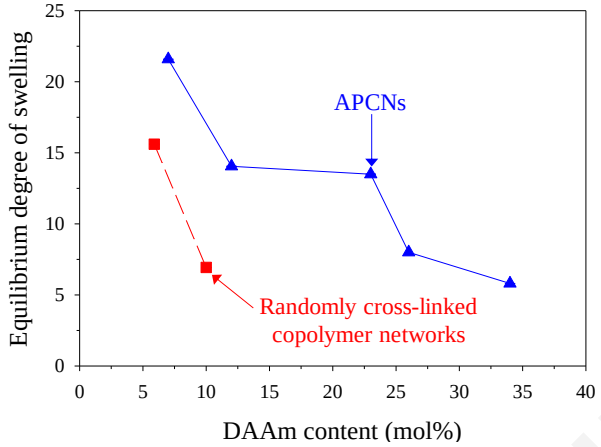

Figure 3.7.13. Effect of the DAAm content in the linear polymer precursors on the equilibrium aqueous degrees of swelling (aqueous buffer solution of pH 7.4) of the oxime cross-linked polymer networks. The gels were initially formed at the stoichiometric ratio at a total solids concentration of 15.0% w/v in an aqueous buffer solution of pH 4.5 or in an EtOH : buffer solution of pH 4.5 mixture at a 1:2 volume ratio.

Figure 3.7.13 shows that the aqueous equilibrium degrees of swelling of the polymer networks prepared using both the random copolymers and the pentablock terpolymers decreased when the DAAm content in the polymer precursors was increased. Thus, increasing the number of the DAAm monomer repeating units in the polymer precursors, and, consequently, the cross-linking density in the final polymer networks results in a tighter gel structure, which, in turn, results in reduced water uptake. In particular, when the DAAm content in the APCN precursor was the lowest, 7.0 mol%, the particular polymer network displayed the highest value of equilibrium DS, ~21.6, whereas when this value was the highest, 34.0 mol%, the particular APCN exhibited the lowest DS value, ~5.8, lower than its preparation DS of ~6.7.

Furthermore, the equilibrium DSs of the randomly cross-linked copolymer networks prepared using the DMAAm$_{100}$-*co*-DAAm$_5$ and DMAAm$_{100}$-*co*-DAAm$_{10}$ random copolymers exhibited lower values than the APCNs based on the pentablock terpolymers and possessing the same DAAm content, *i.e.*, DAAm$_3$-*b*-DMAAm$_{50}$-*b*-EG$_{46}$-*b*-DMAAm$_{50}$-*b*-DAAm$_3$ and DAAm$_6$-*b*-DMAAm$_{50}$-*b*-EG$_{46}$-*b*-DMAAm$_{50}$-*b*-DAAm$_6$. This can be mainly attributed to the random distribution of the DAAm monomer repeating units along the polymer chain, and, consequently, the random distribution of cross-links in the produced polymer networks, resulting in a more tightly cross-linked structure. In contrast, the polymer networks based on the pentablock terpolymers are obtained after the cross-linking

of the linear precursors at their two termini. The implication of this is that the structure of the produced APCNs is less tightly cross-linked, allowing for higher water uptake, and, consequently, higher values of DSs.

3.7.9 Mechanical Properties of the Oxime Cross-linked Polymer Networks

In order to elucidate the effect of cross-linking density (DAAm content) and cross-link distribution in the polymer networks on their mechanical properties, selected polymer networks were characterized using compression experiments. The polymer networks prepared using the linear precursors with the lowest DAAm contents, the $DMAAm_{100}$-*co*-$DAAm_5$ random copolymer and the $DAAm_3$-*b*-$DMAAm_{50}$-*b*-EG_{46}-*b*-$DMAAm_{50}$-*b*-$DAAm_3$ pentablock terpolymer, were not characterized, as their cross-linking density was very low, and they were very soft. In addition, the polymer networks prepared using the $DAAm_{12}$-*b*-$DMAAm_{50}$-*b*-EG_{46}-*b*-$DMAAm_{50}$-*b*-$DAAm_{12}$ and $DAAm_{16}$-*b*-$DMAAm_{50}$-*b*-EG_{46}-*b*-$DMAAm_{50}$-*b*-$DAAm_{16}$ pentablock terpolymers were also not characterized, as these gels formed very quickly, leading to increased inhomogeneity, and, consequently, to a fragile behavior. Thus, only the three remaining oxime cross-linked polymer networks were characterized in terms of their compressive mechanical properties. These were the networks based on the $DMAAm_{100}$-*co*-$DAAm_{10}$ random copolymer, the $DAAm_6$-*b*-$DMAAm_{50}$-*b*-EG_{46}-*b*-$DMAAm_{50}$-*b*-$DAAm_6$ pentablock terpolymer, and the $DAAm_{25}$-*b*-$DMAAm_{50}$-*b*-EG_{46}-*b*-$DMAAm_{50}$-*b*-$DAAm_{25}$ pentablock terpolymer. In the case of the polymer networks based on the $DMAAm_{100}$-*co*-$DAAm_{10}$ random copolymer and the $DAAm_6$-*b*-$DMAAm_{50}$-*b*-EG_{46}-*b*-$DMAAm_{50}$-*b*-$DAAm_6$ pentablock terpolymer, the compression experiments were performed on the as-prepared samples. In contrast, the compression experiments were performed on equilibrium swollen samples in the case of the oxime cross-linked APCN based on the $DAAm_{25}$-*b*-$DMAAm_{50}$-*b*-EG_{46}-*b*-$DMAAm_{50}$-*b*-$DAAm_{25}$ pentablock terpolymer, that was prepared in an EtOH : buffer solution of pH 4.5 mixture at a 1:2 volume ratio and was then equilibrium swollen in a buffer solution of pH 7.4.

Figure 3.7.14 presents the stress-strain curves obtained from the compression experiments for the oxime cross-linked polymer networks prepared from the reaction of PDH and the $DMAAm_{100}$-*co*-$DAAm_{10}$ random copolymer (part (a)), the $DAAm_6$-*b*-$DMAAm_{50}$-*b*-EG_{46}-

b-DMAAm$_{50}$-*b*-DAAm$_{6}$ pentablock terpolymer (part (b)), and the DAAm$_{25}$-*b*-DMAAm$_{50}$-*b*-EG$_{46}$-*b*-DMAAm$_{50}$-*b*-DAAm$_{25}$ pentablock terpolymer (part (c)).

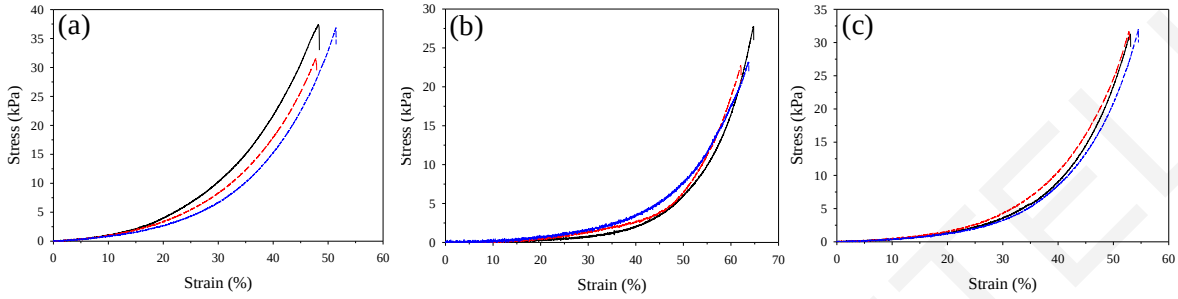

Figure 3.7.14. Compressive stress-strain curves for the oxime cross-linked polymer networks formed from PDH and (a) the DMAAm$_{100}$-*co*-DAAm$_{10}$ random copolymer, (b) the DAAm$_{6}$-*b*-DMAAm$_{50}$-*b*-EG$_{46}$-*b*-DMAAm$_{50}$-*b*-DAAm$_{6}$ pentablock terpolymer (total solids concentration = 15% w/v, aqueous buffer solution of pH 4.5), and (c) the DAAm$_{25}$-*b*-DMAAm$_{50}$-*b*-EG$_{46}$-*b*-DMAAm$_{50}$-*b*-DAAm$_{25}$ pentablock terpolymer (total solids concentration = 15% w/v, EtOH : buffer solution of pH 4.5 mixture of a 1:2 volume ratio and equilibrium swollen in a buffer solution of pH 7.4).

Figure 3.7.14 shows that all the polymer networks exhibited compressive fracture stress values between 25 and 35 kPa, and compressive fracture strain values between 49 and 64%. These low values of fracture stress may be attributed to the fast gelation that occurs during the formation of the oxime cross-linked polymer networks. In particular, these polymer networks can be formed even at low conversions, and, therefore, exhibit a relatively soft nature.

Part (a) shows that the polymer network prepared using the DMAAm$_{100}$-*co*-DAAm$_{10}$ random copolymer exhibited a higher fracture stress value, 35.4 ± 1.8 kPa, compared to the corresponding value of the APCN prepared using the DAAm$_{6}$-*b*-DMAAm$_{50}$-*b*-EG$_{46}$-*b*-DMAAm$_{50}$-*b*-DAAm$_{6}$ pentablock terpolymer, 24.6 ± 1.6 kPa (part (b)). However, the fracture strain value of the gel prepared using the random copolymer was only 49.1 ± 1.1%, whereas the APCN based on the particular pentablock terpolymer exhibited a higher fracture strain of 63.5 ± 0.8%. This difference in the mechanical properties of these materials may be attributed to the distribution of cross-links in the gels; the randomly cross-linked gel exhibits a more tightly cross-linked structure, and, consequently, an increased fracture stress value and a reduced fracture strain value, compared to the other gel. In addition, the APCN prepared using the pentablock terpolymer comprises a PEG middle segment that is highly flexible. As a result, the fracture stress value is lower and the

fracture strain value is higher than the corresponding values of the randomly cross-linked copolymer network.

Part (c) shows that the APCN prepared using the $DAAm_{25}$-*b*-$DMAAm_{50}$-*b*-EG_{46}-*b*-$DMAAm_{50}$-*b*-$DAAm_{25}$ pentablock terpolymer exhibited values of fracture stress of 31.6 ± 0.2 kPa and fracture strain of 53.4 ± 0.5%. The value of the fracture stress was higher than the corresponding value for the APCN prepared using the $DAAm_{6}$-*b*-$DMAAm_{50}$-*b*-EG_{46}-*b*-$DMAAm_{50}$-*b*-$DAAm_{6}$ pentablock terpolymer, while the fracture strain value was lower than the corresponding value of the latter APCN. These differences may be attributed to the increased cross-linking density in the APCN prepared using the pentablock terpolymer possessing a higher DAAm content, *i.e.*, bearing a total of 50 DAAm monomer repeating units, compared to the 12 DAAm monomer repeating units in the other pentablock terpolymer.

Finally, its worth mentioning that the randomly cross-linked copolymer network prepared using the $DMAAm_{100}$-*co*-$DAAm_{10}$ random copolymer displayed a Young's modulus value of 15.3 ± 1.5 kPa, while the APCNs prepared using the $DAAm_{6}$-*b*-$DMAAm_{50}$-*b*-EG_{46}-*b*-$DMAAm_{50}$-*b*-$DAAm_{6}$ and $DAAm_{25}$-*b*-$DMAAm_{50}$-*b*-EG_{46}-*b*-$DMAAm_{50}$-*b*-$DAAm_{25}$ pentablock terpolymers exhibited Young's moduli values of 2.2 ± 0.4 kPa and 6.4 ± 0.6 kPa, respectively. The highest value of the Young's modulus for the gel based on the $DMAAm_{100}$-*co*-$DAAm_{10}$ random copolymer can once again be attributed to its random distribution of cross-links, as a lower number of monomer repeating units is present between the cross-links, resulting in a higher Young's modulus value. In contrast, due to the end-linking of the pentablock terpolymers at their two termini, more monomer repeating units are between the cross-links, leading to a lower Young's modulus value. The APCN prepared using the pentablock terpolymer with the highest DAAm content, 34.0 mol%, exhibited a higher Young's modulus value than the other APCN owing to its higher number of cross-links.

3.7.10 Self-Healing Ability

In order to explore the dynamic nature of the oxime bonds, all polymer networks were evaluated in terms of their self-healing potential. To this end, after their maturing, each of the thus-prepared polymer networks were cut into two pieces and pressed together for 48 hours to induce self-healing. However, it was found that both the randomly cross-linked copolymer networks and the oxime cross-linked APCNs did not exhibit self-healing ability. The self-healing experiments were also performed using polymer networks prepared in methanol, or in the presence of TFA on the gel surfaces. However, once again, none of the polymer networks exhibited any self-healing ability.

Finally, a particular amphiphilic pentablock terpolymer, $DAAm_{16}$-*b*-$DMAAm_{50}$-*b*-EG_{46}-*b*-$DMAAm_{50}$-*b*-$DAAm_{16}$, was reacted with adipic acid dihydrazide that bears two acylhydrazide groups, in aqueous buffer solution of pH 4.5 (total solids concentration = 10% w/v, stoichiometry 1:1), in order to investigate the self-healing ability of the produced acylhydrazone-cross-linked polymer network. As the acylhydrazone bonds are less stable (more dynamic) than the oxime bonds, the resulting polymer network should be self-healable. It was indeed found that, in contrast to the APCNs end-linked using the oxime bonds, this APCN was able to self-heal in less than 24 hours. This last observation confirms the increased stability of the oxime bonds, leading to non-self-healable materials.

3.7.11 Gel-to-Sol Transition

All the oxime cross-linked polymer networks were subjected to hydrolysis in the presence of 3 eq. of TFA relative to the cross-links in the polymer networks. It was found that increasing the DAAm content in the linear random copolymers and pentablock terpolymers, and, therefore, the cross-linking density in the resulting polymer networks, resulted in an increased stability of the gels towards hydrolysis, as the DAAm-rich gels were not transformed into a solution. In particular, the randomly cross-linked copolymer network prepared using the $DMAAm_{100}$-*co*-$DAAm_5$ random copolymer required 5 h to convert into a solution, whereas the corresponding polymer network based on the $DMAAm_{100}$-*co*-$DAAm_{10}$ random copolymer did not convert into a solution even after 30 days. The same behavior was also observed in the case of the oxime cross-linked APCNs,

as only the APCNs containing lower cross-linking densities were able to be converted into solution. In particular, the APCN based on the $DAAm_3$-*b*-$DMAAm_{50}$-*b*-EG_{46}-*b*-$DMAAm_{50}$-*b*-$DAAm_3$ pentablock terpolymer required 7 d to be converted into a solution, while the APCN based on the $DAAm_6$-*b*-$DMAAm_{50}$-*b*-EG_{46}-*b*-$DMAAm_{50}$-*b*-$DAAm_6$ pentablock terpolymer required 11 d. In contrast, the APCNs based on the $DAAm_{12}$-*b*-$DMAAm_{50}$-*b*-EG_{46}-*b*-$DMAAm_{50}$-*b*-$DAAm_{12}$, $DAAm_{16}$-*b*-$DMAAm_{50}$-*b*-EG_{46}-*b*-$DMAAm_{50}$-*b*-$DAAm_{16}$, and $DAAm_{25}$-*b*-$DMAAm_{50}$-*b*-EG_{46}-*b*-$DMAAm_{50}$-*b*-$DAAm_{25}$ pentablock terpolymers were not converted into a solution even after 30 d.

3.7.12 Conclusions

We employed the hydrophobic DAAm monomer, bearing a ketone group in the pendant, and the hydrophilic DMAAm monomer for the synthesis of linear amphiphilic pentablock terpolymers and random copolymers of various compositions using RAFT polymerization. All these linear polymers were used as precursors for the preparation of oxime-cross-linked APCNs, which were formed through the reaction of these linear precursors with the PDH cross-linker that bears two aminooxy groups. In order to verify the formation of the oxime bond, a particular pentablock terpolymer was reacted with a monofunctional aminooxy compound, and the functionalized polymer was characterized using ^{1}H NMR spectroscopy, which indicated the formation of the expected product at a satisfactory yield. Subsequently, the reaction between all linear precursors and PDH was performed in aqueous buffer solutions of pH 4.5 and at the stoichiometric ratio; both of these conditions were found to be the optimum for this reaction. Then, the particular reaction was performed by varying the polymer concentration, in order to elucidate the effect of this parameter on the gel formation time, which was determined from both tube inversion and rheology measurements. Increasing the polymer concentration in the aqueous buffer solution or the DAAm content in the linear precursors resulted in faster gel formation. The gel formation times determined from the rheology measurements were higher than, but close to, the corresponding times determined from the tube inversion experiments. When the reaction was performed in methanol, the oxime cross-linked APCNs required a much longer time to form. The characterization of the obtained oxime cross-linked polymer networks in terms of their equilibrium degrees of swelling indicated reduced values of degrees of swelling upon increasing the DAAm content in the linear precursors. Increasing the DAAm content in the gels resulted in increased values of fracture stress and Young's modulus, but, in reduced values of fracture strain, as indicated from compression experiments. Finally, the frequency-dependent rheology measurements indicated that the oxime bonds exhibited increased stability, as the exchange reaction between the oxime bonds is very slow. Consequently, the polymer networks could not self-heal, even in the presence of TFA, while only the polymer networks containing a low cross-linking density were converted into a solution upon the addition of TFA, and after several days.

3.8 APCNs Based on Heptablock Quaterpolymers of DMAAm, DDAAm, and DAAm Prepared Using RAFT Polymerization and End-linked Using Oxime Bonds

3.8.1 Synthesis of the Pentablock Terpolymers and the Heptablock Quaterpolymers

The pentablock terpolymer precursors and the final heptablock quaterpolymers were prepared in two or three steps, respectively, using RAFT polymerization. Similar to the previous work, the heptablock quaterpolymers were end-linked using oxime bonds, as they comprised polyDAAm segments at their two termini. However, in this case, the heptablock quaterpolymers also consisted of inert hydrophobic polyDDAAm segments, in addition to the reactive hydrophobic polyDAAm segments, the inert hydrophilic polyDMAAm segments and the inert hydrophilic PEG middle segment.

Once again, the total degree of polymerization of the inert hydrophilic DMAAm monomer repeating units was always constant and equal to 100, while the total degree of polymerization of the inert hydrophobic DDAAm monomer repeating units was systematically varied, acquiring values between 12 and 44, and, therefore, covering a range of compositions and molecular weights. In contrast, the total degree of polymerization of the reactive DAAm monomer repeating units in the final heptablock quaterpolymers was almost constant, ranging between 18 and 28, so as to obtain oxime cross-linked APCNs with a constant cross-linking density.

Figure 3.8.1 presents the structures and the procedure followed for the synthesis of the linear amphiphilic ABCBA pentablock terpolymer precursors, the final ABCDCBA heptablock quaterpolymers, and the produced oxime cross-linked APCNs. In the first step, upon the polymerization of DMAAm and the formation of the $DMAAm_{50}$-*b*-EG_{46}-*b*-$DMAAm_{50}$ triblock copolymer, this precursor was used as macro-CTA for the polymerization of DDAAm and the formation of the $DDAAm_x$-*b*-$DMAAm_{50}$-*b*-EG_{46}-*b*-$DMAAm_{50}$-*b*-$DDAAm_x$ pentablock terpolymers. In the next step, after its isolation, the ABCBA pentablock terpolymer was used as macro-CTA for the polymerization of DAAm and the formation of the $DAAm_y$-*b*-$DDAAm_x$-*b*-$DMAAm_{50}$-*b*-EG_{46}-*b*-$DMAAm_{50}$-*b*-$DDAAm_x$-*b*-$DAAm_y$ heptablock quaterpolymers. In total, five pentablock terpolymers, and, consequently, five heptablock quaterpolymers were prepared, in which the total

degree of polymerization of the DDAAm monomer acquired values of 12, 18, 24, 34, and 44, while the total degree of polymerization of the DAAm monomer acquired values of 18, 20, 28, 24, and 28, respectively.

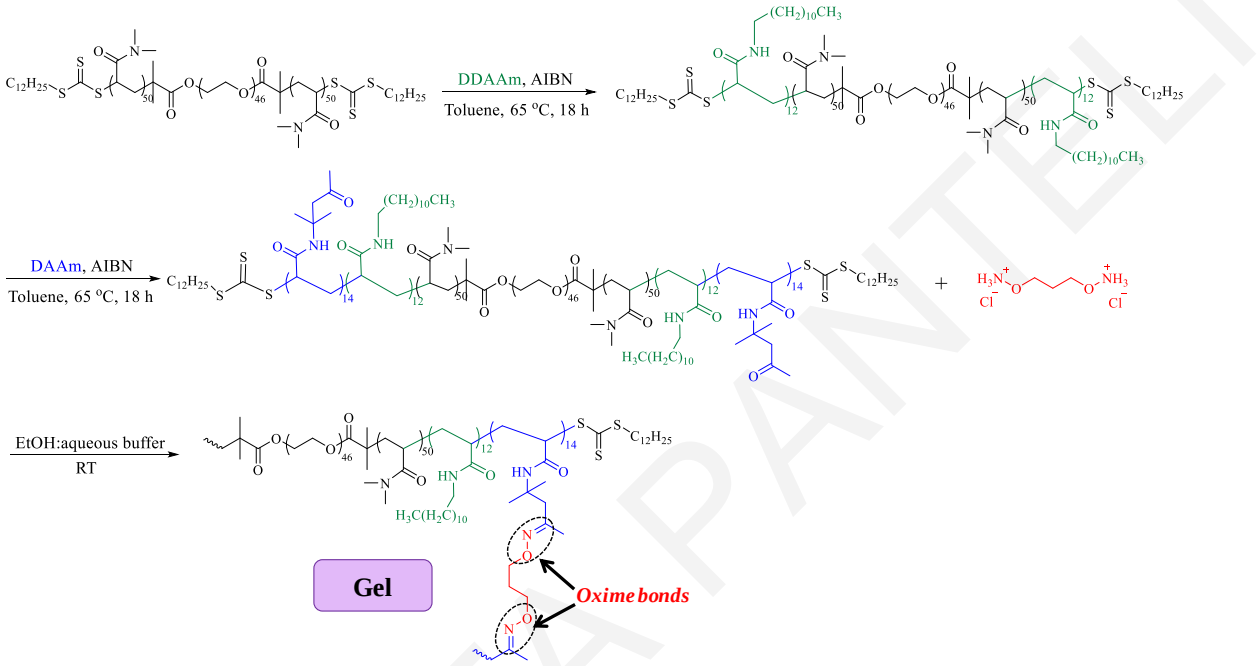

Figure 3.8.1. Procedure followed for the synthesis of the linear amphiphilic ABCBA pentablock terpolymers and the final ABCDCBA heptablock quaterpolymers, which were subsequently used for the preparation of the oxime cross-linked APCNs.

3.8.2 Molecular Weights and Compositions of the Linear Precursors

The synthesized triblock copolymer and pentablock terpolymer precursors, and the final heptablock quaterpolymers, were characterized using GPC and ^{1}H NMR spectroscopy for the determination of their molecular weights and molecular weight distributions, and compositions, respectively. These results and listed in Table 3.8.1, together with the theoretical values of the molecular weight and composition, calculated from ^{1}H NMR spectroscopy and the polymerization feed ratio, respectively. The determination of the theoretical molecular weight of the pentablock terpolymers was accomplished by comparing the area under the peak of the terminal methyl protons (–$(CH_2)_{11}$–CH_3, δ = 0.85 ppm) in the DDAAm monomer repeating units to the area under the peak of the PEG protons (–OCH_2CH_2O–, δ = 3.60-3.75 ppm), while the theoretical molecular weight of the heptablock quaterpolymers was determined by comparing the area under the peak of the

methyl protons next to the ketone group (–(C=O)–CH_3, δ = 2.00 ppm) in the DAAm monomer repeating units to the area under the peak of the PEG protons.

Table 3.8.1. Experimental results of molecular weights and compositions, obtained using GPC and ^{1}H NMR spectroscopy, respectively, and their corresponding theoretically calculated values.

No.	Polymer [a,b]	Theory MW [c] (kg mol^{-1})	GPC Results			DDAAm (mol%)		DAAm (mol%)	
			M_p (kg mol^{-1})	M_n (kg mol^{-1})	$Đ$	Theory[d]	NMR[e]	Theory[d]	NMR[e]
	Triblock Copolymer								
1	DM_{50}-*b*-EG_{46}-*b*-DM_{50}	12.7	14.7	11.2	1.3	0.0	0.0	0.0	0.0
	Pentablock Terpolymers								
2	DD_6-*b*-DM_{50}-*b*-EG_{46}-*b*-DM_{50}-*b*-DD_6	13.8	18.1	12.9	1.5	10.7	10.1	0.0	0.0
3	DD_9-*b*-DM_{50}-*b*-EG_{46}-*b*-DM_{50}-*b*-DD_9	15.3	18.7	13.3	1.6	15.2	14.5	0.0	0.0
4	DD_{12}-*b*-DM_{50}-*b*-EG_{46}-*b*-DM_{50}-*b*-DD_{12}	18.5	22.4	17.8	1.4	19.4	19.5	0.0	0.0
5	DD_{17}-*b*-DM_{50}-*b*-EG_{46}-*b*-DM_{50}-*b*-DD_{17}	19.6	26.1	19.8	1.4	25.4	25.8	0.0	0.0
6	DD_{22}-*b*-DM_{50}-*b*-EG_{46}-*b*-DM_{50}-*b*-DD_{22}	21.7	28.6	20.0	1.5	30.6	30.6	0.0	0.0
	Heptablock Quaterpolymers								
7	DA_9-*b*-DD_6-*b*-DM_{50}-*b*-EG_{46}-*b*-DM_{50}-*b*-DD_6-*b*-DA_9	16.0	18.7	12.4	1.6	9.2	8.5	12.6	14.0
8	DA_{10}-*b*-DD_9-*b*-DM_{50}-*b*-EG_{46}-*b*-DM_{50}-*b*-DD_9-*b*-DA_{10}	16.5	20.5	13.0	1.7	13.1	12.5	13.3	14.0
9	DA_{14}-*b*-DD_{12}-*b*-DM_{50}-*b*-EG_{46}-*b*-DM_{50}-*b*-DD_{12}-*b*-DA_{14}	22.5	26.1	18.0	1.6	15.8	15.9	15.1	18.4
10	DA_{12}-*b*-DD_{17}-*b*-DM_{50}-*b*-EG_{46}-*b*-DM_{50}-*b*-DD_{17}-*b*-DA_{12}	23.9	28.6	19.1	1.6	21.5	22.5	16.0	15.0
11	DA_{14}-*b*-DD_{22}-*b*-DM_{50}-*b*-EG_{46}-*b*-DM_{50}-*b*-DD_{22}-*b*-DA_{14}	24.7	31.3	19.5	1.7	25.6	25.8	17.1	16.2

[a] DA, DD, DM: Further abbreviations for DAAm, DDAAm, and DMAAm, respectively. [b, c, e] Calculated from the ^{1}H NMR spectra. [d] Calculated from the polymerization feed ratio.

The table shows that in most cases the molecular weights (M_n values) obtained using GPC were close to but lower than the corresponding theoretical values. The molecular weight dispersity values for the pentablock terpolymers and the heptablock quaterpolymers were found to range between 1.4 and 1.7, and found to slightly increase as the number of blocks

increased from 5 to 7. Figure 3.8.2 displays the GPC traces for the $DMAAm_{50}$-*b*-EG_{46}-*b*-$DMAAm_{50}$ triblock copolymer precursor and the amphiphilic $DDAAm_x$-*b*-$DMAAm_{50}$-*b*-EG_{46}-*b*-$DMAAm_{50}$-*b*-$DDAAm_x$ pentablock terpolymer precursors (part (a)), and the final $DAAm_y$-*b*-$DDAAm_x$-*b*-$DMAAm_{50}$-*b*-EG_{46}-*b*-$DMAAm_{50}$-*b*-$DDAAm_x$-*b*-$DAAm_y$ heptablock quaterpolymers (part (b)). Both parts of the figure show that when the molecular weight of the polymers was increased, the peak eluted at shorter times, as expected. Furthermore, in both cases, the peaks were monomodal, indicating that both the chain extension of the triblock copolymer precursor with the DDAAm monomer, and the chain extension of the pentablock terpolymers with the DAAm monomer were successful.

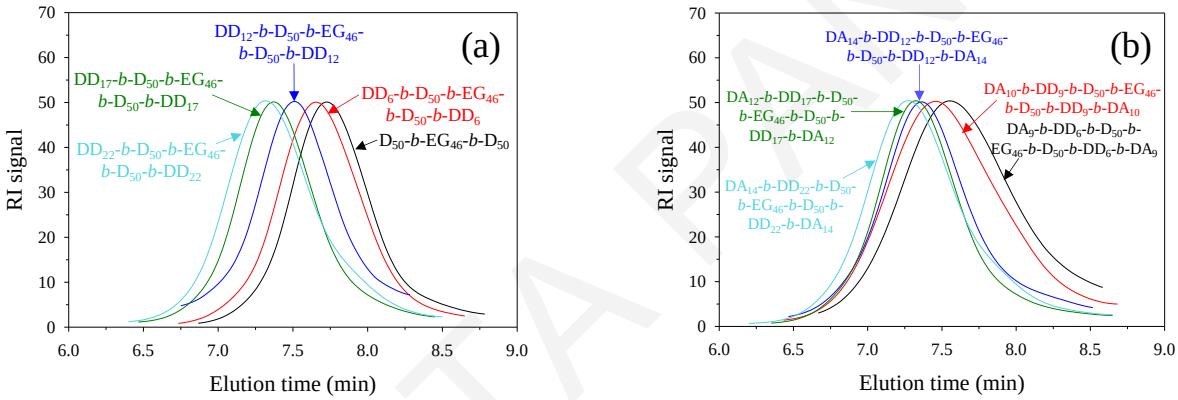

Figure 3.8.2. GPC traces of (a) the $DMAAm_{50}$-*b*-EG_{46}-*b*-$DMAAm_{50}$ triblock copolymer precursor and the $DDAAm_x$-*b*-$DMAAm_{50}$-*b*-EG_{46}-*b*-$DMAAm_{50}$-*b*-$DDAAm_x$ pentablock terpolymers and (b) the final $DAAm_y$-*b*-$DDAAm_x$-*b*-$DMAAm_{50}$-*b*-EG_{46}-*b*-$DMAAm_{50}$-*b*-$DDAAm_x$-*b*-$DAAm_y$ heptablock quaterpolymers.

Figure 3.8.3 presents the ^1H NMR spectra in $CDCl_3$ of the $DMAAm_{50}$-*b*-EG_{46}-*b*-$DMAAm_{50}$ triblock copolymer (part (a)), the $DDAAm_{12}$-*b*-$DMAAm_{50}$-*b*-EG_{46}-*b*-$DMAAm_{50}$-*b*-$DDAAm_{12}$ pentablock terpolymer (part (b)), and the final $DAAm_{14}$-*b*-$DDAAm_{12}$-*b*-$DMAAm_{50}$-*b*-EG_{46}-*b*-$DMAAm_{50}$-*b*-$DDAAm_{12}$-*b*-$DAAm_{14}$ heptablock quaterpolymer (part (c)). In the case of the ABCBA pentablock terpolymers, the theoretical DDAAm content was determined by comparing the area under the peak corresponding to the terminal methyl protons ($-(CH_2)_{11}-CH_3$, δ = 0.85 ppm) in the DDAAm monomer repeating units to the area under the peak corresponding to the methyl protons on the nitrogen atom ($-(C=O)-N(CH_3)_2$, δ = 2.80-3.20 ppm) in the DMAAm monomer repeating units. In the case of the ABCDCBA heptablock quaterpolymers, the theoretical DDAAm content was determined by comparing the area under the corresponding peak of the terminal methyl protons in the DDAAm monomer repeating units to the area under the

peak of the methyl protons next to the ketone group (–(C=O)–CH_3, δ = 2.00 ppm) in the DAAm monomer repeating units, and to the area under the peak of the methyl protons on the nitrogen atom (–(C=O)–N(CH_3)$_2$, δ = 2.80-3.20 ppm) in the DMAAm monomer repeating units. The same calculation was performed for the determination of the DAAm content in the heptablock quaterpolymers.

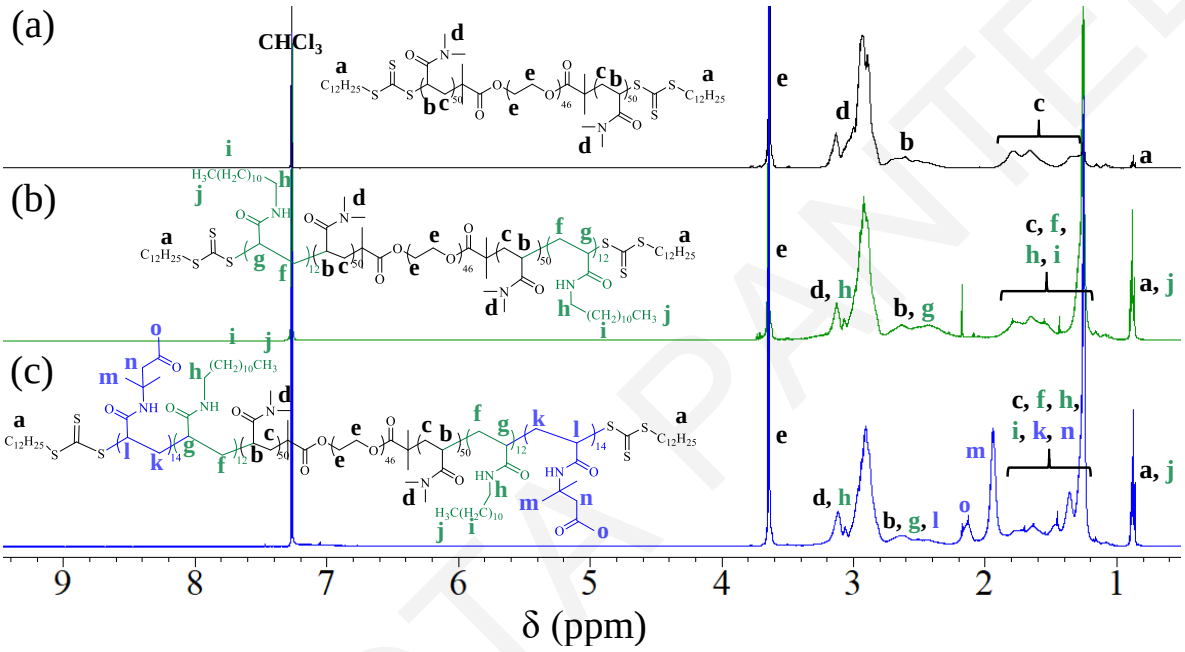

Figure 3.8.3. ^{1}H NMR spectra in $CDCl_3$ of (a) the DMAAm$_{50}$-*b*-EG$_{46}$-*b*-DMAAm$_{50}$ triblock copolymer precursor, (b) the DDAAm$_{12}$-*b*-DMAAm$_{50}$-*b*-EG$_{46}$-*b*-DMAAm$_{50}$-*b*-DDAAm$_{12}$ pentablock terpolymer and (c) the DAAm$_{14}$-*b*-DDAAm$_{12}$-*b*-DMAAm$_{50}$-*b*-EG$_{46}$-*b*-DMAAm$_{50}$-*b*-DDAAm$_{12}$-*b*-DAAm$_{14}$ heptablock quaterpolymer.

The values of the DDAAm content in both the pentablock terpolymer precursors and the final heptablock quaterpolymers determined from the ^{1}H NMR spectra were found to be in good agreement with the corresponding theoretical values calculated from the polymerization feed ratio. In the case of the pentablock terpolymers, the DDAAm content acquired values between 10.1 and 30.6 mol%, while the same values ranged between 8.5 and 25.8 mol% for the heptablock quaterpolymers. In contrast, the experimental values of the DAAm content in the heptablock quaterpolymers were found to be slightly different from the theoretical values calculated from the polymerization feed ratio. However, these values were found to vary between 14.0 and 18.4 mol%, indicating relatively constant values of the DAAm content in the linear heptablock quaterpolymers, and, therefore, constant values of the cross-linking density in the final oxime cross-linked APCNs.

3.8.3 Investigation of the Effect of the Volume Ratio of Ethanol to the Aqueous Buffer Solution in their Mixture on the Gel Formation Time of the Oxime Cross-Linked APCNs

The linear amphiphilic heptablock quaterpolymers are not water-soluble due to the presence of the hydrophobic DDAAm and DAAm monomer repeating units. Therefore, the reactions were performed in mixtures of ethanol and aqueous buffer solution at various volume ratios. Having established in the previous work that the optimum pH value of the aqueous buffer solution is 4.5, and the optimum stoichiometry of the reaction is 1:1, all reactions between the linear precursors and the PDH cross-linker were performed in mixtures of ethanol and aqueous buffer solution of pH 4.5 at the stoichiometric ratio. The reactions between the linear amphiphilic heptablock quaterpolymers and the PDH cross-linker were performed at a total solids concentration of 15% w/v, while the final concentration of the buffer in the mixture of ethanol and aqueous buffer solution was always 200 mM. Figure 3.8.4 plots the dependence of the gel formation time of the oxime cross-linked APCNs based on the $DAAm_{10}$-*b*-$DDAAm_{9}$-*b*-$DMAAm_{50}$-*b*-EG_{46}-*b*-$DMAAm_{50}$-*b*-$DDAAm_{9}$-*b*-$DAAm_{10}$ (part (a)) and $DAAm_{12}$-*b*-$DDAAm_{17}$-*b*-$DMAAm_{50}$-*b*-EG_{46}-*b*-$DMAAm_{50}$-*b*-$DDAAm_{17}$-*b*-$DAAm_{12}$ (part (b)) heptablock quaterpolymers on the volume ratio of the ethanol : aqueous buffer solution. Figure 3.8.5 displays the effect of the DDAAm content in the linear amphiphilic heptablock quaterpolymers on the minimum volume ratio of ethanol to the aqueous buffer solution in their mixture required to maintain polymer solubility.

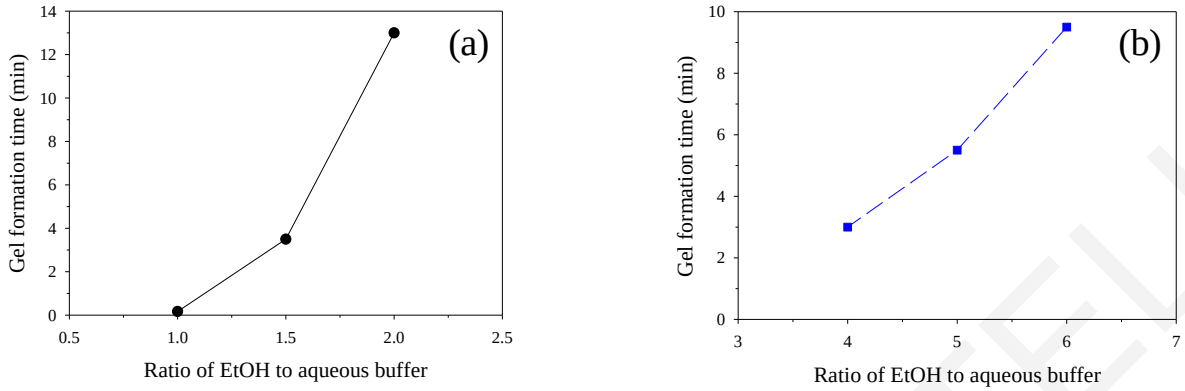

Figure 3.8.4. Effect of the volume ratio of ethanol : aqueous buffer solution mixture on the gel formation time of the oxime cross-linked APCNs based on PDH and the (a) $DAAm_{10}$-*b*-$DDAAm_{9}$-*b*-$DMAAm_{50}$-*b*-EG_{46}-*b*-$DMAAm_{50}$-*b*-$DDAAm_{9}$-*b*-$DAAm_{10}$ and (b) $DAAm_{12}$-*b*-$DDAAm_{17}$-*b*-$DMAAm_{50}$-*b*-EG_{46}-*b*-$DMAAm_{50}$-*b*-$DDAAm_{17}$-*b*-$DAAm_{12}$ heptablock quaterpolymers. The reactions were performed at the stoichiometric ratio at a total solids concentration of 15% w/v in a mixture of EtOH and an aqueous buffer solution of pH 4.5 at a final buffer concentration of 200 mM.

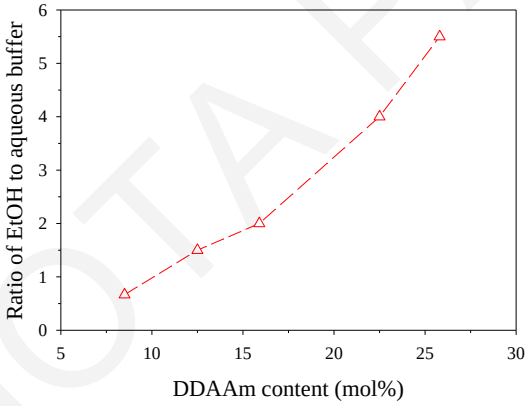

Figure 3.8.5. Dependence of the minimum volume ratio of ethanol to the aqueous buffer solution in their mixture on the DDAAm content in the linear amphiphilic heptablock quaterpolymers required for complete polymer solubility. The reactions were performed at the stoichiometric ratio at a total solids concentration of 15% w/v in an EtOH : aqueous buffer solution of pH 4.5 at a final buffer concentration of 200 mM.

Both parts of Figure 3.8.4 show that the volume ratio of ethanol to the aqueous buffer solution in their mixture had a significant impact on the gel formation time of the oxime cross-linked APCNs. Increasing the relative volume of ethanol in the mixture resulted in increased gel formation times, and this was the case for all the linear amphiphilic heptablock quaterpolymers. This is expected, as a higher relative volume of ethanol in the mixture is accompanied by a lower relative volume of water, which is known to favor the formation of the oxime bond.

On the other hand, the ethanol : aqueous buffer volume ratio could not be reduced, arbitrarily as this would cause polymer insolubility. In particular, a minimum volume fraction of ethanol was required in the mixture to keep the polymer in solution. This fraction expectedly increased as the DDAAm content increased. This dependence was experimentally determined, and the results are plotted in Figure 3.8.5.

3.8.4 Investigation of the Dependence of the Gel Formation Time on the Composition of the Oxime Cross-Linked APCNs

In order to investigate the effect of the composition of the oxime cross-linked APCNs on their formation time, all linear amphiphilic heptablock quaterpolymers were reacted with the PDH cross-linker in mixtures of ethanol and aqueous buffer solution of pH 4.5 at the minimum possible volume ratio. All reactions were performed at the stoichiometric ratio and at total solids concentrations of 12.5, 15.0, and 20.0% w/v. Figure 3.8.6 plots the effect of the DDAAm content (part (a)) and DAAm content (part (b)) in the linear amphiphilic heptablock quaterpolymers on the gel formation time of the obtained oxime cross-linked APCNs.

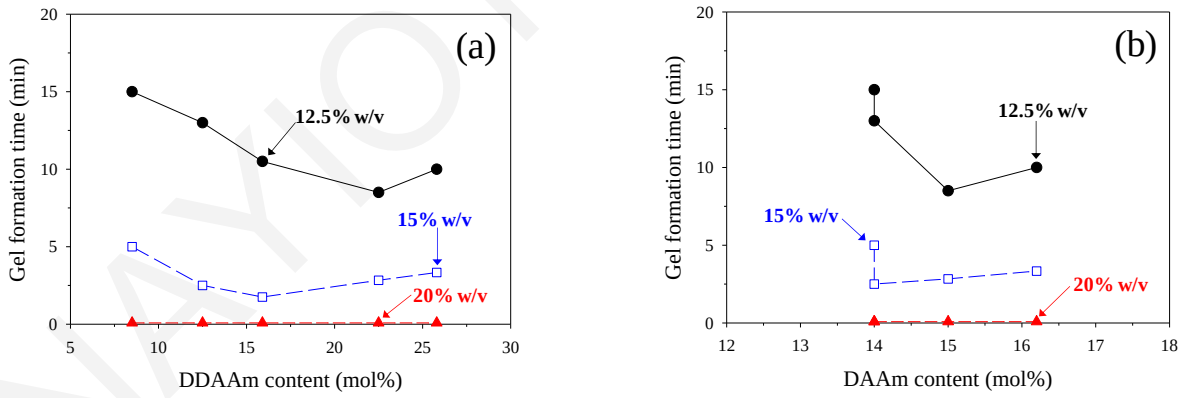

Figure 3.8.6. Effect of (a) DDAAm content and (b) DAAm content in the heptablock quaterpolymers on the gel formation time of the oxime cross-linked APCNs. The reactions were performed at the stoichiometric ratio in a solvent mixture containing the minimum volume fraction of ethanol (to ascertain polymer solubility; different for each polymer) and an aqueous buffer solution of pH 4.5 at a final buffer concentration in the mixture of 200 mM.

Both parts of Figure 3.8.6 show that the gel formation time was independent of the DDAAm and DAAm contents when the total solids concentration was the highest, 20.0% w/v, as it remained constant at 5 s for all APCNs. On the other hand, a more complex dependence of the gel formation time on the DDAAm and DAAm contents was observed

at lower total solids concentrations, 12.5 and 15.0% w/v. The expected trend was a reduction in the gel formation times with both the DDAAm and DAAm contents, which was clearly observed in the lower DDAAm content range, from 7 to 16 mol%.

3.8.5 Investigation of the Effect of Total Solids Concentration on the Gel Formation Time of the Oxime Cross-Linked APCNs

Subsequently, in order to elucidate the dependence of the gel formation time on total solids concentration, each polymer precursor was reacted with the PDH cross-linker in the EtOH : aqueous buffer solution mixtures at three total solids concentrations, 12.5, 15.0, and 20.0% w/v. Figure 3.8.7 presents the effect of total solids concentration on the gel formation time for each oxime cross-linked APCN.

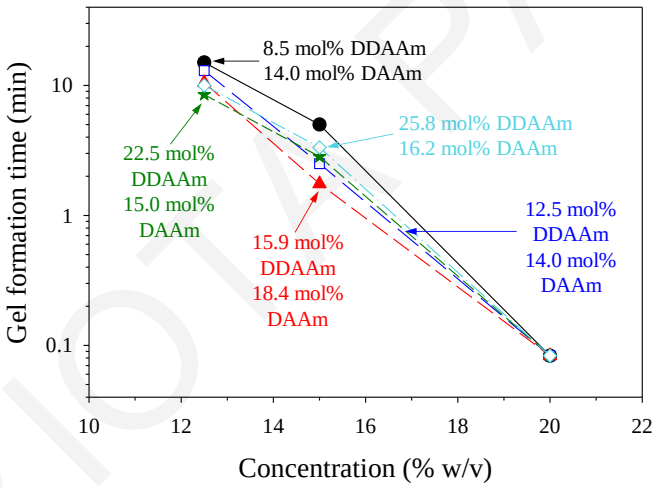

Figure 3.8.7. Effect of total solids concentration on the gel formation time of the oxime cross-linked APCNs. The reactions were performed at the stoichiometric ratio in mixtures of EtOH and aqueous buffer solution of pH 4.5 at a final buffer concentration in the mixtures of 200 mM.

Figure 3.8.7 shows than for all the oxime cross-linked APCNs, the gel formation time decreased linearly in the semi-logarithmic plot (equivalent to an exponential decrease in the linear plot) with increasing total solids concentration, as expected. However, the gel formation times for the oxime cross-linked APCNs at each total solids concentration were not always identical, and, particularly, at the lowest concentrations, due to the slightly different DAAm content values in the linear amphiphilic heptablock quaterpolymers which are not constant.

According to the Flory-Stockmayer equation, the gel point conversion values for the oxime cross-linked APCNs are similar, as they range between 0.19 and 0.23, and, consequently, the gel formation times are also expected to be close to each other. This is indeed proved experimentally but only at the highest total solids concentration, 20.0% w/v, and for some oxime-cross-linked APCNs prepared at the lowest total solids concentrations (12.5 and 15.0% w/v).

It is worth mentioning that when the total solids concentration was lower, 10.0% w/v, gel formation was not observed at all, even in the case of the linear amphiphilic heptablock quaterpolymer with the highest DAAm content, 18.4 mol%. Increasing the polymer concentration also led to increased viscosity of the final polymer solution. Thus, a total solids concentration higher than 20.0% w/v was not pursued.

3.8.6 Investigation of the Effect of the Addition of Aniline as Catalyst on the Gel Formation Time of the Oxime Cross-linked APCNs Prepared in Organic Solvents

The formation of the oxime cross-linked APCNs was also investigated in organic solvents, by performing the reactions of the linear polymer precursors and the PDH cross-linker in methanol or DMF in the presence of two equivalents of TEA to neutralize the aminooxy groups in the PDH cross-linker. Furthermore, the reactions in DMF were also performed in the presence of 10% v/v aniline, in order to evaluate the impact of aniline on the gel formation time. It is worth mentioning that when the reactions were performed in methanol in the presence of aniline, the gel formation times were slightly reduced in comparison with those obtained in methanol without aniline, and, therefore, these reactions were performed in the absence of aniline.

When the reactions were performed in MeOH in the presence of TEA, it was found that the formation of the APCNs was faster with increasing the DDAAm content in the linear heptablock quaterpolymers. However, in contrast to the reactions performed in an EtOH : aqueous buffer solution mixture which always led to the formation of APCNs, the linear amphiphilic heptablock quaterpolymers with the lowest DDAAm contents, 8.5 and 12.5 mol%, upon their reaction with the PDH cross-linker, did not form a polymer network. The oxime cross-linked APCNs prepared with PDH and the $DAAm_{14}$-*b*-$DDAAm_{12}$-*b*-

$DMAAm_{50}$-*b*-EG_{46}-*b*-$DMAAm_{50}$-*b*-$DDAAm_{12}$-*b*-$DAAm_{14}$, $DAAm_{12}$-*b*-$DDAAm_{17}$-*b*-$DMAAm_{50}$-*b*-EG_{46}-*b*-$DMAAm_{50}$-*b*-$DDAAm_{17}$-*b*-$DAAm_{12}$, and $DAAm_{14}$-*b*-$DDAAm_{22}$-*b*-$DMAAm_{50}$-*b*-EG_{46}-*b*-$DMAAm_{50}$-*b*-$DDAAm_{22}$-*b*-$DAAm_{14}$ heptablock quaterpolymers required 28, 15, and 13 min, respectively, to form, which are times longer than those required for the formation of the corresponding APCNs prepared in the mixtures of EtOH and the aqueous buffer solution.

On the other hand, none of the oxime cross-linked APCNs was formed when the reactions were performed in DMF in the presence of TEA. In contrast, when the reactions were performed in the presence of aniline, only the heptablock quaterpolymers with low DDAAm contents (8.5 and 12.5 mol%) did not form a polymer network, as was the case for the reactions performed in MeOH. Once again, the oxime cross-linked APCNs were formed faster when the DDAAm content in the linear precursors was increased. In particular, the oxime cross-linked APCNs based on PDH and the $DAAm_{14}$-*b*-$DDAAm_{12}$-*b*-$DMAAm_{50}$-*b*-EG_{46}-*b*-$DMAAm_{50}$-*b*-$DDAAm_{12}$-*b*-$DAAm_{14}$, $DAAm_{12}$-*b*-$DDAAm_{17}$-*b*-$DMAAm_{50}$-*b*-EG_{46}-*b*-$DMAAm_{50}$-*b*-$DDAAm_{17}$-*b*-$DAAm_{12}$, and $DAAm_{14}$-*b*-$DDAAm_{22}$-*b*-$DMAAm_{50}$-*b*-EG_{46}-*b*-$DMAAm_{50}$-*b*-$DDAAm_{22}$-*b*-$DAAm_{14}$ heptablock quaterpolymers required 80, 30 and 20 min, respectively, to form.

3.8.7 Investigation of the Dynamic Nature of the Oxime Bonds

The dynamic nature of the oxime bonds was evaluated by subjecting the oxime cross-linked APCNs to frequency-dependent oscillatory rheology. To this end, after their preparation in an EtOH : aqueous buffer solution mixture, the polymer networks were allowed to mature for three days and to reach swelling equilibrium in water, and they were subsequently compressed at a 10% strain. Figure 3.8.8 presents the rheology graphs obtained from the frequency sweep measurements on the oxime cross-linked APCNs based on PDH and the $DAAm_{14}$-*b*-$DDAAm_{12}$-*b*-$DMAAm_{50}$-*b*-EG_{46}-*b*-$DMAAm_{50}$-*b*-$DDAAm_{12}$-*b*-$DAAm_{14}$ (part (a)), $DAAm_{12}$-*b*-$DDAAm_{17}$-*b*-$DMAAm_{50}$-*b*-EG_{46}-*b*-$DMAAm_{50}$-*b*-$DDAAm_{17}$-*b*-$DAAm_{12}$ (part (b)), and $DAAm_{14}$-*b*-$DDAAm_{22}$-*b*-$DMAAm_{50}$-*b*-EG_{46}-*b*-$DMAAm_{50}$-*b*-$DDAAm_{22}$-*b*-$DAAm_{14}$ (part (c)) heptablock quaterpolymers.

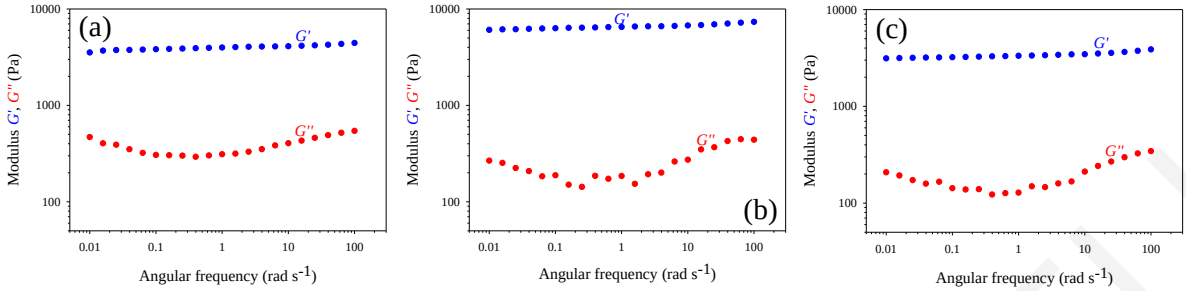

Figure 3.8.8. Dependence of G' and G'' on the angular frequency of the oxime cross-linked APCNs based on PDH and (a) the DAAm$_{14}$-*b*-DDAAm$_{12}$-*b*-DMAAm$_{50}$-*b*-EG$_{46}$-*b*-DMAAm$_{50}$-*b*-DDAAm$_{12}$-*b*-DAAm$_{14}$, (b) the DAAm$_{12}$-*b*-DDAAm$_{17}$-*b*-DMAAm$_{50}$-*b*-EG$_{46}$-*b*-DMAAm$_{50}$-*b*-DDAAm$_{17}$-*b*-DAAm$_{12}$, and (c) the DAAm$_{14}$-*b*-DDAAm$_{22}$-*b*-DMAAm$_{50}$-*b*-EG$_{46}$-*b*-DMAAm$_{50}$-*b*-DDAAm$_{22}$-*b*-DAAm$_{14}$ heptablock quaterpolymers, prepared at the stoichiometric ratio at a total solids concentration of 15% in EtOH : aqueous buffer solution of pH 4.5 mixtures of different volume ratios. The measurements were performed at a 10% strain.

The figure shows that in all cases the values of the elastic modulus, G', were much higher than the values of the loss modulus, G'', indicating the successful formation of the oxime cross-linked APCNs. In addition, the values of G' were found to be nearly constant over the whole frequency range investigated, indicating the formation of elastic materials with solid characteristics. Due to the similar degrees of polymerization of the DAAm monomer repeating units in the three linear amphiphilic heptablock quaterpolymers, the final oxime cross-linked APCNs possessed similar cross-linking densities (and similar values of equilibrium aqueous degrees of swelling), and, consequently, similar values of G' and G''. Once again, the almost frequency-independent values of G'' indicate that the exchange reaction between the oxime bonds is very slow and not detectable from rheology.

3.8.8 Degrees of Swelling of the Oxime Cross-Linked APCNs in Water and Organic Solvents

The equilibrium DSs were determined by allowing the thus-prepared oxime cross-linked APCNs to reach swelling equilibrium in water, EtOH, THF, $CHCl_3$, and toluene. The results are plotted in Figure 3.8.9, as a function of the DDAAm content in the linear amphiphilic heptablock quaterpolymers.

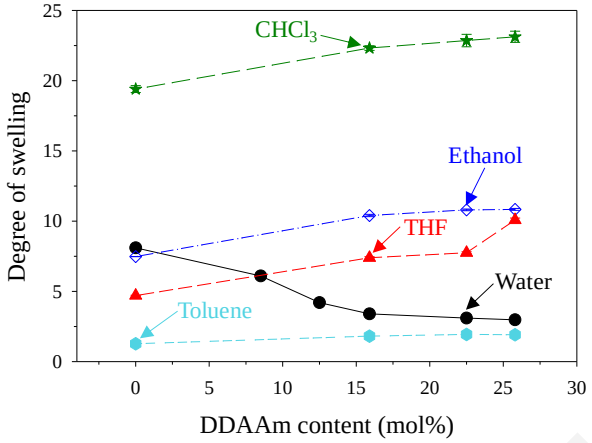

Figure 3.8.9. Effect of the DDAAm content on the equilibrium degrees of swelling of the prepared oxime cross-linked APCNs. The polymer networks were formed in mixtures of EtOH and aqueous buffer solution of pH 4.5 of different volume ratios.

Figure 3.8.9 shows that the aqueous equilibrium DSs decreased with increasing the DDAAm content in the linear precursors, in contrast to the corresponding values in the organic solvents, which increased with the DDAAm content. Increasing the DDAAm content in the linear amphiphilic heptablock quaterpolymer precursors resulted in a decrease in the values of the equilibrium aqueous DSs, as a higher DDAAm content leads to increased hydrophobicity of the linear precursors, and, consequently, the final oxime cross-linked APCNs exhibit a reduced water uptake capability.

On the other hand, the equilibrium DSs in the organic solvents were dependent on the selectivity of each solvent for this system. In particular, the equilibrium DSs of the polymer networks swollen in $CHCl_3$ exhibited the highest values and increased with increasing the DDAAm content, as this solvent is non-selective and compatible with all three monomers and their homopolymers, and, therefore, their block copolymers. In contrast, the oxime cross-linked APCNs swollen in toluene exhibited the lowest values of equilibrium DSs, as toluene is a compatible solvent for all constituents, but is most suitable for the hydrophobic DDAAm and DAAm monomer repeating units. Finally, the equilibrium DSs of the oxime cross-linked APCNs swollen in THF and EtOH exhibited intermediate values.

3.8.9 Mechanical Properties of the Water-Swollen Polymer Networks

3.8.9.1 Stress-Strain Curves

Figure 3.8.10 displays the three repetitions of the stress-strain curves obtained from the compression experiments performed on the equilibrium water-swollen oxime cross-linked APCNs. In particular, the figure presents the stress-strain curves for the APCNs prepared from the reaction of the PDH cross-linker and the $DAAm_{16}$-*b*-$DMAAm_{50}$-*b*-EG_{46}-*b*-$DMAAm_{50}$-*b*-$DAAm_{16}$ pentablock terpolymer (part (a)), the $DAAm_{14}$-*b*-$DDAAm_{12}$-*b*-$DMAAm_{50}$-*b*-EG_{46}-*b*-$DMAAm_{50}$-*b*-$DDAAm_{12}$-*b*-$DAAm_{14}$ heptablock quaterpolymer (part (b)), the $DAAm_{12}$-*b*-$DDAAm_{17}$-*b*-$DMAAm_{50}$-*b*-EG_{46}-*b*-$DMAAm_{50}$-*b*-$DDAAm_{17}$-*b*-$DAAm_{12}$ heptablock quaterpolymer (part (c)), and the $DAAm_{14}$-*b*-$DDAAm_{22}$-*b*-$DMAAm_{50}$-*b*-EG_{46}-*b*-$DMAAm_{50}$-*b*-$DDAAm_{22}$-*b*-$DAAm_{14}$ heptablock quaterpolymer (part (d)). It is worth mentioning that the water-swollen oxime cross-linked APCNs prepared in an EtOH : aqueous buffer solution mixture exhibited a soft nature, and, therefore, the polymer networks were prepared in DMF in the presence of aniline. In particular, the APCNs were prepared at the stoichiometric ratio at a total solids concentration of 20.0% w/v in the presence of 10.0% v/v aniline, and, after their maturing, they were allowed to reach swelling equilibrium in water.

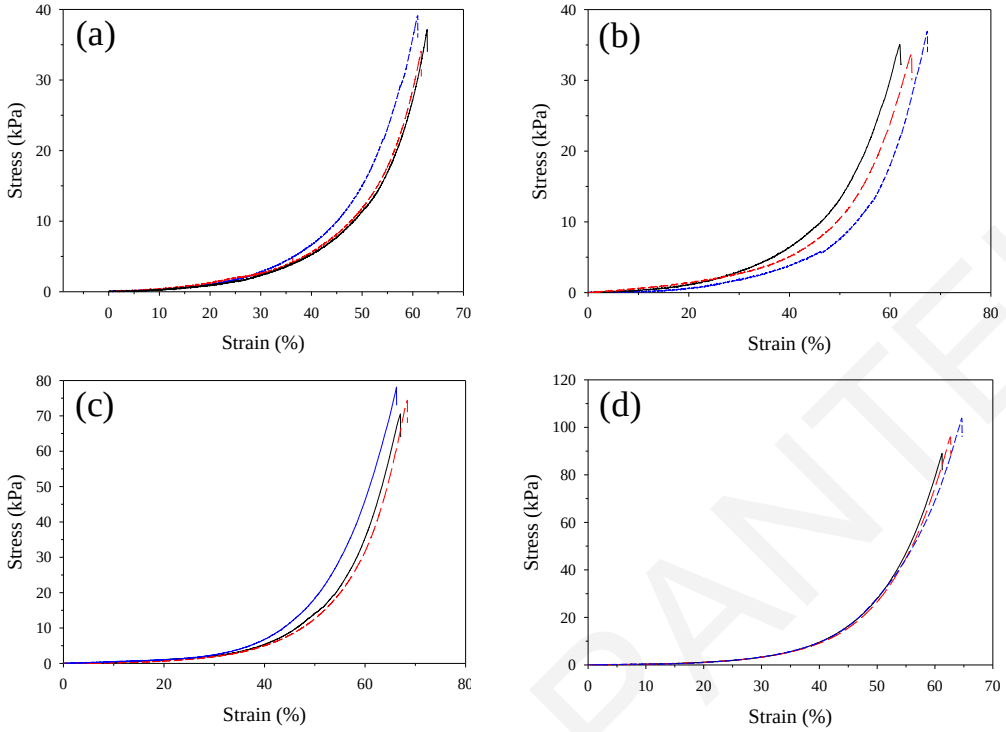

Figure 3.8.10. Compressive stress-strain curves for the oxime cross-linked APCNs formed using PDH and (a) the $DAAm_{16}$-*b*-$DMAAm_{50}$-*b*-EG_{46}-*b*-$DMAAm_{50}$-*b*-$DAAm_{16}$ pentablock terpolymer, (b) the $DAAm_{14}$-*b*-$DDAAm_{12}$-*b*-$DMAAm_{50}$-*b*-EG_{46}-*b*-$DMAAm_{50}$-*b*-$DDAAm_{12}$-*b*-$DAAm_{14}$, (c) the $DAAm_{12}$-*b*-$DDAAm_{17}$-*b*-$DMAAm_{50}$-*b*-EG_{46}-*b*-$DMAAm_{50}$-*b*-$DDAAm_{17}$-*b*-$DAAm_{12}$, and (d) the $DAAm_{14}$-*b*-$DDAAm_{22}$-*b*-$DMAAm_{50}$-*b*-EG_{46}-*b*-$DMAAm_{50}$-*b*-$DDAAm_{22}$-*b*-$DAAm_{14}$ heptablock quaterpolymers. The APCNs were prepared at the stoichiometric ratio at a total solids concentration of 20.0% w/v in DMF in the presence of 10.0% v/v aniline, and then swollen in water.

3.8.9.2 Fracture Stress and Fracture Strain

Figure 3.8.11 plots the effect of the DDAAm content in the linear amphiphilic heptablock quaterpolymers on the fracture stress values (part (a)) and the fracture strain values (part (b)) of the water-swollen oxime cross-linked APCNs. The oxime cross-linked APCN containing the highest DDAAm content, 25.8 mol%, exhibited the highest value of fracture stress, 96 kPa, whereas the lowest fracture stress value of 35 kPa was presented by the oxime cross-linked APCN consisting of 15.9 mol% DDAAm.

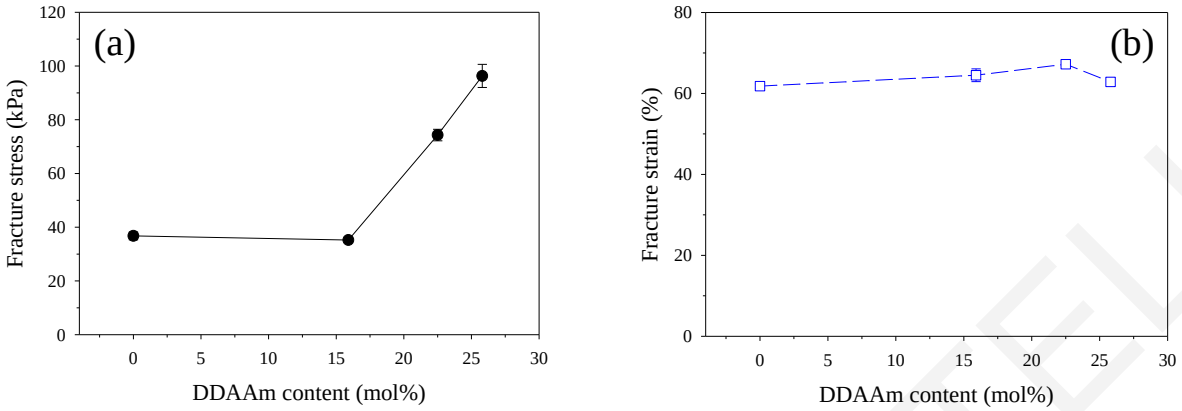

Figure 3.8.11. Dependence of (a) the fracture stress and (b) the fracture strain on the DDAAm content in the oxime cross-linked APCNs.

Part (a) of the figure shows that increasing the DDAAm content in the linear amphiphilic heptablock quaterpolymers resulted in an increase in the fracture stress values. The oxime cross-linked APCNs based on the heptablock quaterpolymers possessed higher fracture stress values than the oxime cross-linked APCN prepared from the reaction of the PDH cross-linker and the $DAAm_{16}$-*b*-$DMAAm_{50}$-*b*-EG_{46}-*b*-$DMAAm_{50}$-*b*-$DAAm_{16}$ pentablock terpolymer precursor due to the extra presence of hydrophobic DDAAm monomer repeating units in the former type of APCNs. As explained before, the presence of the DDAAm hydrophobic units results in associations and internal organization in the networks, enhancing their mechanical strength. However, similarly to the previous work, the fracture stress values are relatively low for all APCNs, possibly due to the low critical conversion required to achieve gelation and form the oxime cross-linked APCNs.

On the other hand, part (b) of the figure shows that the fracture strain values were relatively constant and independent of the DDAAm content in the linear amphiphilic heptablock quaterpolymers, as they ranged between 62 and 67%.

Finally, its worth mentioning that the APCNs prepared using the $DAAm_{16}$-*b*-$DMAAm_{50}$-*b*-EG_{46}-*b*-$DMAAm_{50}$-*b*-$DAAm_{16}$ pentablock terpolymer, the $DAAm_{14}$-*b*-$DDAAm_{12}$-*b*-$DMAAm_{50}$-*b*-EG_{46}-*b*-$DMAAm_{50}$-*b*-$DDAAm_{12}$-*b*-$DAAm_{14}$, $DAAm_{12}$-*b*-$DDAAm_{17}$-*b*-$DMAAm_{50}$-*b*-EG_{46}-*b*-$DMAAm_{50}$-*b*-$DDAAm_{17}$-*b*-$DAAm_{12}$, and $DAAm_{14}$-*b*-$DDAAm_{22}$-*b*-$DMAAm_{50}$-*b*-EG_{46}-*b*-$DMAAm_{50}$-*b*-$DDAAm_{22}$-*b*-$DAAm_{14}$ heptablock quaterpolymers exhibited Young's moduli values of 4.9 ± 0.5 kPa, 4.5 ± 1.6 kPa, 4.4 ± 0.8 kPa, and 3.8 ± 0.7 kPa, respectively. These values are relatively low, similar to those of the APCNs based

on the pentablock terpolymers of the previous work. These values were found to decrease upon increasing the DDAAm content in the linear polymer precursors, implying that the total number of monomer repeating units between cross-links in the resulting gels is more important than the hydrophobe content that was expected to have the opposite effect on the Young's moduli values.

3.8.10 Conclusions

We have reported the synthesis of linear amphiphilic heptablock quaterpolymers of various compositions consisting of the hydrophilic polyDMAAm and PEG segments, and the hydrophobic polyDDAAm and polyDAAm segments. The linear ABCBA pentablock terpolymer precursors and the ABCDCBA heptablock quaterpolymers were characterized in terms of their molecular weights and compositions. It was found that the experimental values of the molecular weight and composition exhibited similar values to the expected ones. It was also found that the molecular weight dispersity increased with the increase in the number of blocks. Then, these linear amphiphilic precursors were end-linked through oxime bonds *via* their reaction with the PDH cross-linker in order to obtain the APCNs. These reactions were performed in mixtures of EtOH and aqueous buffer solution of pH 4.5 of varying volume ratios and at varying total solids concentrations, or in methanol and DMF, in the presence or absence of aniline. It was found that the oxime cross-linked APCNs were formed much faster in the mixtures of EtOH and aqueous buffer solution, while the gel formation time was reduced when the total solids concentration was increased. When the reaction solvent was DMF, the oxime cross-linked APCNs were not formed; however, when aniline was added into the reaction mixture, the polymer networks with the highest DDAAm contents were formed within 30 min. Subsequently, the oxime cross-linked APCNs were characterized in terms of their equilibrium degrees of swelling in water and organic solvents and of their mechanical properties in water. Increasing the DDAAm content in the gels resulted in a decrease in the equilibrium aqueous degrees of swelling and an increase in the values of the equilibrium degrees of swelling in the organic solvents. Finally, the compression experiments performed on the water-swollen oxime cross-linked APCNs indicated an increase in the fracture stress values and a decrease in the Young's moduli values with increasing the DDAAm content, and nearly constant fracture strain values, independent of the DDAAm content.

3.9 References

1. Gong, J. P.; Katsuyama, Y.; Kurokawa, T.; Osada, Y. Double-network hydrogels with extremely high mechanical strength. *Adv. Mater.* **2003**, *15*, 1155-1158.
2. Nakajima, T.; Furukawa, H.; Tanaka, Y.; Kurokawa, T.; Osada, Y.; Gong, J. P. True chemical structure of double-network hydrogels. *Macromolecules* **2009**, *42*, 2184-2189.
3. Shams Es-haghi, S.; Leonov, A. I.; Weiss, R. A. Deconstructing the double-network hydrogels: The importance of grafted chains for achieving toughness. *Macromolecules* **2014**, *47*, 4769-4777.
4. Shestakova, P.; Willem, R.; Vassileva, E. Elucidation of the chemical and morphological structure of double-network (DN) hydrogels by high-resolution magic angle spinning (HRMAS) NMR spectroscopy. *Chem. Eur. J.* **2011**, *17*, 14867-14877.
5. Wang, Z. *Comprehensive Organic Name Reactions and Reagents*; Wiley, New York, 2010, 1807-1810.
6. O' Connell, P. B. H.; Brady, C. J. Polyacrylamide gels with modified cross-linkages. *Anal. Biochem.* **1976**, *76*, 63-73.
7. Nayak, S.; Gan, D.; Serpe, M. J.; Lyon, A. L. Hollow thermoresponsive microgels. *Small* **2005**, *1*, 416-421.
8. Hu, X.; Tong, Z.; Lyon, A. L. Multicompartment core/shell microgels. *J. Am. Chem. Soc.* **2010**, *132*, 11470-11472.
9. Kaneko, D.; Tada, T.; Kurokawa, T.; Gong, J. P.; Osada, Y. Mechanically strong hydrogels with ultra-low frictional coefficients. *Adv. Mater.* **2005**, *17*, 535-538.
10. Ducrot, E.; Chen, Y.; Bulters, M.; Sijbesma, R. P.; Creton, C. Toughening elastomers with sacrificial bonds and watching them break. *Science* **2014**, *344*, 186-189.
11. Argun, A.; Can, V.; Altun, U.; Okay, O. Nonionic double and triple network hydrogels of high mechanical strength. *Macromolecules* **2014**, *47*, 6430-6440.
12. Rubinstein, M.; Colby, R. H. *Polymer Physics;* Oxford University Press, New York, 2003, Ch. 7, 253-305.
13. Gent, A. N.; Liu, G. L.; Mazurek, M. Experimental study of molecular entanglement in polymer networks. *J. Polym. Sci., Part B: Polym. Phys.* **1994**, *32*, 271-279.

14. Sperling, L. H.; Mishra, V. The current status of interpenetrating polymer networks. *Polym. Adv. Tech.* **1995**, *7*, 197-208.
15. Michalke, W.; Lang, M.; Kreitmeier, S.; Göritz, D. Comparison of topological properties between end-linked and statistically cross-linked polymer networks. *J. Chem. Phys.* **2002**, *117*, 6300-6307.
16. Wang, E.; Escobedo, F. Swelling and tensile properties of tetra-polyethylene glycol via coarse-grained molecular models. *Macromol. Theory Simul.* **2017**, *26*, 1600098.
17. Webber R. E.; Creton, C.; Brown, H. R.; Gong, J. P. Large strain hysteresis and Mullins effect of tough double-network hydrogels. *Macromolecules* **2007**, *40*, 2919-2927.
18. Rikkou-Kalourkoti, M.; Kitiri, E. N.; Patrickios, C. S.; Leontidis, E.; Constantinou, M.; Constantinides, G.; Zhang, X.; Papadakis, C. M. Double networks based on amphiphilic cross-linked star block copolymer first conetworks and randomly cross-linked hydrophilic second networks. *Macromolecules* **2016**, *49*, 1731-1742.
19. Okay, O. Macroporous copolymer networks. *Prog. Polym. Sci.* **2000**, *25*, 711-779.
20. Mitsumata, T.; Gong, J. P.; Osada, Y. Shape memory functions and motility of amphiphilic polymer gels. *Polym. Adv. Technol.* **2001**, *12*, 136-150.
21. Bilici, C.; Okay, O. Shape memory hydrogels via micellar copolymerization of acrylic acid and *n*-octadecyl acrylate in aqueous media. *Macromolecules* **2013**, *46*, 3125-3131.
22. Gulyuz, U.; Okay, O. Self-healing poly(acrylic acid) hydrogels with shape behavior of high mechanical strength. *Macromolecules* **2014**, *47*, 6889-6899.
23. Shiblee, MD N. I.; Ahmed, K.; Khosla, A.; Kawakami, M.; Furukawa, H. 3D printing of shape memory hydrogels with tunable mechanical properties. *Soft Matter*, **2018**, *14*, 7809-7817.
24. Luo, R.; Zhu, M.; Yuan, X.; Li, S. An autonomic and "off–on–off"-switchable polymer microreactor. *RSC Adv.* **2015**, *5*, 5598-5603.
25. McCormick, C. L.; Nonaka T.; Johnson, C. B. Water-soluble copolymers: 27. Synthesis and aqueous solution behavior of associative acrylamide/*N*-alkylacrylamide copolymers. *Polymer* **1988**, *29*, 731-739.
26. Hiemenz, P. C. *Polymer Chemistry: The Basic Concepts*; Marcel Dekker, New York, 1984, Ch. 1, 48-65.

27. Mukherjee, S.; Bapat, A. P.; Hill, M. R.; Sumerlin, B. S. Oximes as reversible links in polymer chemistry: Dynamic macromolecular stars. *Polym. Chem.* **2014**, *5*, 6923-6931.
28. Kalia, J.; Raines, R. T. Hydrolytic stability of hydrazones and oximes. *Angew. Chem. Int. Ed.* **2008**, *47*, 7523-7526.
29. Dirksen, A.; Hackeng, T. M.; Dawson, P. E. Nucleophilic catalysis of oxime ligation. *Angew. Chem.* **2006**, *118*, 7743-7746.
30. Kölmel, D. K.; Kool, E. T. Oximes and hydrazones in bioconjugation: Mechanism and catalysis. *Chem. Rev.* **2017**, *117*, 10358-10376.
31. Grover, G. N.; Braden, R. L.; Christman, K. L. Oxime cross-linked injectable hydrogels for catheter delivery. *Adv. Mater.* **2013**, *25*, 2937-2942.
32. Lin, F.; Yu, J.; Tang, W.; Zheng, J.; Defante, A.; Guo, K.; Wesdemiotis, C.; Becker, M. L. Peptide-functionalized oxime hydrogels with tunable mechanical properties and gelation behavior. *Biomacromolecules* **2013**, *14*, 3749-3758.
33. Bissot, T.C.; Parry, R. W.; Campbell, D. H. The physical and chemical properties of the methylhydroxylamines. *J. Am. Chem. Soc.* **1957**, *79*, 796-800.
34. Tung, C.-Y. M.; Dynes, P. J. Relationship between viscoelastic properties and gelation in thermosetting systems. *J. Appl. Polym. Sci.* **1982**, *27*, 569-574.
35. Winter, H. H.; Chambon, F. Analysis of linear viscoelasticity of a cross-linking polymer at the gel point. *J. Rheol.* **1986**, *30*, 367-382.
36. Chambon, F.; Winter, H. H. Linear viscoelasticity at the gel point of a cross-linking PDMS with imbalanced stoichiometry. *J. Rheol.* **1987**, *31*, 683-697.
37. Flory, P. J. Molecular size distribution in three dimensional polymers. II. Trifunctional branching units. *J. Am. Chem. Soc.* **1941**, *63*, 3091-3096.
38. Stockmayer, W. H. Theory of molecular size distribution and gel formation in branched-chain polymers. *J. Chem. Phys.* **1943**, *11*, 45-55.

CHAPTER 4: CONCLUSIONS AND FUTURE WORK

We explored three different approaches to improve the mechanical properties of polymer network hydrogels, materials which are known to be very fragile. These approaches included multiple network interpenetration, introduction of a hydrophobic monomer, and introduction of reversible cross-links, the first two of which proved more successful. Most monomers and cross-linkers used for the preparation of the present materials were acrylamides. In particular, the nonionic *N*,*N*-dimethylacrylamide (DMAAm) was employed as the hydrophilic monomer, the rather uncommon and crystalline *N*-dodecylacrylamide (DDAAm) served as the hydrophobic monomer, whereas diacetone acrylamide (DAAm) was utilized as the ketone-bearing reactive monomer for the oxime cross-link formation. On the other hand, the hydrophilic diacrylamides *N*,*N*′-methylenebisacrylamide (MBAAm) and *N*,*N*′-(1,2-dihydroxy-ethylene)bisacrylamide (DHEBA) were utilized as the non-degradable and degradable cross-linkers, respectively.

The multiple network hydrogels based on DMAAm and MBAAm proved particularly successful, as increasing network multiplicity and monomer concentration led to an increase in all the mechanical properties in uniaxial compression, including the Young's modulus, the fracture stress and strain, and the fracture energy density. The best network was the quintuple (five-fold) network made at the highest monomer concentration of 5 M, presenting a Young's modulus of 2.1 MPa, a fracture stress of 51 MPa, a fracture strain of 88%, and a fracture energy density of 5.5 MJ m^{-3}. These very promising results warrant further investigations on multiple networks, by employing other hydrophilic monomers, such as acrylamide, temperature-sensitive monomers, such as *N*-isopropylacrylamide, or even hydrophobic monomers, such as *N*-hexylacrylamide. This Thesis also included preliminary characterization (at the lowest monomer concentration) of some of the multiple networks using the modern technique of nanoindentation, by which the hardness of the samples was determined, the trends of which were consistent with the results on the Young's modulus obtained through the above-mentioned uniaxial compression characterization. A complete characterization of all multiple network samples (at all monomer concentrations) by nanoindentation could also be performed in the future, and compare these new results with the ones from uniaxial compression. Again within the

multiple network direction, and focusing on just double-network hydrogels, we provided a first estimation of the degree of interconnection between the two networks which was found to correspond to a percentage of grafting of the second network onto the first of up to 20%. This was accomplished by using a combination of degradable (DHEMA) and non-degradable (MBAAm) cross-linkers to prepare partially degradable double-network hydrogels based on DMAAm.

The second major part of the work involved preparation and characterization of amphiphilic polymer networks resulting from the combination of the hydrophilic DMAAm and hydrophobic DDAAm monomers. Networks of two architectures were prepared, randomly cross-linked networks and well-defined based on block copolymers. Robust polymer networks were obtained for both architectures, whose mechanical properties increased with the hydrophobe content, reaching values of fracture stress of 7 and 11 MPa for the best randomly cross-linked and well-defined network, respectively. Extremely interestingly, some of the randomly cross-linked amphiphilic polymer networks displayed shape memory, with original shape being recoverable from seconds to minutes, depending on DDAAm hydrophobe content and temperature (range between 50 and 70 °C). The amphiphilic nature of these polymer networks leads to their self-assembly in water, and the resulting organized structure greatly contributes to their enhanced mechanical properties. This structure should be fully characterized in the future using scattering, diffraction and microscopy techniques. However, within this Doctoral Thesis, several linear amphiphilic block copolymers, bearing polyDMAAm and polyDDAAm segments, were prepared and characterized in dilute aqueous solutions using small-angle neutron scattering, dynamic light scattering, and atomic force microscopy, and were found to form spherical micelles or multimicellar aggregates, with the latter structures favored in the more hydrophobic samples. Furthermore, the samples presenting shape memory should be characterized in the future in terms of their thermophysical properties, and, in particular, the temperature-dependence of their elastic modulus using dynamical mechanical analysis or rheology, and melting and crystallization transitions using differential scanning calorimetry (DSC). It is noteworthy that preliminary DSC experiments on bulk polymer network samples did not show a clear melting point, although the DDAAm monomer clearly shows the expected

melting transition at 50 °C. Possibly, the presence of water could help the melting transition.

The final part of the work involved the preparation of amphiphilic polymer networks by the combination of DAAm-bearing linear precursor polymers with a diaminooxy cross-linker to form oxime cross-links. The gel formation times of these networks were determined using the tube inversion technique and rheology, as a function of polymer concentration, polymer composition, stoichiometry, solution pH, solvent type and presence of aniline. Rheology was also used to determine the bond lifetime for the oxime cross-links which was found to be very long, and the cross-links difficult to exchange. This was the reason why self-healing was not possible at all for these materials, and the gel-to-sol transition required days. Future work within this section might involve a switch from slow oxime to the more dynamic hydrazone chemistry for the cross-links, by keeping the same linear polymer precursors bearing the ketone reactive side-groups (in DAAm), and combining them with a dihydrazide rather than a diaminooxy cross-linker.